UNIVERSITÄT PADERBORN

FAKULTÄT FÜR ELEKTROTECHNIK, INFORMATIK UND MATHEMATIK

Load Profiling and Demand Side Management Methods for Optimized and Sustainable Microgrids in East Africa

Von der Fakultät für Elektrotechnik, Informatik und Mathematik
der Universität Paderborn

zur Erlangung des akademischen Grades

Doktor der Ingenieurwissenschaften (Dr.-Ing.)

genehmigte Dissertation

von

Josephine Nakato Kakande

Erster Gutachter: Prof. Dr.-Ing. habil. Stefan Krauter
Zweiter Gutachter: Prof. Dr.-Ing. Henning Meschede

Tag der mündlichen Prüfung: 09.03.2026

Paderborn 2026

Diss. EIM-E/399

UNIVERSITÄT PADERBORN

FAKULTÄT FÜR ELEKTROTECHNIK, INFORMATIK UND MATHEMATIK

Load Profiling and Demand Side Management Methods for Optimized and Sustainable Microgrids in East Africa

Submitted to the Faculty of Electrical Engineering, Computer Science and Mathematics
of the University of Paderborn

for the award of the degree of

Doctor of Engineering (Dr.-Ing.)

approved dissertation

by

Josephine Nakato Kakande

First examiner: Prof. Dr.-Ing. habil. Stefan Krauter
Second examiner: Prof. Dr.-Ing. Henning Meschede

Date of oral examination: March 9, 2026

Paderborn 2026

Diss. EIM-E/399

Paderborn University
Faculty of Electrical Engineering, Computer Science and Mathematics
Electrical Energy Technology - Sustainable Energy Concepts (EET-NEK)

DOCTORATE THESIS

in Fulfilment of the Requirements for the Degree of Doctor of Philosophy in Electrical Engineering

Load Profiling and Demand Side Management Methods for Optimized and Sustainable Microgrids in East Africa

Author:

Josephine Nakato Kakande
(6956686)

Supervised by:

Prof. Dr.-Ing. habil. Stefan Krauter

Date: 10th March 2026

Declaration

I, **JOSEPHINE NAKATO KAKANDE**, do hereby declare to the Senate of the University of Paderborn that this dissertation is my original work and that it has not been submitted for a degree or similar award in any other Institution.

Josephine Nakato Kakande

10 March 2026

Name and signature of candidate **Date**

Dedication

Dedicated to

Ephraim, Edmund, Elijah and Freda, to Sam,

and my parents Bridget Kakande and Prof. Ignatius Kakande

Acknowledgements

First and foremost, I wish to express my gratitude to Almighty God for the blessing of life and for enabling me to undertake and complete my PhD research. He has sustained me spiritually, physically, materially, intellectually and in all aspects.

To God, be all the glory!

I am indebted and full of gratitude to my supervisor, Prof. Dr.-Ing. Stefan Krauter. Your guidance, mentorship, technical knowledge imparted, field expertise shared and input into the research, publications and thesis have formed an integral part of the PhD journey. My deepest thanks for all your support and contributions.

I would also like to express my sincere gratitude to Prof. Dr.-Ing. Henning Meschede for reviewing and examining the dissertation, as well as to the entire Doctoral committee. I truly appreciate the opportunity to benefit from your shared knowledge and feedback.

My thanks to all my colleagues from the Electrical Energy Technology - Sustainable Energy Concepts (EET-NEK) Chair at Paderborn University. Thank you very much Godiana Hagile Philipo, Jörg Bendfeld for the valuable expertise and guidance shared, Marius Möller, Dorothea Hermann, Hala Fares-Alhaddad and Dirk Prior.

I would like to thank the German Federal Ministry of Education and Research (BMBF) for funding this research under the Art-D Grids Project.

To my colleagues and all the partners on the ART-D Grids project, it has been a pleasure and great experience working and interacting together. Thank you Mark Geofrey Kagarura, Ibrahim Mwammenywa, Henrik Bode, Paul Bogere, Septimus Boshoff, Lillian Donna Namujju, Henrietta Acquah-Swanzy, Teddy Mangeni, Henry Asiimwe and Tobias Klaus.

I acknowledge and thank Waddah Alturk and Nisha Shilpakar. A big thank you to Simon Mabala, Aminu Bugaje and all other colleagues and friends for their support and encouragement.

I am grateful to Makerere University for granting me study leave to pursue my PhD studies at Paderborn University.

My thanks to Winch Energy, the Lwak Convent community, Silale microgrid personnel and the various microgrid communities for all their support and collaboration; it is greatly appreciated.

Words cannot adequately express my immense gratitude to my family for all their support, prayers, encouragement, sacrifices and for standing in for me while I have been undertaking this PhD. I am eternally indebted to you. Thank you to my parents Prof. Ignatius Kakande and Bridget Kakande, to my siblings Betty, Mary, Charles, Barbara, Anne, Joseph, to Sarah and Naomi and all who have played a role. May God bless and reward you a thousandfold.

My dear father Prof. Ignatius Kakande, forever loved, your example of a life well lived in love and service of God and others will always be a lifelong blessing and inspiration.

To my beloved husband Samuel Lutalo, you have been an integral, invaluable companion on this journey, and your contribution has been immeasurable - I am beyond grateful! To my dear children Ephraim, Edmund, Elijah and Freda, I cannot thank you enough for your prayers, encouragement, sacrifices, love and presence in my life.

May God bless you all richly.

Paderborn, 16 September 2025

Josephine Nakato Kakande

Abstract

About 600 million people in Sub-Saharan Africa (SSA) remain without access to electricity, representing three-quarters of the world's unelectrified population. Microgrids, particularly solar-based systems, are increasingly recognized as a viable pathway to bridging this gap, given the region's abundant solar resources. However, the inherent intermittency of renewable energy calls for battery storage as well as effective demand side management (DSM) strategies to ensure microgrid system reliability and sustainability.

This dissertation investigates DSM approaches for rural East African microgrids, focusing on solar PV-battery and hybrid systems. The rapidly growing refrigeration sector in Africa, projected to increase from 80 million to 200 million appliances by 2030, presents a critical but underexplored area of intervention for DSM. A combination of modeling, simulation, and experimental studies was conducted. Refrigeration scheduling for a site in Kenya was optimized based on appliance temperature evolution data, giving an 8% overall demand reduction and a shift by 1 hour in the time of the evening peak. A revision of energy efficiency labeling standards for East Africa was proposed to account for ageing and efficiency degradation in refrigeration appliances, which can lead to a 23% increase in energy consumption after 10 years. Experimental investigation of battery state of charge and temperature-based control for refrigeration appliances demonstrated improved alignment of refrigeration demand with elevated battery charge and PV generation periods and resulted in an average 14% reduction in daily refrigeration energy use for three appliances, with performance improvements varying across appliances.

Analysis of system and customer load profiles from microgrids in Uganda and Tanzania highlighted the importance of DSM strategies such as strategic load growth to enhance PV utilization. A novel approach integrating electric two-wheelers and portable storage into a microgrid in Uganda was investigated. Results showed a 57% reduction in Levelized Cost of Energy (LCOE) to USD 0.35 USD/kWh, a 98.5% reduction in kWh of curtailed PV energy, and avoided annual CO_2 emissions of 73.27 tons, equivalent to annual emissions from 57 fossil-fuel two-wheelers travelling 50 km daily. Furthermore, 160 additional customers could be served annually as off-microgrid consumers without requiring investment in distribution infrastructure.

These findings demonstrate the considerable potential of DSM to improve the sustainability, efficiency, and scalability of microgrids and energy systems in general in East Africa, through approaches addressing refrigeration, battery storage and e-mobility.

Zusammenfassung

Etwa 600 Millionen Menschen in Subsahara-Afrika (SSA) haben nach wie vor keinen Zugang zu elektrischem Strom, was drei Viertel der weltweit nicht elektrifizierten Bevölkerung entspricht. Microgrids, insbesondere auf Solarenergie basierenden Systeme, werden angesichts der reichlich vorhandenen Sonnenenergie in der Region zunehmend als gangbarer Weg zur Überbrückung dieser Lücke anerkannt. Die inhärente Unbeständigkeit erneuerbarer Energien erfordert jedoch Batteriespeicher sowie effektive Strategien zum Nachfragemanagement (DSM), um die Zuverlässigkeit und Nachhaltigkeit von Microgridsystemen zu gewährleisten.

Diese Dissertation untersucht DSM-Ansätze für ländliche Microgrids in Ostafrika, wobei der Schwerpunkt auf Solar-PV-Batterie- und Hybridsystemen liegt. Der schnell wachsende Kühlungssektor in Afrika, der bis 2030 voraussichtlich von 80 Millionen auf 200 Millionen Geräte anwachsen wird, stellt einen kritischen, aber noch wenig erforschten Bereich für DSM-Maßnahmen dar. Es wurde deshalb dafür eine Kombination aus Modellierung, Simulation und experimentellen Studien durchgeführt. Die Kühlplanung für einen Standort in Kenia wurde auf der Grundlage von Daten zur Temperaturentwicklung der Kühlschränke und Gefriertruhen optimiert, was zu einer Gesamtreduzierung des Bedarfs um 8% und einer Verschiebung der Abendspitzenzeit um 1 Stunde führte. Es wurde eine Überarbeitung der Energieeffizienz-Kennzeichnungsstandards für Ostafrika vorgeschlagen, um der Alterung und Effizienzverschlechterung von Kühlgeräten Rechnung zu tragen, die nach 10 Jahren zu einem Anstieg des Energieverbrauchs um 23% führen kann. Experimentelle Untersuchungen zur Ladezustands- und temperaturbasierten Steuerung von Kühlgeräten zeigten eine verbesserte Abstimmung des Kühlbedarfs mit erhöhten Batterieladezustands- und PV-Erzeugungszeiten und führten zu einer durchschnittlichen Reduzierung des täglichen Energieverbrauchs für die Kühlung von drei Geräten um 14 %, wobei die Einsparungen je nach Gerät variierten.

Die Analyse der System- und Kundenlastprofile von Mikronetzen in Uganda und Tansania unterstrich die Bedeutung von DSM-Strategien wie dem strategischen Lastwachstum zur Verbesserung der PV-Nutzung. Ein neuartiger Ansatz zur Integration von Elektro-Zweirädern und tragbaren Speichern in ein Microgrid in Uganda wurde untersucht. Die Ergebnisse zeigten eine Senkung der Stromgestehungskosten (LCOE) um 57 % auf 0,35 USD/kWh, eine Reduzierung der nichtgenutzten PV-Energie um 98,5 % in kWh und eine Vermeidung von jährlichen CO_2-Emissionen in Höhe von 73,3 Tonnen, was den jährlichen Emissionen von 57 konventionellen, mit fossilen Brennstoffen betriebenen Zweirädern entspricht, die täglich 50 km zurücklegen. Darüber hinaus könnten jährlich 160 zusätzliche Kunden als Off-Microgrid-Verbraucher versorgt werden, ohne dass Investitionen in die Verteilungsinfrastruktur erforderlich wären.

Diese Ergebnisse zeigen das beträchtliche Potenzial von DSM zur Verbesserung der Nachhaltigkeit, Effizienz und Skalierbarkeit von Microgrids und Energiesystemen im Allgemeinen in Ostafrika durch übergreifende Konzepte, die Kühlung, Batteriespeicherung und E-Mobilität miteinbeziehen.

Acronyms

2&3W	Two- and Three-Wheelers
AF	Alternative Framework
AfDB	African Development Bank
AfEMA	Africa E-Mobility Alliance
Ah	Ampere hour
AMI	Advanced Metering Infrastructure
API	Application Programming Interface
ASM	Ancillary Services Market
BAU	Business as Usual
BESS	Battery Energy Storage System
CFL	Compact Fluorescent Lamp
CLI	Command-Line Interface
CMP	Capacity Market Program
CPP	Critical Peak Pricing
CRF	Capital Recovery Factor
DBB	Demand Bidding/Buyback
DLC	Direct Load Control
DOD	Depth of Discharge
DP	Dynamic Programming
DR	Demand Response
DSM	Demand Side Management
EAC	East African Community
EACREEE	East African Centre of Excellence for Renewable Energy and Efficiency
EDR	Emergency Demand Response
EELA	Energy Efficient Lighting and Appliances
EMS	Energy Management System
EPRA	Energy and Petroleum Regulatory Authority

EPRI	Electric Power Research Institute
ESMAP	Energy Sector Management Assistance Program
ESS	Energy Storage System
FERC	Federal Energy Regulatory Commission
GA	Genetic Algorithm
GFA	Grid Friendly Appliance
HFPSO	Hybrid Firefly Particle Swarm Optimization
HOMER	Hybrid Optimization of Multiple Energy Resources
HVDC	High Voltage Direct Current
ICS	Interruptible Curtailable Service
IEA	International Energy Agency
IIR	International Institute of Refrigeration
IoT	Internet of Things
IPP	Independent Power Producer
JNHPP	Julius Nyerere Hydro Power Plant
KenGen	Kenya Electricity Generating Company
KPLC	Kenya Power and Lighting Company
LCOE	Levelized Cost of Energy
LED	Light-emitting diode
LoRaWAN	Long Range Wide Area Network
LP	Linear Programming
LPSP	Loss of Power Supply Probability
LS	Load Shifting
M2M	Machine-to-machine
MEPS	Minimum Energy Performance Standards
MILP	Mixed-Integer Linear Programming
MINLP	Mixed-Integer Nonlinear programming
MPC	Model Predictive Control
MQTT	Message Queuing Telemetry Transport

MTF	Multi-Tier Framework
NASA	National Aeronautics and Space Administration
NDC	Nationally Determined Contribution
NPC	Net Present Cost
O&M	Operation and Maintenance
OCR	Optical Character Recognition
PAYG	Pay-As-You-Go
PC	Peak Clipping
PCC	Point of Common Coupling
PCM	Phase Change Materials
PSO	Particle Swarm Optimization
PUE	Productive Use of Energy
PUR	Polyurethane
PV	Photovoltaic
RCA	Rainflow Counting Algorithm
RE	Renewable Energy
RTP	Real-time Pricing
SADC	Southern African Development Community
SDG	Sustainable Development Goal
SHS	Solar Home System
SOC	State of Charge
SSA	Sub-Saharan Africa
STC	Standard Test Conditions
SVR	Support Vector Regressor
TANESCO	Tanzania Electric Supply Company
TCL	Thermostatically Controlled Load
TOU	Time-of-use
U4E	United for Efficiency
UEC	Unit Energy Consumption

UEDCL	Uganda Electricity Distribution Company Limited
UETCL	Uganda Electricity Transmission Company Limited
UFLS	Under Frequency Load Shedding
USD	United States Dollar
UVLS	Under Voltage Load Shedding
VM	Virtual Machine
VPN	Virtual Private Network
VRLA	Valve Regulated Lead Acid
WFS2ACSO	Wingsuit Flying Search algorithm and Artificial Cell Swarm Optimization

List of Symbols

a	Weighting coefficient for EC_{16}
A	Thermal conductance (W/℃)
A_{dh}	Devices of type d available for control in hour h
AEC	Annual energy consumption (kWh/ year)
β_{bat}	Upper bound of battery size
B_d	Earliest time device d can start running
β_{pv}	Upper bound of PV size
b	Weighting coefficient for EC_{32}
B_D	Battery degradation rate
B_r	Number of battery replacements over project lifetime
c_1	Cognitive acceleration constant
c_2	Social acceleration constant
C_{Bat}	Battery capital cost (USD/kWh)
C_{conv}	Converter capital cost (USD/kW)
$connect(h)$	Shiftable loads connected at hour h
C_r	Number of converter replacements over project lifetime
CRF	Capital Recovery Factor
c_v	Isochoric (constant volume) heat capacity (J/K)
DOD	Depth of discharge
DOD_{port}	Portable battery depth of discharge
d	Type of device
$disconnect(h)$	Shiftable loads disconnected at hour h
d_τ	Decay constant (min^{-1})
$d_{\tau_{max}}$	Decay constant factor (min^{-1})
E_B	Battery energy (kWh)
E_{Bmax}	Maximum battery energy (kWh)

E_{Bmin}	Minimum battery energy (kWh)
EC_T	Energy consumption based on ambient temperature T (Wh / day)
E_d	Latest time device d can finish running
E_L	Hourly base load energy (kWh)
E_{mob}	Energy for e-mobility loads (kWh)
$E_{n_{x_n daily}}$	Energy supplied to load of type x_n daily (kWh)
$E_{port_{usable}}$	Usable energy of portable battery storage (kWh)
E_{PS}	Energy for portable storage (kWh)
E_{PV}	PV energy produced (kWh)
E_y	Normalised energy consumption at age y years
f	Inflation rate
f_d	Derating factor for PV modules
F_j	Frost adjustment factor for the jth compartment
f_h	PSO objective function
f_{obj}	MILP objective function
G	Incident solar radiation (kW/m^2)
g_d	Operation duration of device type d (hours)
G_{ref}	Incident solar radiation at STC (kW/m^2)
h	Hour
H	Number of hours in a day
i	Swarm particle number
ICC	Initial capital cost
i_{nom}	Nominal interest rate
INS	Installation costs
INS_{BAT}	Battery installation costs
INS_{CONV}	Converter installation costs
INS_{PV}	PV installation costs
$iter$	Iteration number

$iter_{max}$	Maximum number of iterations
k	Heat transfer coefficient (W/(m^2 K))
K_j	Volume adjustment factor for the jth compartment
K_T	Temperature coefficient of power for solar PV modules (/℃)
L_{bat}	Battery lifetime (years)
LCC	Lifecycle cost
LCOE	Levelized Cost of Energy
$load_{fc_h}$	Forecasted load at hour h (kW)
$\Delta load_h$	Change in load at hour h (kW)
m_c	Thermal mass (J/℃)
$MG_{customer_{kwh_{daily}}}$	Average annual energy consumption per microgrid customer
N	Project lifetime (years)
η	Coefficient of performance
η_{cc}	Charge controller efficiency
η_{ch}	Battery charging efficiency
N_d	Total number of types of devices
η_{disch}	Battery discharging efficiency
η_{conv}	Converter efficiency
$n_{cycles(DOD)}$	Number of battery cycles as a factor of DOD
nx	Component X's operational lifetime (years)
n_{x_n}	Number of loads of type x_n
$n_{x_n daily}$	Number of loads of type x_n charged daily
η_{port}	Portable battery converter efficiency
Off_{MG}	Number of off-microgrid customers served annually
$OPEX_{BAT}$	Battery operational costs
$OPEX_{CONV}$	Converter operational costs
$OPEX_{PV}$	PV operational costs
p	Refrigeration appliance power

P_{Bat}	Battery power (kW)
P_{conv}	Converter power rating (kW)
$P_{g_{best}}$	Global best position from the entire swarm population
P_{Grid}	Grid power (kW)
φ_1 , φ_2	Random numbers in the range [0, 1]
$P_{i_{best}}$	Personal best position of particle i
P_L	Load power (kW)
P_L^{max}	Maximum AC load power demand (kW)
P_{md}	Power consumption of device d in its m^{th} hour of operation
P_{PV}	PV generated power (kW)
$P_{pv_{excess}}$	Excess PV power (kW)
P_r	PV rated power at STC (kW)
PR_{FUEL}	Present value of fuel costs
PR_{OPEX}	Present value of operating costs
PR_{REP}	Present value of replacement costs
P_{x_n}	Charging power of load x_n
REP_{BAT}	Battery replacement costs
REP_{CONV}	Converter replacement costs
r	Discount rate
R	Energy consumption index
R_{adj}	Energy consumption index with ageing factor
RLM_h	Reducible load margin at hour h
S	Surface area (m^2)
s_d	Maximum possible delay of device d
soc_{TH}	SOC threshold
σ	Battery self discharge
τ	Temperature sampling interval
t	Time

T_1	Reference ambient temperature (℃)
T_2	Fresh food compartment reference temperature (4°C)
T_{amb}	Ambient temperature (℃)
$Targ_h$	Hourly load power target (kW)
T_{band}	Range of water temperature deadband (℃)
T_c	Cell temperature (℃)
T_h	Upper water temperature deadband value (℃)
T_{high1}	Upper temperature threshold for appliance (℃) for SOC >soc_{TH}
T_{high2}	Upper temperature threshold for appliance (℃) for SOC ≤ soc_{TH}
T_j	Temperature of the jth compartment (℃)
T_l	Lower water temperature deadband value (℃)
T_{low1}	Lower temperature threshold for appliance (℃) for SOC >soc_{TH}
T_{low2}	Lower temperature threshold for appliance (℃) for SOC ≤ soc_{TH}
T_{ref}	Reference temperature (℃)
T_{set}	Water heater temperature setpoint (℃)
v_i	Current velocity vector for particle i
$v_i(t+i)$	Next velocity vector for particle i
V_j	Volume in the jth compartment (L)
v_{max}	Maximum velocity for PSO algorithm
v_{min}	Minimum velocity for PSO algorithm
w	Inertia weight
W_{x_n}	Priority weighting of load x_n
x_i	Swarm particle i current position
$x_i(t+1)$	Swarm particle i next position
x_n	Type of e-mobility or portable storage load
$x_{n_{bat_{cap}}}$	Battery capacity of load x_n (kWh)
$x_{port_{bat_{cap}}}$	Portable battery capacity (kWh)

X_r	Number of times component X is replaced over project lifetime
y	Age of appliance (years)

Table of Contents

List of Figures

List of Tables

Publications

Kakande, J.N.; Philipo, G.H.; Krauter, S. Optimized Demand Side Management for Refrigeration: Modeling and Case Study Insights from Kenya. *Energies* 2025, 18, 3258. https://doi.org/10.3390/en18133258

J. N. Kakande, G. H. Philipo and S. Krauter. Smart Demand Side Management Using Battery SOC-Based Control for Refrigeration in a Solar Hybrid System. 2025 IEEE 7th Global Power, Energy and Communication Conference (GPECOM 2025), Bochum, Germany, 2025. doi: 10.1109/GPECOM65896.2025.11062012

Kakande, J.N.; Philipo, G.H.; Krauter, S. Optimized E-Mobility and Portable Storage Integration in an Isolated Rural Solar Microgrid in Uganda. *Solar* 2024, 4, 694-727. https://doi.org/10.3390/solar4040033

J. N. Kakande, G. H. Philipo and S. Krauter. Demand Side Management Potential of Refrigeration Appliances. 2023 IEEE PES/IAS PowerAfrica, Marrakech, Morocco, 2023. doi: 10.1109/PowerAfrica57932.2023.10363161

J. Nakato Kakande, G. Hagile Philipo, S. Krauter. Optimal Design of a Semi Grid-Connected PV System for a Site in Lwak, Kenya Using HOMER. 8th World Conference on Photovoltaic Energy Conversion (WCPEC-8 / EU PVSEC 2022), 2022, Milan, Italy. doi: 10.4229/WCPEC-82022-4CV.1.8

J.N. Kakande, G.H. Philipo, S. Krauter. Load Data Acquisition in Rural East Africa for the Layout of Microgrids and Demand–Side–Management Measures. In: Proceedings of the 38th European Photovoltaic Solar Energy Conference and Exhibition (EUPVSEC 2021), 2021, pp. 1505-1510. doi: 10.4229/EUPVSEC20212021-6BV.5.38

Philipo, G.H.; Kakande, J.N.; Krauter, S. Neural Network-Based Demand-Side Management in a Stand-Alone Solar PV-Battery Microgrid Using Load-Shifting and Peak-Clipping. *Energies* 2022, 15, 5215. https://doi.org/10.3390/en15145215

Philipo, G. H., Kakande, J. N., and Krauter, S. Combined Economic and Emission Dispatch of a Microgrid Considering Multiple Generators. 2023 IEEE PES/IAS PowerAfrica, Marrakech, Morocco, 2023. doi: 10.1109/PowerAfrica57932.2023.10363325

Philipo, G. H., Kakande, J. N., and Krauter, S. Demand-Side Management for Optimal Dispatch of an Isolated Solar Microgrid. 2023 IEEE AFRICON, Nairobi, Kenya, 2023. doi: 10.1109/AFRICON55910.2023.10293343

Publications Under review

Kakande, J.N.; Philipo, G.H.; Krauter, S. Integrating Ageing into Minimum Energy Performance Standards (MEPS) for Sustainable and Efficient Refrigeration in East Africa. *Environmental Research: Infrastructure and Sustainability*. (Manuscript under Review and Revision)

1 Introduction

1.1 Background

Global energy needs are on the rise due to population growth, increased development levels and advancements in technology. Sufficient, sustainable, quality and reliable energy supply is critical for the development of nations as it spurs economic advancement and brings social and environmental benefits [1]. For an energy system to be described as sustainable, it is essential that it meets the following criteria: environmental friendliness, affordability, reliability, safety, convenience of use and equitable access [2].

Sustainable Development Goal (SDG) 7 targets the achievement of affordable, sustainable, modern and reliable energy for all by 2030. It also targets an increased renewable fraction in the energy mix as well as a doubling of the rise in energy efficiency by 2030.

While 2015 to 2021 saw global electrification increase from 87% to 91%, unfortunately this improvement was not reflected in developing economies [3]. Projections indicate that by 2030, 685 million people will be unelectrified worldwide [4].

In Sub-Saharan Africa (SSA), 600 million people or about three quarters of the unelectrified population worldwide lack electricity access. Furthermore, there is a huge urban-rural electricity access disparity; more than 80% of Africa's unelectrified population reside in rural areas [5]. The SSA rural electrification rate is less than 25%, while urban electrification is at 71% [6].

Africa utilizes less than 6% of the world's energy despite comprising nearly 18% of the global population, with South Africa alone consuming a significant 16% of the continental demand. Wood fuel and wastes comprise almost two thirds of the cooking fuels in Africa [5], with only 30% of Africa's populace in 2022 accessing clean cooking solutions and more than 900 million people, predominantly rural, deprived thereof. Installed electricity capacity continent-wide was 245 GW but inefficiencies meant that transmission and distribution losses were as high as 17.1% as shown in Table 1-1 [7].

Table 1-1: Energy statistics for Africa in 2015 and 2022

Indicator	2015	2022	Reference
Population with access to electricity in Africa (%)	42	56	[7]
Population with access to electricity in Sub Saharan Africa (%)	39	50	[3]
Total installed electricity capacity (GW)	168	245	[7]
Installed renewable capacity (GW)	33	56	[7]
Population with access to clean cooking solutions (%)	32	30	[7]
Electricity losses through transmission, distribution, collection (%)	15	17.1	[7]

In 2021, 844 TWh of electricity was generated on the continent, of which 185 TWh or 22% was from renewable sources [8]. Despite an abundance of renewable resources, fossil fuels account for 75% of Africa's electricity production [7]. This presents a significant challenge due to emissions, energy security risks and rising fuel costs on account of global market, political and supply chain disruptions. Fortunately though, falling solar equipment costs are driving renewable energy (RE) as energy carriers of choice.

Africa's electricity consumption rose from 639.2 TWh in 2015 to 680.2 TWh in 2019 [9]. Demand in 2040 is projected to be 1,614 TWh, of which 76% could be met by RE in form of hydro, solar and wind power if existing and planned plants are implemented and operating at full capacity [10]. Africa's 2021 electricity consumption per capita was 600 kWh [11] but at 180 kWh, SSA's per capita energy consumption (excluding South Africa) is dwarfed by the 6500 kWh and 13000 kWh per capita values of Europe and USA respectively [12].

There are different tier structures for categorising the level of residential electricity consumption. The World Bank and Energy Sector Management Assistance Program (ESMAP) in 2015 proposed a 6-level Multi-Tier Framework (MTF) ranging from Tier 0 for no access to Tier 5 with highest reliability and daily energy consumption of 8 kWh, thus redefining the binary 'connected' or 'not connected' evaluation metric of electricity access [1]. A simpler alternative framework (AF) was proposed by Pelz et. al., with Tier 1 characterised by lighting, phone charging and fans, Tier 2 usage extending to use of

refrigeration appliances, televisions or air conditioners and Tier 3 indicating use of other electrical appliances [13] [14]. This comparison is depicted in Table 1-2 [14].

Table 1-2: Alternative Framework (AF) versus Multi-Tier Framework (MTF) categorisation of electricity access [14]

Alternative Framework (AF) electricity access categorisation [14] [15]						
	Tier 0	**Tier 1**	**Tier 2**	**Tier3**		
Availability	None	< 8 hours	8 – 16 hours	> 16 hours		
Service Level	None	Minimal (Lighting & Phone charging)	Decent (plus TV, refrigeration and cooling appliances)	Affluent (plus other electrical appliances)		
Affordability (percentage of budget)		> 10%	5 – 10 %	< 5%		
Multi-Tier Framework (MTF) electricity access categorisation [14]						
	Tier 0	**Tier 1**	**Tier 2**	**Tier 3**	**Tier4**	**Tier5**
Duration		≥ 4 hours	≥ 4 hours	≥ 8 hours	≥ 16 hours	≥ 23 hours
Quality					Voltage problems do not affect use of desired appliances	
Reliability (Disruptions/ week)				≥ 14 hours	≤ 3 of total duration < 2 hours	
Capacity		≥ 3 W	≥ 50 W	≥ 200 W	≥ 800 W	≥ 2 kW
Consumption (Wh / day)	< 12	≥ 12	≥ 200	≥ 1000	≥ 3425	≥ 8219
Affordability				Cost of standard consumption of 365 kWh per annum is < 5% of household income		

To improve incomes and affordability of power, productive use of energy (PUE) is often promoted alongside energy access and extension programs, particularly in developing countries and for new connections.

1.2 Classification of electricity supply options

1.2.1 Centralised versus decentralised systems

The centralised grid was traditionally the main electricity supply solution used to provide energy access but focus has since shifted to deployment of decentralised energy systems [2]. The traditional grid uses AC, with High Voltage Direct Current (HVDC) networks becoming a more recent phenomenon. The benefits of grid electrification include sizeable capacity and long distance coverage. In addition, generation from thermal and hydro sources provides inertia to the system and makes it more resilient to load and frequency changes. However disadvantages associated with the grid include the cost of infrastructure required to evacuate power to load centres, relatively high connection costs, inefficiencies such as losses and lengthy rollout times. According to Power for All, in Africa connection to the grid costs on average United States Dollars (USD) 2,500 per connection [16], while [17] cites a USD 1,200 per rural connection cost for Uganda and USD 180,000 transmission cost per km for a 132 kV line.

Decentralised energy systems provide energy to localised areas and typically serve smaller communities. They are a favourable energy supply option in areas with difficult terrain, remoteness, sparsely scattered populations and low consumption, such as rural areas. They are also suitable for locations rich in renewable resources such as solar or wind and are a viable option due to falling costs of equipment, innovative business models, conducive regulatory environments and technological advancements. With quick installation times and lower costs, electricity can be provided on a smaller scale than the grid.

1.2.2 Grid, Solar home systems and Microgrids

Electricity connectivity is typically achieved through grid extension or densification, microgrids and solar home systems (SHS). For connectivity by 2030, the International Energy Agency (IEA) recommends grid extension as the most economical and sensible solution for nearly 45% of new connections, and for rural locations, microgrids and standalone systems as being most optimal [5].

- Characterised by large area coverage and a big population served, the centralised grid has generation, transmission and distribution assets serving loads scattered over a large area which may be residential, commercial and industrial loads. Due to the lengthy transmission distances and associated losses, transformers are employed to step up and down voltages. However ageing, insufficient, inefficient and unreliable infrastructure and climate related generation shortfalls are some challenges of grid electrification. South Africa for instance in 2023 experienced significant power reliability challenges. Over the period from January 01 2023 to December 11 2023, South Africa had a 99% occurrence of daily load-shedding (332 days) due to demand exceeding supply [12]. Lack of power stunts Africa's GDP growth by 2% to 4% yearly. Thus, power cuts rob African companies of 5% of sales values [18], and in the case of Ghana and Tanzania, an exorbitant 15% of the value of sales [19], with adverse impacts on national and continental development.

- Standalone solar home systems work best in low demand and sparse population scenarios and can be quickly installed. The typical SHS rating of 200W is insufficient for productive and commercial applications [16]. SHS proved popular in Africa due to the Pay-As-You-Go (PAYG) instalment payment models and mobile money services, with Kenya being a trendsetter in their rapid uptake.

- Microgrids are suitable for locations that are distant from the grid and financially viable due to sufficient, higher population concentration and demand. It is estimated that microgrids will be the least cost access option for 430 million people worldwide by 2030, of whom 380 million will reside in Sub-Saharan Africa [20]. A microgrid is a smaller scale electricity system consisting of generation and distribution assets that supply a limited number of customers. Some microgrids also include storage. The typical microgrid structure as depicted in Figure 1-1 [21] contains both AC and DC components. Microgrids can operate either in grid-connected mode whereby they interface with the grid via a Point of Common Coupling (PCC), or in isolated mode. Renewable energy resources such as solar and wind are often used due to their environmental friendliness and localised availability. Fossil fuel gensets and hydro power are can also serve as microgrid generation resources. Microgrids may also be interconnected.

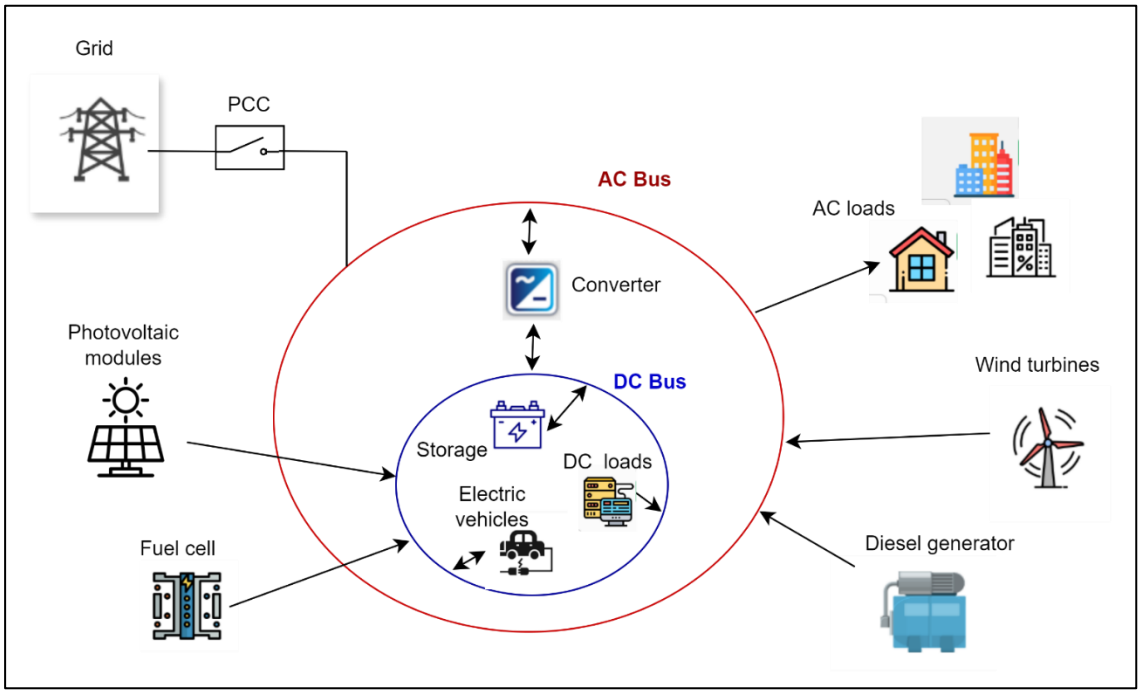

Figure 1-1: Typical layout of a grid-connected microgrid system

While most analyses of microgrids have been carried out for hybrid combinations of PV, wind, diesel genset, battery storage, grid, biomass generators and/or fuel cell set-ups [22] [23][24][25][26][27][28][29], the lifecycle analyses of setups with PV and battery only are few [22]. Microgrid systems with diesel gensets or other power generation sources are often preferred to those with a 100% renewable fraction on account of the relatively high expenses associated with RE installation and storage equipment [30]. With the trend going towards avoiding the emissions associated with diesel gensets, more research on sustainable options for PV with battery microgrids is needed.

1.3 Problem description

Microgrids are gaining prominence as a suitable option for achieving electricity access in unserved and underserved communities, including in East Africa. They, along with solar

home systems are projected by IEA as being the best method of bridging the energy gap for 55% of Africa's unelectrified population by 2030 [5].

Electricity supply and demand mismatch creates system and market inefficiencies. Demand side management (DSM) strategies aim to align supply with demand by influencing power usage time and consumption levels, which helps to improve energy system stability. DSM is broadly categorised into several strategies: peak clipping, valley filling, strategic conservation, strategic load growth, load shifting, and flexible load shape [31]. These approaches are typically driven by efforts to improve energy efficiency and cut unnecessary or untimely consumption. Measures like peak clipping and load shifting can be carried out through means such as time-of-use pricing, consumer incentives, or automating appliance operation. Together, these tactics enable energy system developers, utilities and consumers to reshape demand patterns in impactful ways.

Microgrids are typically characterised by low day time consumption and a poor load factor, which is the average to peak demand ratio, resulting in a high levelized cost of energy and sustainability challenges due to insufficient income generation for financial viability [32]. Renewable based systems using solar technology, on the other hand, have maximum production during the day. Thus shifting of loads to the daytime as well as increasing daytime demand would ensure optimal use of the solar generation resources and limit reliance on battery storage or gensets to meet peak evening demand.

Given the increasing prevalence of renewable energy sources for on-grid and isolated electricity supply, the need for mechanisms to better match demand and supply and to increase the flexibility of power systems has resulted in a heightened focus on research and implementation of demand side management practices to boost technology and market efficiencies.

Different approaches to DSM have been undertaken. Several studies have focused on water heaters with tanks as suitable for demand side management due to their large power rating and resistive nature [33][34] as well as air-conditioning [35][36], but these are not commonly used in Africa, and especially not in the power-limited microgrid communities. Refrigeration appliances are more prevalent than water heaters and are typically among the biggest residential energy consuming appliances [37][38], with their numbers and thus electricity consumption projected to increase significantly in Africa [5]. Despite substantial interest in demand side management, limited attention has been paid to the potential of refrigeration for DSM applications, particularly in renewable energy and energy storage contexts and in rural Africa settings. Hence DSM for refrigeration is investigated in this work.

Prior studies commonly rely on the aggregation and grouping of homogeneous devices for load control and load shifting [39][40] [41]. However, such assumptions overlook the diversity of real-world appliances and performance. Accordingly, research that considers non-homogeneous devices, through both modelling and experimental studies, presents a critical avenue for advancing understanding of refrigeration operation and control in off-grid and hybrid energy systems

Although Africa accounts for nearly one-fifth of the world's motorcycles, less than 0.2% of these are electric [42]. Electric two- and three-wheelers (2&3W) therefore provide a low-hanging entry point for transport electrification and decarbonization in emerging and developing economies in Africa [43], yet their adoption is constrained by the limited availability and relatively high cost of energy systems for charging infrastructure in off-grid and weak grid areas, thus limiting deployment largely to urban areas. Concurrently, rural microgrids, which are increasingly used to expand energy access, often have limited distribution footprints (typically 1 km radius [44]), and also face challenges of surplus PV generation and curtailment. These challenges highlight a critical research problem; the lack of integrated solutions that simultaneously address the underutilization of renewable energy in rural microgrids and the energy needs of e-mobility and rural off-microgrid communities. Investigating how e-mobility charging stations and portable storage can be integrated as additional loads into microgrids could unlock significant benefits, reducing PV curtailment, improving microgrid sustainability, and enabling wider adoption of clean transport in rural Africa.

Overall, with the growing deployment of microgrids in East Africa, there is a need for context-specific studies on demand-side management strategies that account for the region's energy, socio-economic, and infrastructural conditions, particularly for solar-powered systems with storage. This points to the need for further investigation into how tailored strategies for isolated and hybrid microgrids can optimize renewable energy utilization, enhance microgrid sustainability, and facilitate the integration of both existing and emerging technologies, such as refrigeration and e-mobility.

1.3.1 Objective

The objective of this research is to investigate how sustainable operation of microgrids and renewable energy systems in East Africa can be achieved, using load profile information from several microgrids in East Africa and demand side management techniques.

1.3.1 Research questions

The following research questions were addressed as part of this research:

- How effectively can refrigeration appliances be operated and controlled using demand side management measures such as load shifting?

This was answered by modelling DSM potential for a site in Lwak, Kenya using HOMER and load profile data obtained from measurements at the site. The incorporation of peak clipping and load shifting were evaluated as means of rightly sizing a hybrid PV system, with the aim of achieving sustainable operation. Then load profile and refrigeration appliance temperature and power measurements were carried out at the site, Lwak Convent in Kenya to evaluate possible fridge control options. Particle Swarm Optimisation was used to model DSM load shifting and strategic conservation for the refrigeration appliances at the site for a hybrid solar system setup.

- How can demand response be implemented based on refrigeration appliance temperature and battery SOC values?

Experimental control of refrigeration appliances was undertaken within a solar system setup at Lwak Convent, Siaya District, Western Kenya. The experimental tests aimed to assess the energy savings and performance improvements achievable when appliance operation was modulated using both the battery state of charge and freezer temperature as control parameters. The results highlighted how targeted demand-side interventions can reduce demand and storage discharge requirements, thereby enhancing the sustainability of rural microgrid operations.

- What demand side management measures are viable given insights gained from load profiling of microgrids in East Africa?

Lod profile measurements were made for a microgrid in Silale, Tanzania. The data obtained showed the need for measures such as strategic load growth to raise consumption during high PV generation but low demand periods. The average load profiles for 866 customers of 8 microgrids in Uganda were analysed, and most of them displayed an evening peak while during the day there was generally low consumption, indicating the untapped potential to elevate the daytime demand and improve the load factor.

- What is the potential for implementing DSM in a rural standalone microgrid by integrating electric two wheelers and serving off-microgrid customers beyond the microgrid's distribution network footprint using portable storage?

A study involving modelling was carried out on strategic load growth for a rural off-grid microgrid in Uganda through integrating electric two wheelers and portable storage as flexible loads, in a novel analysis of off-microgrid electrification potential. Results show a reduction in PV curtailment and Levelized Cost of Energy (LCOE), as well as the possibility of supplying 160 off-microgrid customers annually. This could be pursued by collaboration of microgrid developers with e-mobility and portable battery companies.

1.4 Methodology

The research was conducted by carrying out desk-based research, field data collection as well as experimental testing and investigation of appliances and an energy system setup at Lwak in Kenya. Data from operational microgrids in East Africa was obtained and analyzed, providing insights on rural microgrid consumption in the East African context, and Uganda and Tanzania in particular. Modelling and simulation was done with the data from the microgrids and field measurements. Comparison with work described in the literature was done, to evaluate the effectiveness of the demand side approaches proposed.

1.5 Contributions

The significance of this research lies in its contribution to the understanding of demand side management in the context of sustainability of microgrids in East Africa. It broadens knowledge on designing resilient, technologically flexible, and financially sustainable microgrid systems, with a focus on both technical and socio-economic outcomes.

The study focuses on refrigeration appliances, often among the largest residential energy consumption devices, and explores decarbonization of transport through electric two-wheelers while extending off-grid access using portable storage.

For a site in Kenya, temperature evolution measurements of refrigeration appliances are used to demonstrate DSM potential. Load management strategies, including load shifting, are modeled, and cross-system interactions between storage and loads investigated through experimental implementation of SOC- and temperature-based control in a hybrid PV-battery setup. These interventions achieve demand reduction and improve alignment of appliance operation with energy production and storage levels. Cross-system analysis and integration is underexplored in the literature: in particular, the interactions between refrigeration loads and battery storage are rarely addressed, despite their potential to significantly influence system reliability, cost, and scalability. Considering these cross-system dynamics has introduced a critical perspective, opening opportunities for more impactful demand-side management strategies in both grid-connected and stand-alone microgrids.

The research also proposes integrating ageing into Minimum Energy Performance Standards (MEPS) for East Africa, thus addressing a critical gap, not only in the region but globally, of lifetime energy performance consideration of existing standards.

Load profiles of microgrids and customers are analyzed to identify DSM opportunities. A novel DSM strategy for strategic load growth is proposed, combining electric two-wheelers and portable storage to enable off-microgrid electrification. This approach is evaluated using actual microgrid customer and load data and lifecycle analysis to quantify additional customers served, PV curtailment reduction, cost savings, and avoided emissions. These results highlight a pathway for integrating productive energy use, transport decarbonization, portable storage, and renewable energy optimization in the planning and operation of rural microgrids.

Collectively, these contributions demonstrate the novelty and practical significance of this work, providing a framework for deploying demand-side management, improving energy efficiency, reducing costs, and supporting sustainable electrification in East Africa.

1.6 Thesis Outline

The rest of this thesis contains the following chapters:

Chapter 2 – Literature Review: This chapter contains an overview of the electricity sector in Uganda, Kenya and Tanzania, and also covers the role of microgrids. Demand side management aspects as well as microgrid control and optimisation, and load management options are also discussed.

Chapter 3 - Research Methodology: In this chapter the methodology, study sites and case study details are described. The data collection tools and setup as well as the experimental, modelling and simulation aspects for the five case studies is also presented, including where applicable, the optimisation methods utilised.

Chapter 4 - Results: The results obtained and discussion of the research outputs are contained in this chapter.

Chapter 5 - Conclusion and Future work: This chapter contains the overall conclusion and future work recommendations relating to the research work described in the thesis.

2 Literature Review

This chapter provides an overview of the electricity sector in the East African countries Uganda, Kenya and Tanzania. It also describes concepts related to microgrids, demand side management, optimisation, electricity applications and load management.

2.1 Electricity sector in East Africa

East Africa, including Uganda and Kenya which are crossed by the equator and Tanzania, is blessed with high solar irradiation.

Figure 2-1 shows the worldwide average global horizontal irradiation [45]. The average daily irradiation for the three countries ranges between 5 to 6 kWh/m^2. This translates to a specific yield in the range of 1300 to 1900 kWh/kW$_p$ as depicted in Figure 2-2. Specific yield refers to the total annual energy produced per kW$_p$ of installed solar capacity and is an important metric in comparing solar output at different locations.

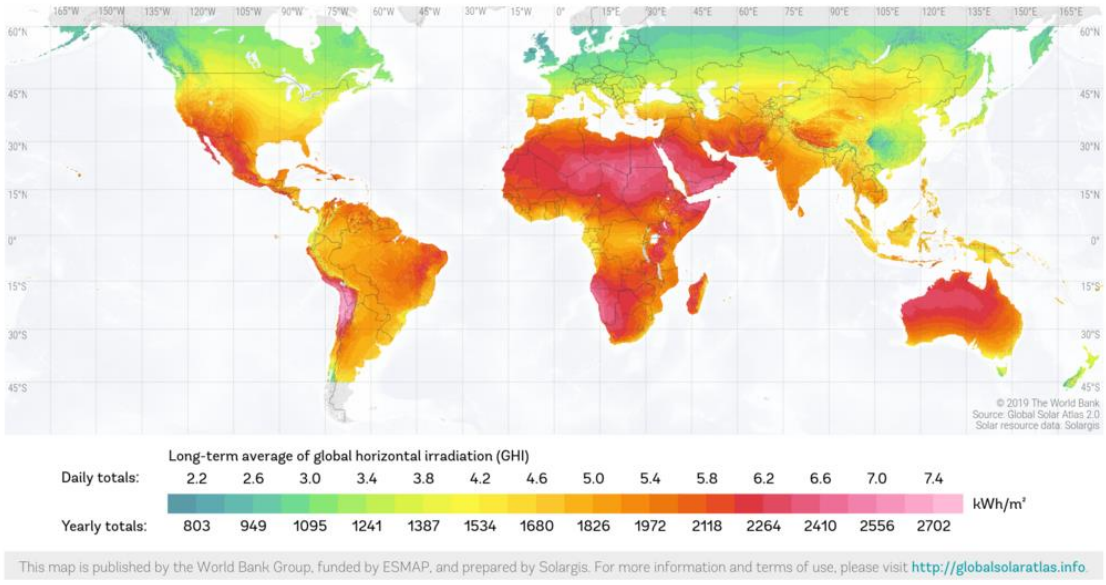

Figure 2-1: Global horizontal irradiance map [45]

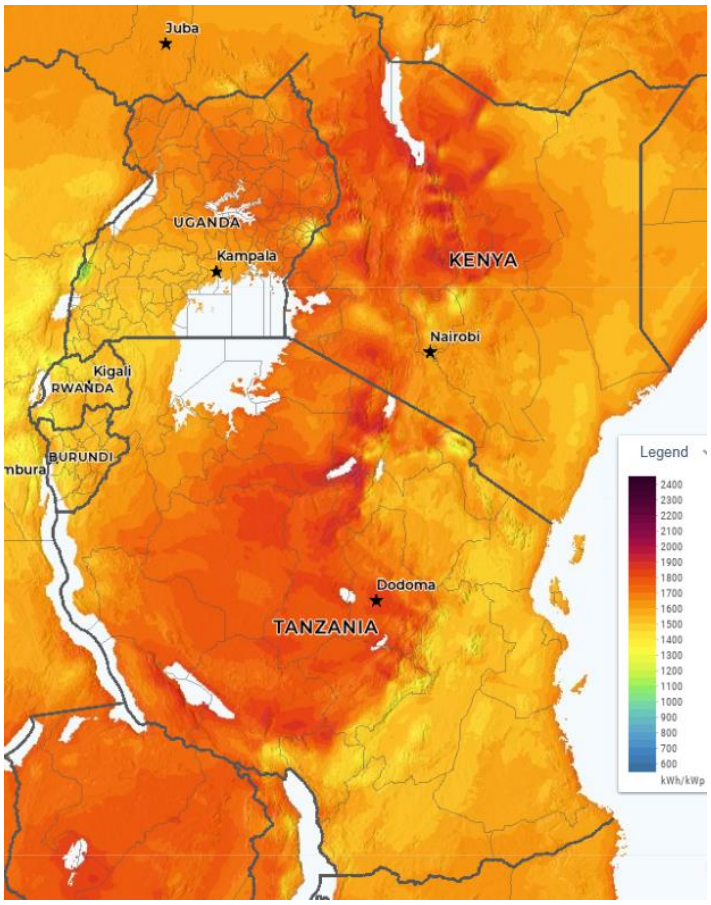

Figure 2-2: Specific yield map for Uganda, Kenya and Tanzania [46]

2.1.1 Uganda

Uganda has a population of 46.5 million people [47]. Uganda's installed electricity capacity in 2022 was 1,401.96 MW. Of this 1,394.97 MW was on-grid and 6.99 MW from off-grid systems [48]. The installed generation mix is depicted in Figure 2-3. Renewable energy comprises 93% of the installed capacity, i.e. hydro (78%), cogeneration plants based on sugarcane bagasse (10%) and solar PV (5%).

Public utility company Uganda Electricity Transmission Company Limited (UETCL) is the single bulk buyer responsible for all grid transmission. However in 2022 the regulations were changed to allow selected customers to purchase power directly from the grid rather than from a distribution utility. The amended Electricity Act also allows private sector participation in transmission and net metering. However these changes are yet to be operationalised [49]. Figure 2-4 shows the sources of the energy purchased by UETCL from 2018 to 2022.

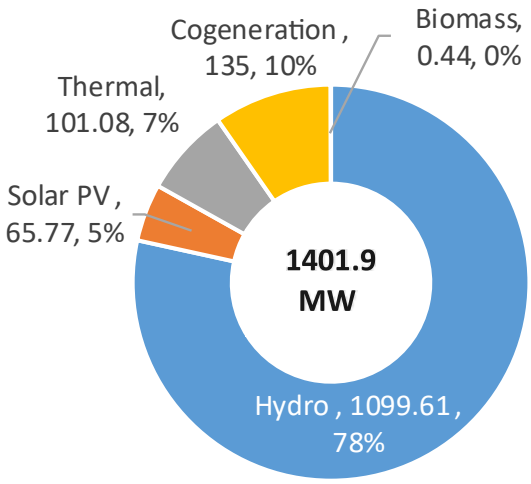

Figure 2-3: Uganda's installed capacity in 2022 (MW) [48]

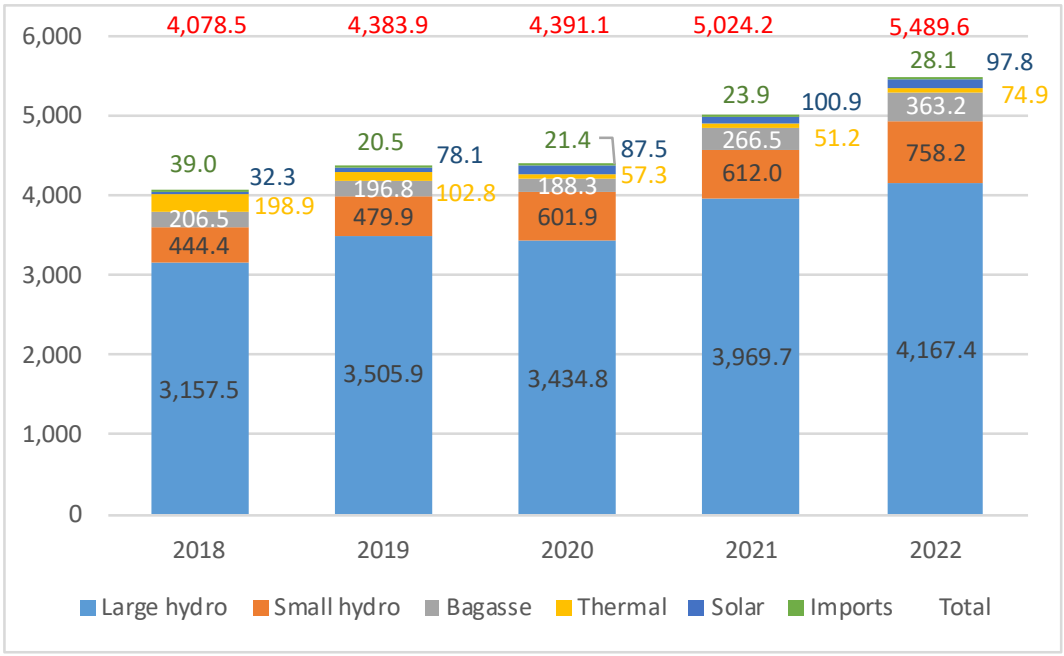

Figure 2-4: UETCL energy purchased in GWh (total in red) from 2018 - 2022 (Source of data: [48]*)*

Peak domestic demand in 2022 was 784.7 MW while the corresponding peak amount inclusive of power exports was 843 MW. Private distribution utility Umeme was responsible for 97.6% of distribution network energy sales. Uganda Electricity

Distribution Company Limited (UEDCL) is the public distribution counterpart. 3,942.6 GWh was the energy consumed from the national grid in 2022, with the customer allotments as shown in Figure 2-5. Transmission losses were 4.83% while Umeme reported 16.9 % distribution losses [48].

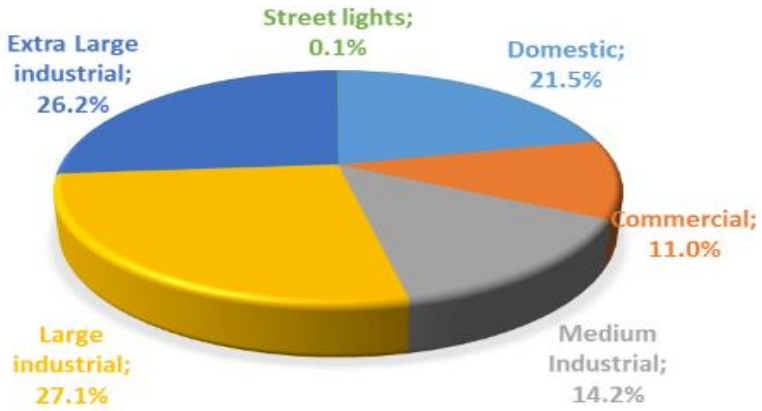

Figure 2-5: Uganda's grid consumption per category (%) in 2022 [48]

Grid connectivity in Uganda is 43%, primarily in urban areas (78%) while rural grid connectivity is only 17%. The main source of electricity for rural areas (25%) is solar home systems. Reliability remains a challenge, as electricity access for more than 4 hours daily was experienced by only 25% of the population in 2021 [50].

With Uganda's oil and gas extraction plans gaining momentum and the imminent commencement of oil extraction in the Albertine Graben region of Uganda, the Lake Albert Infrastructure Project (LAIP) is planned as a 52 MW electricity power plant fuelled by the excess gas from oil extraction activities. A long term power purchase agreement is to be entered into between UETCL and the LAIP project developers [51].

Uganda's Vision 2040 spells out the economic and development targets for 2040, including a per capita electricity consumption of 3668 kWh and 80% electricity access by 2040 [52]. To meet these targets, as per the Energy Policy for Uganda 2023, the forecasted energy mix by 2040 is shown in Figure 2-6. It can be seen that there are plans to introduce nuclear generation, green hydrogen, gas, waste to energy, wind, thermal and peat to the generation mix, thus increasing the generation capacity to 52,400 MW [53].

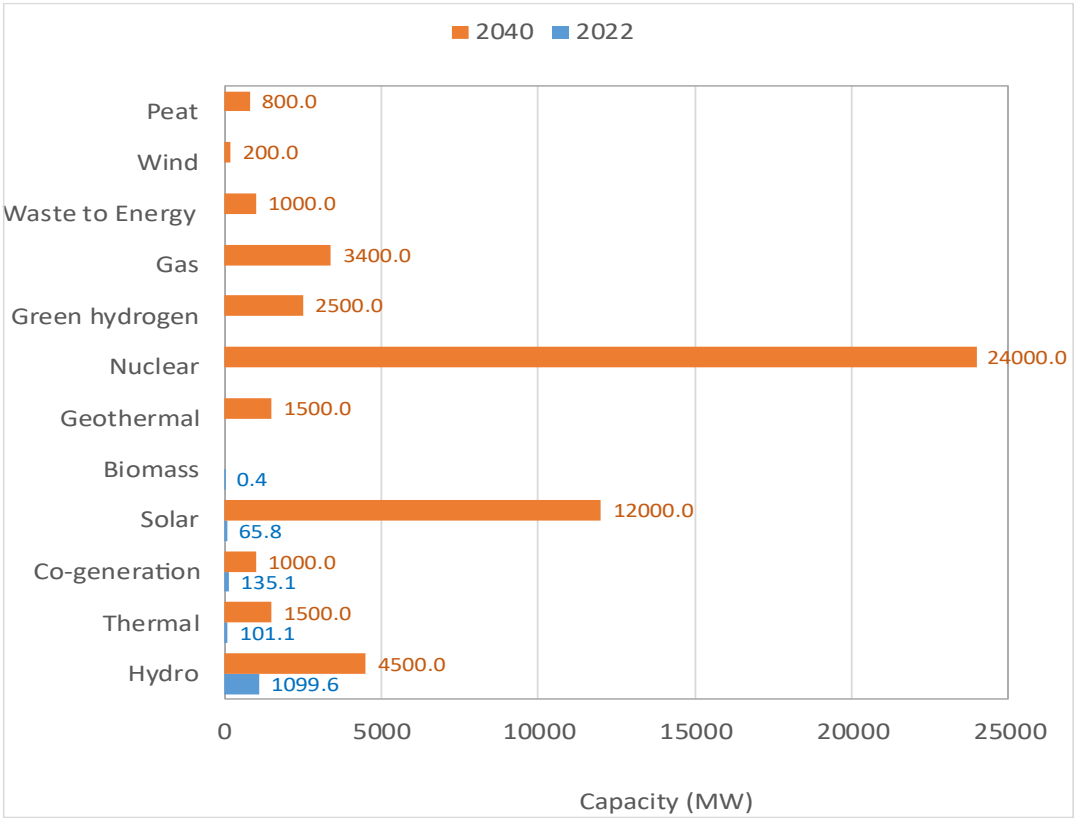

Figure 2-6: Uganda's generation mix in 2022 and generation targets for 2040 (MW) (Source of data: [53]*)*

Of the total 24.7% emissions reductions target, Uganda's updated Nationally Determined Contribution (NDC) of 2022 includes a commitment to a 5.9% unconditional reduction in emissions by 2030 through cost-effective investments, renewable energy expansion, and improved energy efficiency [49].

2.1.2 Kenya

Kenya's installed capacity in 2023 was 3,243.6 MW, with 75% of the installed capacity being renewable resources namely geothermal, biomass, wind, solar and hydro resources. 6% is via the 500 kV High Voltage Direct Current (HVDC) line to Ethiopia and fossil fuels account for the remainder as depicted in Figure 2-7 [54].

It is estimated that by 2030 the installed generation capacity will be 5 GW. About two thirds of the installed generation capacity is owned and operated by the utility Kenya Electricity Generating Company (KenGen), and the rest by IPPs (Independent Power Producers) and off-grid developers. Kenya Power and Lighting Company (KPLC) is the

sole distribution utility company in Kenya. With geothermal providing the base load demand and only 950 MW developed so far of the potential 10,000 MW geothermal capacity [12], the country possesses an abundance of green and climate-resilient energy resources.

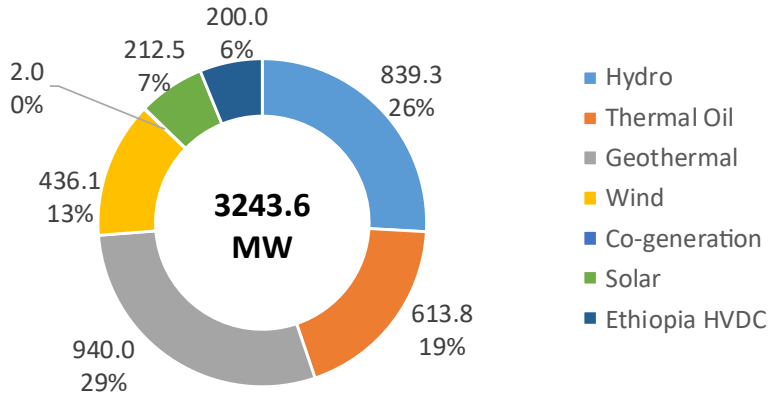

Figure 2-7: Kenya's installed electricity capacity in 2023 (MW) (Source of data: [54]*)*

Electricity demand is concentrated in the capital city and urban areas, as exemplified by almost half of the country's demand in 2018 being in the capital city and its environs despite these having only 8% of the then 50 million citizens. This highlights the need for stimulating demand and employing alternative access means like microgrids and SHS in non-metropolitan areas where grid connection and extension costs are not offset by the energy sales. In 2023, the country's domestic consumption was 10,320.6 GWh, distributed as shown in Figure 2-8 [54]. Figure 2-9 shows Kenya's electricity generation and imports in GWh from 2019 to 2023.

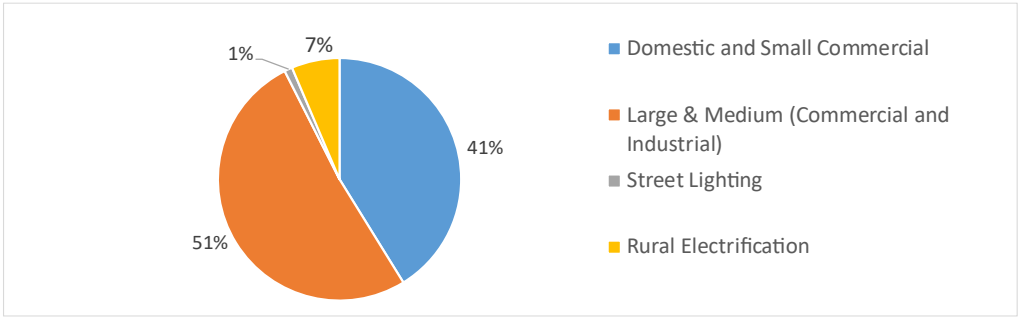

Figure 2-8: Kenya electricity consumption per sector (%) in 2023 (Source of data: [54]*)*

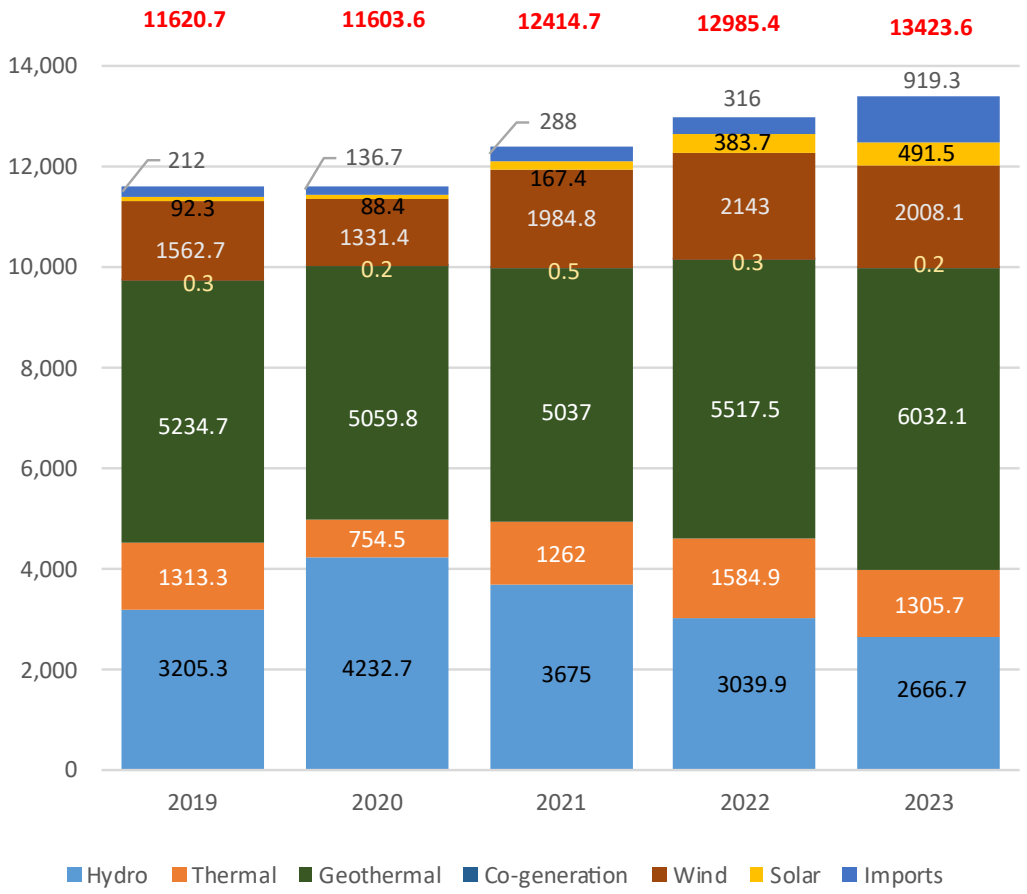

Figure 2-9: Kenya's electricity generation and imports in GWh (total in red) from 2019 - 2023 (Source of data: [54]*)*

Kenya has set a target of adding to its energy mix between 350 MW and 450 MW of green hydrogen power generated from renewable sources like wind or solar by 2032 [55].

2.1.3 Tanzania

Tanzania is richly endowed with a wide range of energy resources including wind, solar, hydropower, geothermal, biomass and fossil fuels. The country's abundant renewable energy potential is depicted in Figure 2-10 [56]. However biomass accounts for a huge 80% to 85% of the country's energy demand, primarily for cooking [56].

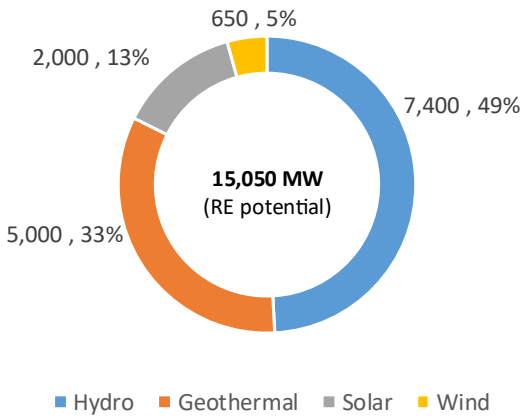

Figure 2-10: Tanzania renewable energy potential in MW [56]

Tanzania Electric Supply Company (TANESCO), owned by the Tanzanian Government, is responsible for power generation, transmission, and distribution in the country, and operates natural gas power plants, hydro power plants, and thermal plants.

As of December 2023, Tanzania's installed generation capacity was 1938.35 MW, of which 1899.05 MW was on-grid and 39.03 MW was off-grid. Of the installed grid capacity, 1193.82 MW (63%) was natural gas, 601.60 MW (32%) hydropower, fuel-based sources comprised 83.93 MW (4%) and biomass 10.5 MW, as illustrated in Figure 2-11. The peak demand, occurring in August 2023, was 1482.80 MW [57].

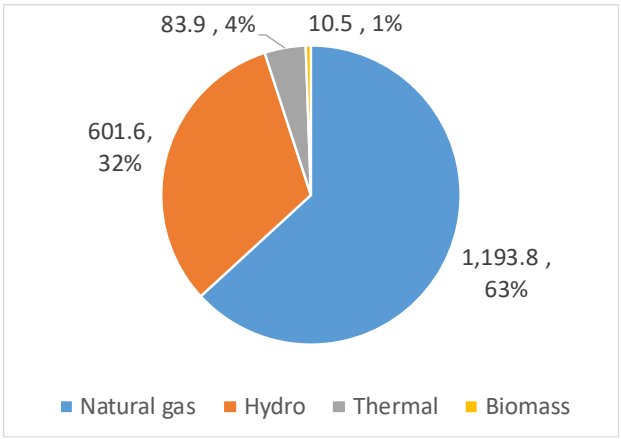

Figure 2-11: Tanzania installed grid capacity in 2023 (in MW) [57]

The trend in electricity generation from different sources (in GWh) from 2018 to 2022 for Tanzania [58] is shown in Figure 2-12. About 151 GWh of electricity was imported in 2022 from Uganda and Zambia.

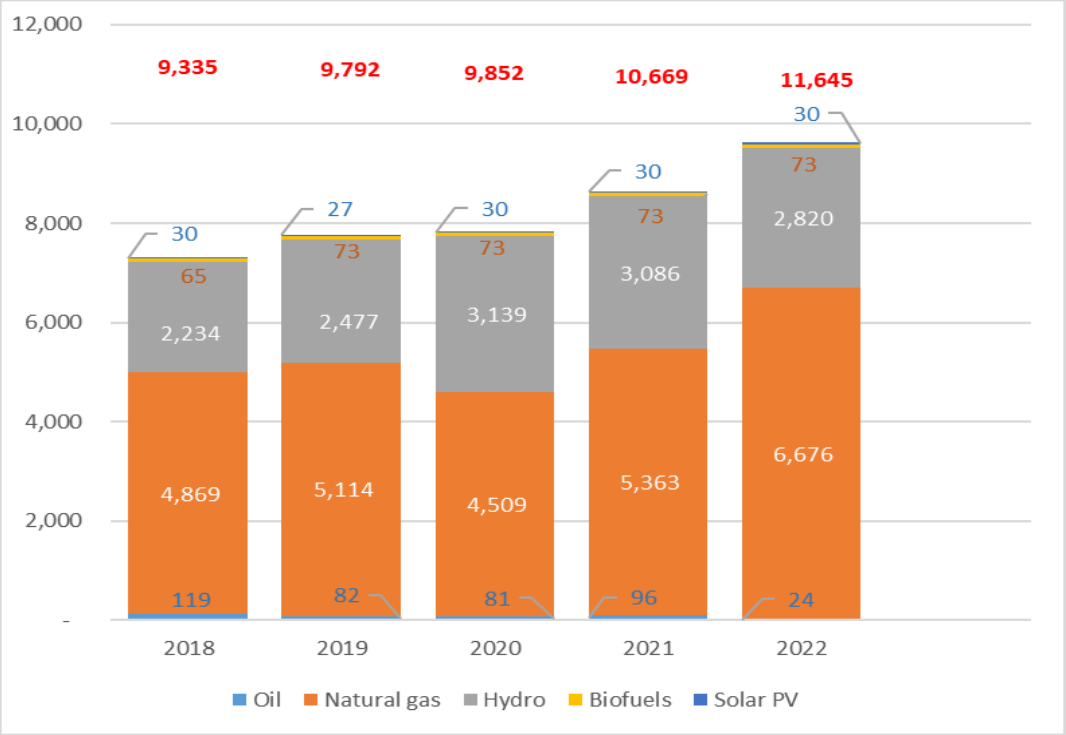

Figure 2-12: Tanzania electricity generation (GWh) from 2018 – 2022 (Source of data: [58])

Of the 60 million people in Tanzania in 2020, only 38% had electricity access, with a large disparity between rural - urban access [59]. The country's population in 2024 was 69.4 million people [60]. According to the IEA [58], in 2022 the annual per capita electricity consumption was 122 kWh, while the electricity consumption per sector was 21.4% for industry, 44.3% residential, 31.7% for commercial and public services and 2.6% for other applications, as shown in Figure 2-13.

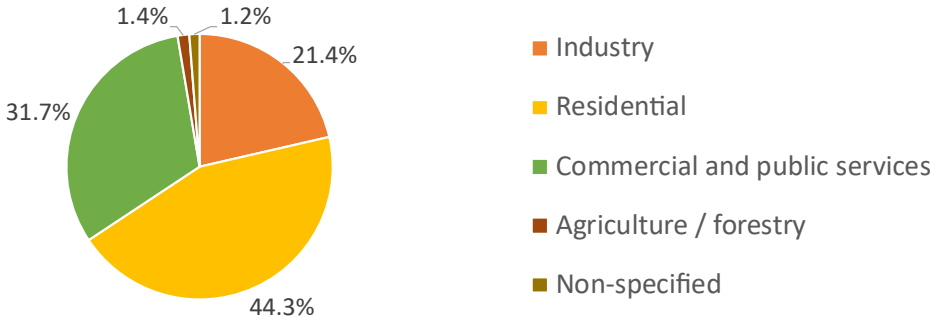

Figure 2-13: Tanzania electricity consumption per sector (%) in 2022 [58]

Despite the surplus in generation capacity relative to peak demand, load shedding was common in 2023 due to drought and hence low water levels at the hydro plants. In 2021/2022, the system energy losses were 14.5% [61]. The country had a target of increasing grid capacity from 1.5 GW in 2015 to 10 GW by 2025/2026, but due to the associated costs and other constraints, demand side management has been proposed as better alternative to ensuring sufficient and increased electricity access [62].

The 2115 MW Julius Nyerere Hydro Power Plant (JNHPP), slated for completion in 2024, had by July 2024 added an additional 662 MW to Tanzania's grid [63].

2.2 Microgrids overview

2.2.1 Principles of microgrids

Countries worldwide are experiencing major grid reliability challenges for reasons that include aging infrastructure, extreme weather damage and climate change-related power disruptions. Decentralised local energy systems such as microgrids, and particularly those using renewable resources such as solar, wind and hydro, provide a favourable solution not only for electricity access, but also to meet energy security, reliability and resilience needs.

A microgrid is a set of generation source(s) and associated loads, typically covering a localized scope, and sometimes including storage elements [64]. They may be grid connected, or stand-alone. When disconnected from the grid, this is referred to as island mode operation. In developing economies, microgrids present a less costly and more efficient

means of providing electricity to sparsely populated, demand-limited and commercially or industrially immature populations. In developed countries which are not as energy poor, microgrids are relevant for energy security, climate resilience and greening of energy consumption. As load centres are often distant from generation plants, microgrids reduce on the power losses associated with AC transmission of power. DC systems are however gaining traction due to their improved efficiencies and lower costs relative to similarly sized AC systems [65].

Microgrids have been classified as power-limited and energy-limited. Power-limited refers to the use of approaches such as residential wiring stipulations on permitted number and type of sockets and lights, or the type of electrical devices allowed, or requirements for notification of the energy supplier in case of additional loads. This is done to limit peak power. Instituting power limits requires a trade-off between protecting the system from excessive demand and enabling customer demand growth, ensuring that customers prepared for upgrades are not unnecessarily constrained [66].

With energy-limited, the concern is more on the amount of energy stored by the system as would apply to intermittent sources like solar with battery storage, whereby the battery capacity and constraints limit the energy available. The hugest proportion of microgrid lifecycle costs stem from the storage replacement [67]. For microgrids in developing countries, the batteries are a major cause of system unsustainability due to inability to replace the batteries at the end of their lifetime [68]. This is because of the low demand and income levels typical of off-grid remote rural communities. The inverse relation between the lifespan of the battery and its use means that replacement is inevitable, either due to capacity degradation over time caused by processes like corrosion, sulphation and stratification, or due to reaching the battery cycling limit [69][65][70]. For decentralised microgrids with storage, both power and energy limitations are important considerations [71].

Microgrid customers are typically within a 2-3 km radius of the power generation plant, and potential customers beyond this coverage are unable to connect to and access the microgrid electrification infrastructure [37]. Thus portable storage provides an easy way to extend electricity access beyond microgrids' distribution networks. These findings align with the reported average 45% connection ratio of microgrids to their people in their locality and 35% ownership of SHS in the areas studied in [37] .

2.2.2 Load profiles and demand patterns

Load profiles depict the variation of power demand by customers over a day. Many electricity projects assume linear demand growth, but 75% of projects in a study [72] were found to ignore, non-realistically, the demand evolution over time. Consumption trends can however be deduced from load profile data.

For a decentralised power system such as a microgrid, granular insight into customer consumption is integral for reliable, sufficient, good quality, economically viable, minimally lossy, energy efficient and demand evolution-aligned electricity supply. Advanced metering infrastructure (AMI) incorporating smart meters enables two-way communication between the consumer meters and the energy supply company.

Smart meters have availed a large volume of data on consumption of electricity customers, from which load profiles can be extracted and the benefits of prediction accessed. In [73], machine learning is used for prediction and classification of microgrid consumers. Demographic data such as income, energy sources and desired appliances is used to predict average consumption, load profile and demand growth for prospective customers, while behavioural data like hourly consumption and meter top-up frequency and top-up amounts of existing customers generates economic viability insights. However only about 3% of smart meter data is being used to improve grid operations [74].

Smart meters that provide metering data in intervals ranging from 5 minutes to an hour enable demand response measures to be instituted [75]. In a study on SparkMeter meters deployed in 36 microgrid sites in three Sub Saharan Africa countries i.e. Kenya, Nigeria, and Tanzania, data was averaged and recorded in 15-minute intervals for parameters such as voltage, frequency, power factor, active power consumption, cost of electricity and power limits imposed on users [66]. While power quality metrics indicated generally satisfactory performance, it was recommended that targeted mitigation measures be implemented to detect and resolve underlying power quality problems. Notably, poor power quality can result in technology lock-in into inefficient appliances, as it acts as a deterrent to investment in more efficient appliances [76]. Thus ensuring good power quality supply can help promote the uptake of energy efficiency measures and equipment.

Load profile analysis for the 36 sites revealed four general demand patterns: Morning and Evening peaks for 31% of the microgrids (11 sites); Daytime Bump with late afternoon drop and evening peak for 19% (7 sites); Daytime Baseload showing a gradual increase in demand during the day and significant evening peak but smaller loads than daytime bump for 22% (8 sites); and Mostly Daytime with low evening and nighttime consumption for 28% of the microgrids (10 sites) [66].

Five distinct load profile clusters for Tanzania microgrid customers were identified in [77], with commercial customers exhibiting high daytime usage and households large evening peaks with relatively low overall consumption. For Mpale microgrid in Tanzania an evening peak in consumption and higher weekend consumption were identified [78].

While the typical approach to sizing a microgrid at the design stage has been to carry out surveys to estimate the future customers' expected demand, studies using practical microgrid data found errors in survey-based individual customer demand projection to exceed 65% [73]. The non-correlation between projected and actual consumption is attributable in part to an overestimation by previously unelectrified customers of their actual capability to pay for electricity, the appliances they will acquire and use, and disparities between region and location specific activities [73]. Additional insights from field data would thus be a useful addition to the body of knowledge.

Using k-means clustering and smart meter data, customers of microgrids in Tanzania were classified on the basis of normalised average daily load profiles as well as daily energy consumption [77]. By classifying customers according to their load profile and average daily consumption, their consumption in terms of both quantity and patterns were assessed. Insights about the distribution of consumer categories across different consumption levels and load profiles for the case under study highlighted that for businesses, the type of business did not determine the level of consumption or type of profile. This suggests that demand management approaches should not be based only on consumer category.

In [79], from actual consumption data, K-means clustering was used to develop a random forest model for load profile prediction based on energy usage patterns and demographics indicators from pre-survey information for Tanzanian microgrid customers.

Regarding energy consumption, low tier energy consumption in urban and rural areas in East Africa by 2030 has been projected as being 160 and 44 kWh/person/year, or at a higher tier, 423 and 160 kWh/person/year, for urban and rural areas respectively [80].The 44 kWh loads are generally lighting, fan and television, 160 kWh loads extend to light food processing and washing machines, and the 423 kWh loads span refrigeration, microwaves, water heaters, water pumps and irons (i.e. medium or continuous use devices).

The authors of [32] analysed the load profiles of 11 microgrids that were installed from 2014 and 2016 in East Africa, with 7 of the microgrids being situated in Kenya and the other 4 in Tanzania. They provided day-to-day variability and timestep variability factors that could be used in HOMER (Hybrid Optimization of Multiple Energy Resources) software for simulating energy systems. The average daily consumption for the 11 microgrids was found to range between 585 Wh/day and 40067 Wh/day, while the mean daily energy demand for all 11 sites was 6702 Wh/day [32]. Using k-means clustering, Tanzania microgrid customers were grouped based on daily electricity consumption into low (< 140 Wh), medium (140-450 Wh), and high (> 450 Wh) segments in [77].

As per 2018 data, solar home systems customers in Kenya had an estimated average daily energy consumption ranging between 50 Wh/day and 204 Wh/day, with the mean being 64.5 Wh/day [37].

Additional insights into microgrid consumption characteristics from smart meter data would be beneficial for stakeholders in the microgrid regulation, development, operation, financing and utilisation space. The classification of customers and understanding the various consumption patterns also facilitates the development of suitable tariffs, which can be used to implement demand management.

2.3 Microgrid control and optimization

Energy management systems have the role of matching demand with generation, a role that is important for managing the fluctuations of renewable resources that lack a spinning reserve to maintain frequency and thus, in the absence of a grid connection are less able to cope with spurious ramps or changes in demand. Storage systems such as batteries and flywheels provide frequency fluctuation handling support, thus improving system stability [81].

Microgrids without storage, whether grid connected or decentralised, have relatively simpler control requirements, but with the addition of storage for stability, reliability and to accommodate the intermittency and fluctuations of renewable sources like solar and wind, control becomes more complex. The storage helps to offset the mismatch between surplus power generation during periods of resource richness, and the demand requirements during periods of resource scarcity at which time the surplus stored energy can then be redistributed to consumers [64].

There are various means of representing microgrid control schemes. One scheme is based on a three tier control hierarchy involving (from bottom to top) primary, secondary and tertiary levels [82] [83] [84] as depicted in Figure 2-14. The two bottom layers relate to power quality and grid stability, and the tertiary level to optimal operation of generation sources, storage and load management.

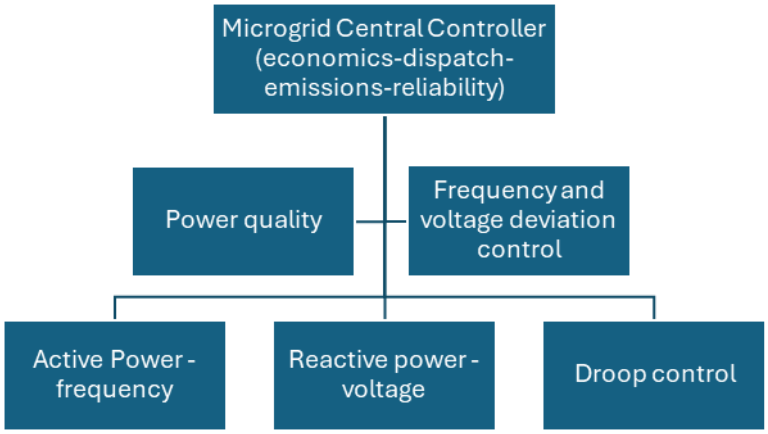

Figure 2-14: Microgrid Control hierarchy [82]

The primary control level is concerned with local voltage and frequency control using droop control for instance, as well as local active and reactive power sharing. The secondary level assumes a grid connection, and relates to voltage and frequency control at the point of common coupling (PCC), while the tertiary level spans the control of power flow, emissions management and economic dispatch [84].

Among the economic considerations discussed in literature are the minimisation of net present cost, levelized cost of energy (LCOE), generation costs including for start-up and shut down, power losses, emissions, operation costs, fuel costs, battery degradation costs, peak load, loss of power supply probability (LPSP) and dumped energy [85]. Maximisation objectives span renewable energy factor (REF), availability, user comfort and revenue [86] [26].

Another approach visualizes the microgrid Energy Management System (EMS) responsible for controlling the microgrid operations from a timing perspective [83]. Figure 2-15 highlights the short-term roles scaling from microseconds, to minutes, of power dispatch

by the different energy sources, and which are related to power quality, voltage and frequency control. On the longer-term scale are tasks that include but are not limited to energy management, prediction of load and supply, storage management, load shifting and peak shaving as well as emissions control and cost optimization.

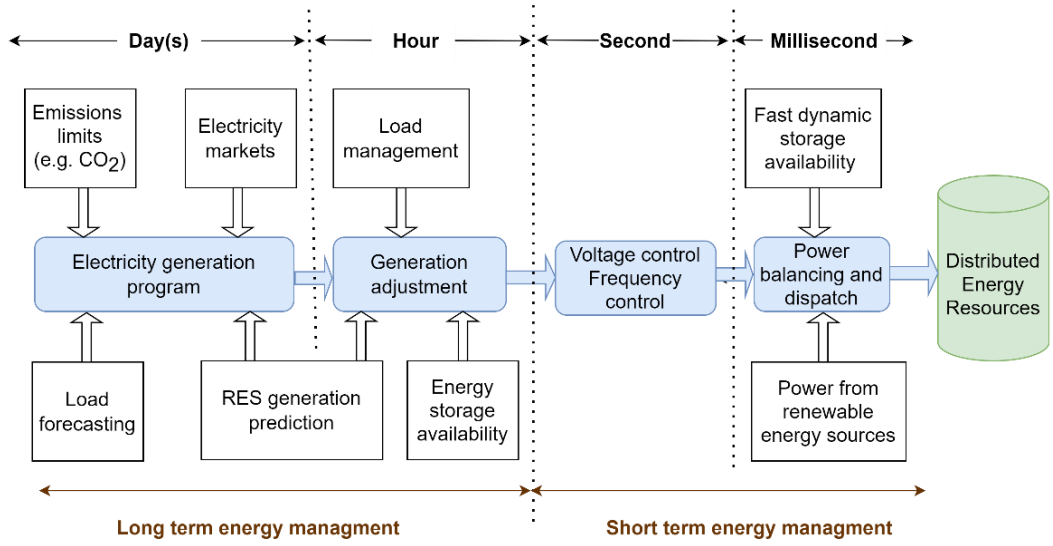

Figure 2-15: Key functions of microgrid control (adapted from [83]*)*

In the work described in this dissertation, we approached the control functionality from a tertiary or long-term perspective.

While solar generation tends to peak in the mid-morning and peter out in the afternoon, the typical demand profile for microgrids and communities and households tends to peak in the evening and early hours of the night, when there is no solar generation. This necessitates additional energy sources such as the grid or genset or battery or other storage for the load requirements to be met during this period of peaking consumption.

Power networks require a fine balance between supply and consumption in order to maintain reliable and quality supply of electricity. The power management function of the EMS must target this balance, while keeping within constraints such as those imposed by component capacity limitations, permissible ramping rates, economic or cost bounds and power quality (grid) regulations or codes. Increased RE integration into traditional grids

creates a need for additional and quickly available spinning reserve and power sources capable of providing ancillary services such as voltage control and frequency control [87].

Under frequency load shedding (UFLS) and under voltage load shedding (UVLS) are typically deployed as a last resort for an energy system's stability. Both techniques adversely impact system reliability and have economic ramifications. When renewable systems are deployed, reduced system inertia and intermittency makes the system more susceptible to abrupt ramping in demand or supply. Battery storage can provide a fast and dynamic response to these variations [34].

Optimization algorithms are important for handling power dispatch problems in RE systems and also to effectively manage conflicting technical, economic, environmental and customer satisfaction objectives [21] [88].

2.3.1 Optimization methods

Optimization can be described as the process of choosing the best solution to a problem from among several options given specific limitations (constraints) in order to achieve a certain objective. Possible objectives include cost minimisation, energy reduction, emissions minimisation, maximisation of user comfort, etc. If there is one objective, this is single objective optimization. When more than one objective is sought, this is referred to as multi-objective optimization.

Several optimization methods have been used for energy system studies and management. Some of these optimization methods include Linear Programming (LP), Mixed-Integer Linear Programming (MILP), Mixed-Integer Nonlinear programming (MINLP), Dynamic Programming (DP), and metaheuristic algorithms like genetic algorithms (GAs) and Particle Swarm Optimization (PSO). These are discussed briefly below.

Linear programming

Most optimisation models use Linear Programming (LP), whereby an objective function with variables is minimised or maximised subject to some constraints. For LP, the objective function and constraints must be linear. The general LP equation is given below:

Minimise $c^T x$

Subject to: $Ax \leq b$

$$A_{eq}x = b_{eq}$$

$$b_l \leq x \leq b_u$$

where vector x represents the variables while matrices A, A_{eq} and vectors c, b, b_{eq}, b_l and b_u specify the objective function and constraints [89].

Maximising $c^T x$ is equivalent to minimising $(-c)^T x$.

Mixed-Integer Linear programming

For Mixed-Integer Linear Programming, the constraints and objective function are linear and one or more variables are integers [90] [91] .

Mixed-Integer Nonlinear programming

When the objective or constraints are non-linear and the decision variables include one or more integers, this is referred to as a Mixed-Integer Nonlinear programming (MINLP) problem [92].

Dynamic Programming

Dynamic Programming (DP) decomposes a complex, multi-stage decision-making process into a series of interconnected sub-problems, whose individual solutions are retained for future reference. At each step, a choice is selected from a finite set of possible actions according to a specified optimization criterion. This method offers a systematic framework for determining a sequence of interdependent decisions in an optimal manner, making it particularly well-suited for applications involving dynamic systems [93] [89].

Genetic algorithms

A Genetic Algorithm (GA) is a metaheuristic algorithm modelled upon evolutionary processes, mutation and natural selection [94] [95]. A population of individuals representing possible solutions is created within the search space and their fitness is evaluated based on their objective function values. The best members are used to create a new generation by crossover (combining two parent individuals to create a new child individual) and mutation (small changes to individuals). The process is repeated for the new generation until a termination criterion is reached [89].

Particle Swarm Optimization

Particle Swarm Optimization (PSO) is a metaheuristic optimization method that imitates the migratory behaviour of animals to achieve a given objective. It involves communication and continual learning in which the best individual's position is retained in memory and other individuals informed thereof to move them in that direction, so as to attain a sufficiently good solution within a given search space. This is done until a stop criterion is met [96] [97].

The different optimization methods are compared in Table 2-1.

Table 2-1: Comparison of optimisation methods

Optimisation Method	**Advantages**	**Disadvantages**	**References**
LP	• Global optimum solution assured if problem can be expressed in a linear format • Short computation times • Scales well with big problems • Availability of reliable, fast solvers	• Possibility of poor modelling accuracy due to the linearity restrictions • Difficult to use for complex interactions	[98] [99] [89]
MILP	• Global optimum solution assured if problem can be expressed in a linear format • Short computation times • Availability of reliable, fast solvers • Scales well to big problems • Can handle complex interactions	• Possibility of poor modelling accuracy due to the linearity restrictions • For MILP problems, complexity increases with the number of integer variables • Increased temporal and spatial granularity negatively affects MILP more that LP problems	[98] [99] [89]

MINLP	• Greater accuracy possible than the LP and MILP models • Can fully represent complex problems	• More computationally-intensive than LP • Convergence to global optimum not assured • Problematic scaling to big problems	[89]
DP	• Improved optimization speed and throughput can be achieved by dividing the problem into smaller sub-problems thus enabling parallel computation • Works for non-convex, non-continuous, non-differentiable and black-box functions	• Long computation time for big problems	[93] [89] [100]
GA	• The randomness of mutation increases the probability of escaping local optima and finding the global optimum • Can be applied to most optimization problems including non-convex, discrete, mixed-integer and black-box problems	• Convergence to global optimum not assured • Long computation time for big problems	[89] [101]
PSO	• Reaches a near-optimal solution with simpler implementation and less computational requirements than GAs • Fewer parameters required for tuning adjustment than GAs • Can be used to optimize large dimensional problems	• Convergence to global optimum not assured	[96] [102]

Some energy optimization methods discussed in the literature include techniques such as binary linear programming [103] and Model Predictive Control (MPC) using binary quadratic programming [104] for appliance scheduling and management. However, such

methods are ill-equipped to efficiently handle large numbers of heterogeneous controllable devices with different power usage patterns and specifications, and are computationally intensive and time-consuming [105] [106].

Metaheuristic optimization algorithms like Particle Swarm Optimization (PSO), Genetic Algorithms (GAs), the firefly algorithm (FA) and Ant Colony Optimization are nature-inspired techniques that use populations to search a solution space for near-optimal solutions [96]. These methods have been widely studied for demand-side management (DSM) and load scheduling. For instance, a GA was applied to appliance scheduling for residential, commercial, and industrial users, achieving energy and cost savings and reduced peak demand compared to the scenario without DSM [107]. However a disadvantage of GAs is that they are computationally intensive and time-consuming.

PSO and variations thereof have also been applied for similar purposes [106] [39], and studies done comparing its performance to other techniques such as the Grasshopper Optimization Algorithm (GOA) [40] and the Firefly Algorithm [108]. Hybrid methods such as wingsuit flying search algorithm and artificial cell swarm optimization (WFS2ACSO) [41] and hybrid firefly particle swarm optimization (HFPSO) [108] have also been proposed, incorporating dynamic pricing schemes and optimizing appliance schedules to minimize energy costs [41] and reduce thermal energy consumption and carbon emission [108].

2.3.2 Particle Swarm Optimization

Particle Swarm Optimization (PSO) is a population-based metaheuristic optimisation method inspired by the collective migratory movement of birds or fish. It iteratively updates candidate solutions - represented by particles - through position and velocity (direction or displacement) changes to arrive at a sufficiently good solution from all possible solutions within a given search space. The exploration phase begins with setting the initial swarm parameters, followed by the exploitation phase during which particles adjust their velocity and position across multiple iterations. PSO handles various optimization types including discrete, binary, constrained, combinatorial and multi-objective optimization. Convergence is determined by a maximum number of iterations limit or attaining an output that is sufficiently close to the desired result, with the best-performing particle selected as the final, near-optimal solution [109].

Figure 2-16 depicts the flow of the general PSO algorithm operation [96].

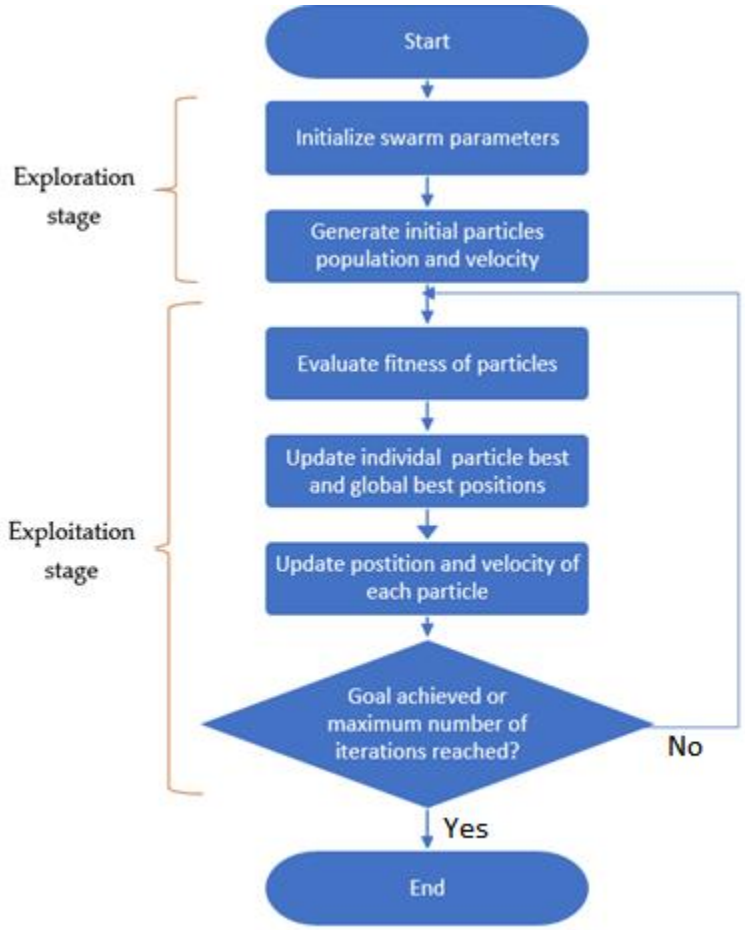

Figure 2-16: PSO algorithm flow

The individual and global best position and cost are stored at each evaluation and used to update the position and velocity of the particles as per Equations 3.13 and 3.14.

$$x_i\,(t+1) = x_i\,(t) + v_i\,(t+1) \tag{3.13}$$

$$v_i\,(t+1) = w\,v_i\,(t) + \varphi_1\,c_1\left(P_{i_{best}} - x_i\,(t)\right) + \varphi_2\,c_2\left(P_{g_{best}} - x_i\,(t)\right) \tag{3.14}$$

where i is particle's number ($i = 1,..,N$; N being the number of particles in the swarm), $x_i\,(t+1)$ and $x_i\,(t)$ are vectors describing the next and current positions of each particle, respectively, and velocity vector $v_i\,(t+1)$ indicates the next movement direction of each

particle in the population [96] [109]. v_i (t) is restricted to [- v_{max}, v_{max}]. An excessively large maximum velocity v_{max} widens the exploration range, while if it is excessively small, particles will tend to prioritize local search.

The inertia weight w governs the trade-off between global exploration and local exploitation. During the optimization process, the exploration scope is gradually reduced, guiding particles from broad exploration to more precise adjustment upon entering a good location [109]. A larger w encourages broader search across the solution space, while a smaller w concentrates the search locally for fine-tuning. Accordingly, w is dynamically adjusted, as defined in Equation 3.15.

$$w = w_{min} + (w_{max} - w_{min}) \cdot \left(\frac{iter_{max} - iter}{iter_{max}}\right) \tag{3.15}$$

where w_{max} represents the predefined maximum value of w and w_{min} represents the predefined minimum value, usually 0.9 and 0.4 respectively. $iter$ and $iter_{max}$ are the current iteration of the algorithm and the maximum number of iterations respectively [39] [110].

$P_{i_{best}}$ and $P_{g_{best}}$ represent the best position found so far by an individual particle and the best position identified across the entire swarm, respectively. φ_1 and φ_2 are independent random numbers within the interval [0, 1], while c_1 and c_2 are the cognitive acceleration constant and social acceleration constant, respectively. c_1 and c_2 are also called trust parameters and indicate the level of confidence in self, and neighbors, respectively. These constants influence how strongly a particle is attracted toward its own best-known position and the swarm's global best. Since cooperation is the underlying strength of the swarm optimization, they generally are most effective for well-balanced c_1 and c_2 ($c_1 \approx c_2$). Usually, static values of c_1 and c_2 are used, and most commonly $c_1 = c_2$.

Among the advantages of PSO relative to similar nature-inspired algorithms are [96] [102]:

- It is able to reach a near-optimal solution with simpler implementation and less computational requirements than other heuristic algorithms e.g. GAs.
- Needs fewer parameters for tuning adjustment.
- PSO uses historical memory of all particles in searching unlike GAs which cannot harness historical memory because they change the population in each generation, replacing the old population with a newer and more efficient one.

- High applicability since it is less sensitive to the nature of the objective function and can be used for varying optimization problems.
- PSO can be used to optimize large dimensional problems.

2.4 Energy Modelling tools and approaches

Several energy system modelling tools exist, including EnergyPLAN [111], HOMER (Hybrid Optimisation of Multiple Energy Resources) [112], LEAP (Low Emissions Analysis Platform, formerly known as Long-range Energy Alternatives Planning) [113], LUT-ESTM (LUT Energy System Transition Model) [114] [115], MARKAL (MARKet ALlocation model) [116], Oemof (Open Energy Modelling Framework) also called Solph [117], OSeMOSYS (Open Source Energy Modelling System) [118], PyPSA (Python for Power System Analysis) [119], RETScreen Clean Energy Project Analysis Software [120] and TIMES (The Integrated MARKAL-EFOM System) [121]. GAMS stands for General Algebraic Modeling System and is used in TIMES.

Table 2-2 summarises the key features of some of the more common energy modelling software tools. Some terms in Table 2-2 are described below [92]:

- Scenario – Comparison of long term options for the energy or electricity sector e.g. policy implications
- Operation Decision Support – Optimising of dispatch and operation of energy or electricity systems
- Investment Decision Support – Optimising of energy or electricity system investments
- Power System Analysis Tools – Used for detailed power system studies such as dynamic operation and power flows
- Partial Equilibrium models –These focus on only one market i.e. the energy or electricity market, without considering the whole economy.

Table 2-2: Comparison of Energy Modelling Tools

(IDS - Investment Decision Support, ODS - Operation Decision Support, PSAT - Power System Analysis Tool)

Tool	**Purpose**	**Methodology**	**Resolution**	**Temporal horizon**	**Geographical scope**	**Availability**	**Software**	**References**
Energy Plan	Scenario, IDS	Simulation	Hourly	1 year	Local to Continental	Free	Stand-alone	[92]
HOMER	IDS, ODS	Simulation	Minutes, Hourly	Multi-Year	Local	Commercial	Stand-alone	[92]
LEAP	Scenario	Simulation, Linear Programming	Yearly, Weekly, Daily, Hourly	Usually 20–50 years	Local to Global	Free & Commercial	Stand-alone	[92] [122]
LUT-ESTM	Scenario, IDS, ODS	Linear Programming	Hourly	Long-term, up to 2100	Local to Global	Closed source, with plans to make it open source	MATLAB + Solver (MOSEK/ Gurobi/ CPLEX)	[114] [115] [123]
MARKAL	Scenario	Linear Programming / Mixed Integer Programming, Partial Equilibrium	Multiple years (user-determined time-slices within a year)	Long-term (user-determined)	Local to Regional	Commercial, Free demo version	GAMS + Solver (VEDA)	[92]
Oemof	Scenario, IDS, ODS	Linear Programming, Mixed Integer	Seconds to years	User determined	User determined	Open Source	Python + Solver	[92]

		Linear Programming, Partial Equilibrium						
OSeMOSYS	IDS	Linear Programming	User-determined (intra-annual)	User-determined (10–100 years)	Community to Continental	Open Source	GNU MathProg, Python, GAMS	[92] [124]
PyPSA	IDS, ODS, PSAT	Linear Programming	Hourly	1 year	Local to Continental	Open Source	Python	[92]
RETScreen	Scenario, IDS	Simulation	Daily/ Monthly/ Yearly	Maximum 100 years	Single-system to Global	Free	Windows with .NET	[92]
TIMES	IDS, ODS	Linear Programming, Mixed Integer Programming, Partial Equilibrium	Multiple years with user-determined time-slices	Long-term (user-determined)	Local to Global	Commercial, Free demo version	GAMS + Solver (VEDA)	[92]

2.5 Demand side management

2.5.1 Principles of Demand Side Management

A load profile describes the variation in the electrical demand of a customer or group of customers over a given period of time. The term demand side management (DSM) was defined by the Electric Power Research Institute (EPRI) as ‘‘*the planning, implementation, and monitoring of activities designed to influence customer use of*

electricity so as to produce desired changes in the utility's load profile shape, namely the time pattern and magnitude of a utility's load" [125] [126] [100].

Demand Side Management (DSM) seeks to align electricity consumption with supply, thereby mitigating issues such as system overloads, excessive battery discharge, brown-outs, unplanned outages, and shortened equipment lifetime. Common DSM objectives include cost minimisation, efficiency improvement, maximising reliability, emissions reduction, fuel reduction and customer satisfaction [127].

The centralised grid is frequently over-dimensioned to cater for the peak loading [100]. The need for DSM is of paramount importance in microgrids because oversizing the microgrid system at the design stage results in underutilization of the system and hence a higher levelized cost of energy (LCOE) [72] [21]. The LCOE is the average cost per kWh of useful energy produced by an energy system over its lifetime and is a technology-independent way of comparing generation sources and technologies.

Furthermore, microgrids, with their relatively small number of consumers, typically exhibit higher demand instability, while the use of intermittent renewable generation creates supply-side fluctuations [128]. Diesel gensets and battery storage are commonly used to meet demand during insufficient supply periods, but this carries cost implications. Under-dimensioning of a microgrid on the other hand results in overloading, damage and shortened equipment lifetime as well as low reliability. This impacts microgrid sustainability negatively as, according to Crossboundary, there is 10 times more consumption at higher reliability sites than low reliability sites [129].

It is thus important to introduce measures to reduce energy system capacity sizing requirements. DSM reduces the need for, and therefore costs of, supply side investments in generation, transmission and / or distribution assets.

The key techniques for DSM are presented in Figure 2-17.

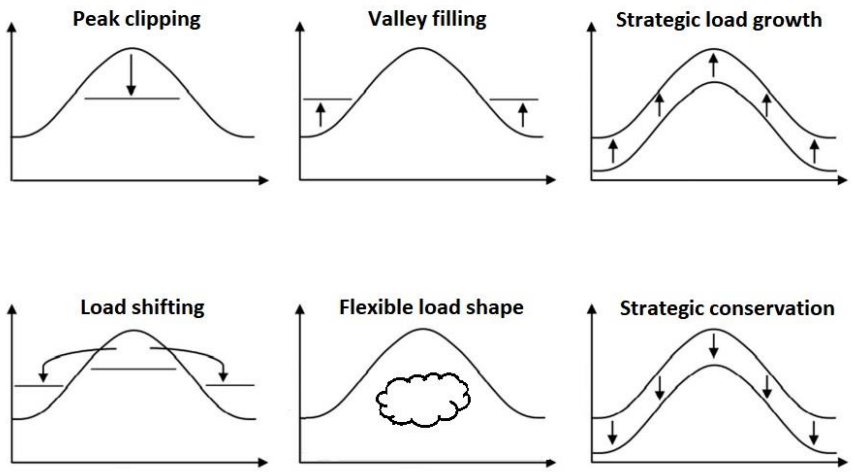

Figure 2-17: Techniques for DSM (adapted from [31]*)*

The common demand side management approaches are described in [125] [130] [31] [131] [24] [132].

- Load shifting means customers are incentivized to change their demand from peak to off-peak hours, and thus the maximum or peak demand is reduced, while total energy consumed remains unchanged. It can be done by changing the operational times of loads.
- Peak clipping or peak shaving means some loads are dropped in order to limit the maximum power. This helps consumers to avoid peak demand charges, and also reduces overall energy consumption. This however can result in increased user discomfort and higher customer dissatisfaction. When the demand is lower, the loads can be restored.
- Strategic conservation minimises energy requirements, for instance through implementing energy efficiency measures.
- Strategic load growth aims at raising energy consumption over a given extended period such as a year or season. It targets the increase of not only valley demand but also peak demand for lengthy periods.
- Valley filling has as its goal increasing energy consumption during off-peak periods, usually if low cost fuels ae available during low demand periods. It increases energy consumption without increasing the maximum power, and can be attained by for instance introducing new electric loads that formerly used other fuels e.g. electric vehicles charging at night.

- Flexible load shape enables customers to modify their consumption patterns by purchasing power at reduced reliability or quality of service levels. For instance, the energy supply company can cut off some loads.

In a broader sense, DSM has been described as consisting of energy efficiency and demand response (DR) [21] [133].

Energy efficiency is one of the simplest means to reduce energy consumption, emissions and energy costs hence the attribution to energy efficiency of being the 'first fuel' by the IEA [134]. DSM strategies based on energy efficiency (EE) can generally be applied to any grid and are particularly suitable for developing countries, while DR-based ones require more advanced smarter grid technologies [135]. In general, it has been stated that energy conservation steps as well as efficiency improvement measures e.g. customers ensuring they switch off lights when not needed or replacing incandescent bulbs and compact fluorescent lamps (CFLs) with LED (light-emitting diode) lamps, are cheaper than buying more efficient but higher consumption appliances such as refrigerators. However refrigeration uptake is on the increase, so refrigeration appliance energy conservation and efficiency strategies need to be considered and studied.

The Federal Energy Regulatory Commission (FERC) defines demand response (DR) as a modification of the consumption of electric energy by customers from their typical consumption in response to changes electricity prices or incentive payments. Their initial definition focused on reducing demand during peak hours [136] but was later expanded to include effecting profile changes at any time [133].

Figure 2-18 illustrates the main measures by which DR is achieved, through incentive-based and price-based methods.

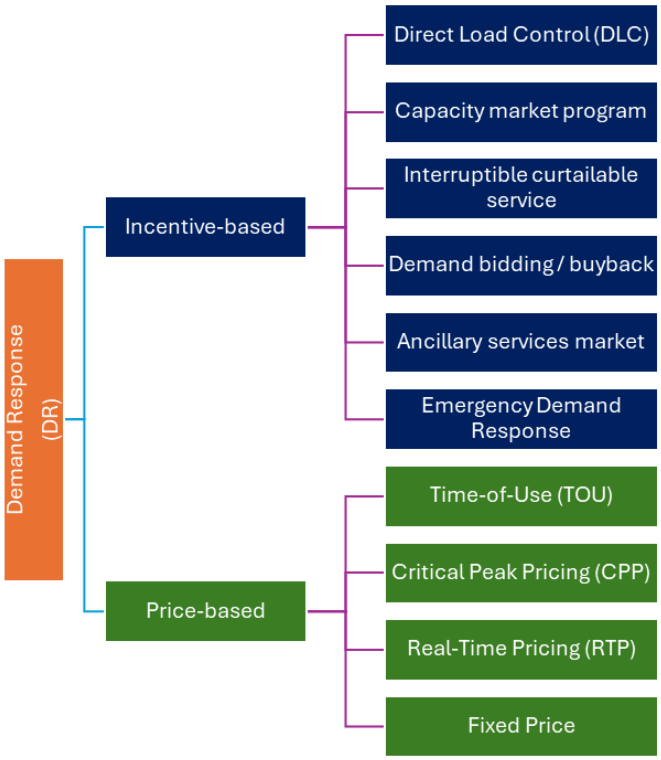

Figure 2-18: Demand response options [137]

Incentive-based DR programmes include the following [137] [138]:

- Direct Load Control (DLC) means energy providers can directly and remotely control consumer appliances to achieve the desired supply-demand balance, targeting mainly residential and small commercial consumers. Loads like air conditioning can be controlled by the generation company, and typically the number of hours or days are stipulated to minimise customer discomfort.
- Emergency Demand Response (EDR) programmes provide financial benefits to customers for decreasing their power draw when the power system is stressed. Both DLC and EDR are voluntary for consumers.
- Capacity market programs (CMP) oblige customers to curtail loads so as to lower demand to levels required by the utility to maintain the energy system in balance, thus in effect replacing typical generation resources.
- Interruptible Curtailable Service (ICS) is a mandatory version of EDR implemented to achieve system stability, whereby mainly industrial customers receive discounts or credits for lowering their demand.

- In Demand Bidding/Buyback (DBB) programs, large customers offer curtailment capacity bids to the supplier as the amount of load they are willing to shed.
- Ancillary Services Market (ASM) participation is possible by some customers. Ancillary services enable an electricity system to manage fluctuations in generation and demand, hence providing flexibility and maintaining stability. These services include inertia, operating reserve, frequency control and voltage control [139].

Price-based DR aims to modulate the consumption patterns of customers to improve the supply and demand balance, lower peak demand and minimise supply side interventions by means of the following price related approaches [137] [138]:

- Time-of-use (TOU) pricing is such that at different times typically during a diurnal 24-hour span, different tariffs, typically peak, off-peak and shoulder rates are imposed. In Kenya and Uganda commercial and industrial grid consumers are the major beneficiaries of this.
- Critical peak pricing (CPP) is when a higher rate is applied during periods of peak demand or when system reliability is stressed, typically for a few hours or days annually.
- Real-time pricing (RTP) involves dynamic adjustment of rates that reflects market dynamics and the supply-demand fluctuations. The energy supplier publicises these vacillating rates hourly or the day before, with the aim of lowering consumption during periods of low supply or high demand.
- With fixed prices, the tariffs are set and unchangeable for a given period or season.

CPP, TOU and RTP elicit better responsiveness to supply-demand constraints than fixed tariffs [130].

Tariffs based on load curves rather than economic activity category have been recommended [140]. Savings of almost 20% on costs have been reported as a result of managing 40% of controllable loads using DR measures. The classification of customers and understanding the various consumption patterns facilitates the development of suitable tariffs, which can be used to implement DSM.

2.5.2 Load management approaches

For load management to be possible, appliances need to be classified and controlled accordingly. Load classification approaches described in the literature include the following [137]:

- Classification based on operation time: Loads can be grouped into deferrable or shiftable loads and non-deferrable or non-shiftable loads. The appliances in the different classifications are not strictly demarcated. Examples of priority or non-shiftable loads include lights, computers, TVs, radios. Examples of shiftable loads include washing machines, dryers, refrigerators, water pumps, water heaters, dish-washers. Deferrable loads, sometime referred to as interruptible loads, can have their operation moved to low price or high renewable energy periods [40] [141]. Deferable loads are suitable for DSM applications.
- Classification based on flexibility of power rating: Loads are grouped into adjust-able loads for which power drawn can be adjusted and those for which the power is non-adjustable. For example thermal loads like ovens, water heaters, or irons can operate at lower voltages and thus lower power requirements unlike others like refrigeration appliances and water pumps [142]. Adjustable loads can partic-ipate in DSM, unlike non-adjustable ones.
- Classification based on the energy consumption of the appliances: Loads are grouped as those requiring a lot of energy and those with low energy requirements. Low consumption devices like TVs, lighting, computers are exempted from DSM control, while those with large power draws such as air conditioning are suitable for load management [143].

Residential loads have also been categorised as follows [36]:

- Resistive loads such as electric cookers and ovens, incandescent lamps, space and water heaters. For these devices, power consumption can be decreased by decreasing voltage.
- Power electronics loads such as computers, laptops, monitors, TVs.
- Energy efficient light loads such as LED loads and CFLs.
- Directly-connected motors such as fridges, freezers, water pumps, washing machines, dryers, dishwashers and drive-controlled motors such as air conditioners.

Various approaches have been adopted to manage loads in power networks. Load management measures that can be deployed include banning of appliances that consume higher power than appropriate for a microgrid, use of circuit breakers and remote meters with relays that can be programmed to interrupt supply to or turn off certain deferrable appliances [144].

In [142], the use of Grid Friendly Appliance (GFA) Controllers to autonomously respond to over- and under- frequency occurrences is described. Loads like dryers and water heaters can be dropped if frequency drops below the lower frequency bound. Electric vehicles can also provide voltage regulation and frequency regulation services. However it is important to avoid oscillatory transient responses by scheduling the appliance reconnections appropriately.

A direct load control (DLC) approach for residential customers that uses dynamic voltage control is described in [36]. Voltage control smart plugs utilising triacs and thyristors are used to control the power consumption of passive loads like heaters or ovens. By reducing voltage upon receipt from the utility of a DLC signal such as a price signal or load curtailment request, power consumption is reduced. Thus customer discomfort is avoided as would be the case if the loads were switched off completely. It was proposed in [36] that for refrigerator, iron, toaster, kettle, hair dryer and AC loads, power consumption reductions of 6% – 20% were possible, but not for electronic loads like computers. Also, it should be noted that for loads containing motors such as refrigeration appliances which require a given power to operate, voltage reduction results in current increases which can cause overheating and burnout.

In [135], energy savings of 9% were deemed achievable from actions taken by consumers to improve energy conservation such as disconnection of unused device plugs and switching off of unnecessary loads, while load shifting measures meant 15% of the total energy usage was shifted from peak to off-peak hours.

2.6 Some energy uses

2.6.1 Lighting

Considering energy efficiency as a demand side management measure, lighting has been widely addressed in Africa [145] and Asian countries like India [146].

15% of global electricity use is for lighting, with higher proportions occurring in electricity consumption- and access-limited areas [147]. In developing nations, lighting contributes approximately 15% of overall electricity demand and is responsible for around 5% – 6% of total greenhouse gas emissions [146]. In urban Nigeria, 35% of the residential electricity consumption was stated as being for lighting [148]. Fluorescent bulbs usage and adoption of more efficient lighting, equipment and appliances would significantly reduce emissions in 65% of the countries worldwide [147]. A 2020 South African study found lights to contribute 31% - 57% of electricity expenditure in schools, with replacement of fluorescent bulbs by more energy efficient LED bulbs reducing costs by 21% to 39% [149].

The Energy Efficient Lighting and Appliances (EELA) project seeks to promote energy efficient lighting and appliances across East and Southern Africa through market incentives, policy and regulation, capacity building and awareness raising [145]. It was estimated in a 2017 report that from energy efficiency measures in Uganda, 2,224 GWh of energy savings (31% of demand) plus 341 MW of on-grid and 15 MW of off-grid peak demand reduction could be achieved and 10.6 million tonnes of CO_2 emissions prevented [150].

Other DSM approaches such as load shifting are not as applicable to lighting loads.

2.6.2 Refrigeration

According to the International Institute of Refrigeration (IIR), the refrigeration sector, which spans refrigeration, air-conditioning and heat pumps, accounts for 20% of global electricity use [151]. Rising global temperatures, as evidenced by the National Aeronautics and Space Administration (NASA) report that 2024 was the year with the highest recorded global average surface temperature [152], as well as growing refrigeration needs in both developed and developing nations [5], indicate that the refrigeration portion of electricity demand is expected to increase.

Thanks to their thermal inertia, refrigeration and thermal (such as water heating and cooling) systems can act as flexible buffer technologies, offering real-time demand-side management potential by allowing brief shutdowns while still meeting operational and food safety requirements [153] [154].

To prevent food spoilage, recommended refrigerator temperatures generally fall between 1.1°C to 4.4°C [155], with other guidelines suggesting 2°C to 4°C, but not exceeding 5°C to 6°C for ready-to-eat foods [156], or even up to 8°C [157]. For freezers, recommended temperatures are below -12°C [158], with -18°C being the most common recommended upper freezer threshold [159], while another study cited -15°C [160].

The internal temperature of a fridge or freezer is influenced by several factors including the ambient temperature, frequency and duration of door openings, its insulation properties, and how full the appliance is. Higher ambient temperatures increase heat transfer into the appliance, requiring more energy to maintain cooling targets. A fuller fridge or freezer retains cold better due to the thermal mass of its contents, reducing the energy needed to restore the regulated temperature after being opened. Power usage is also affected by the thermostat setting [161], the installation setup i.e. ventilation and clearance from walls and neighbouring bodies, and how often contents are added or removed [162]. Importantly, overfilling should be avoided, as it can obstruct air circulation and hinder efficient cooling [159].

Although advances in energy efficiency are reducing the power draw of increasingly larger refrigeration appliances, high upfront costs, limited market availability, and long appliance lifespans averaging around 16 years [163] present barriers that can hinder access to newer, more efficient appliance models in developing countries. In many African households and businesses, fridges and freezers are frequently switched off to reduce electricity costs, with usage in some cases limited to just 1 to 2 hours per day. These extended off periods can present risks to food safety.

A study in Ghana revealed that due to the widespread importation of inefficient, used or discarded refrigeration appliances and the higher ambient temperatures typical of Ghana, in 2005 the average Ghanaian household refrigeration appliance consumed approximately 924 kWh annually, significantly higher than the corresponding 250 kWh/year and 400 kWh/year averages in Europe and the USA [164].

It is worth noting that energy efficiency programmes can have unexpected outcomes. For instance, energy savings from providing more efficient air conditioners and refrigerators in Mexico were less than projected due to underestimation of the efficiencies of the replaced equipment, with an average refrigeration energy drop of only 11 kWh per month (i.e. an 8% reduction), while air conditioner electricity consumption actually increased due to more usage [165]. The latter result would give the impression that, contrary to expectations, energy saving gains are higher when the replacement devices are of lower efficiency. This indicates that a judicious choice of which devices to replace with more efficient ones should be made, accompanied by public and consumer sensitization and awareness initiatives.

Ageing impacts

Insulation effectiveness highly impacts the energy consumption of a refrigeration appliance [166]. Performance and insulation degradation is expected over time due to ageing. Insulation degradation results from processes such as the inward diffusion of ambient air and water vapour into the insulation which is typically polyurethane (PUR) foam, and the outward diffusion of the cell gas in the insulation material which plays a critical role in reducing convective heat transfer.

Elevated ambient temperatures accelerate ageing, while extremely low temperatures also result in faster internal temperature rise due to increased insulation thermal conductivity from water vapour condensing into liquid [167].

Small insulation width, combined with reduced effectiveness from ageing, increase appliance wear and shorten compressor lifespan as the compressor must operate for longer durations [167] [166]. A study was done on the optimal wall thickness of refrigeration units, aimed at minimising heat losses and determining the appropriate sizing to achieve a target energy efficiency index [167].

Implications for off-grid and on-grid energy systems

In many rural African communities served by microgrids, refrigerators remain uncommon in households, largely due to limited purchasing power [80]. According to the East African Centre of Excellence for Renewable Energy and Efficiency (EACREEE), even when refrigeration appliances are present, their usage is often restricted because of the high cost of operation, due to their lengthy usage patterns [168]. This underutilization not only reduces demand for electricity, impacting the long-term viability of microgrid

operators and utilities, but also undermines the practical benefits of refrigeration, such as food preservation and household convenience. Furthermore, it weakens consumer motivation to invest in cold storage appliances. However, initiatives focused on productive energy use and appliance financing are increasingly being adopted to encourage wider adoption and use of refrigeration devices [25] (see Figure 2-19).

Figure 2-19: Shop with a chest freezer (to the left) for productive energy use at Senyondo microgrid in Uganda

A 2022 study in Uganda highlighted a lack of accessible information on the energy consumption of refrigeration appliances, which hinders consumers from making informed purchasing decisions [169]. To address this gap, the study recommended the enactment and enforcement of legislation similar to that implemented by Kenya's Energy and Petroleum Regulatory Authority (EPRA) and the Rwanda Standards Board. It also recommended the establishment of a national appliance or product registration database modeled after EPRA's system to publicly disclose energy consumption data as well as mandatory labeling that displays the unit energy consumption (UEC) in kWh/year.

Efforts are underway to establish and implement Minimum Energy Performance Standards (MEPS) for residential refrigerators and air conditioners across the East African Community (EAC), led by EACREEE in collaboration with SADC Centre for Renewable Energy and Energy Efficiency (SACREEE) from the Southern African Development Community (SADC) [168][170]. The IEC 62552:2015 standard, which is adaptable to local climate conditions and internal appliance temperatures, is used in Kenya [171]. It is also widely used in the EU. However, these standards currently overlook the increase in energy consumption as appliances age.

There is a lack of lifetime energy consumption and lifetime energy efficiency studies for refrigeration appliances in the African context, which calls for further investigation.

DSM studies of refrigeration

Various studies have explored DSM strategies in refrigeration, such as price-based DSM, pre-cooling, coordinated refrigerator scheduling using real-time thermal mass estimation [157] [104] and time-of-use based control [172]. A study in Slovenia evaluated domestic refrigerators' internal, contents and air temperatures and household user behaviour over 24 hours using 15-minute interval data [156]. Coordinated scheduling experiments of refrigerator compressors showed potential energy savings of nearly 30% while adhering to minimum on/off durations of 3.6 to 6.3 minutes On and 1.6 to 4 minutes Off to avoid compressor stress due to frequent switching [104]. Other research examined the role of refrigerators in grid frequency regulation and the risks of simultaneous restarts after outages [154] [173], as well as surplus power utilisation through extra refrigeration system cooling to lower later energy demand [174].

Energy efficiency refers to achieving the same outcome or accomplishing the same task with lower energy input [175]. The use of Phase Change Materials (PCM) in refrigeration systems carries several benefits, including enhanced temperature stability [143][176][177][178], improved energy efficiency and reduced energy consumption [160][179][176]. Additional advantages include lower operational costs [180], increased resilience to power blackouts [177], and less compressor on and off cycling [179][176][178]. Compared to chemical battery storage, PCM are considered as more cost-effective, environmentally friendly and durable [181].

Precooling strategies aim to shift cooling-related electricity demand from periods of peak consumption or high electricity prices to periods of lower demand or reduced prices [182] [157]. This makes precooling an effective DSM approach for load shifting, valley filling, and strategic energy conservation [183], particularly in systems with renewable energy sources [182]. PCM can thus support load shifting by being cooled during periods of low demand or high photovoltaic (PV) generation, and allowing the later usage of stored cooling capacity during periods of high energy demand [143].

Time-of-use (TOU) tariffs are a commonly employed DSM mechanism in refrigeration for peak load reduction and increased off-peak energy consumption [181]. However, prior

related studies have highlighted several limitations, including no integration of smart grid technologies for dynamic price-based costs control [180][184], and the lack of user cost savings analysis from peak shaving and valley filling in an aggregated refrigeration appliance control study for Ireland [185]. The latter study modelled thermostat setpoint adjustments based on demand signals, which reduced peak loads through overcooling but increased overall energy consumption. Refrigerator DSM using precooling and varying electricity prices is modelled in [157], with pre-defined precooling start times. Varying the pre-cooling start times yields different price savings, depending in part on the refrigerator's initial temperature at the beginning of the precooling period. In [186], the operation of fridges within an elevated temperature band between 8 pm and 11 pm yielded energy savings during the 3-hour period, but these savings were offset and the gains lost once normal uncontrolled operation resumed.

As noted in [181], real-time predictive control of refrigeration appliances is made more complex by random user interactions such as appliance door openings, or insertion and removal of items of varying temperatures, which must be handled without violating food safety temperature constraints. Predictive control of aggregated freezers using generalized assumptions about stochastic door openings was modelled, and shorter control intervals of 15 minutes for DSM were recommended to mitigate synchronisation and avoid demand rebound effects [187].

Load shifting alters the timing of energy consumption but does not necessarily reduce the total energy used by appliances as any temporary reduction is often offset by subsequent increases, known as load recovery. The length and timing of the adjustments depend on the characteristics of the specific load [178]. Previous studies have often assumed that a fixed portion of the load such as 20% [132] or up to 20% [23] can be shifted without accounting for appliance-specific requirements [140, 46].

However in the case of refrigeration, additional constraints related to food safety, beyond basic load shifting, must be considered.

2.6.3 E-mobility

In Africa, over 650 million rural inhabitants primarily rely on walking, cycling, or public transportation that is usually imported two- and three-wheeler (2&3W) vehicles, for

mobility [188]. With high national 2&3W fleet proportions in African countries e.g. 70% in Uganda, 53% in Rwanda [42], 37% in Kenya, 34% in Tanzania and 23% in Ghana [189], these vehicles are also a major source of employment in East Africa [190] [191]. Electric two and three wheelers thus present a promising entry point for transport electrification in the region.

While Africa accounts for approximately 20% of the global motorcycle fleet, only 0.2% are electric [42], with internal combustion engines (ICEs) being dominant. Figure 2-20 shows a typical rural fuel station at Senyondo microgrid on Bunjako Island in Uganda.

Several companies are introducing e-mobility solutions in Africa, including in East Africa [188][192][193]. The expansion of electric mobility is hindered by factors such as unavailable or unreliable electricity supply, limited charging infrastructure which confines usage largely to urban areas, high upfront costs and unfavourable regulatory and policy frameworks. Some companies offer portable batteries and battery-swapping services for e-motorbikes, but the high capital costs of off-grid solar-based charging stations continue to pose a significant challenge.

(a) (b)

Figure 2-20: (a) Fuel station served by Senyondo solar PV microgrid at Bunjako in Uganda (b) Lake Victoria shores at Senyondo microgrid showing a stationary ICE 2-wheeler motorbike (mid-left)

Rural microgrids which are typically powered by renewable solar energy suffer from low daytime electricity consumption and poor load factors, resulting in high levelized cost of energy and financial sustainability challenges [18]. These microgrids often serve a limited geographic area (within a 1 km radius) [44], leaving potential users outside that footprint without access.

There is a little explored / exploited opportunity for microgrids to reduce PV energy curtailment and increase their supplied energy and hence sustainability by integrating e-

mobility charging stations and portable storage as additional loads. This bears further investigation.

3 Research Methodology

3.1 Methodology approach

A mixed-methods research approach is used. This includes qualitative data collection through conducting surveys and interviews with energy users, technical personnel and microgrid operators plus site observations, as well as secondary data collection from publications and reports. For acquisition of quantitative data, measurement equipment is installed and used at the sites. Quantitative data is also accessed from online databases such as that of NASA, from microgrid system equipment data portals and smart meter data repositories.

Modelling, simulation and experimental studies are carried out. The work undertaken is categorised into 5 case studies from sites situated in Uganda, Kenya and Tanzania.

3.2 Site descriptions

The sites chosen are representative of microgrids and residential energy use cases in rural East Africa. Measurements for this research were carried out at three sites: Lwak in Kenya, Silale in Tanzania and Bunjako in Uganda.

3.2.1 Lwak Convent in Kenya

Lwak Convent in Siaya District, Western Kenya is located at 0° 8.4’ S, 34° 21.4’ E, as shown in Figure 3-1. Consisting of three buildings, each with its own power meter, the site is grid connected with, at the start of the research, a 40kW diesel generator supplying backup power to the Convent and several nearby buildings during outages.

(a) (b)

Figure 3-1: (a) Lwak location (Source: Screenshot from HOMER Pro) (b) Lwak site in Siaya, Western Kenya (Source: Google maps)

The site has several electrical consumption devices including TVs, radios, water dispensers, fridges, freezers and irons. The biggest energy consuming loads in terms of power ratings and continuous operation are 3 refrigerators and 5 freezers listed in Table 3-1. Thus focus was placed on the fridges and freezers for demand side management. Building 1 contains one fridge and two freezers, Building 2 has one fridge and two freezers while Building 3 is equipped with one freezer and one fridge.

Table 3-1: Refrigeration appliances at Lwak Convent

Appliance	Location	Description
Freezer 1	Building 1	Bruhm BCF-398SD
Fridge 2	Building 1	Toshiba GR-EF 33
Freezer 3	Building 1	HTCF208A2
Fridge 5	Building 3	Haier
Freezer 6	Building 3	ArmCoAF-C38(K)
Fridge 8	Building 2	Goldstar GR-312S
Freezer 9	Building 2	-
Freezer 10	Building 2	Bruhm BCF-398SD

Installed PV system description

Later on a PV system was setup at Lwak Convent, under the Art-D Grids project. The 12

kW_p solar PV system has 37.58 kWh battery storage. Figure 3-2 shows some of the installed system equipment.

The PV system consist of 3 strings of 10 JA Solar JAM72S10-415W PV modules, with each string connected to one of three SMA Sunny Boy 5.0 inverters (rated 5kW). Three strings of Hoppecke Sun power VR M 12-105 batteries (nominal voltage 12V) comprising of four batteries per string are connected to each of the three 6kW SMA Sunny Island 8.0H-13 battery inverters, forming the 48V dc storage system. 1 SMA Data Manager and 2 SMA Energy Meters were also installed.

Each of the three buildings was connected as a stand-alone 4 kW_p PV, 12.53 kWh storage microgrid with 1 SMA Sunny Island 8.0H-13 inverter and 1 SMA Sunny Boy 5.0 inverter.

Figure 3-2: Lwak solar system equipment

3.2.2 Senyondo microgrid at Bunjako in Uganda

Operated by Winch Energy Uganda (later renamed NOA Uganda), Senyondo microgrid at Bunjako on Lake Victoria's shores is an off-grid solar PV microgrid with battery

storage serving off-grid communities from four of the 8 villages on Bunjako island (see Figure 3-3a). The containerised Senyondo microgrid equipment is shown in Figure 3-4.

Winch Energy also operates several microgrids in Lamwo District, Northern Uganda (see Figure 3-3b).

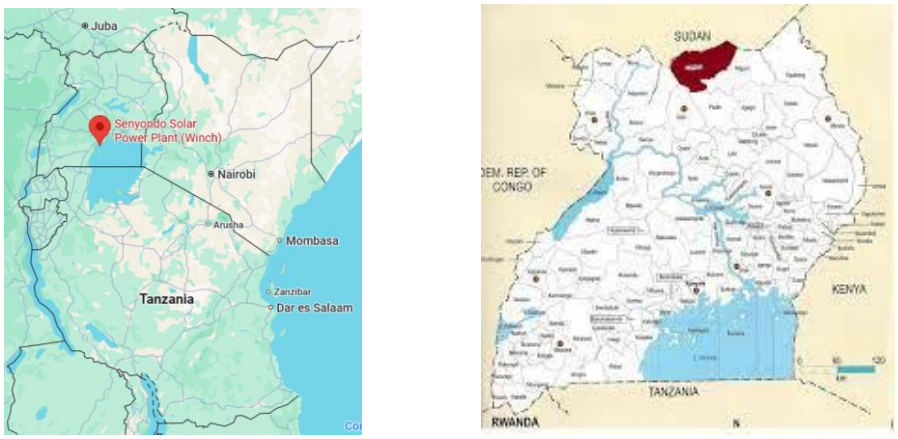

(a) (b)

Figure 3-3: (a) Location of Senyondo microgrid in Uganda (Image source: Google maps) (b) Lamwo District in Northern Uganda (in red) (Image source: Uganda Investment Authority [194]*)*

The 75.8 kWp solar PV microgrid at Senyondo has 296.64 kWh lead–acid battery storage and is equipped with SMA Sunny Tripower 20000 TL-30 and SMA Sunny Island 8.0H-12 inverters. The storage system comprises of Hoppecke OPzV Sun Power VR L 2-1700 batteries.

Customer load profile data for 1 other microgrid in Central Uganda and 6 microgrids in Lamwo District in Northern Uganda is also used in Case Study 5.

Figure 3-4: Senyondo microgrid equipment including the Mavowatt power quality analyzer connection setup at Bunjako, Uganda

3.2.3 Silale microgrid in Tanzania

Silale microgrid, located in Dodoma region in Tanzania (see Figure 3-5), is an isolated solar PV with battery storage microgrid that was installed around 2015, with the local community taking over its operation from around 2019.

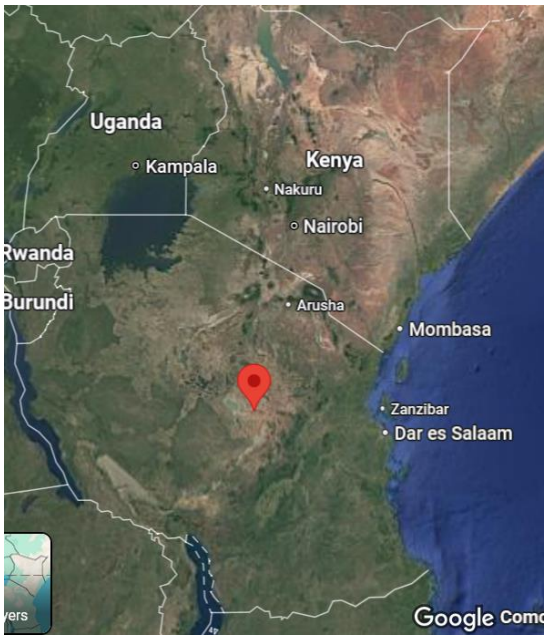

Figure 3-5: Location of Dodoma in Tanzania (Image source: Google maps)

At installation, the microgrid had 55 Solarwatt panels each rated 250W_p and 24 Hoppecke 10 OPzV 2V 1236 Ah batteries forming the 48V DC storage system. Also installed were 1 solar inverter (SMA Sunny Tripower STP 15000 TL-10), 3 battery inverters (SMA Sunny Island SI 6.0H) and 1 Sunny WebBox data logger meant for logging the PV system data.

Two of the batteries were faulty and had been disconnected, and several solar panels were damaged by the time of the 2022 field visit.

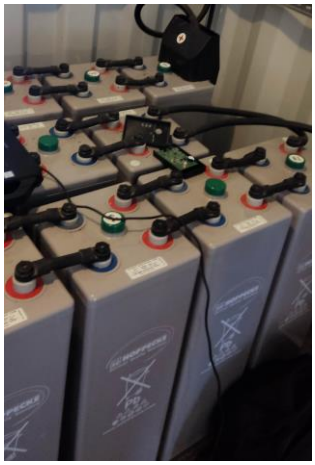

Figure 3-6: Silale microgrid setup

The line allocation during installation was as follows: Line 1 (or Phase A) for organisations like the school and church, Line 2 (or Phase B) for businesses such as salons, bars, shops, restaurants and Line 3 (or Phase C) for residential customers.

Due to a lack of individual customer meters until the installation of a smart meter system in December 2022 [195], all microgrid customers paid a uniform amount (similar to a subscription model [196]) irrespective of actual monthly energy consumption. Prior to that the grid had been extended to Silale village, enabling the community members to choose between a microgrid or grid connection, or both.

3.3 Description of Case Studies

The five case studies are described below.

3.3.1 Case Study 1 - Use of HOMER for design and analysis of a hybrid power system and DSM options at Lwak

Using the simulation tool HOMER Pro (Version 3.14), a grid-interactive system is designed for Lwak Convent in Kenya. The PV, and battery system with diesel genset is simulated based on preliminary site information, with the aim of evaluating system sizing and techno-economic specifications for two proposed demand side management (DSM) strategies, load shifting and peak clipping. The system aims at reducing grid and genset

dependence, minimizing costs and storage requirements, and maximizing renewable energy utilization.

3.3.2 Case study 2 - Refrigeration temperature evolution study at Lwak and appliance efficiency degradation analysis

The second case study involves analysis of the power consumption of the refrigeration appliances at the rural site in Lwak, Kenya, assessing the potential for energy savings through temperature-based control strategies that regulate appliance on/off cycles. Experimental results are compared with model-based temperature evolution simulations, highlighting discrepancies between model-based results and measured performance. The aim of this case study is to provide an initial understanding of feasible refrigeration load shifting timelines and associated energy savings, thereby informing future development of possible control mechanisms for demand side management of refrigeration appliances.

The temperature evolution experimental data of four of the freezers is used in applying the Bonn method for evaluating efficiency degradation over time. Ageing-cognizant Minimum Energy Performance Standards (MEPS) for refrigeration appliances are also proposed for a more realistic evaluation of lifecycle energy efficiency performance.

3.3.3 Case study 3 - DSM modelling using PSO for refrigeration appliances at Lwak

Case Study 3 presents a DSM strategy for refrigeration appliances using Particle Swarm Optimization (PSO), based on the findings from the refrigeration temperature evolution experiments at Lwak described in Case Study 2.

This case study proposes a PSO-based DSM strategy involving refrigeration load-shifting and strategic conservation for a hybrid system, using experimental data from Lwak Convent. The goal is to redistribute energy demand more evenly while reducing overall consumption and costs, without compromising food safety. Unlike some prior studies that utilise time-of-use pricing [39][107], the optimization approach employs an objective function based on average daily power consumption to schedule the operation of refrigerators and freezers, thereby allowing modulation of the site's load profile.

The PSO method builds on approaches from [106] [39], extending them to refrigeration loads and constant tariff conditions typical of Kenya residential tariffs. Constant tariffs are generally the norm in East Africa and SSA microgrids, with TOU tariffs being very rare [197]. Furthermore, a study analysing four solar microgrids in Tanzania showed TOU tariffs as having negligible impact in shifting consumption patterns, raising the daytime-to-total consumption ratio (DTCR) of the microgrids by less than 1% when daytime (off-peak or 10 am to 4 pm) tariffs were reduced to 50% of the rest of the time (peak or 4 pm to 10 am) tariffs [196].

PSO is chosen due to its rapid convergence, relatively low computational overhead, scalability, and adaptability across diverse optimization problems [96] [102]. Additionally, it is well-suited for managing multiple appliances or customer loads in microgrid and grid contexts.

The proposed method combines load shifting and targeted conservation measures to reduce refrigeration energy use through coordinated scheduling of multiple appliances, offering a means for DSM in energy resource-constrained and uniform tariff settings.

3.3.4 Case study 4 - Battery State of Charge and temperature-based control for refrigeration appliances

Case Study 4 tackles an experimental investigation into the control of refrigeration appliances for the solar PV and battery system installed at Lwak Convent in Western Kenya. The study evaluates energy savings achievable through demand-side management (DSM) strategies that automate refrigeration appliance control based on battery state of charge (SOC) and internal appliance temperature.

Control logic was implemented to manage the on-off switching of fridges and freezers using both SOC and specified temperature thresholds. This approach is particularly relevant in off-grid scenarios without generator backup, where the battery serves as the sole energy source during periods of low or no solar generation, making SOC a critical indicator of power availability during night time and low-irradiance conditions.

Unlike prior research described in [186], DSM in this case study is not restricted to fixed hours of the day, allowing greater flexibility and responsiveness to real-time energy

conditions. An aim was to achieve smartness and minimize user involvement by enabling autonomous control based on system parameters.

3.3.5 Case study 5 - E-mobility and portable storage integration for a rural microgrid

Case Study 5 investigates strategic load growth as a demand-side management (DSM) strategy tailored for rural microgrids in East Africa, seeking to address the challenges regarding microgrid sustainability, electricity access, and rollout of electric mobility solutions described in Section 2.6.3. This approach involves integrating electric mobility and portable storage systems, with the objective of utilizing surplus generated PV energy and minimizing PV energy curtailment.

Unlike the DSM methods focusing on peak shaving or valley filling, strategic load growth intentionally increases both off-peak and peak demand over extended periods, making it particularly well-suited for absorbing excess renewable energy through productive and flexible loads.

The proposed approach in this case study aims to mitigate the limitations associated with RE curtailment and demand response strategies such as reduced economic returns and lower reliability [198] or decreased user comfort [199][200] due to forced load shedding or load shifting. In contrast, the proposed DSM method promotes load growth, enhancing system utilization, revenue generation and provision of energy access to the unserved.

To evaluate microgrid energy consumption patterns, load profiles for customers of 8 microgrids in Uganda and for Silale microgrid in Tanzania are analyzed and related insights obtained. Average daily customer consumption for the Uganda microgrids informs the modelling and life cycle assessment of the proposed DSM strategy using MILP optimisation for Senyondo microgrid in Uganda. MILP is chosen because of its simplicity and scalability for linear problems, as summarised in Table 2-1.

3.4 Data Collection Tools

3.4.1 Equipment used

Power and irradiance measurements

For Case Study 1, VectoGraphs Power Quality measurement devices were used to measure power consumption at Lwak Convent for the period 23rd March 2022 to 26th March 2022. The measurements were carried out by Septimus Boshoff and Henrik Bode. A sensor setup was installed at Lwak that measured solar irradiance (W/m²), wind speed (m/s), and ambient temperature (°C) over the period 25th March to 22nd April 2022.

For Case Study 2, a Gossen Metrawatt Mavowatt 230 power quality analyzer was used to measure the power consumption of the three buildings at Lwak from 6th February to 10th February 2023.

For Case Study 5, power measurements were conducted at Silale microgrid using a Gossen Metrawatt Mavowatt 240 power analyzer for the period from 15th December to 29th December 2022. Solar irradiance at Silale was measured using an SP Lite2 irradiance meter. Figure 3-7 illustrates the measurement setup at Silale microgrid as well as visible damage to the Silale microgrid solar panels.

(a) (b) (c) (d)

Figure 3-7: (a) Equipment setup for Silale microgrid measurements (b) Mavowatt and Kipp & Zonen Meteon display for the SP Lite2 irradiance meter (c) Damaged solar panel (d) Stone on the solar panels (in red circle)

Appliance power measurement and control equipment

For Case Study 1, the internal temperatures of the 8 refrigeration appliances at Lwak were monitored using AM2302 sensors connected to Raspberry Pi 3 Model B microcontrollers for temperature data logging. Power consumption measurement and control of the appliances was managed using Edimax SP-2101W V3 smart plugs, which offer remote

switching functionality, as shown in Figure 3-8. Power data for the smart plugs was displayed using the Edismart App and recorded using the open-source Tesseract OCR (optical character recognition) engine in Python 3.8.10 [201]. Appendix A contains the related Python code.

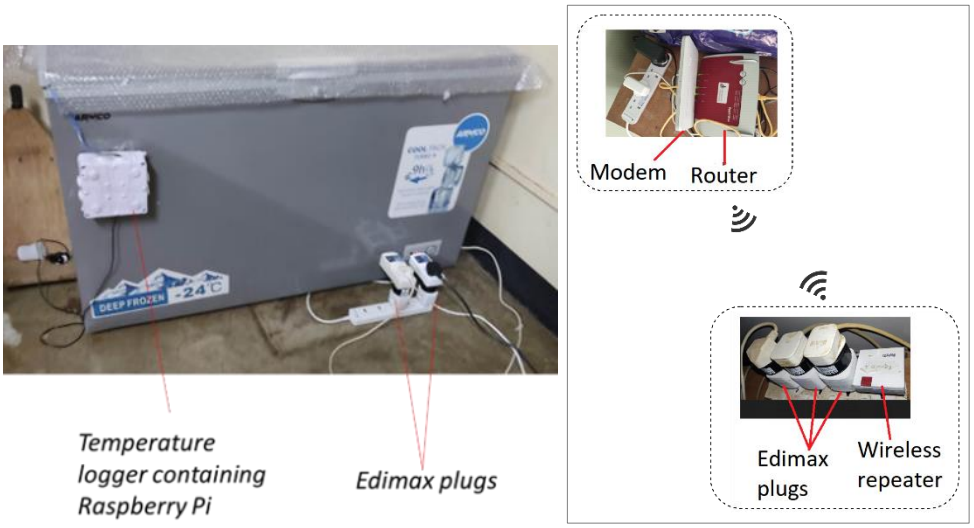

(a) (b)

Figure 3-8: (a) Setup to monitor freezer internal temperature and freezer power as well as to remotely switch on and off the freezer (b) Communications network setup between different rooms and buildings

For Case Study 4, the field setup at Lwak consisted of two Raspberry Pi 4 microcontrollers (named Pi 1 and Pi 2) for refrigeration appliance control and system data logging,. An Internet of Things (IoT)-based platform was implemented using smart plugs fitted with Shelly Plus 1 PM devices and DS18B20 temperature sensors to control device on/off state and measure internal appliance temperatures, respectively, connected to the 8 refrigeration appliances listed in Table 3-1. Figure 3-9 shows the load management setup for the battery and SOC-based control. The general site layout is shown in Figure 3-10.

(a)

(b)

(c)

Figure 3-9: Load management system for the battery and SOC-based control (a) Modem, raspberry pi and main router (b) Shelly smart plug and client side router (c) Temperature sensor setup

Figure 3-10: Lwak site layout (Image source: adapted from Google maps)

A Wi-Fi network was established to connect the refrigeration appliance smart plugs and related network devices to the primary microcontroller (Pi 1) responsible for load management and control. A wired network was used to connect the inverters, other system equipment and the second microcontroller (Pi 2) which were installed in the solar equipment room. Two internet modems were used to provide secure remote access to the system.

Due to distance and vegetation between the solar equipment room (housing Pi 2) and the buildings containing the DSM loads and Pi 1, both Raspberry Pis could not be connected to the same local wireless network. To bridge this gap, a cloud-based HiveMQ MQTT broker was employed to securely transmit battery SOC data from Pi 2 (on the solar PV system network) to Pi 1 (on the load control network) via the Internet. The experimental setup was as shown in Figure 3-11.

The monitoring and control platform was implemented using open-source tools Node-RED, MQTT, InfluxDB and Grafana installed in a Docker environment on both Raspberry Pis. Pi 2 was configured with the node-red-contrib-sma-WebConnect node [222], enabling communication with SMA Sunny Island inverters via the Webconnect functionality. This node allows retrieval of inverter data e.g. battery state of charge (SOC) by configuring the inverter's IP address, user credentials, and specific value_ids (e.g., '6100_00498F00' for battery SOC), as defined in the pySMA library [223].

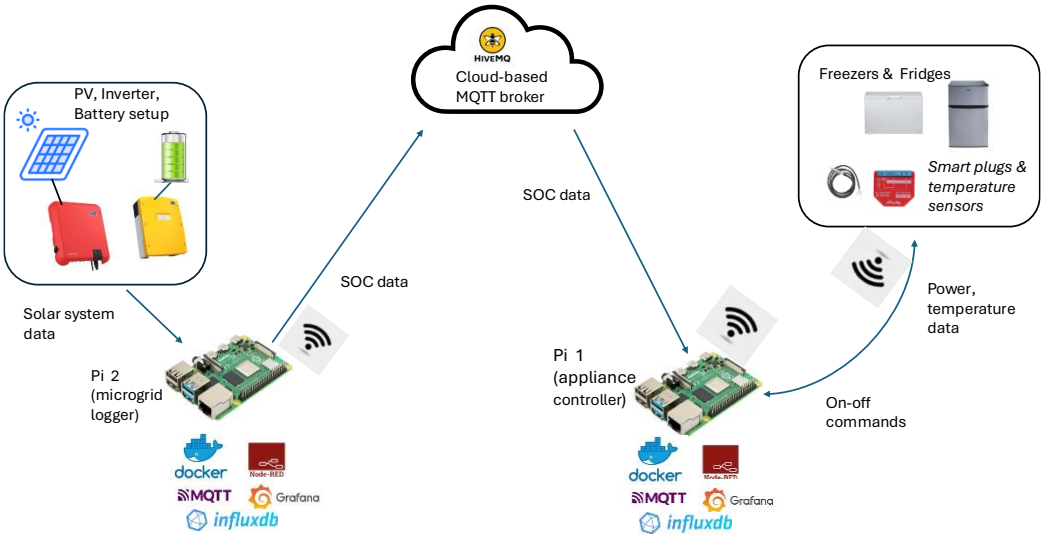

Figure 3-11: Experimental setup for load control at Lwak

3.4.2 Tools and Software

HOMER

HOMER Pro (Hybrid Optimization of Multiple Energy Resources) is a widely utilized tool for the design and analysis of hybrid microgrid and grid-connected energy systems

[202][127]. Its simulation and optimization functions enable comprehensive technical and economic evaluations based on site-specific power demand and local climatic conditions.

For the grid-connected site described in Case Study 1, HOMER Pro Version 3.14 is used to perform a techno-economic assessment of various energy carriers, analyzing potential cost savings and evaluating the effectiveness of DSM strategies like peak shaving and peak clipping. HOMER was selected for its ability to conduct multi-year simulations under both grid-connected and standalone scenarios, while also factoring in grid reliability, making it suitable for evaluating both current performance and long-term planning.

MATLAB/Simulink

MATLAB 2023 is commonly used for modelling and simulating electrical load, control systems, and optimization algorithms.

Simulation of refrigeration appliance operation and appliance temperature modelling for Case Study 2 is done using MATLAB 2023. For Case Study 3, MATLAB 2023 is used to model refrigeration load shifting using PSO and a hybrid PV system at Lwak.

MATLAB 2023 is also utilized for modelling and simulating the technical and economic performance of the MILP-optimised off-grid solar PV system with battery storage and e-mobility and portable storage loads discussed in Case Study 5.

IOT platform tools – Docker, MQTT, Node-RED, InfluxDB, Grafana

The server-client communication setup for the temperature and battery SOC control in Case Study 4 is depicted in Figure 3-12.

Docker is an open-source operating system framework that enables delivery, building, running and management of software in packages referred to as containers. Using the Docker API (application programming interface) or CLI (command-line interface), containers can be created, moved, started, stopped and deleted [203]. In contrast to a virtual machine (VM) that runs on hardware and uses its own operating system, docker enables applications to be run on different operating systems. Docker was used to install MQTT, InfluxDB, Node-RED and Grafana that were used for the load control and data logging, retrieval and visualisation on the raspberry pis.

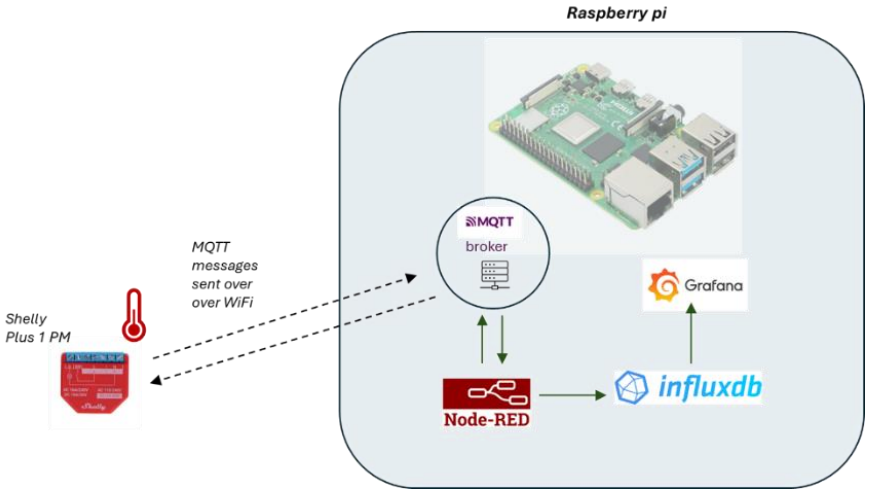

Figure 3-12: Communication and software tools

MQTT (Message Queuing Telemetry Transport) is a messaging protocol that is popularly used on IoT platforms and for machine-to-machine (M2M) communication [204]. It uses publish and subscribe messages to relay and receive information according to the topics subscribed to. MQTT clients publish messages and relay them via an MQTT broker to subscribers which are able to receive the messages. It enables communication over low-bandwidth, high delay and unreliable networks. The Shelly devices were configured to communicate with the MQTT Broker installed on the raspberry Pi 1 and relay power, temperature, current, voltage and other data. Eclipse Mosquito [205] was installed on a Windows computer to access and verify the MQTT setup and operation. HiveMQ broker [206] was installed on Pi 2 to relay the solar system information over the internet to the cloud HIVE MQ broker, and thereafter it was retrieved on Pi 1 and used for device control. Use of MQTT helps avoid some challenges associated with using Modbus Protocol for relaying inverter data, such as the need for additional converters and knowledge of the Modbus register addresses [207].

Node-RED is an open-source browser-based programming tool that uses visual flow editors for programming IoT devices [208]. Node-RED has nodes for MQTT input and output, function nodes, influx in and out nodes, filter and change nodes, etc. MQTT in nodes were used to obtain data for different topics, and the MQTT out nodes were used to send messages such as the control commands. Influxdb nodes were used to store data to the InfluxDB databases on the raspberry pis. The contrib-sma-webconnect node [209] was installed in node-RED on Pi 2 and was used to obtain battery SOC data from the Sunny Island inverters and to log it to an InfluxDB database on Pi 2, and then relay it via

the cloud-based HIVE MQ MQTT broker to Pi 1, where it was used for load control (Figure 3-11). The Node-RED port number is 1880.

InfluxDB is an open-source database used for storing time-series data in real-time [210]. It also enables the data to be visualised by means of suitable queries. The queries can also be used for visualisation of desired information in Grafana. The influxdb port number is 8086 / 8087.

Grafana is open-source software that enables querying, analytics and visualisation of data stored in a database [211]. Grafana was used to retrieve and view the data stored in InfluxDB databases on the two raspberry Pis, and for downloading the data as csv files for further analysis and processing. The Grafana port number is 3000.

As security is an important aspect of IoT systems, the various programs utilised passwords and tokens for secure access. To access the raspberry pis remotely, Twingate and Tailscale were installed on them. Twingate is a cloud-based service that uses zero trust networking to enable secure remote access to network devices. It allows application level access on the device and not network access unlike VPNs (virtual private networks) that allow access to the whole network [212]. Tailscale is a VPN service that enables secure remote access to devices and applications [213].

3.5 Experimental design and approach, Modelling and Simulation

3.5.1 Case Study 1 - Optimal design of a grid-connected PV system

Meteorological data

The monthly solar insolation data used was obtained using HOMER Pro from the National Aeronautics and Space Administration (NASA) solar energy dataset. The average annual insolation is 6.25 kWh/m²/day. February has the highest monthly average of

6.78 kWh/m²/day and July the lowest monthly average of 5.81 kWh/m²/day (see Figure 3-13).

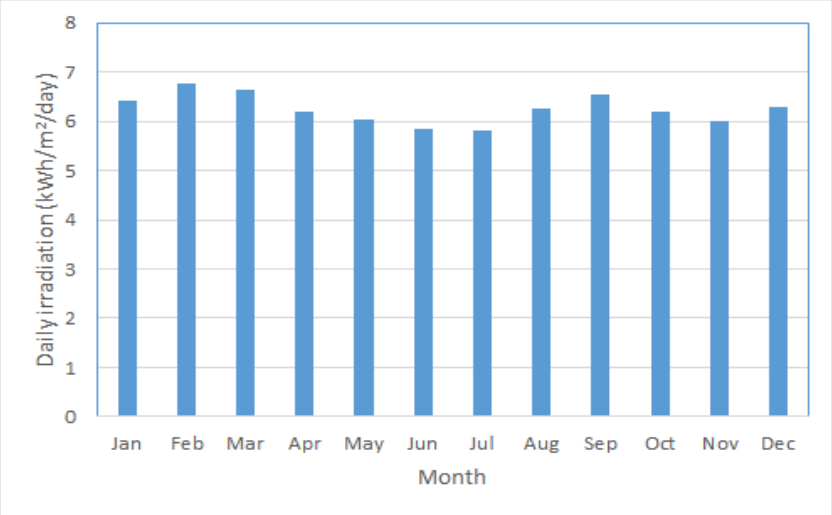

Figure 3-13: Daily average solar Global Horizontal Irradiance (GHI) data, averaged for each month (Source: NASA data downloaded in HOMER Pro)

Figure 3-14 and Figure 3-15 show the measured daily irradiance and ambient temperature profiles from 25th March to 22nd April 2022. Average solar irradiance peaked between 10 am and 2 pm, and ambient temperatures between 10 am and 3 pm.

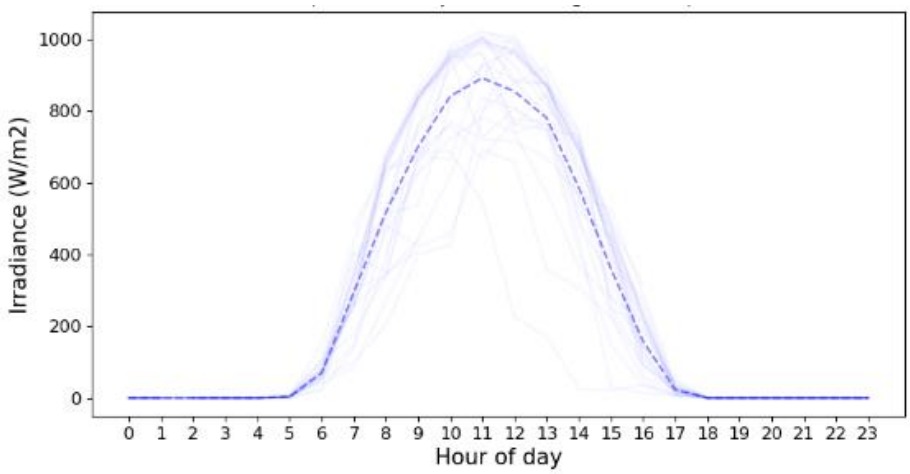

Figure 3-14: Measured daily irradiance profile in the module plane at Lwak for 25 March 2022 to 22 April 2022 (dashed line represents average values)

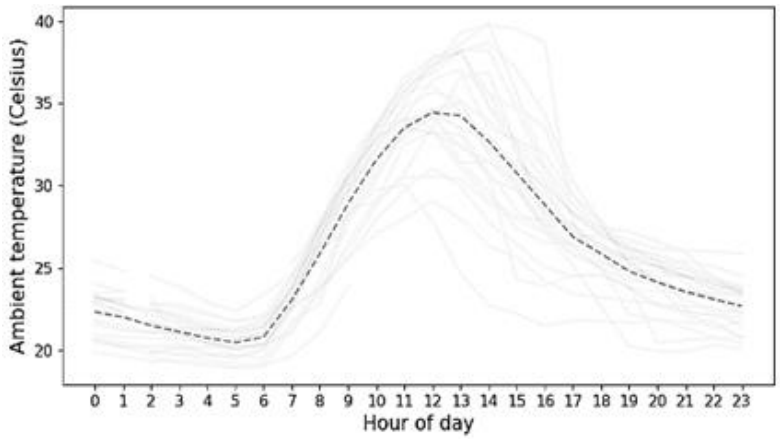

Figure 3-15: Ambient temperature at Lwak from 25 March 2022 to 22 April 2022 (dashed line represents average values)

Load profile

Power measurements at Lwak Convent conducted by Septimus Boshoff and Henrik Bode using VectoGraphs Power Quality equipment from 23rd March to 26th March 2022 gave an average daily power consumption of 2.33 kW over the period. The average daily load profile (see Figure 3-16) has a bimodal pattern. Peak demand occurs between 6 pm and 8 pm, corresponding to return of the residents and evening activities, with a smaller peak between 9 am and 10 am.

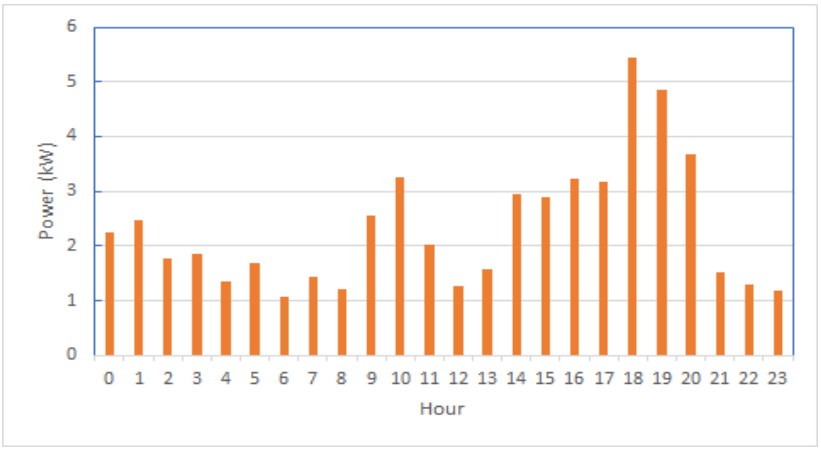

Figure 3-16: Average hourly load profile for Lwak site for 23rd March until 26th March 2022

Reliability metrics were also considered. In 2016, the average annual grid outage duration per customer in Kenya was estimated at 216.3 hours [214]. To estimate grid reliability at the location, generator runtime data from a school located adjacent to Lwak Convent was used as an indicator of local outage conditions. This data was integrated into the HOMER Pro simulation.

Loads

Table 3-2 shows typical power ratings and estimated operation durations for some of the electrical appliances at Lwak [100] [215], including their classification as either deferrable (D) or shiftable loads which can be started at any given time, or non-deferrable (N) loads with inflexible operation times. For this case study, the fridges and freezers are considered to be non-deferrable loads. Additional loads such as lighting are omitted from Table 3-2.

Table 3-2: Load characteristics

Device	Rating (kW)	Quantity	Total (kW)	Duration (hrs)	Deferrable (D) or Non-deferrable (N)	Reference
TV	0.2	2	0.4	3	D	[100]
Radio	0.015	1	0.015	3	D	
Water dispenser	0.53	2	1.06	6	D	
Fridge	0.25	4	1	6.5	N	
Freezer	0.12	2	0.24	6.5	N	
Electric cooker	2	1	2	3	D	[100]
Electric Iron	2	2	4	2	D	[100]
Kettle	2	2	4	0.5	D	[215]

Proposed DSM measures

From Figure 3-16, peak demand occurs between 6 pm and 8 pm, while the load is comparatively low between 11 am and 1 pm, coinciding with high solar irradiance. To address this imbalance, both peak clipping and load shifting strategies are applied.

For peak clipping (PC), if the evening hourly demand (6 - 8 pm) exceeds the peak observed during the morning (10 am), the load is capped at the morning peak value of 3.238 kW. This approach reduces stress on the battery storage system, especially during evening hours [216]. The morning peak demand, rather than the average load [132], is used as the clipping threshold to avoid unnecessary load shedding during periods when solar generation is sufficient to meet demand.

For load shifting (LS), the evening load is limited to the daily average of 2.33 kW, with excess demand redistributed to the low-load, high-solar generation window between 11 am and 1 pm. Since the combined demand of concurrently operating refrigerators and freezers is approximately 1.24 kW (see Table 3-2), sufficient capacity remains to support additional loads during this period. For simplicity, it is assumed that the curtailed evening load is evenly redistributed across the designated daytime hours.

Figure 3-17 shows the PC load profile while Figure 3-18 shows the LS load profile. With peak clipping the effect is a nearly constant load between 2 pm and 8 pm. With load shifting, the peak period shifts to 11 am – 1 pm. With peak clipping, the daily energy reduces to 51.69 kWh from the 55.97 kWh value for the No DSM and LS cases, an 8% reduction.

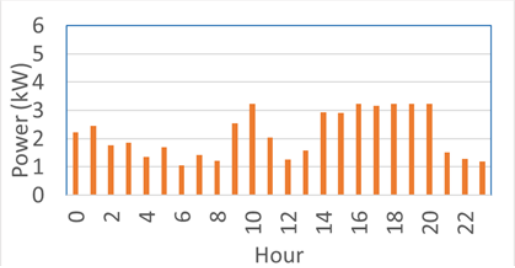

Figure 3-17: Profile after peak clipping (PC)

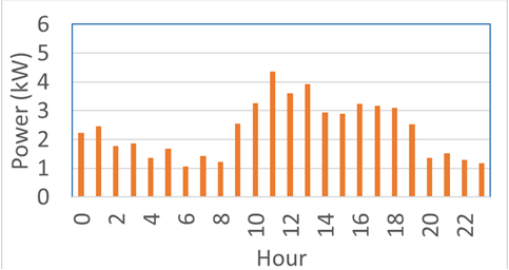

Figure 3-18: Profile after load shifting (LS)

System Design and Simulation in HOMER

The components of the modelled hybrid power system include the grid, solar PV, battery energy storage and a diesel generator. The system is modelled and optimized using HOMER Pro to determine the most cost-effective and technically feasible configuration. Figure 3-19 shows the schematic representation of the system, and Table 3-3 the hybrid system parameters.

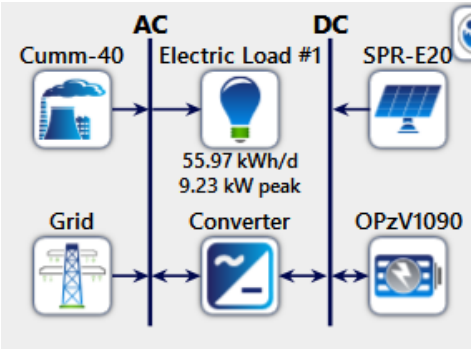

Figure 3-19: System schematic of Lwak convent (screenshot from HOMER Pro)

Table 3-3: System parameters

Component	Parameter	Value	Parameter	Value
PV	Type	SunPower E20-327	Capital cost	USD 3,300 / kW_p
	PV module rating	327 W_p	O&M cost	USD 10 / kW_p
	Efficiency	20.1%		
Converter	Lifetime	15 years	Capital cost	USD 300
	Efficiency	95%	Lifetime	15 years
Battery	Type	Sunlight 2V7 RES OPzV 1090	Capital cost	USD 300
	Capacity	120 kWh	O&M cost	USD 10
	System DC voltage	48 V	Number of Strings	3
Genset	Capacity	40 kW	Replacement Cost	USD 15,000
	Fuel cost	USD 1 / Litre	Diesel cost	USD 1 / Litre

SunPower E20-327 PV modules [217] were selected due to their comparable specifications to the SPR-320E-WHT-D modules used in similar studies for Kenya and Zimbabwe [218] [219].

A 40 kW diesel generator, modelled with the performance characteristics of the Cummins 40 kW genset, is incorporated into the HOMER simulation and the initial capital cost is set to zero.

The Load Following (LF) dispatch strategy is applied, where the generator is operated solely to meet the real-time load demand and does not contribute to battery charging. This differs from the Cycle Charging (CC) method in HOMER, which runs the generator at full capacity and diverts any excess energy to charge the battery bank.

The cost of electricity from the grid is set at USD 0.21 per kWh. As net-metering was not permitted under Kenya's energy regulations, grid export of surplus electricity is not considered in the model. The simulation assumes a discount rate of 7%, an inflation rate of 7.5%, and a project lifespan of 25 years. To ensure high reliability, the system design permits no annual capacity shortage (0%).

(i) Without DSM

Four scenarios are modelled without DSM and using the load profile in Figure 3-16:

- First scenario (S1): HOMER determines the PV system and battery sizes
- Second scenario (S2): System battery DC voltage set to 48 V, HOMER sizes the PV
- Third scenario (S3): System battery DC voltage set to 48 V, PV system size is specified as 16.5 kW
- Fourth scenario (S4): Business as usual (BAU) scenario with only grid and generator supply.

(ii) With DSM (Peak clipping and Load shifting)

Upon incorporating stochastic day-to-day (10%) and timestep (20%) variability factors to the PC load profile and LS load profile in HOMER, the simulation peak demands are 5.53 kW for peak clipping and 7.6 kW for load shifting, as illustrated in Figure 3-20 and Figure 3-21.

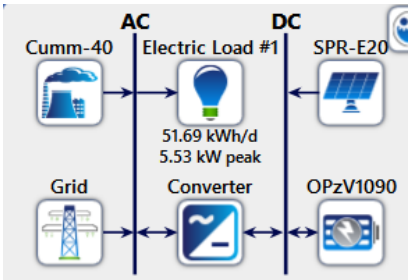

Figure 3-20: Peak clipping system schematic from HOMER

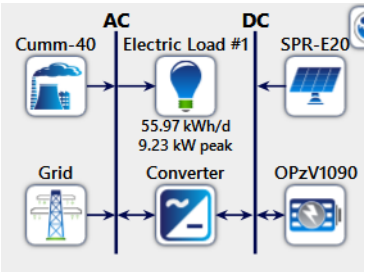

Figure 3-21: Load shifting system schematic from HOMER

3.5.2 Case Study 2 - Refrigeration temperature evolution and appliance ageing effects analysis

Modelling approaches used for Case study 2

(i) Refrigeration Temperature Model

The following equation is commonly used to model the temperature variation of a refrigerator [157] [158]:

$$T_{i+1} = \epsilon\ T_i + (1 - \epsilon)\left(T_{amb} - \frac{\eta p}{A}\right) \tag{3.1}$$

where

$$\epsilon = e^{-\frac{\tau A}{m_c}} \tag{3.2}$$

T_i is the fridge internal temperature (°C), T_{amb} is the ambient room temperature (°C), η is the coefficient of performance, p denotes the power when the fridge compressor is either on or off, A is the thermal conductance for the appliance in W/°C, m_c in J/°C is the thermal mass and τ is the temperature sampling interval.

A, which can also be expressed in SI units as W/K (equivalent to W/°C), represents heat flow per unit temperature difference between inside and outside of the appliance.

The general refrigeration model is applied to model temperature variation for one freezer, Freezer 6. It is important to emphasize that the main goal of this aspect of the research

was not to create a highly precise freezer temperature model, but rather to use a general model as a benchmark for comparison against data measured at Lwak.

(ii) Bonn method for evaluation of refrigeration efficiency and insulation effectiveness

The Bonn approach provides a method for quantifying the decline in refrigeration efficiency over time [167]. This method involves measuring the temperature rise under controlled conditions to assess insulation performance.

Since PUR foam is the most common component of the appliance walls, its degradation directly impacts thermal performance. The Bonn method is modelled as follows.

A decay constant d_τ is defined as:

$$d_\tau = \frac{1}{t}\ln\left(\frac{T_i\,(0)-T_{amb}(0)}{T_i\,(t)-T_{amb}(t)}\right) \tag{3.3}$$

where $T_i\,(t)$ is the internal appliance temperature at time t and T_{amb} is the ambient temperature.

The maximum decay constant value $d_{\tau_{max}}$, referred to in this work as the decay constant factor, can be correlated with the internal temperature rise of an appliance during the period it is switched off using a regression function [167]. This decay constant factor provides a measure of the effectiveness of the appliance's thermal insulation, and is calculated as

$$d_{\tau_{max}} = \max\,(d_\tau) \tag{3.4}$$

According to the Bonn method, $d_{\tau_{max}}$ is related to the heat transfer coefficient k (W/(m^{2}K)) by the equation

$$d_{\tau_{max}} = \frac{S\,k}{c_v} \tag{3.5}$$

where S is the surface area (m^2) and c_v is the isochoric (constant volume) heat capacity (J/K) which is determined by the materials used to build the refrigeration appliance walls [167].

Manufacturer specifications are typically used to determine c_v and S.

If S and c_v are known therefore, the heat transfer coefficient k can be calculated as

$$k = \left(\frac{c_v}{S}\right) d_{\tau_{max}} \tag{3.6}$$

The Bonn method is selected for this study because it is a non-intrusive method of evaluating refrigeration ageing and does not require knowledge of the appliance specifications. Thus it is suited to contexts where detailed information on refrigeration appliances is unavailable.

Determining of the heat transfer coefficients k of the four assessed freezers at Lwak and tracking insulation deterioration over time was beyond the scope of this research, as relevant manufacturer and purchase information was unavailable and due to the limited time over which the measurements were taken.

(iii) Refrigeration Ageing model

Previous studies [167] [220] [221] have examined how refrigeration appliance energy use increases over time. A study on refrigeration appliances in Germany reported an efficiency decline equating to a yearly rise in energy consumption of at least 1% [220]. This suggests that after a decade of operation, a unit's energy consumption could exceed its initial level by more than 10%.

In [221], an ageing model derived from measurements of 32 refrigeration appliances is given as

$$E_y(y) = 1 + 0.295 \left[1 - e^{-\left(y/6.517\right)}\right] \tag{3.7}$$

where

E_y is the normalised energy consumption and y is the appliance age (in years).

Due to the lack of energy performance labelling standards that take efficiency degradation over time into account, we propose a novel, first of the kind, ageing-aware efficiency labelling standards approach for refrigeration appliances. The standards are proposed for East Africa, though the approach could be adopted for other regions and countries.

The ageing model in Equation 3.7 is used to develop the proposed standards.

(iv) Energy Consumption and Efficiency categorisation for refrigeration appliances

The East African Community (EAC) Energy Performance standards are described below [170] [222].

Annual Energy Consumption (AEC) is

$$AEC = EC_T \left(\frac{365}{1000}\right) \quad (3.8)$$

with

$$EC_T = a\ (EC_{16}) + \ b\ (EC_{32}) \quad (3.9)$$

where

AEC is annual Energy Consumption in kWh / year and EC_T is energy consumption in Wh / day based on ambient temperature T and rounded to the nearest integer. EC_{16} is daily energy consumption measured at an ambient temperature of 16°C, EC_{32} is daily energy consumption measured at an ambient temperature of 32°C measured as per IEC 62552-3, and a and b are weighting coefficients corresponding to EC_{16} and EC_{32} respectively, with a and b summing up to 1.

For various reference ambient temperatures, corresponding values of a and b are shown in Table 3-4.

Table 3-4: Reference ambient temperatures for refrigeration appliance daily energy consumption

Reference ambient temperature (°C)	***a***	***b***	**Reference**
20	0.75	0.25	[170]
24	0.5	0.5	[170]
32	0	1.0	[170]
32	-0.014	1.104	[222]

The average ambient temperature is assumed to be 25 °C, so 32°C is used as the reference ambient temperature in the calculations [222]. This is because if the ambient temperature falls between 24 °C and 32 °C, the 2021 U4E (United for Efficiency) report for regional harmonization of MEPS and labels for refrigerators in the EAC and the SADC stipulates the use of 32 °C as the reference ambient temperature for efficiency evaluations [170].

Adjusted volume (AV) is calculated as [170] [222]:

$$AV = \sum_{j=1}^{J} V_j\ K_j\ F_j \quad (3.10)$$

with

$$K_j = \frac{T_1 - T_j}{T_1 - T_2} \tag{3.11}$$

where V_j represents the volume in the jth compartment of the appliance in Litres, K_j is the volume adjustment factor for the jth compartment (to two decimal places) and F_j is the frost adjustment factor for the jth compartment. F_j = 1.1 is applied to frost-free (automatic defrost) frozen food compartments, whereas F_j = 1.0 is assigned to all other compartment types, including manual defrost frozen food compartments.

T_1 is the reference ambient temperature (°C), T_2 is the fresh food compartment temperature (4°C), and T_j is the temperature of the jth compartment (°C).

Table 3-5 presents K values for a reference ambient temperature of 32°C [170] [222].

Table 3-5: Some values of volume adjustment factor K

Reference ambient temperature	**Fresh food compartment**	**Frozen food compartment**	
T_1 = 32°C	K = 1 (T_2 = 4°C)	T_{comp} = - 6°C	K = 1.36
		T_{comp} = - 9°C	K = 1.46
		T_{comp} = -12°C	K = 1.57
		T_{comp} = -15°C	K = 1.68
		T_{comp} = -18°C	K = 1.79

The maximum annual energy consumption (AEC_{max}) in kWh/year for various appliance categories, given a reference ambient temperature of 32 °C, must remain within the limits specified in Table 3-6.

Table 3-6: Values of maximum annual energy consumption (AEC_{max}) [170]

Reference ambient temperature	**Product Category**	AEC_{max} **(kWh/year)**
32°C	Refrigerators	0.220 AV + 137
	Refrigerator-Freezers	0.288 AV + 210
	Freezers	0.268 AV + 247

Using the Energy consumption index R, calculated as

$$R = \frac{AEC_{max}}{AEC} \tag{3.12}$$

the UNEP E4C recommendations for the EAC and SADC regions [170] categorise the refrigeration appliances' efficiency as being low, intermediate or high, as per Table 3-7.

Table 3-7: Labelling categories for refrigeration appliances [170]

Grade	**Refrigerators**	**Refrigerator-Freezers**	**Freezers**
High Efficiency	$1.50 \leq R$	$1.50 \leq R$	$1.50 \leq R$
Intermediate efficiency	$1.25 \leq R < 1.50$	$1.25 \leq R < 1.50$	$1.25 \leq R < 1.50$
Low efficiency	$1.00 \leq R < 1.25$	$1.00 \leq R < 1.25$	$1.00 \leq R < 1.25$

In this work, we go ahead to compare the standard refrigeration efficiency labelling standards for EAC (and SADC) in Table 3-7, with a proposed novel approach that incorporates ageing for the development of more realistic lifetime-aware efficiency labelling standards for refrigeration appliances.

Load profile

The average daily maximum power demand (kW) measured using a Mavowatt 230 power quality analyzer from 6th to 10th February 2023 for all 3 buildings at the Lwak site is plotted in Figure 3-22. There are two distinct peaks, an early morning peak between 4 am and 6 am, and a larger evening peak from 6 pm to 10 pm. For a more robust system design, particularly with regard to solar PV and battery sizing, the maximum measured demand values are utilised and plotted.

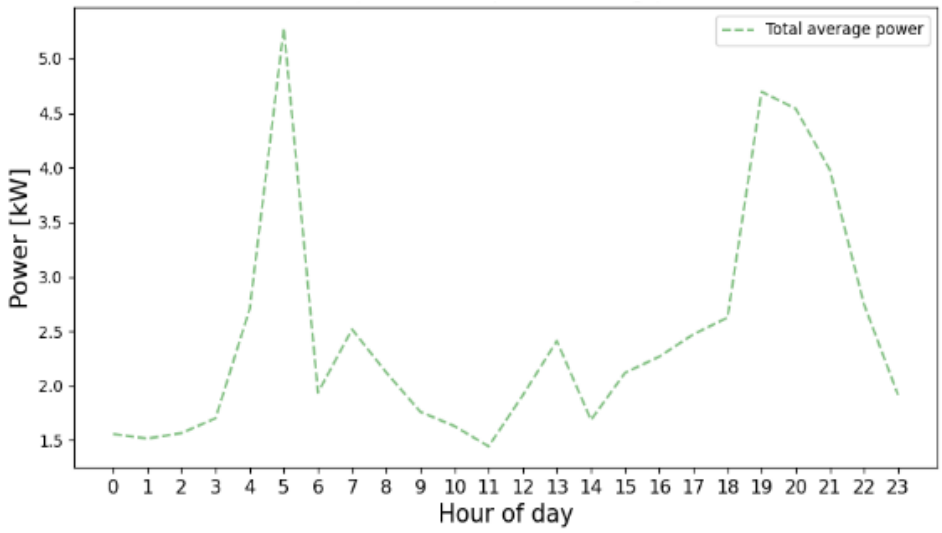

Figure 3-22: Load profile showing average hourly maximum power demand at Lwak from 06 - 10 February 2023

Refrigeration power analysis

Figure 3-23, Figure 3-24 and Figure 3-25 depict the power of the 8 refrigeration appliances, measured at different times using the Edimax SP-2101W V3 smart plugs.

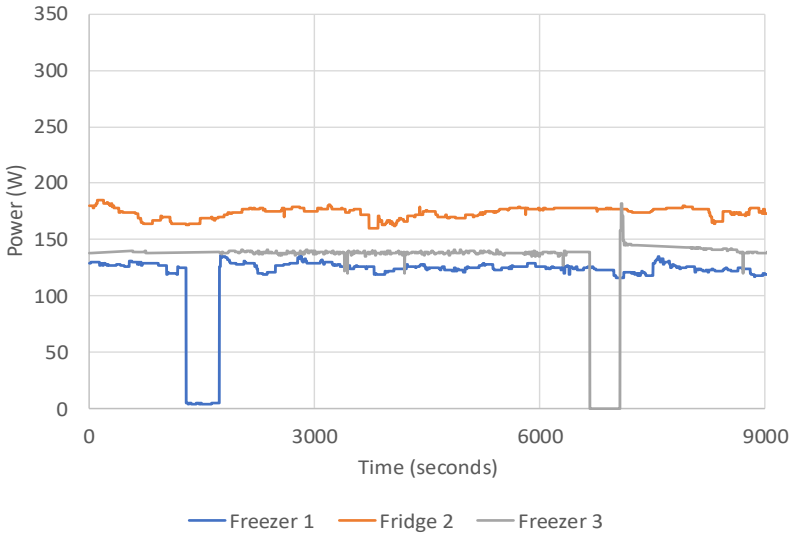

Figure 3-23: Power consumption of Freezer 1, Fridge 2 and Freezer 3 in Building 1

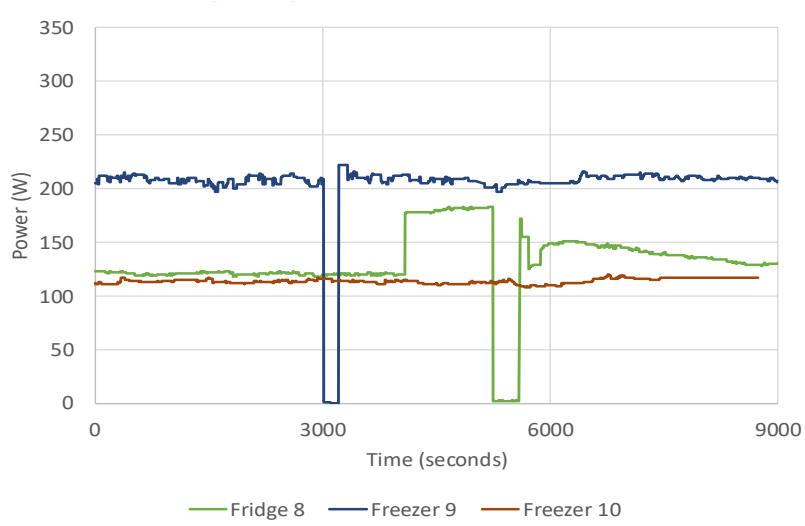

Figure 3-24: Power consumption of Fridge 8, Freezer 9 and Freezer 10 in Building 2

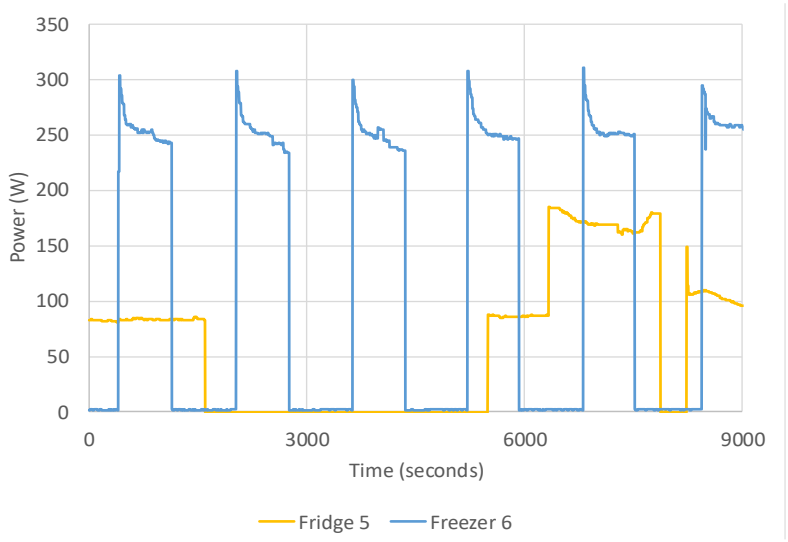

Figure 3-25: Power consumption for Fridge 5 and Freezer 6 in Building 3

Freezer 1, Fridge 2, Freezer 3, Fridge 8, Freezer 9, and Freezer 10 have fairly constant power usage patterns. For these appliances, instances during the measurement interval where the recorded power drops to 0 W are attributed to gaps in data logging.

In contrast, Fridge 5 and Freezer 6 in Building 3 show distinct cyclic behaviour consistent with compressor on–off operation. The large increases in power demand for Fridge 8 at around 4000 seconds and for Fridge 5 at about 6500 seconds are attributed to user actions like door opening and/or addition of warm items.

Table 3-8 shows the details (from the available information) and measured power for the refrigeration appliances. The average total refrigeration load is 1.228 kW for all appliances. For inverter-based systems, peak demand is an important design parameter, hence the peak measured power values are also given in Table 3-8.

Table 3-8: Refrigeration Appliance Details

Appliance	Location	Description	Power rated (W)	Average measured /average ON state Power (W)	Peak measured power (W)
Freezer 1	Building 1	Bruhm BCF-398SD	-	123	139
Fridge 2	Building 1	Toshiba GR-EF 33	-	174	185
Freezer 3	Building 1	HTCF208A2	94	133	182
Fridge 5	Building 3	Haier	-	62 / 83	185
Freezer 6	Building 3	ArmCoAF-C38(K)	210	112 / 265	311
Fridge 8	Building 2	Goldstar GR-312S	120-140	132	183
Freezer 9	Building 2	-	-	204	222
Freezer 10	Building 2	Bruhm BCF-398SD	-	114	120

For Freezers 3 and 6 (see Table 3-8), the measured instantaneous power demand and energy consumption exceeded their rated values. Such discrepancies may arise from reduced heat dissipation capability due to dust on radiator fins, air leakage through degraded door seals, or performance degradation of compressors and fans with age. Mitigation of these inefficiencies can be done for instance, by increasing the effective thermal mass of partially filled units by adding containers with phase-change materials (PCM) or water to slow temperature rise during compressor or appliance off periods. In [177], use of plates containing a commercial PCM was able to keep internal freezer temperatures 4 - 6 °C lower during a three-hour power cut. However this study did not extend to PCM incorporation.

A limitation of this study is that the refrigeration appliances were loaded to different extents. Freezers 6 and 10 were completely full, Freezers 1, 3, and 9 were partially filled,

and all fridges were less than half full. Despite the disparities in stored contents amounts, thermal mass is not considered in this analysis. Ambient temperature effects as well as the frequency and duration of door openings are also not considered in the assessment.

Refrigeration temperature analysis

The objective of this work was to determine the feasible off-time for potential refrigeration load shifting or curtailment DSM for Lwak.

This study examines the temperature trajectories of four freezers, namely Freezers 1, 3, 6, and 10. The rate of internal temperature increase was assessed by switching off their power supply for varying durations (126 minutes, 170 minutes, 7.5 hours and 84 minutes for Freezers 1, 3, 6 and 10 respectively) while recording and logging the temperature changes, after which they are switched on.

Their initial temperatures varied, as shown in Figure 3-26 which illustrates the measured off-state temperature changes of the four freezers.

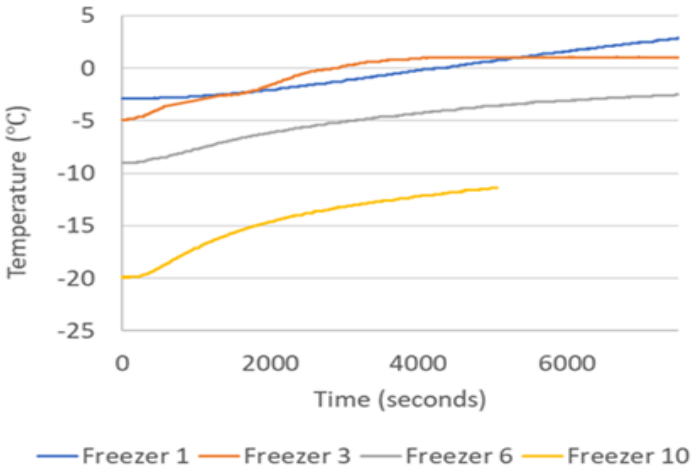

Figure 3-26: Freezers 1, 3, 6 and 10 temperature evolution when switched off

Except for Freezer 10 (refer to Figure 3-26), measured temperatures notably exceed the recommended minimum temperature for freezers (-18°C typically, [158] cites -12°C). Freezers 3, 6, and 10 exhibit relatively comparable temperature gradients below 5000

seconds, and in general the slopes tend to level off with time, indicating a transition towards thermal equilibrium.

The temperature profiles of Freezers 1, 3, 6, and 10 when switched off and then back on using the Edimax SP-2101W V3 smart plugs are presented in Figure 3-27. Each freezer started at a different initial temperature, reflecting variations in thermostat settings and prior operating conditions. It was not monitored whether, or for how long, the appliances were opened during the measurement periods.

Except for Freezer 10, the off temperatures rose above recommended safety thresholds. For off-periods shorter than 5000 seconds, the rates of temperature increase in Freezers 3, 6, and 10 were comparable. With longer off-times, the initially linear temperature rise began to level off. Differences in thermal mass (due to varying load capacities), ambient room temperatures, and door opening were not accounted for in this analysis.

The onset of temperature decline corresponds to power restoration. Freezer 6, which was fully loaded, remained off for the longest interval, exhibiting a rise from -9 °C to -0.8 °C over six hours, and an 8.7 °C increase from -9 °C to -0.3 °C over seven hours.

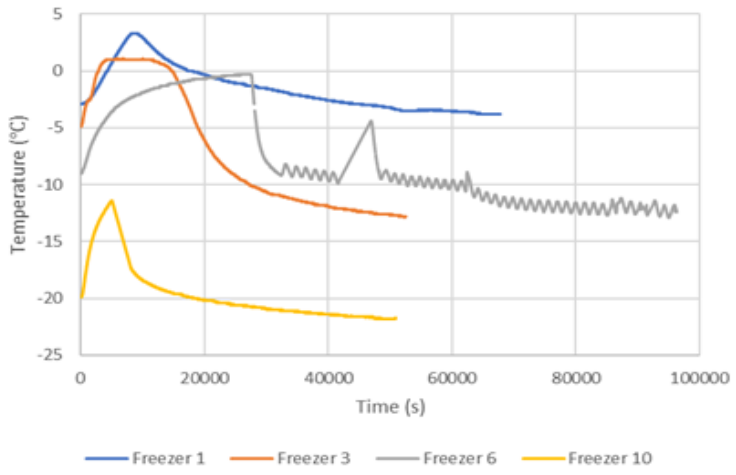

Figure 3-27: Freezer 1, 3, 6 and 10 temperature profiles for off and on states

If the freezer and refrigerator thermostats are adjusted to their lowest temperature settings, and an appliance has sufficient thermal mass and the specifications to achieve the off-state profile observed in Freezer 6, the rise in internal temperature during a 7-hour power outage could be limited to 8 °C or less. Such an extended off-cycle would be advantageous for demand side management, peak load reduction, and load shifting of

refrigeration systems. For example, a conservative controlled cycle could involve 3 - 4 hours of on operation followed by 3 - 4 hours of off time.

3.5.3 Case study 3 - DSM using PSO for refrigeration appliances

From the data collected using the Edimax SP-2101W V3 smart plugs and raspberry pi 3 microcontrollers with AM2302 sensors, the freezer measurements revealed that internal temperatures could remain within an 8 °C range during off periods of 3 - 4 hours, and even up to 7 hours for Freezer 6. This off duration can be further prolonged by increasing the thermal mass of the contents (for instance using water or phase-change materials), by lowering the thermostat settings so that the off cycle begins at a cooler starting point, by reducing the frequency and duration of door openings, or by improving the appliance's insulation.

Using these insights, a conservative demand-side management strategy is suggested as follows. Freezer 6 operates on a 4-hour ON and 2-hour OFF cycle, while the remaining appliances follow a 5-hour ON and 1-hour OFF schedule. This is based on the assumption that the other units have lower thermal inertia and therefore require longer ON periods to ensure food safety (see Table 3-9). It is also assumed that the load profile for the next 24 hours is perfectly known [39], which may be feasible if, for example, forecasting methods are integrated [132].

Table 3-9: Refrigeration appliance control cases

	Freezer 1, Fridge 2, Freezer 3, Fridge 5, Fridge 8, Freezer 9, Freezer 10	**Freezer 6**
Switching cycle	5:1 hourly ON:OFF cycle over 24 hours	4:2 hourly ON:OFF cycle over 24 hours

It is assumed that within each 6-hour interval, Freezer 6 remains off for two hours. Even in cases where two consecutive intervals place the Freezer 6 off periods back-to-back such that the final two hours of one interval and the initial two hours of the next coincide, the maximum continuous off duration is limited to 4 hours. This remains within the acceptable food safety temperature limits for Freezer 6, as established by the measurements discussed in Section 3.5.2.

Some studies have carried out on load shifting with the objective of increasing renewable energy usage such as [23], but in this work the focus is on improving the load factor, but subject to the limitations imposed by food safety considerations of the site's refrigeration loads. Modelling using the DSM load profile is also done for a hybrid solar system setup.

DSM modelling approach for the refrigeration loads

Customer comfort has been recognized as a key objective in the control of thermostatically controlled loads (TCLs) [17]. A study [31] showed that refrigerator-based decentralized refrigerator control, when combined with an energy storage system (ESS), can support autonomous microgrid frequency regulation and simultaneously lower ESS capacity requirements when user comfort and participation considerations are incorporated. Comfort is compromised though when frequency deviations are large, as this translates into larger variations in temperature.

In this case study 3, customer comfort is assumed not to be compromised, since the imposed appliance operation curtailments are taken to be such that internal temperatures remain within acceptable food safety limits.

To simulate load shifting at Lwak, the eight refrigeration units are modeled as shiftable PSO algorithm-scheduled devices in a constant tariff grid-connection setup. The appliance operational times (Table 3-9) are defined based on the temperature measurements in Section 3.5.2. This approach contrasts with that in [32], where temporal staggering was done by incrementally activating additional refrigeration units during the control window.

3.5.3.1 PSO Algorithm model description

The target curve $Targ_h$ is defined as the forecasted hourly load power, where the forecasted load corresponds to the load profile in Figure 3-22. Equation (3.13) was selected to represent the target curve since the Kenyan grid tariff is constant, rendering price-based optimization infeasible. This approach could be adopted in microgrids with constant tariffs as well.

$$Targ_h = \frac{\sum_{h=1}^{H} \left(load_{fc_h} \right)}{H} \tag{3.13}$$

where $Targ_h$ represents the target load power, $load_{fc_h}$ is the forecasted load at hour h and $H = 24$.

The non-shiftable loads are treated as a single aggregated, time-varying load [223][199]. The reducible load margin (RLM) at hour h, defined as the difference between the forecasted load and the target load, is given by

$$RLM_h = load_{fc_h} - Targ_h \tag{3.14}$$

The sign of RLM determines the required marginal load adjustment; a positive value indicates that the forecasted load exceeds the target and thus requires load reduction through device disconnection, while a negative value signifies that additional load should be connected.

To align the actual load with the target, the following objective function f_h is formulated:

$$\text{Minimise: } f_h = [\,|RLM_h| - |\Delta load_h|\,] \tag{3.15}$$

where RLM_h is the desired load adjustment and $\Delta load_h$ is the actual change in load at hour h.

RLM_h represents the desirable change in load necessary to match the load curve to the target curve $Targ_h$, but this adjustment cannot be realized exactly. The objective function f_h therefore seeks to ensure that the implemented load change $\Delta load_h$ matches RLM_h as closely as possible.

The net load change at each hour can be expressed as

$$\Delta load_h = connect\ (h) - disconnect\ (h) \tag{3.16}$$

where $connect\ (h)$ denotes the loads connected at hour h and $disconnect\ (h)$ the loads disconnected at hour h.

The power contribution at hour h from devices whose operation has been shifted to earlier start times is expressed as

$$connect(h) = \sum_{d=1}^{N_d} \sum_{m=1}^{g_d} \sum_{l=1}^{h-1} X_{dl(h-m+1)}\, P_{md} \tag{3.17}$$

where

$connect(h)$ computes the power at hour h due to devices that were shifted to start at earlier times l, such that h is their m^{th} hour of operation. h denotes the hour of the day ($h \in \{1,2,\dots,24\}$), d denotes the types of devices, N_d is the total number of types of devices, m is the hour of operation of device d, g_d is the operation duration (in hours) of device type d, P_{md} denotes power consumption for device type d in its m^{th} hour of operation, X_{dlh} denotes the number of devices of type d shifted to start earlier to hour l from h.

$$disconnect(h) = \sum_{d=1}^{N_d} \sum_{m=1}^{g_d} \sum_{q=h+1}^{h+s_d} X_{d(h-m+1)q}\, P_{md} \tag{3.18}$$

sums up the power that would have existed at hour h as the m^{th} hour of operation for devices that would have started running at $(h-m+1)$, but were shifted later or delayed to start at time q, and s_d is the maximum number of hours device d can be shifted forward or delayed [41] while still completing its operation within its allowed window $[B_d, E_d]$. B_d is the earliest time device d can start running and E_d is the latest time device d can finish running.

The constraints include the following:

$$X_{dhq} = 0, \quad \text{for } q < h\ ,\ q > h + s_d \tag{3.19}$$

i.e. maximum shifting delay for device d should not exceed s_d hours.

$$X_{d_h} \leq A_{dh} \tag{3.20}$$

i.e. at any hour h, the number of devices of type d being either connected or disconnected must not exceed those available for control A_{dh} in that hour.

$$X_{dh} \geq 0 \tag{3.21}$$

i.e. the number of devices for shifting must be non-negative.

These govern the decision to connect or disconnect loads at each time step, with the aim of shaping the load curve to more closely follow the target [106].

The simulation is implemented in MATLAB 2023. A constant electricity tariff of 0.18 USD/kWh, applicable to Kenyan domestic grid customers [224], is used for cost evaluation. The optimization is carried out using particle swarm optimisation (PSO) with a maximum iteration limit of $iter_{max}$=100, inertia weight w varying from 0.4 to 0.9, acceleration constants $c_1 = c_2 = 2$, random coefficients φ_1 and φ_2 within [0,1] [39] and a swarm size of 100.

Load shifting over 24 hours has been discussed in studies such as [132] [39]. DSM (strategic conservation and load shifting) of the refrigeration loads using PSO was applied to the 24 hour average load profile described in Figure 3-22. The shifting capacity is only a few hours, and thus considering one day in this case study is deemed sufficient.

3.5.3.2 Modelling of hybrid solar PV-battery system

A PV system with battery storage was planned for installation at the Lwak site with the specifications below:

- PV array: 12.45 kW_p, comprising 30 JA Solar JAM72S10-415W modules connected to 3 SMA Sunny Boy 5.0 inverters.
- Battery energy storage system (BESS): 37.58 kWh capacity, utilizing 36 Hoppecke Sun Power VR M 12-105 lead-acid batteries connected to 3 SMA Sunny Island 8.0H-13 inverters.

The general system topology is illustrated in Figure 3-28.

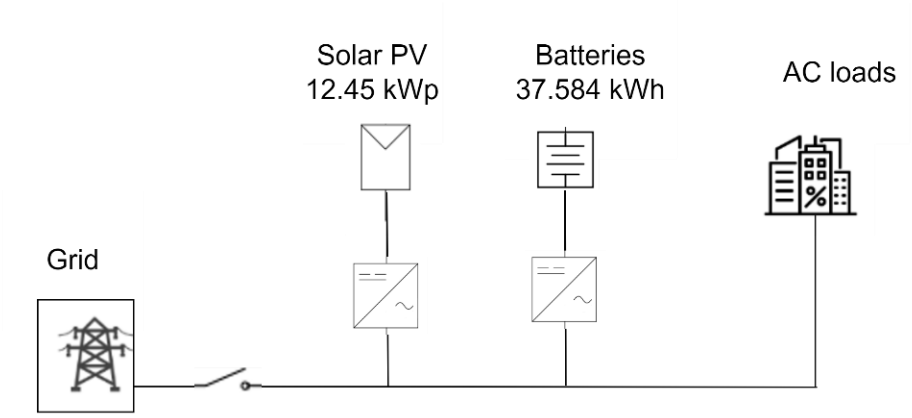

Figure 3-28: Schematic of the proposed hybrid energy system at Lwak

The AC loads are categorized into two groups: non-shiftable (base) loads and shiftable loads (refrigeration appliances). For this analysis, the grid is assumed to be 100% reliable thereby ensuring zero loss of load, hence the shared generator is not considered.

The 24-hour load profiles without DSM [225] and with PSO-based DSM (incorporating strategic conservation and load-shifting) are used in the system modelling. The simulations were done using MATLAB 2023 for the day in 2022 with the lowest solar irradiance and hence the minimum PV generation. Hourly irradiance and temperature data for the Lwak site were obtained from the NASA database [226]. Minimum and maximum battery state of charge (SOC) was specified as 50% and 100% respectively.

PV output is given by:

$$P_{PV}(t) = P_r \, f_d \, \frac{G(t)}{G_{ref}} \left[1 + K_T \left(T_c - T_{ref}\right)\right] \tag{3.22}$$

and

$$T_c = T_{amb} + 0.0256 \, G(t) \tag{3.23}$$

where P_{PV} denotes the PV generated power (kW), P_r is the rated PV capacity under standard test conditions (STC) (kW), $f_d = 0.9$ is the derating factor [227]. $G(t)$ and G_{ref} represent the incident solar radiation in kW/m^2 and at STC of 1 kW/m^2 respectively, the temperature coefficient of power K_T = - 0.0037/°C, T_c, T_{ref} = 25 °C and T_{amb} denote the cell temperature, reference temperature and ambient temperature respectively, in °C.

The equations for battery charging (Equation 3.24) and discharging (Equation 3.25) are

$$E_B(t) = E_B(t-1) + \left(E_G(t) - \frac{E_L(t)}{\eta_{conv}}\right) \eta_{bat}\eta_{ch} \quad (3.24)$$

$$E_B(t) = E_B(t-1) + \left(E_G(t) - \frac{E_L(t)}{\eta_{conv}}\right) / \eta_{bat}\eta_{disch} \quad (3.25)$$

with

$$E_G(t) = P_{PV}(t)\,\eta_{conv} \quad (3.26)$$

where $E_B(t)$ is battery energy at time t, E_G denotes PV AC energy, E_L denotes the load energy, η_{conv} is converter efficiency, η_{ch} is battery charging efficiency, η_{disch} is battery discharging efficiency and η_{bat} is battery inverter efficiency.

The system is subject to the following constraints

$$P_G(t) + P_{Grid}(t) = P_L(t) + P_{Bat}(t) \quad (3.24)$$

$$E_{Bmin} < E_B(t) < E_{Bmax} \quad (3.25)$$

where $P_G(t)$ is PV AC power (kW), P_L is load power (kW), P_{Grid} is grid power (kW) supplied to the load at time t, E_{Bmin} and E_{Bmax} are battery minimum and maximum energy respectively. Battery power P_{Bat} (kW) is positive when charging and negative when discharging.

The model parameters are shown in Table 3-10.

Table 3-10: System parameters for hybrid PV system [227][228][229][224]

Component	Parameter	Value	Parameter	Value
PV	PV module rating	0.415 kWp	Derating factor	0.9
	PV capacity	12.45 kWp		
Battery	Nominal capacity	87 Ah	Charging efficiency	98%
	Nominal voltage	12 V	Discharging efficiency	98%
	System DC voltage	48 V	Minimum SOC (%)	50%
	System storage capacity	37.584 kWh	Maximum SOC (%)	100%
			Initial battery SOC (%)	50%

Converter	Power rating	15 kW	Efficiency	96%
	Battery inverter efficiency	96%		
Grid	Tariff	0.18 USD/kWh		

The dispatch algorithm depicted in Figure 3-29 prioritizes load supply from PV generation. When PV generation exceeds the demand, the excess PV energy is used to charge the batteries if SOC < 100%. Any surplus PV generation beyond the load and charging requirements is curtailed. When PV energy is insufficient to cover the demand, the battery discharges if the SOC > 50%. If the battery energy is insufficient, then the grid supplies the unmet demand. Grid reliability is assumed to be 100%.

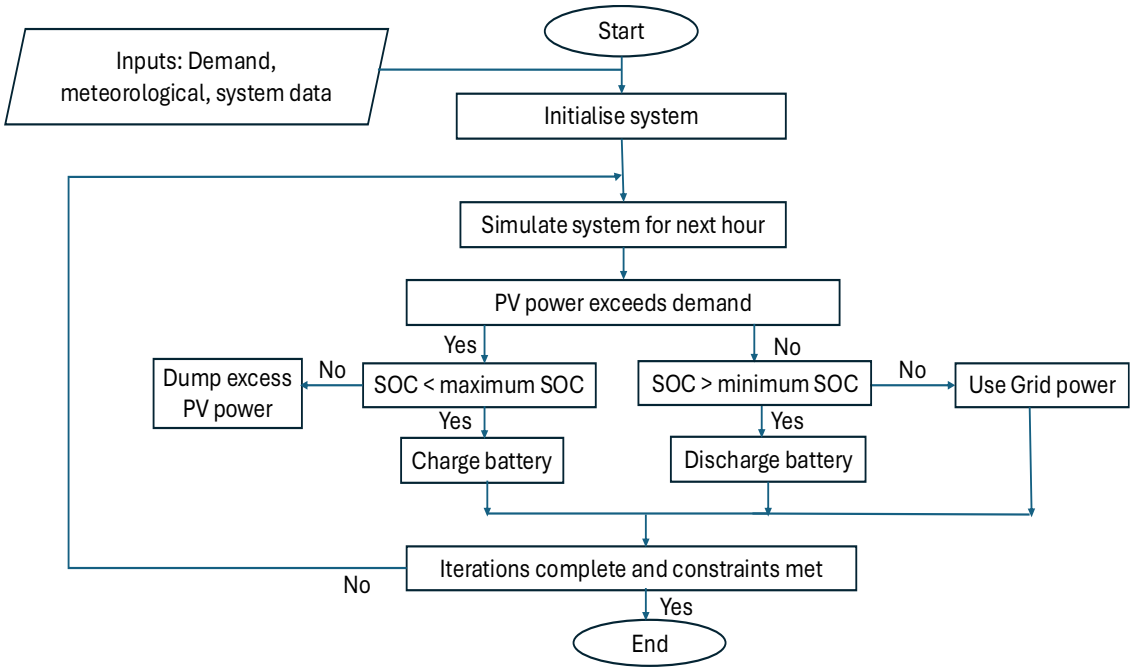

Figure 3-29: Dispatch algorithm for the hybrid PV system at Lwak

The two scenarios were modelled are:

- Scenario 1: No DSM + PV + battery storage + grid
- Scenario 2: DSM + PV + battery storage + grid

3.5.4 Case study 4 - Battery SOC and temperature-based refrigeration control

This study experimentally investigated demand-side management (DSM) of refrigeration appliances by utilizing battery state of charge (SOC) and freezer temperature values for automated control, thereby eliminating the need for user intervention. For the fridges, the DS18B20 temperature sensors were placed within the freezer compartments. The study was conducted for the solar PV with battery system deployed at the Lwak site, described in Section 3.2.1. A limitation is that in this experimental study, the effects of door opening, food loading and unloading, ambient temperature and thermal mass are not considered.

This experimental setup is illustrated in Figure 3-30.

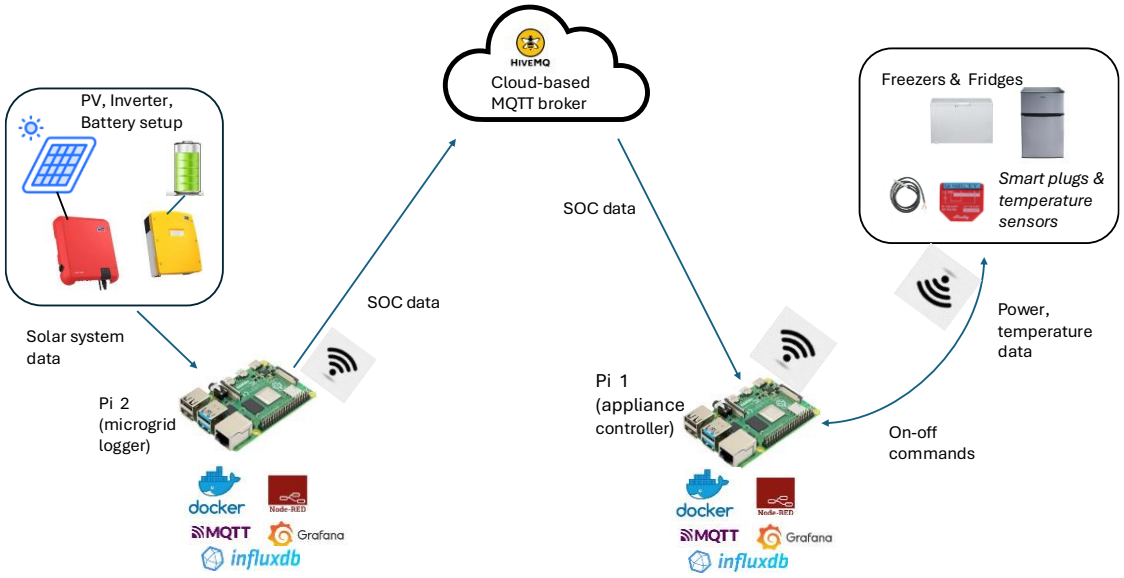

Figure 3-30: Experimental setup for temperature and battery SOC-based load control

Two cases are evaluated:

Case 1: No control (baseline)

Power consumption of three refrigerators and five freezers was measured without any control intervention. It was observed that the majority of the appliances operated above the recommended temperature threshold of -18 °C for freezers.

Case 2: SOC and Temperature-based control

The control decision flow is depicted in Figure 3-31.

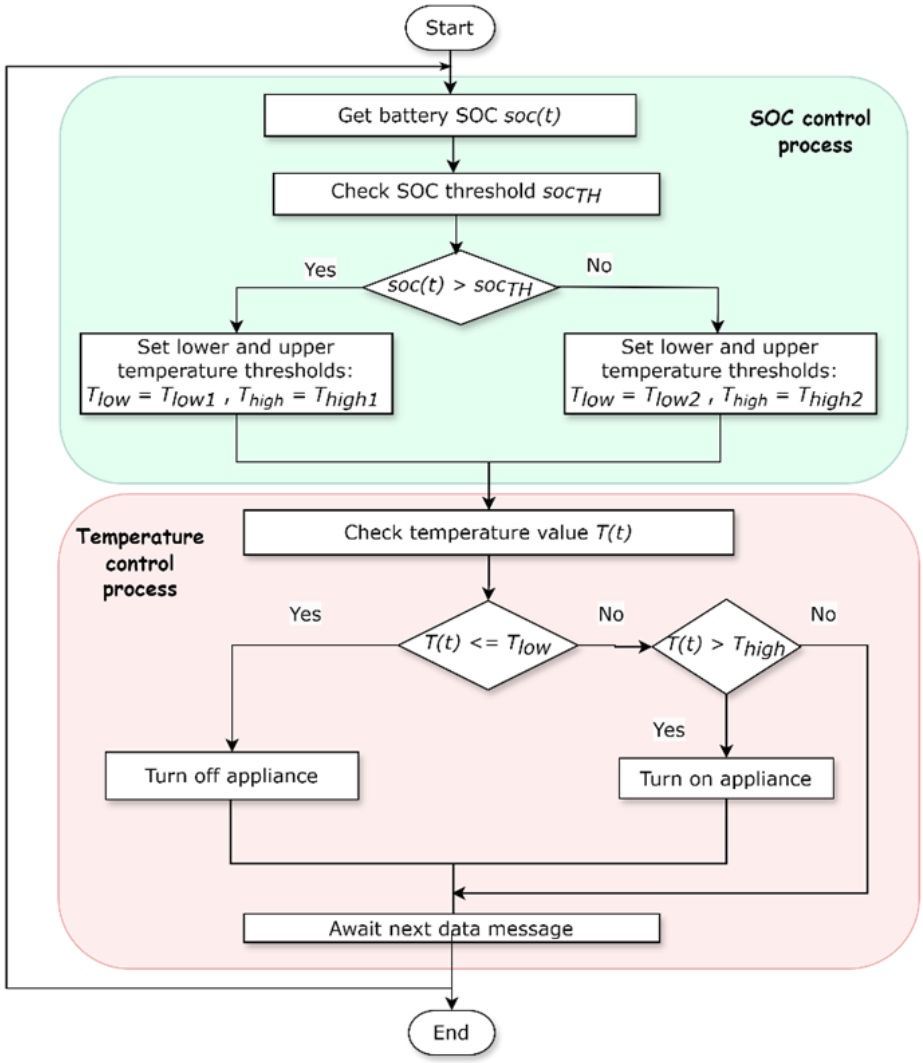

Figure 3-31: Decision flow for SOC and temperature-based control

Two sets of appliance control temperature thresholds were defined for Case 2. Appliance temperature data, measured continuously using DS18B20 sensors, was relayed to the controller (Pi 1). SOC control was based on the battery SOC for Building 3. A SOC threshold (soc_{TH}) of 75% was used for switching between the two sets of temperature control thresholds. In the microgrid system, the battery minimum state of charge (SOC) was set to 50%.

When SOC >75%, the appliance controller (Pi 1) was configured to regulate the operation of fridges and freezers according to the temperature thresholds specified in Table 3-11. Since the appliances had different baseline temperatures, the T_{low1} thresholds varied. When an appliance's temperature drops to or below the lower threshold T_{low1}, Pi 1 sends a signal to the corresponding Shelly smart plug to switch the appliance off. As the internal temperature subsequently rises above the upper threshold T_{high1}, Pi 1 switches on the appliance.

Table 3-11: Temperature thresholds for temperature based control

Appliance	Lower temperature threshold T_{low1} (°C)	Upper temperature threshold T_{high1} (°C)	Description
Freezer1	-15	-12	Bruhm BCF-398SD
Fridge2	-15	-12	Toshiba GR-EF 33
Freezer3	-14	-12	HTCF208A2
Fridge 5	-18	-12	Haier
Freezer6	-14	-12	ArmCoAF-C38(K)
Fridge 8	-15	-12	Goldstar GR-312S
Freezer9	-14	-12	-
Freezer10	-18	-12	Bruhm BCF-398SD

The difference between the upper and lower temperature thresholds is called a deadband [230]. In this study, the same upper deadband thresholds (T_{low2} and T_{high2}) were applied to all appliances when SOC ≤ soc_{TH}. Being below freezing point, it is taken that they are sufficient to maintain the safety of freezer food contents. The aim is to reduce refrigeration power consumption during periods with lower battery energy reserves.

When SOC ≤ 75% therefore, the temperature thresholds were increased to $T_{low2} = -10$ °C and $T_{high2} = -6$ °C. These higher thresholds were chosen primarily because they are higher than the ones in Table 3-11, so as to reduce appliance power consumption under low SOC conditions.

For appliances with lower baseline temperatures, both sets of control temperature thresholds would be set to lower values, to align closer to recommended freezer temperatures.

The strategy presented in this study is analogous to precooling, a technique that shifts cooling load from peak to off-peak hours [231], often based on TOU tariffs [184]. In this experimental setup however, appliance operation is governed by the battery SOC rather than dynamic pricing.

It can also be seen as relating to [33], where the authors investigate the application of electric water heaters (EWHs) as a means of frequency regulation, with a temperature setpoint of 55°C (T_{set}), and upper and lower water temperature deadband values of 60°C (T_h) and 50°C (T_l) at which the devices turn off and on respectively. When frequency is high and all EWHs are already on, to lower the frequency, participating EWHs have their temperature setpoint (T_{set}) raised by $T_{band} = T_h - T_l$ so as to raise the power demand.

The rebound effect, characterized by a sharp surge in demand when multiple refrigeration units restart simultaneously after load shedding or an outage, can lead to transient overloading and loadshedding to recur. However, because in this study the appliances are at different internal temperatures when the SOC threshold is reached, the rebound effect is not considered.

3.5.5 Case study 5 - E-mobility and portable storage integration in a microgrid

3.5.5.1 Energy consumption of microgrid customers in Uganda

Winch Energy (WE) Limited / NOA Uganda operates several off-grid renewable energy microgrids in Uganda, including Senyondo and Buzaami-Bugoma microgrids at Bunjako on the shores of Lake Victoria and 25 microgrids in Lamwo district, Northern Uganda [232]. The microgrids use containerised Remote Power Units (RPUs), modular systems that combine solar PV equipment with battery storage.

For this study, customer power consumption data from eight Winch Energy microgrids located in Central Uganda and Lamwo district, Northern Uganda was analysed (see Figure 3-3). These microgrids, situated in rural communities, have 100% renewable energy supply. An overview of the system configuration is illustrated in Figure 3-32.

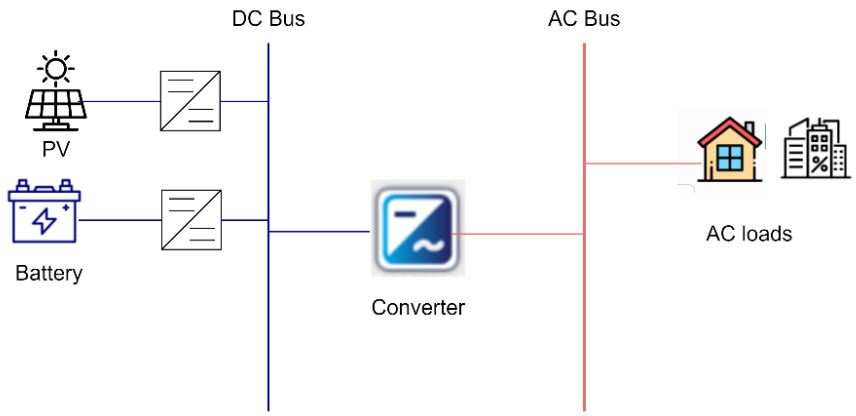

Figure 3-32: General setup of the 8 mentioned microgrids (MGs) in Uganda

The 8 microgrids commenced operation in 2022, providing an opportunity to analyse relatively recent datasets that reflect current consumer behaviour under fully renewable, off-grid electrification schemes. Using smart meter data logs from 866 customers, the average customer load profile per microgrid was generated as presented in Figure 3-33.

Most of the aggregated profiles reveal a distinct evening peak in demand, which is characteristic of rural and residential-dominated energy consumption. Consumption during daytime hours remains comparatively low, reflecting limited daytime use of electricity characteristic of businesses. Such patterns point to a significant untapped potential for DSM and productive use stimulation, aimed at elevating daytime electricity demand. Enhancing daytime demand would improve the load factor and increase both the technical and economic efficiency of the microgrids.

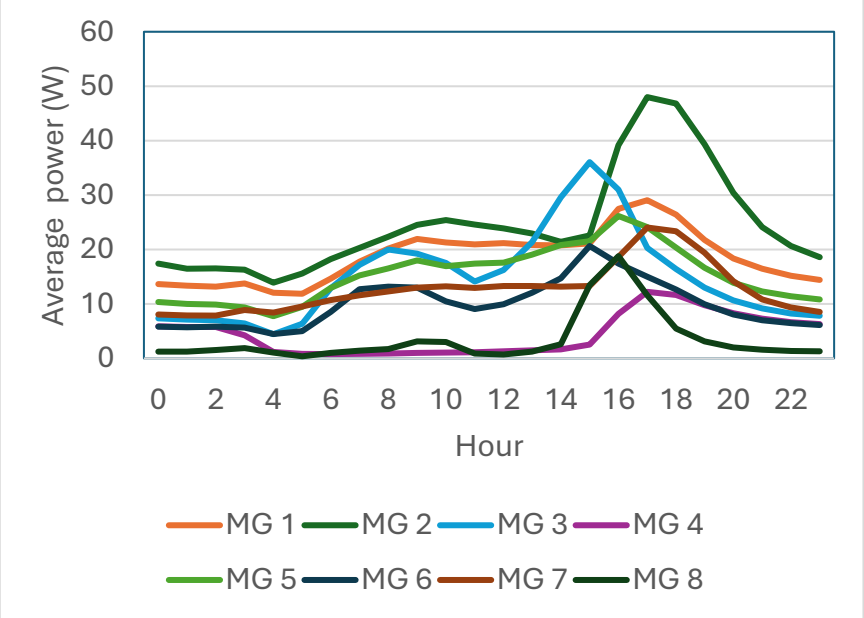

Figure 3-33: Average daily consumption of customers of 8 microgrids (MGs) in Uganda

For the purposes of this study, no distinction is made between residential and commercial customers. While customer types tend to exhibit different load characteristics, the objective here is to establish the average microgrid customer consumption, irrespective of category. This approach ensures that this analysis captures the average daily customer energy needs, which feeds into subsequent analysis.

The analysis of smart meter records from the 866 customers across the 8 microgrids revealed an average daily consumption of approximately 312 Wh per customer. This relatively modest demand is consistent with the typical consumption patterns of rural off-grid households in sub-Saharan Africa, where electricity is primarily utilised for basic services such as lighting, phone charging, and limited appliance use.

This value of 312 Wh/customer/day (about 9.4 kWh/customer/month) is subsequently adopted as a representative benchmark for the microgrid lifecycle analysis presented in later sections. Using this calculated consumption value helps ensure that the modelling and techno-economic evaluation better reflect real-world conditions of rural microgrids, thereby improving the accuracy and relevance of the results.

3.5.5.2 Senyondo microgrid modelling

Load Profile

The microgrid demand profile for the period 04 March 2022 to 21 September 2023, obtained from the SMA Sunny Portal, is plotted in Figure 3-34. It is similar to the typical microgrid load profiles [25], and has an evening peak attributed to residential demand [24].

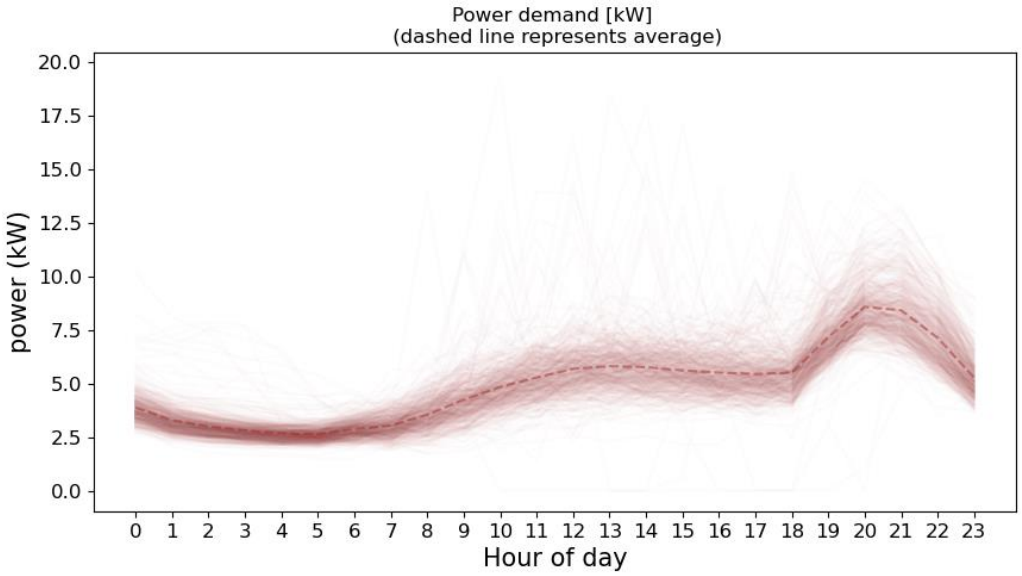

Figure 3-34: Load profile for Senyondo microgrid from March 2022 to September 2023

For modelling and subsequent analysis, Senyondo microgrid demand data for the 1-year period spanning 01 September 2022 to 31 August 2023 was utilised. The weekday consumption distribution for this interval is presented in Figure 3-35. The results indicate a generally uniform demand profile across the week, with only marginal deviations. Weekend consumption, particularly on Saturdays and Sundays, is slightly higher than on weekdays, with Sunday exhibiting the highest average demand, though the difference is comparatively small. This relative homogeneity across days implies that DSM interventions can be formulated in a manner that is applicable uniformly throughout the week, rather than tailored exclusively to specific weekdays.

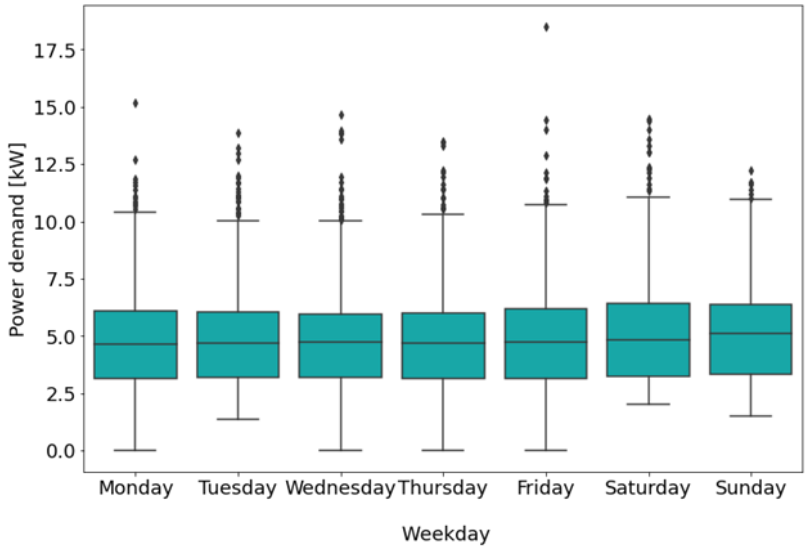

Figure 3-35: Average load per week day for Senyondo microgrid from 01 September 2022 to 31 August 2023 (rectangle lower border, inner line, and top border indicate the first quartile, median, and third quartile, respectively)

The issue of missing or anomalous data in smart meter datasets has been widely addressed in the literature [233] [234]. Such irregularities may arise from a variety of causes, including communication network interruptions, equipment downtime, environmental influences, or unstable transmission between sensors and databases. Broadly, two strategies are employed to manage missing data; elimination, which involves discarding missing data, and imputation, where absent values are substituted with estimated ones. Although elimination is straightforward, it has the drawback of discarding potentially valuable information and may introduce bias by distorting temporal data patterns.

In the context of energy system modelling, preserving the continuity and accuracy of time-series load data is important. Demand side management models, renewable generation simulations and life-cycle analyses rely on hourly and sub-hourly datasets to capture diurnal cycles, peak loads, and seasonal variations. Missing or omitted data points can therefore misrepresent system behaviour, compromise model validity, and weaken the robustness of subsequent policy or operational insights. To mitigate these risks, this study employs imputation for reliable analysis.

Various imputation techniques have been developed to address missing values in time-series datasets, including simple substitution methods such as last observation carried forward, mean, median, and mode replacement. Other techniques include Maximum Likelihood Estimation and Multiple Imputation [235][233]. Machine learning-based strategies have gained prominence, including Support Vector Regressor (SVR), Bayesian missing values imputers, k-Nearest Neighbours (KNN), and Random Forest Imputation [241]. Among these, KNN and Random Forest methods are widely used due to their ability to capture nonlinear dependencies in the data [236]. Some studies have shown Random Forest-based approaches, like the missing forest algorithm, to outperform KNN and other imputational methods in terms of predictive accuracy and robustness [237] [238].

For the one-year data used in this study, 0.15% of the average hourly demand data was missing, likely due to network failures or temporary data logger downtime. To address these gaps, the Missing Forest algorithm, implemented in Python, was applied. This approach enabled the construction of a complete hourly demand dataset for 8,760 hours, representing an uninterrupted annual load profile. The resulting dataset was subsequently used as the base load for energy system modelling and life cycle assessment.

It is noted that for this study, annual growth in load demand was not considered.

Meteorological data

To capture site-specific solar irradiance data, an irradiance meter was installed at the Senyondo microgrid site. Figure 3-36 illustrates the measured daily irradiance distribution for the period spanning 10 March 2022 to 21 September 2023. Ambient temperature values for Senyondo were obtained from the NASA website [226].

For modelling of the microgrid operation, the measured irradiance data and ambient temperature values from 01 September 2022 to 31 August 2023 were used. The average monthly ambient temperature from the NASA dataset and the average measured monthly irradiance (September 2022 – August 2023) are shown in Figure 3-37.

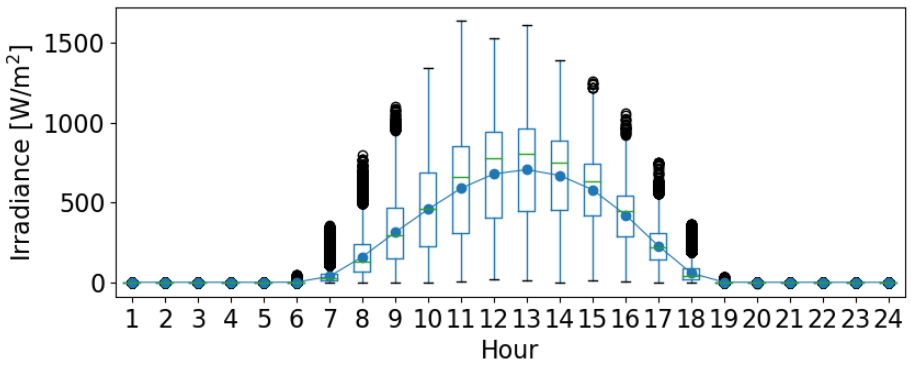

Figure 3-36: The daily irradiance distribution per hour (curve indicates mean) for Senyondo microgrid. The rectangle lower border, inner line, and top border indicate the first quartile (Q1), median, and third quartile (Q3), respectively. The circles outside the rectangles represent outliers i.e. data points outside the range of 1.5 times the IQR (interquartile range) from Q1 and Q3

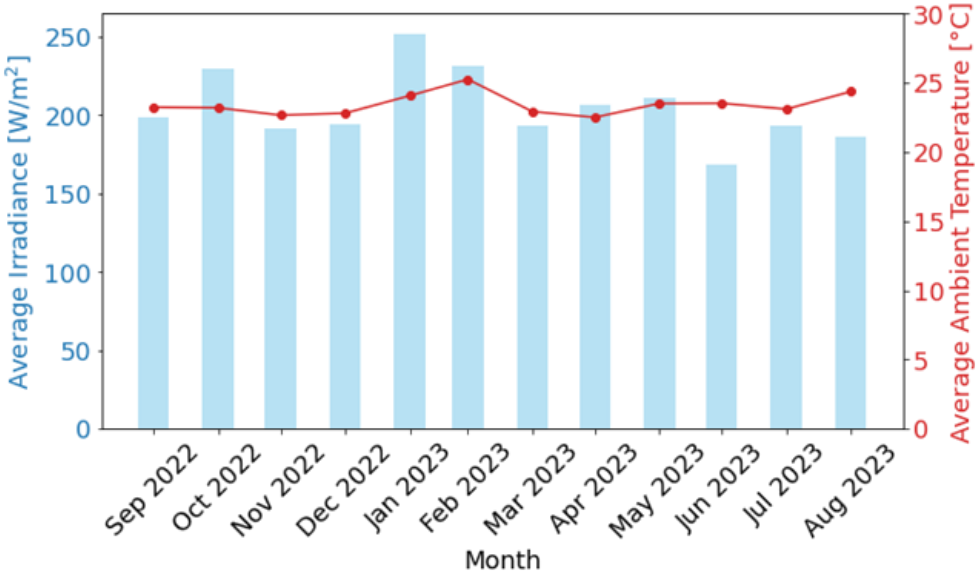

Figure 3-37: Monthly average irradiance and ambient temperature for Senyondo from September 2022 to August 2023

Solar PV system

PV generation, which is a function of solar irradiance and ambient temperature, is modelled as shown below [97] [239] [240].

$$P_{PV}(t) = P_r\, f_d\, \frac{G(t)}{G_{ref}} \left[1 + K_T \left(T_c - T_{ref}\right)\right] \quad (3.26)$$

and

$$T_c = T_{amb} + 0.0256\, G(t) \quad (3.27)$$

P_{PV} is the PV output power (kW), P_r is the rated PV capacity under STC (kW), $f_d = 0.9$ is the derating factor [227], $G(t)$ is the incident solar radiation in kW/m^2, G_{ref} = 1 kW/m^2 is the solar radiation at STC, K_T = - 0.0037/°C is the temperature coefficient of power, T_c is the cell temperature (°C), T_{ref} = 25°C is the reference temperature and T_{amb} is ambient temperature (°C).

Hourly PV energy production is given by

$$E_{PV}(t) = P_{PV}(t)\, \Delta t \quad (3.28)$$

where Δt denotes an hour.

The PV specifications are summarised in Table 3-12.

Table 3-12: PV, battery and converter specifications for Senyondo microgrid

Component	Parameter	Value	Parameter	Value
PV [97]	Average PV panel rating	395 Wp	Installation cost	20% of C_{PV}
	Lifetime	25 years	Annual O&M cost	2.5% of C_{PV}
	Capital cost (C_{PV})	USD 400		
Battery [241][242] [24]	Nominal capacity	1545 Ah	Minimum SOC (%)	50%
	Nominal voltage (V_{Bat})	2 V	Maximum SOC (%)	100%
	System DC voltage	48 V	Capital cost (C_{Bat})	USD 300/kWh
	Self-discharge rate (σ)	0.2%	Installation cost	3% of C_{Bat}
	Round trip efficiency (η_{Bat})	86%	Annual O&M cost	2.5% of C_{Bat}
	Charge controller efficiency (η_{cc})	90%		
Converter [24][243][244]	Power rating	80 kW	Installation cost	3% of C_{conv}
	Lifetime	15 years	Annual O&M cost	2.5% of C_{conv}
	Capital cost (C_{conv})	USD 300/kW	Efficiency (η_{conv})	98%

Battery storage

Battery charging dynamics are represented as follows [245]:

$$E_B(t) = E_B(t-1) + \left(E_G(t) - \frac{E_L(t)}{\eta_{conv}}\right) \eta_{cc}\, \eta_{bat} \tag{3.29}$$

and

$$E_G(t) = E_{PV}(t)\, \eta_{conv} \tag{3.30}$$

where $E_B(t)$ denotes the battery energy at time t, E_G is the generated electrical energy, E_L is the hourly base load energy. System conversion losses are incorporated through the converter efficiency (η_{conv}), the charge controller efficiency (η_{cc}) and the battery round trip efficiency (η_{bat}).

During discharging, the battery energy is computed as:

$$E_B(t) = (1-\sigma)E_B(t-1) + \left(E_G(t) - \frac{E_L(t)}{\eta_{conv}}\right) / \eta_{cc}\, \eta_{bat} \tag{3.31}$$

where σ is the battery hourly self-discharge.

It is assumed that the maximum charging and discharging power of the battery are sufficient to meet the base load demand.

Battery self-discharge varies according to technology. For lead-acid batteries, typical monthly self-discharge ranges between 2–5%, whereas for lithium-ion batteries the value is around 1% [246]. The initial state of charge (SOC) of the battery was set to 70% in the model.

Battery degradation

A significant portion of the lifecycle costs of microgrids is due to battery replacement [67]. This issue is particularly pronounced in off-grid systems deployed in developing countries, where the high cost of battery replacement poses a critical challenge to system sustainability. In many rural and remote communities, limited income levels and low electricity demand often render end-of-life battery replacement financially unfeasible [68].

Over time, batteries experience capacity degradation due to mechanisms such as sulphation, corrosion, and stratification, or as a result of reaching their maximum number of charge-discharge cycles [69][65][70]. Ambient temperature also influences battery longevity. An increase in operating temperature from 20 °C to 30 °C can reduce battery life by approximately 50% [247] [248], highlighting the sensitivity of storage systems to local environmental conditions. Typical industry standards for stationary storage systems define the battery end-of-life as occurring when the battery's usable capacity declines to 80% of its initial rated value [248].

Several studies have underscored the importance of incorporating battery degradation modelling in microgrid lifecycle assessments, to improve the accuracy of economic evaluations and to inform optimal operational and replacement strategies.

Rainflow cycle analysis is widely employed for modelling and quantifying battery degradation over time. In one study a rainflow counting algorithm (RCA) was used for translating battery DOD data into equivalent full and half cycles, and filtering was applied to calculate capacity decline [249]. Another study assigned a cost component to battery capacity reduction of valve regulated lead acid (VRLA) and Li-ion batteries, evaluated using a rainflow counting analysis of the number of cycles and DOD [250]. A dispatching approach that considers battery cycling ageing costs derived from filtered RCA outputs is described in [251], allowing operational strategies to account for degradation. A degradation model that integrates DOD analysis with microcycle resolution and battery temperature in evaluating the benefits of hybridizing a lead-acid BESS with supercapacitors is presented in [252].

In this study, the rainflow cycles counting algorithm [253][254] is applied to estimate battery lifetime, with failure defined on the basis of charge–discharge cycles. Manufacturer information on cycle numbers and DOD is used to construct the degradation model [253], based on the specifications of the Hoppecke OPzV Sun/Power VR L 2-1700 batteries installed at Senyondo microgrid (see section 3.2.2).

Using the cycle number, DOD, and temperature characteristics provided by the manufacturer [248], a semi-logarithmic plot of the number of cycles against DOD at 25 °C is generated (see Figure 3-38). This curve serves as the input to the rainflow counting simulation for Senyondo microgrid, which translates the battery's DOD data into cycle-based quantification of degradation over time.

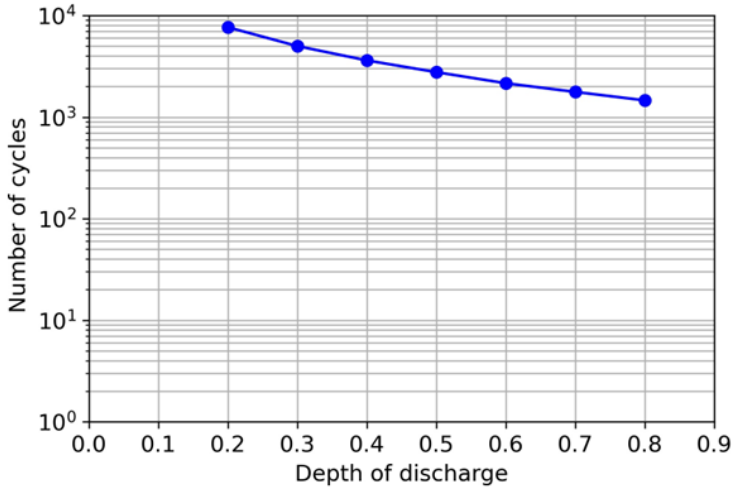

Figure 3-38: Semi-log plot of number of cycles to failure versus DOD at 25°C for the Hoppecke VR-L battery

The site average ambient temperature was 23.4°C, so data for 25°C is used to obtain the following expression for the cycles to failure as a function of DOD [247] [253]:

$$n_{cycles(DOD)} = 18927.43\, e^{(-8.9220\, DOD)} + 6563.71\, e^{(-1.9022\, DOD)} \tag{3.32}$$

The aging rate per cycle is the inverse of $n_{cycles(DOD)}$.

The battery degradation rate B_D for the entire period is thus calculated as

$$B_D = \sum_k \frac{1}{n_{cycles(DOD_k)}} \tag{3.33}$$

where k represents the cycle index.

The battery lifetime in years L_{bat} is given by

$$L_{bat} = \frac{1}{B_D} \tag{3.34}$$

The Battery parameters used in the modelling [241] [242] [24] are shown in Table 3-12. The battery minimum SOC is set to 50% in the model, which is typically recommended

for lead acid batteries, and is also recommended by the Hoppecke battery manufacturer [248].

Converter

The converter is responsible for power conversion, enabling the transformation of DC to AC (for supplying loads) and AC to DC (for charging the battery storage system). The converter rating P_{conv} (kW) is generally computed as [245]:

$$P_{conv} = \frac{P_L^{max}}{\eta_{conv}} \tag{3.35}$$

where P_L^{max} denotes the maximum AC load demand and η_{conv} is the converter efficiency.

For this study, the converter was sized at 80 kW, a rating that minimises PV generation curtailment. Table 3-12 contains the technical specifications of the converter [24] [243][244].

Electric bikes and portable storage

Reported values for the energy consumption of electric two- and three-wheelers (2&3W) vary significantly depending on the vehicle type and testing conditions. Table 3-13 shows the difference between documented certified performance and field operation [255], underscoring the importance of using real-world values in energy planning for e-mobility integration in microgrids.

Table 3-13: Energy consumption per 100 km for electric vehicles [255]

Category	**Parameter**	**Certified energy consumption (kWh/100km)**	**Real world energy consumption (kWh/100km)**	**Reference**
Electric bikes & Bike-like three-wheelers	Range	0.17 - 2.25	0.41 - 1.45	[255]
	Average	0.54	0.71	
Electric motorcycles (two- & three-wheelers)	Range	1.07 - 17.5	6.0 - 13.5	
	Average	4.62	9.3	

Travel behaviour studies provide insight into potential mobility-related energy demand. In Uganda, urban electric motorbike riders reported average daily travel distances of 150 km, while Zembo motorcycles had lower averages at 70 km per day [191].The Bodawerk bike has a range of 100-120 km [256].

An 8.55 kW_p PV system with 9.6 kWh of battery storage in Uganda could support the recharging of 20-30 Zembo motorcycles daily, according to [258]. A passenger-carrying Bodawerk e-bike can cover 50-120 km per day, while the Zembo e-bike range is 50–80 km [259]. Such studies are important in establishing realistic charging demands for microgrids serving electric mobility.

For the purposes of this analysis, an average daily distance of 50 km is assumed [257].

Three categories of electric two-wheelers in use in Uganda are considered as representative mobility loads in this study; the Bodawerk e-motorcycle [260] [257] [192] [261], the Zembo e-motorcycle [262] [191] [261], and the AfricroozE e-bicycle [263] [261]. Their specifications are presented in Table 3-14. In addition, the bodawerk 4.6 kWh smart battery [260] is considered as a portable storage solution for off-microgrid customers, and a charging rate of 1000 W is assumed.

Table 3-14: Electric bike and portable storage specifications

Load type	**Charging rate (W)**	**Battery capacity (Wh)**	**E-bike energy (Wh) required for 50 km**	**References**
Bodawerk	900	2200	1950	[257]
Zembo	1100	2160	1830	[191]
Africrooze	200	500	500	[261]
Portable storage	1000	4600	--	

The number of additional loads of each type charged daily $n_{x_n daily}$ is computed as

$$n_{x_n daily} = \frac{E_{n_{x_n daily}}}{x_{n_{bat_{cap}}}} \tag{3.36}$$

x_n represents the type of load, with $x_n = 1,2,3,4$ corresponding to Bodawerk, Zembo, Africrooze and portable storage loads respectively, $E_{n_{x_n daily}}$ is the energy supplied to load type x_n daily in kWh, and $x_{n_{bat_{cap}}}$ is the battery capacity of x_n in kWh.

Daily charging targets were defined for each load type in order to minimise PV curtailment. The Bodawerk, Zembo, and AfricroozE loads were each allocated a daily charging target of 20 units, while the portable storage load was assigned a daily charging target of 60 units. These targets were selected to ensure effective utilisation of PV energy, thereby reducing excess PV production that would otherwise remain unused.

For modelling user behaviour, it is assumed that each e-mobility rider covers an average distance of 50 km per day. Conventional ICE motorbikes' petrol consumption is about 1.5 litres of petrol / 50 km [42] [188]. This provides the basis for quantifying the equivalent fuel savings when substituting ICE motorbikes with electric 2&3W.

The equivalent annual savings in fuel consumption from using electric 2&3W can be calculated by summing up the equivalent litres of petrol that would have been required to meet the daily 50 km distance coverage of each type of e-bike.

From this, the annual CO_2 emissions avoided by using electric transport can be computed as

$$CO_2\ avoided/year = (\sum_{d=1}^{365} Daily\ litres\ of\ petrol\ avoided\ for\ all\ bikes)\ CO_2\ per\ litre \quad (3.37)$$

with CO_2 emissions being 2.32 kg CO_2 / litre of petrol.

For the Li-ion bodawerk portable storage, a depth of discharge (DOD) of 80% and a conversion efficiency of 85% are assumed. The usable energy of the portable storage $E_{port_{usable}}$ (kWh) is thus

$$E_{port_{usable}} = x_{port_{bat_{cap}}}\ DOD_{port}\ \eta_{port} \quad (3.38)$$

where $x_{port_{bat_{cap}}}$ is the portable battery capacity (kWh), DOD_{port} is the portable battery depth of discharge and η_{port} is the portable battery converter efficiency.

The average number of off-microgrid customers that can be served annually is therefore

$$Off_{MG} = \left[\left(\sum_{d=1}^{365} n_{portable_{daily}}\right) E_{port_{usable}}\right] / \left(365\, MG_{customer_{kwh_{daily}}}\right) \quad (3.39)$$

where Off_{MG} is the number of off-microgrid customers that can be served annually using portable storage, and $MG_{customer_{kwh_{daily}}} = 0.312$ kWh is the average daily energy consumption per customer obtained from analysis of the 8 microgrids in Uganda (Section 3.5.5.1).

Reliability considerations

One of the most important performance indicators for microgrids, particularly in off-grid rural electrification contexts in Africa, is the Loss of Power Supply Probability (LPSP) [264]. The LPSP provides a quantitative measure of system reliability, defined as the probability that an energy system is unable to supply the load demand at a given time. A lower LPSP indicates a more reliable system, while a higher value reflects frequent or prolonged shortages in power supply.

The reliability of a microgrid, expressed through LPSP, is influenced by several interdependent factors. These include:

- Weather resource variability: Fluctuations in solar irradiance and ambient temperature directly affect PV generation and battery performance.
- System size and design: The installed capacities of PV arrays, battery storage, and converters determine the ability of the system to meet peak and average loads.
- Energy storage characteristics: The DOD, round-trip efficiency, and self-discharge rates of batteries strongly influence the ability to supply demand during periods of low solar generation.
- Load demand patterns: Sharp evening peaks or highly variable usage can significantly increase the likelihood of unmet demand.
- Energy management or load management strategies: DSM, smart scheduling, and load prioritisation can help reduce supply deficits.

While the LPSP can be reduced by oversizing system components, such an approach increases both capital and lifecycle costs, raising concerns about affordability and long-term sustainability in rural electrification projects. Therefore, system sizing must balance technical reliability and economic viability.

The LPSP is calculated as

$$LPSP = \frac{\sum_{t=1}^{T} P_{deficit}(t)}{\sum_{t=1}^{T} E_L(t)} \quad (3.40)$$

where $P_{deficit}$ denotes the deficit of power required to serve the demand.

In Africa, some typical microgrid LPSP values are 0.12 in Morocco [26] and 0.1 for Uganda [265] [25]. Lower LPSP values can be achieved through increasing storage capacity or oversizing the PV system, both of which provide greater resilience against intermittency and demand fluctuations. However, this increases capital expenditure and lifecycle costs. Consequently, system developers and operators must weigh the marginal cost of additional reliability against the financial sustainability of the microgrid and the willingness- or ability-to-pay of customers.

Economic parameters

In the economic assessment of energy systems, the Life Cycle Cost (LCC) and the Levelized Cost of Energy are important parameters [24][69] [245]. The cost evaluation of the modelled microgrid system is carried out using an LCC analysis, from which the LCOE is obtained.

The installation costs (INS), with adjustments for inflation and discounting over the project lifetime, are given by

$$INS = INS_{PV} + \left(INS_{BAT} \sum_{b=1}^{B_r} \frac{(1+f)^{nb-1}}{(1+r)^{nb}}\right) + \left(INS_{CONV} \sum_{c=1}^{C_r} \frac{(1+f)^{nc-1}}{(1+r)^{nc}}\right) \quad (3.41)$$

where INS_{PV}, INS_{BAT} and INS_{CONV} represent the PV, battery and converter installation costs. B_r and C_r represent the number of battery and converter replacements over the project lifetime.

X_r denotes how many times component X is replaced over the project lifetime N, and is calculated as

$$X_r = int\left(\frac{N-nx}{nx}\right) \quad (3.42)$$

where nx is the operational lifetime of component X.

The discount rate r is adjusted for inflation, and is given by

$$r = \frac{i_{nom}-f}{1+f} \quad (3.43)$$

where f is the inflation rate and i_{nom} is nominal interest rate.

The present value of operating costs PR_{OPEX} is calculated as

$$PR_{OPEX} = [OPEX_{PV} + OPEX_{BAT} + OPEX_{CONV}] \sum_{n=1}^{N} \frac{(1+f)^{n-1}}{(1+r)^n} \quad (3.44)$$

whereby $OPEX_{PV}$, $OPEX_{BAT}$ and $OPEX_{CONV}$ represent the PV, battery and converter operational costs.

PR_{REP} denotes the present value of the replacement costs. Battery and converter replacement costs (REP_{BAT} and REP_{CONV} respectively), are included whenever their operational lifetime expires within the project lifetime:

$$PR_{REP} = REP_{BAT} \sum_{b=1}^{B_r} \frac{(1+f)^{nb-1}}{(1+r)^{nb}} + REP_{CONV} \sum_{c=1}^{C_r} \frac{(1+f)^{nc-1}}{(1+r)^{nc}} \quad (3.45)$$

The LCC represents the total cost of owning and operating the system over its entire project lifetime, expressed in present value terms as

$$LCC = ICC + INS + PR_{OPEX} + PR_{REP} + PR_{FUEL} \quad (3.46)$$

where ICC is the initial capital cost. The present value of the fuel cost PR_{FUEL} is zero since the system has no diesel or biomass generator.

The salvage values of the converter and battery storage at the end of the project lifetime are subtracted from the LCC to avoid overestimating the replacement costs.

$LCOE$ is computed, inclusive of the mobility and portable storage loads, as

$$LCOE = \left(\frac{LCC}{\sum_t^T (E_L(t) + E_{mob}(t) + E_{PS}(t))} \right) CRF \quad (3.47)$$

with $E_L(t)$, $E_{mob}(t)$ and $E_{PS}(t)$ representing the energy for the met load demand, e-mobility loads and portable storage respectively, at time t.

The capital recovery factor (CRF), given by [243] as

$$CRF = \frac{i_{nom}\,(1+i_{nom})^N}{(1+i_{nom})^N - 1} \quad (3.48)$$

allows the conversion of a one-time capital expenditure into an equivalent annualized cost over the project lifetime.

Table 3-15 displays the values used in the economic modelling [24] [266][265].

Table 3-15: Economic parameters for Senyondo microgrid model

Parameter	**Value**	**Parameter**	**Value**
Project lifetime (N)	25 years	Inflation rate (f)	7.5%
Nominal interest rate (i_{nom})	13%	Tariff	USD 0.30 / kWh

The capital and operational costs associated with the charging stations for the additional loads are excluded from this analysis, as it is assumed that such infrastructure is deployed and managed by third-party operators rather than being part of the core microgrid investment.

Optimization approach

The primary objective of the adopted control strategy is the minimization of PV energy curtailment. To achieve this, additional loads, i.e. e-mobility loads and portable storage, are incorporated into the system as flexible, curtailable loads. These loads do not compromise the reliability of the microgrid since they are supplied only when surplus power is available after meeting the base load and stationary storage requirements.

By structuring the energy dispatch in this manner, the system ensures that:

- Critical (base) demand is always prioritized, safeguarding reliable supply to consumers.
- Surplus PV generation is effectively absorbed, reducing energy wastage.
- Flexible loads enhance system economics, as energy that would otherwise be curtailed is productively used.

This approach seeks to improve the overall load factor of the PV system, while also providing a pathway for integrating productive uses of energy, particularly in rural contexts where demand during daytime hours is typically low.

The microgrid control strategy prioritizes supplying the base load demand. Once the base load is satisfied, any excess PV generation is used to charge the stationary battery storage. If additional surplus energy remains after meeting both the base load and the BESS charging requirements, it is allocated to charging the electro-mobility loads and portable storage. In this way, system utilization is maximized, and PV energy curtailment is minimized.

The flow chart in Figure 3-39 illustrates the basic control strategy.

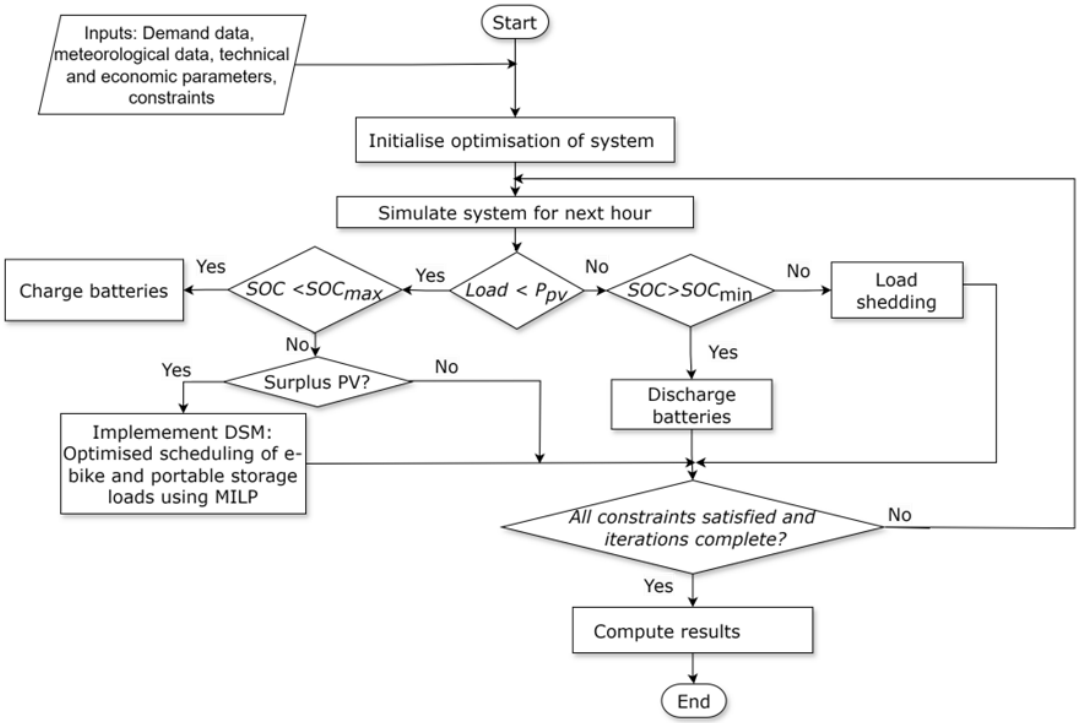

Figure 3-39: Flow chart illustrating dispatch and optimisation approach

MATLAB is used for the system modelling and simulation of the technical and economic aspects of the microgrid. Mixed-Integer Linear Programming (MILP) optimisation is used to implement DSM control of the e-mobility and portable storage loads.

The general MILP problem can be expressed as

$$\min_x f^T x \text{ subject to } \begin{cases} Ax \leq b \\ A_{eq}x = b_{eq} \\ lb \leq x \leq ub \end{cases} \tag{3.49}$$

where vector x of the variables has some integer values, $f^T x$ is the objective function and f is a vector, matrices A, A_{eq} and vectors b, b_{eq} describe the linear inequalities and linear equations that along with bounds lb and ub specify the constraints [89] [267].

To maximise the objective function, it is multiplied by -1.

MILP Optimisation for e-mobility and portable storage loads

To optimally allocate surplus PV energy to additional curtailable loads, a Mixed-Integer Linear Programming (MILP) framework was developed. The formulation builds on prior work [268][269] and includes priority weights, technical limits, and load balance constraints for realistic integration of e-mobility and portable storage into the microgrid.

The decision variable is

$n_{x_n} \epsilon \mathbb{Z}^+$: Number of loads of type x_n supplied at time t

The objective function f_{obj} to be maximised is

$$\max \quad f_{obj} = \sum_{x_n=1}^{x_N} W_{x_n} \; P_{x_n} \; n_{x_n}(t) \tag{3.50}$$

where $n_{x_n}(t)$ is the number of loads of type x_n charged at time t, W_{x_n} is the assigned priority weighting of load x_n and P_{x_n} is the charging power of load x_n. x_n={1,2,3,4} corresponds to the bodawerk, zembo, africrooze and portable storage loads, respectively.

The assigned charging priorities are $W_1 = W_2 = W_3 = 1$ and $W_4 = 0.5$.

The constraints include the following:

- Capacity bounds

$$0 \leq \beta_k \leq \beta_k^{max}, \qquad \beta_k \in \{\beta_{pv}, \beta_{bat}\} \tag{3.51}$$

where β_k denotes the upper bounds of the PV and battery sizes.

- Energy balance

$$P_{PV}(t) = P_L(t) + P_{Bat}(t) \tag{3.52}$$

At every time step, the energy balance in (3.52) (regarding the base load) must hold. The battery power $P_{Bat}(t)$ is positive for charging and negative for discharging.

- Battery limits

The battery state of charge is bounded by

$$E_{Bmin} < E_B(t) < E_{Bmax} \tag{3.53}$$

where $E_{Bmin} = 0.5\, E_{Bmax}$.

- Excess PV allocation constraint

$$\sum_{x_n=1}^{x_N} \left(P_{x_n}\, n_{x_n}(t) \right) \leq P_{pv_{excess}}(t)\, \eta_{conv} \tag{3.54}$$

where x_N is the number of types of e-mobile and portable loads, i.e. $x_N = 4$. $P_{pv_{excess}}(t)$ is the excess PV power at time t after supplying the base load and charging the battery.

- Load parity constraint (fairness between e-bike types)

$$\left| n_{x_n}(t) - n_{x_n+1}(t) \right| \leq 2\,, \quad x_n = 1 \tag{3.55}$$

The daily difference between the number of Bodawerk and Zembo e-motorcycles charged should not exceed 2 units, such that both types of e-bikes are charged in nearly equal numbers.

- Daily charging bounds

The maximum number of batteries of each type to be charged daily is $n_{x_n daily_{max}}$, where

$$0 \leq n_{x_n daily} \leq n_{x_n daily_{max}} \tag{3.56}$$

The charging priority weights and targeted daily number of each type of load are shown in Table 3-16. The actual daily number of batteries charged on a given day for each load type ($n_{x_n daily}$) depends on that day's surplus PV energy.

Table 3-16: E-bike and portable storage daily targets

Load Type	**Charging Rate (W)**	**Battery Capacity (Wh)**	**Charging Priority/Weight**	**Daily Maximum Batteries Charged ($n_{x_n daily_{max}}$)**
Bodawerk	900	2200	1	20
Zembo	1100	2160	1	20
Africrooze	200	500	1	20
Portable storage	1000	4600	0.5	60

Several studies have modelled e-mobility charging patterns and energy profiles using estimated charging times. For instance, [269] employed peak sun hours and charging time estimates for e-bike load scheduling, while [270] analysed e-mobility integration in PV and wind systems with battery storage based on annual renewable energy, storage supply capacity and charging time estimates. In contrast, this work adopts a more granular

approach, computing the hourly energy balance each hour in the year to determine the supply to the e-mobility and portable storage loads.

4 Results

4.1 Case Study 1 - Optimal design of a grid-connected solar PV system

(i) Without DSM

Table 4-1 shows key techno-economic results for the four scenarios, defined as below:

- S1: HOMER sizes both PV and battery
- S2: Battery voltage fixed at 48 V, HOMER sizes PV
- S3: Battery voltage fixed at 48 V, PV size fixed at 16.5 kW
- S4: Business-as-usual (grid + generator only).

The renewable fraction for all 3 systems with PV exceeds 90%, indicating significant utilization of the PV generated energy. Scenario S3's excess electricity is 8,080 kWh/year for the 16.5 kWp configuration, far exceeding that of S2 of 1,015 kWh/year. This surplus could be channelled into applications such as refrigeration, water heating, water purification or e-mobility.

Table 4-1: Results without DSM

Scenario	PV (kW)	Converter (kW)	Excess Electricity (%)	Renewable Fraction (%)	NPC (USD)	LCOE (USD/kWh)
S1	12	4.96	6.1	91.4	91,559	0.169
S2	12.3	6.27	4.2	94.9	94,589	0.174
S3	16.5	6.13	25.8	98.8	104,360	0.192
S4	0	0	0	0	134,595	0.248

Both Net Present Cost (NPC) and LCOE are reduced for the hybrid PV systems compared to the BAU grid and genset only setup, indicating the economic advantage of integrating solar generation over the project lifetime due to reduced grid and generator reliance. The LCOE reduces by 32%, 30% and 23% for the hybrid PV systems in S1, S2, and S3 respectively, compared to the BAU grid and genset only setup (S4). LCOE values for S1,

S2 and S3 do not exceed 0.192 USD/ kWh, compared to 0.248 USD/ kWh for the BAU case (S4).

(ii) With DSM (Peak clipping and Load shifting)

Table 4-2 summarises the results from simulation of the four scenarios for the load shifting and peak clipping DSM.

Table 4-2: Peak Clipping (PC) and Load Shifting (LS) results

Scenario	DSM measure	PV (kW)	Converter (kW)	Excess Electricity (%)	Renewable Fraction (%)	NPC (USD)	LCOE (USD/ kWh)
S1	PC	11	4.55	5.1	91.9	80,831	0.161
	LS	12.4	5.18	7.9	94.0	80,410	0.148
S2	PC	11.7	5.30	5.8	96.8	84,476	0.169
	LS	12.8	6.56	7.2	97.5	86,012	0.158
S3	PC	16.5	4.88	31.3	99.7	97,355	0.194
	LS	16.5	5.75	26.6	99.5	95,243	0.175
S4	PC	0	0	0	0	125,681	0.251
	LS	0	0	0	0	134,723	0.248

S2 yields a renewable energy fraction of 96.8% for peak clipping and 97.5% for load shifting, indicating that most of the load-supplied energy comes from renewable PV generation. Generator utilisation is low, contributing only 0.14% and 0.18% of total energy for peak clipping and load shifting, respectively.

For S3, the renewable fraction exceeds 99% for both DSM cases, with the grid supply being only 0.14% and 1.96% for peak clipping and load shifting respectively, underscoring the system's near-total dependence on solar generation. The higher excess energy observed in S3 compared to S1 and S2 is expected, as the larger PV array produces more total energy. This creates an opportunity to redirect excess solar power to, for example, thermal applications such as water heating or refrigeration, rather than curtailing the surplus PV, adding to the cost benefits of reduced grid consumption and less generator use.

Comparing the no DSM case with the DSM cases for S1, S2 and S3 reveals that both excess electricity and the renewable fraction are higher when DSM is implemented, except in the case of peak clipping for S1 which has the lowest excess electricity at 5.1% due to the system components being sized for a smaller demand.

The key technical and economic results are summarised in Figure 4-1, showing that in general, business-as-usual has the highest LCOE, thus the installation of PV with battery storage is recommended for the Lwak Convent site. Furthermore, load shifting gives a lower LCOE than peak clipping, and thus load shifting as a DSM strategy is suitable for further investigation.

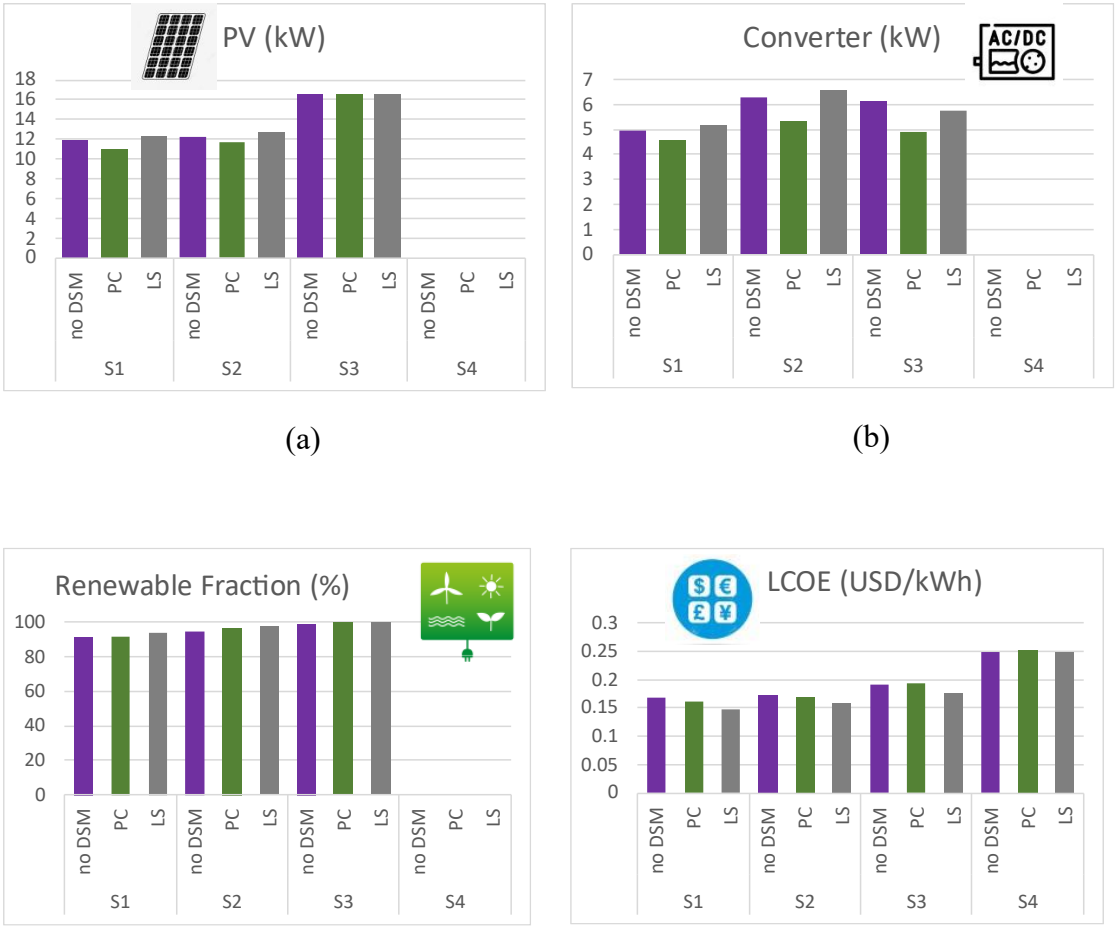

Figure 4-1: Simulation results for the 4 scenarios showing (a) PV capacity (b) Converter Capacity (c) Renewable Fraction (d) LCOE

4.2 Case study 2 – Refrigeration temperature evolution and ageing impact analysis

Refrigeration appliance temperature modelling

Freezer 6 is further analyzed and compared with results from modelling with MATLAB the refrigerator temperature model defined in Equations 3.1 and 3.2. The freezer's measured temperature range during the off state period was -12.9 ℃ to -0.3 ℃. Two on-state power values for Freezer 6 (Table 3-8) are modelled, p = 265 W (average ON power) and $\bar{p}$ =112W (average power), and from [157], T_{amb} =24 °C, ɳ =3, A = 3.21 W/°C, τ = 30 s and m_c = 86400 J.

Figure 4-2 illustrates the model results and the measured temperature plots.

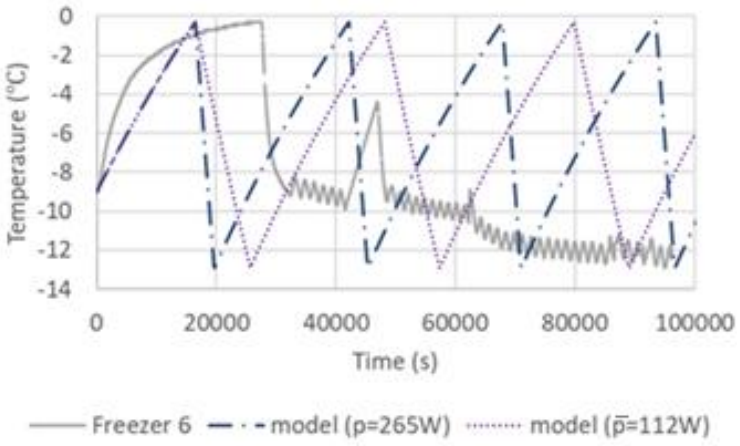

Figure 4-2: Modelled and measured temperature profiles for Freezer 6

The model shows faster cooling is achievable for the larger p value, while using the smaller $\bar{p}$ gives a slower cooling rate. The measured data shows a leveling-off in temperature rise over time that is not captured in the model. The discrepancy between the measured temperature values and the models can be attributed to use of estimated model inputs such as T_{amb}, ɳ, A, τ and m_c drawn from [157], leading to parameter mismatch with the actual appliance. Door opening and item loading/unloading, ambient variations and the

air circulation patterns inside the freezer compartment are other possible causes of differences.

The observation aligns with [187], where deviations between modeling and experimental results were attributed to thermostat hysteresis, non-uniformity of compartment air temperature, and simplifications inherent in lumped-parameter models. In practice, freezer air temperature often continues to fall or stabilize briefly after the compressor switches off as thermal energy redistributes, whereas the model assumes temperature decreases only during compressor operation.

Therefore, model results may not provide sufficiently realistic inputs for investigating demand side management applications, particularly if estimated parameters are used.

Energy and cost savings

In April 2023, Kenya increased its electricity tariff for domestic consumers using more than 100 kWh per month by 32.7%, from 15.8 KES to 20.97 KES per kWh (0.18 USD/kWh) [224]. In the energy and cost calculations, the peak power demand values of Fridge 5 and Freezer 6 (Table 3-8) are used. Based on the measurements and data in Table 3-8, implementing a generic 4-hour ON and 2-hour OFF load management cycle for all refrigeration appliances would yield annual energy and cost savings of 33% for refrigeration loads alone, as indicated in Table 4.4. When considering the total power consumption of all loads, the projected yearly savings are 17%, as shown in Table 4.5. These estimates assume that the suggested 4:2 ON:OFF switching strategy maintains internal appliance temperatures of all appliances within food safety limits.

Table 4-3: Annual potential refrigeration energy and refrigeration cost savings

	Without DSM	With DSM	Savings	Percentage reduction
Energy (kWh/yr)	10757.28	7171.52	3585.76	33%
Cost (USD/yr)	1936.31	1290.87	645.44	33%

Table 4-4: Overall annual energy and cost savings for the site considering all loads

	Without DSM	With DSM	Savings	Percentage reduction
Energy (kWh/yr)	21575.66	17989.90	3585.76	17%
Cost (USD/yr)	3883.62	3238.18	645.44	17%

Assuming uniform on-off patterns for all appliances however does not give sufficient consideration to the heterogeneity of the appliances, hence more granular considerations of the appliance switching patterns and how they are scheduled is of interest.

Evaluation of insulation effectiveness

When computing the decay constant, the first 20% of the appliance temperature data from Lwak shown in Figure 3-26 is omitted, to avoid the transient effects that occur when refrigeration appliances are powered off. These residual transient phenomena arise mainly from downstream cooling effects from the evaporator and/or stabilization of pressure within the refrigeration system. This is similar to what was done in [167], where the first 20% and last 20% of the temperature data was disregarded when estimating the delay constant. The decay constant d_τ (min^{-1}) was evaluated over durations in which the appliance's internal temperature exhibited an approximately linear gradient with time. The maximum decay constant $d_{\tau_{max}}$, which we refer to as the decay constant factor, was defined as the threshold beyond which the initially increasing d_τ values began to decline [167].

The selected measurement interval (i.e. the latter 80% of the appliance temperature data in Figure 3-26) is deemed adequate for d_τ (min^{-1}) computation, and T_{amb} = 25 °C is assumed (Equation 3.3), which is consistent with the approach in [167] given the approximately linear temperature slope for the four appliances.

The d_τ (min^{-1}) values for the four freezers are plotted in Figure 4-3.

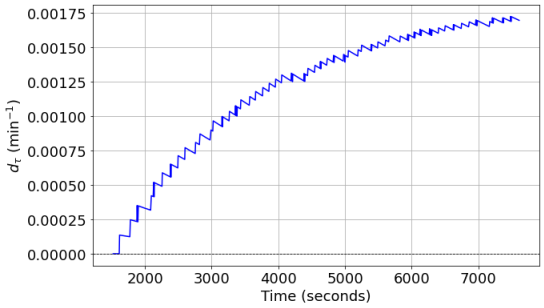

(a) Freezer 1

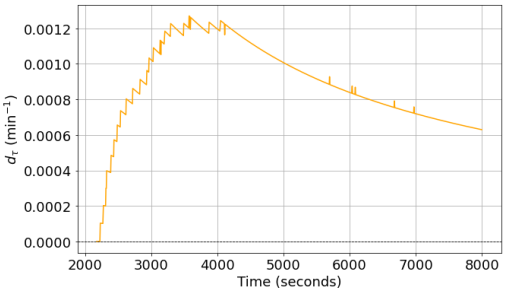

(b) Freezer 3

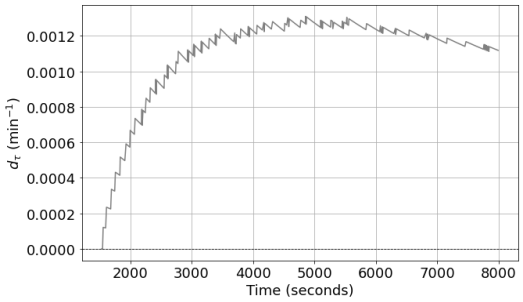

(c) Freezer 6

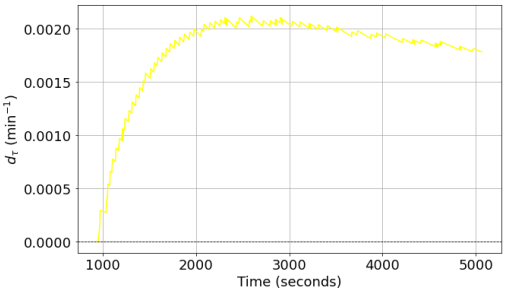

(d) Freezer 10

Figure 4-3: Refrigeration appliance delay constant $d_\tau(t)$ in min^{-1} for Freezers 1, 3, 6 and 10

As the decay constant d_τ values for Freezer 1 are still rising and have not yet peaked and started to decline over the measurement interval (see Figure 4-3a), the available measurement data is found to be insufficient to determine $d_{\tau_{max}}$ for Freezer 1. Hence Freezer 1 results are not considered.

Table 4-5 shows the decay constant factors $d_{\tau_{max}}$ (min^{-1}) for Freezers 3, 6 and 10. At 0.127 x10^{-2} min^{-1}, 0.131 x10^{-2} min^{-1}and 0.212 x10^{-2} min^{-1} for Freezers 3, 6 and 10 respectively, they are less than the 0.28 x10^{-2} min^{-1}, 0.49 x10^{-2} min^{-1} and 0.49 x10^{-2} min^{-1} values given in [167].

Table 4-5: Decay constant factor for three freezers at Lwak

Decay constant factor	**Freezer 3**	**Freezer 6**	**Freezer 10**
$d_{\tau_{max}}$ (min^{-1})	0.127 x10^{-2}	0.131 x10^{-2}	0.212 x10^{-2}

The decay constant factor values for the appliances at Lwak, calculated at the time of measurement, are not sufficient for a rigorous comparison across appliances as they are influenced by differences in design and operating parameters. It is also noted that the temperature measurements were conducted at different times and not concurrently. Nevertheless, they provide a useful baseline for subsequent evaluations of insulation degradation effects. For a given appliance, an increase in $d_{\tau_{max}}$ is indicative of higher energy consumption and thus of energy efficiency degradation.

The computation of appliance heat transfer coefficients k as well as the assessment of insulation performance over time was beyond the scope of this study, as manufacturer specifications and purchase information for the appliances were unavailable.

With ageing, the decay constant factor $d_{\tau_{max}}$ is expected to increase, resulting in rising energy consumption due to the positive correlation between $d_{\tau_{max}}$ and energy use.

As reported in [167], the decay constant factor decreases with the addition of insulation, suggesting that improved insulation can serve as an effective strategy to reduce the energy demand of refrigeration appliances. Accordingly, enclosing appliances with supplementary insulating materials, as demonstrated in [167], is recommended to lower energy requirements.

The use of advanced insulation technologies is also recommended. For example vacuum–perlite composites, currently being introduced by Liebherr as part of what is promoted as the first cradle-to-cradle circular refrigeration technology, offer reusability and environmental benefits through the use of volcanic rock [271].

Efficiency labelling grades considering ageing

Based on the ageing model in Equation 3.7, the values in Table 4-6 denote the expected growth in refrigeration appliance energy consumption for each year of operation, up to 20 years.

E_y represents the normalised energy consumption after y years, and ΔE_y is the percentage appliance energy increase after year y of operation. Thus a 23% increase in energy consumption is expected after 10 years, and a 27% increase after 16 years, pointing to declining energy efficiency with age.

Table 4-6: Increase in refrigeration appliance energy consumption with ageing

Year (y)	E_y	ΔE_y (%)	Year (y)	E_y	ΔE_y (%)
1	1.04	4.2	**11**	1.24	24.0
2	1.08	7.8	**12**	1.25	24.8
3	1.11	10.9	**13**	1.25	25.5
4	1.14	13.5	**14**	1.26	26.1
5	1.16	15.8	**15**	1.27	26.5
6	1.18	17.8	**16**	1.27	27.0
7	1.19	19.4	**17**	1.27	27.3
8	1.21	20.9	**18**	1.28	27.6
9	1.22	22.1	**19**	1.28	27.9
10	1.23	23.1	**20**	1.28	28.1

E_y is the normalised energy consumption after y years
ΔE_y is the percentage appliance energy increase after y years

The findings from incorporating ageing into the labelling standards using the results in Table 4-6 are described below.

Energy Consumption and Efficiency categorisation for refrigeration appliances

In this work, the ageing factor is incorporated into the computation of the energy consumption index R in order to more realistically reflect long-term appliance performance. The adjustment to R is based on the ageing model which predicts a 23% increase in energy consumption after 10 years of operation. Although the mean lifetime of refrigeration appliances is estimated at approximately 16 years [163], a 10-year duration is selected for illustration as a conservative representative evaluation period. The adjusted energy consumption index with ageing is denoted as $R_{adj_{age}}$.

The calculation of $R_{adj_{age}}$ is carried out using the reference refrigerator–freezer values provided in Annex A.2 of the Draft East African Standard: Refrigerating appliances for household and similar use - minimum energy performance requirements [222].

Specifically, the appliance considered contains a 137 litre fresh food compartment and a 63 litre automatic-defrost frozen food compartment at -18 °C. The corresponding energy consumption index R, computed using the standard approach, is compared with $R_{adj_{age}}$ calculated by applying the ageing adjustment for 10 years, as described in Section 3.5.2. The results are shown in Table 4-7.

Table 4-7: Energy Consumption Index computed without and with an ageing factor

Parameter	**Value**	***Energy consumption index calculation***	
Reference ambient temperature (°C)	32	**Energy consumption index without ageing adjustment**	**Value**
Fresh food compartment temperature (°C)	4	Daily energy consumption at 32°C, EC_{32} (kWh / day)	0.724
Frozen food compartment temperature (°C)	-18	Annual Energy Consumption, AEC (kWh / year)	264.3
Fresh food compartment volume (L)	137	Maximum Annual Energy Consumption, AEC_{max} (kWh / year)	286.1
Frozen food compartment volume (L)	63	Energy Consumption Index, R	1.08
Fresh food compartment volume adjustment factor	1.00	**Energy consumption index with ageing adjustment**	**Value**
Frozen food compartment volume adjustment factor	1.79	Daily energy consumption at 32°C after 10 years, $EC_{32_{adj_{10}}}$ (kWh / day)	0.891
Fresh food compartment frost adjustment factor	1.0	Annual Energy Consumption with 10-year ageing factor adjustment, $AEC_{adj_{10}}$ (kWh / year)	325.3
Frozen food compartment frost adjustment factor	1.1	Maximum Annual Energy Consumption with ageing factor, $AEC_{max_{adj_{10}}}$ (kWh / year)	303.7
Fresh food compartment adjusted volume (L)	137	Energy Consumption Index with ageing factor, $R_{adj_{age}}$	0.93

As indicated in Table 3-7, the minimum energy performance requirement corresponds to R=1.00, defining the threshold for low-efficiency devices. The computed R=1.08 value places the appliance within the allowable range but at the lower end of efficiency. After the inclusion of the 10-year ageing factor, however, the adjusted index $R_{adj_{age}}$= 0.93 falls below the minimum compliance threshold (i.e. $R_{adj_{age}}$< 1), reclassifying the appliance as non-compliant with the minimum energy performance standards.

These results demonstrate that reliance solely on initial efficiency ratings can significantly underestimate long-term energy performance. The integration of ageing effects

into the definition of energy labelling standards thus a more robust framework for evaluating appliance efficiency, considering its operational lifespan.

A sensitivity analysis is performed to quantify the influence of assumed equipment lifetimes on the ageing-adjusted $R_{adj_{age}}$ values. The results, presented in Table 4-8, show the key parameters for no ageing and for ageing with operational lifetimes of 10, 15, and 20 years, for the appliance whose data is in Table 4-7.

Table 4-8: Sensitivity analysis for different appliance lifetimes

Parameter	**Standard approach (no ageing)**	**With ageing (lifetime y in years)**		
		y **=10**	y **=15**	y **=20**
$EC_{32_{adj_y}}$ (kWh / day)	0.724	0.891	0.916	0.927
AEC_{adj_y} (kWh / year)	264.3	325.3	334.3	338.5
$AEC_{max_{adj_y}}$ (kWh / year)	286.1	303.7	306.3	307.5
R	1.08	-	-	-
R_{adj_y}	-	0.93	0.92	0.91

The ageing-adjusted index $R_{adj_{age}}$ displays a 14 - 16% reduction relative to the standard R = 1.08, with values of 0.93, 0.92, and 0.91 for 10-year, 15-year, and 20-year operational lifetimes.

For a more realistic efficiency categorisation, a revised labelling framework is proposed, that introduces an ageing factor R_{age} based on from the 20-year lifetime. This choice ensures stricter standards than would be achieved under shorter design lifetimes, such as 10 years.

$$R_{age} = \frac{R}{R_{adj_{20}}} = \frac{1.08}{0.91} = 1.2 \quad \text{(to 1 decimal place)}$$

R_{age} is then applied as a multiplier to each of the limits listed in Table 3-7. This generates the revised minimum energy labelling categories shown in Table 4-9.

Table 4-9: Proposed energy labelling categories with ageing for refrigeration appliances

Grade	**Refrigerators**	**Refrigerator-Freezers**	**Freezers**
High Efficiency	$1.80 \leq R$	$1.80 \leq R$	$1.80 \leq R$
Intermediate efficiency	$1.50 \leq R < 1.80$	$1.50 \leq R < 1.80$	$1.50 \leq R < 1.80$
Low efficiency	$1.20 \leq R < 1.50$	$1.20 \leq R < 1.50$	$1.20 \leq R < 1.50$

By incorporating the ageing factor into a more conservative grading scheme, it is expected that the East African market, as well as other regional markets, will be directed toward refrigeration appliances that are more energy efficient and also exhibit improved long-term reliability and performance. Accounting for ageing helps ensure that appliances maintain their efficiency categorization over their operational lifetime, reducing unforeseen increased energy consumption and operating costs.

Although the revised MEPS calculations including the ageing adjustment were performed for the specific appliance described, it is envisaged that these proposed ageing-aware energy labeling standards would be broadly applicable across a diverse range of refrigeration appliances.

Overall summary

We recommend that ageing factors be incorporated into the development of minimum energy performance standards (MEPS) for the EAC region, and extended to other regions such as SADC and elsewhere. Integrating such considerations would provide a more realistic representation of long-term appliance performance, ensuring that only appliances with sustained efficiency are permitted to enter the market. This adjustment is expected to reduce lifecycle energy costs, particularly given the lengthy operational lifetimes of refrigeration appliances.

Implementation of such standards could incentivize manufacturers to produce higher-quality, longer-lasting appliances, while supporting consumers in selecting products with lower lifecycle energy costs. Furthermore, these standards provide a regulatory

framework for periodically updating minimum performance requirements in line with appliance ageing trends and technological advancements.

Improved appliance efficiency also has broader system-level benefits, including the reduction of stress on both microgrid and grid infrastructure during peak demand periods. Sensitization and awareness campaigns on the importance of and adherence to efficiency standards will be critical to foster consumer and market uptake of compliant appliances. Second hand appliances should not be permitted on the market.

Furthermore, a monitoring method like the Bonn method provide a useful means of quantifying insulation degradation over several years. As insulation deterioration directly influences the decay constant and hence appliance energy consumption, the Bonn method can serve as a practical tool for tracking insulation effectiveness and assessing long-term refrigeration appliance energy demand.

In scenarios where cold storage facilities are built using materials and construction methods that are locally sourced and tailored to the regional context, due to for example lower initial investment and maintenance costs, easier access to materials and spare parts, or easier local capacity skilling, the Bonn method offers a practical, low-cost solution to assess the effectiveness of insulation material and monitor its performance over time. By applying this method, designers can evaluate different insulation options and track degradation, enabling them to evaluate both energy and cost efficiency and the long-term durability of cold storage systems built using locally accessible resources.

4.3 Case study 3 - DSM using PSO for refrigeration appliances

The resulting load profiles from the DSM strategic load conservation (due to appliance on time curtailment) and load shifting are shown in Figure 4-4, and the results given in Table 4-10. The refrigeration curtailment arises from switching off of appliances for some hours as described in Table 3-9.

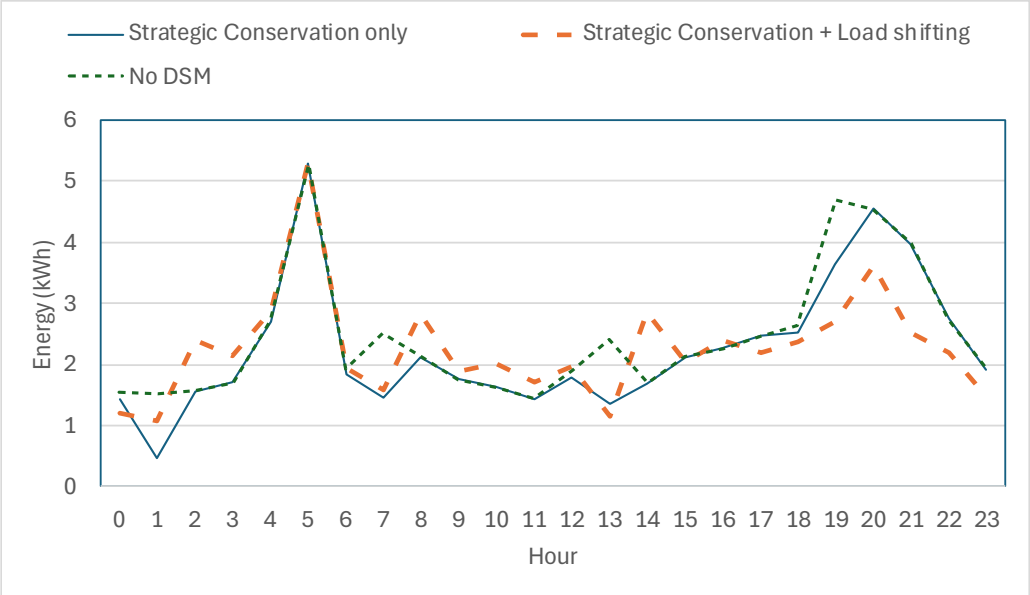

Figure 4-4: Load profiles for the No DSM case (dotted line) and DSM case with refrigeration curtailment (strategic conservation) and load shifting (long dashed line)

Table 4-10: Results from PSO optimized load shifting of refrigeration appliances

	No DSM	**Strategic Conservation only**	**DSM (Strategic Conservation & Load shifting)**
Total daily energy (kWh)	59.11	54.45	54.45
Minimum daily energy (kWh)	1.44	0.46	1.09
Peak daily load (kW)	5.28	5.28	5.28
Peak hour daily (hour)	5	5	5
Average daily load (kW)	2.46	2.27	2.27
Peak evening load (kW)	4.70	4.54	3.61
Peak evening hour (hour)	19	20	20
Load Factor (Average to Peak ratio)	0.47	0.43	0.43
Reduction in daily refrigeration energy (%)		18%	18%
Reduction in refrigeration energy annual cost (USD/year)		306	306
Overall reduction in total daily energy (%)		8%	8%

With strategic energy conservation and load shifting the average load reduces to 2.27 kW from 2.46 kW (Table 4-10). The load factor declines by 8.5% from 0.47 to 0.43 with the

introduction of the DSM. This relatively small reduction is attributable to the dual-peak load profile, which limits the scope for load shifting, particularly during morning hours. The morning peak remains largely unaffected due to the relatively small load-shifting window size (6 hours) and the small number of shiftable devices. Increasing both the quantity and variety of shiftable loads could increase the load-shifting potential and gains, as in [39]. In microgrid scenarios with load profiles exhibiting the typical "duck curve" [33] of a low morning peak, dampened daytime consumption and peak consumption in the evening, even greater improvements in load factor may be achievable.

With DSM, the evening peak occurs an hour later, around 20:00 hrs, than for the no DSM case (Figure 4-4). When only strategic conservation is applied, the evening peak decreases by 3%, whereas a combined approach of strategic conservation and load shifting achieves a more substantial 23% reduction relative to the No DSM scenario. Daily refrigeration energy is reduced by 18% due to the on-off operational patterns specified in Table 2, resulting in an overall demand reduction of 8%.

It is expected that by extending the permissible load-shifting period (e.g. to 48 hours instead of 24 hours), greater benefits from load shifting could be achieved. Using smaller time steps for DSM control, such as 15-minute intervals rather than hourly, could further improve load-shifting benefits. The inclusion of additional deferrable or shiftable electrical devices could yield greater improvements in load factor.

PV System modelling results

The PV generation and the load profiles with and without DSM as plotted in Figure 4-5 show the surplus in PV relative to the load. The modelling results are given in Table 4-11.

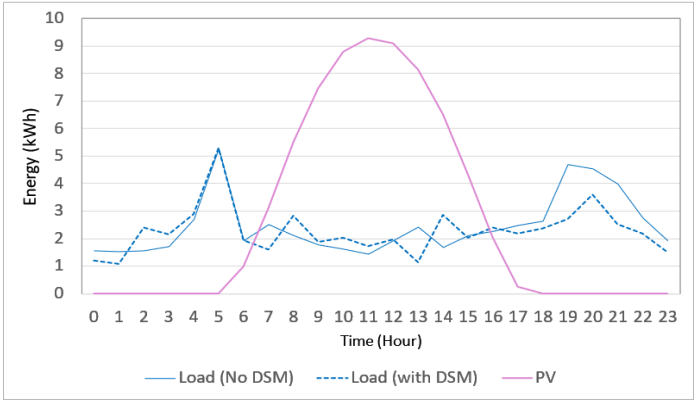

Figure 4-5: Load profiles without and with DSM and PV energy (kWh for each hour of the day, averaged)

Table 4-11: Results from modelling of the DSM for a hybrid system at Lwak

Parameter	**No DSM**	**DSM**
Average daily demand (kWh)	2.46	2.27
Minimum daily demand (kWh)	1.44	1.09
Maximum daily demand (kWh)	5.28	5.28
Total daily demand (kWh)	59.11	54.45
Total annual demand (kWh)	21,576.24	19,874.00
Total daily grid energy (kWh)	20.87	16.34
Grid fraction of load supply (%)	35%	30%
Percentage reduction in daily grid energy (%)		22%
Estimated Annual total grid energy (kWh)	7618.21	5963.59
Grid tariff (USD/kWh)	0.18	0.18
Estimated annual grid energy cost (USD)	1371	1073
Reduction in annual grid energy cost (USD)		297.88
Total daily PV production (kWh)	65.53	65.53
Total PV energy supplied daily to load (kWh)	20.88	21.31
Percentage of PV in load supply (%)	35%	39%

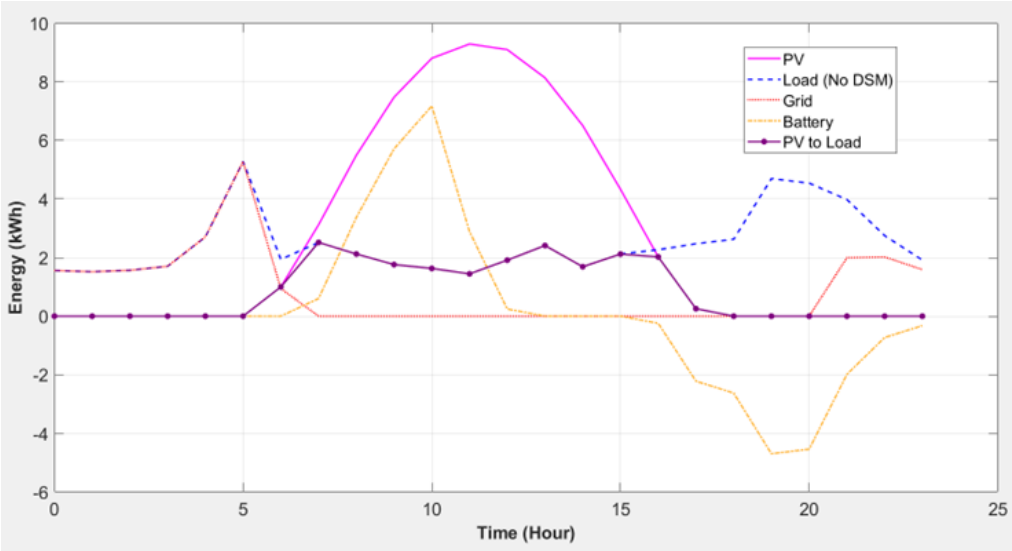

Figure 4-6: Energy and SOC plots for Lwak with no DSM

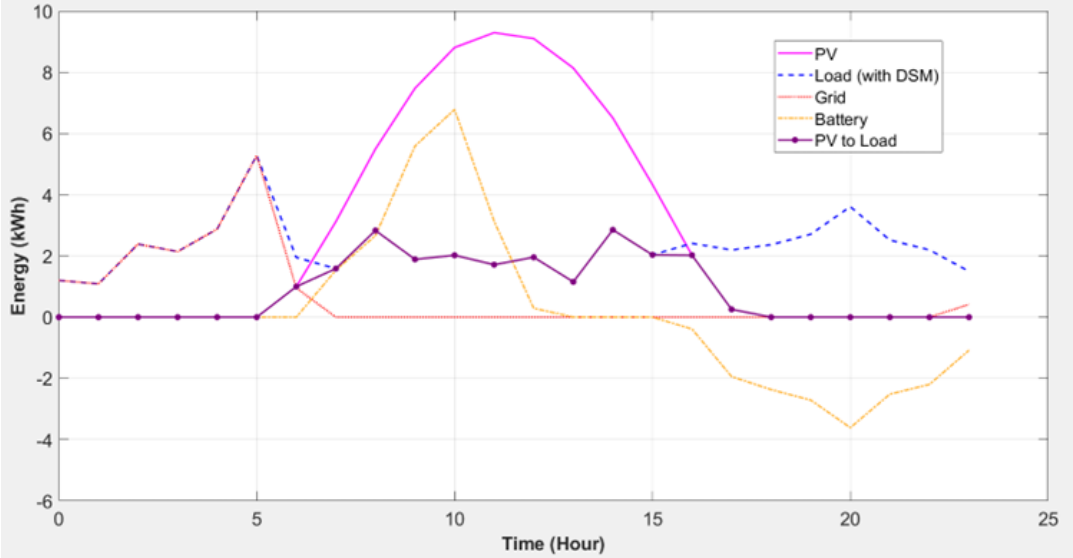

Figure 4-7: Energy and SOC plots for Lwak with load shifting DSM

- **Reduced Grid Dependence**

Grid energy contributions to the load supply decrease from 35% to 30% with DSM (strategic conservation and load shifting), corresponding to a 22% reduction in daily grid energy costs, and to an estimated annual grid costs saving of USD 297.88 at a grid tariff of

USD 0.18/kWh [224]. Over 10 year and 15 year appliance lifetimes, this translates to significant cumulative cost savings of approximately USD 2979 and USD 4468 respectively, assuming a fixed grid tariff and ignoring ageing effects such as insulation degradation. Corresponding energy savings are about 16,546 kWh over 10 years and 24,819 kWh over 15 years.

- **PV Utilization**

The PV system, with a peak hourly output of 9.29 kWh and a possible daily PV production of 65.53 kWh (Table 4-11), delivers only 20.88 kWh under the non-DSM scenario and 21.31 kWh under the DSM scenario (roughly one-third of available generation). The remainder is curtailed, primarily during midday hours (12:00 - 15:00), as illustrated in Figure 4-6 and Figure 4-7. This highlights a system efficiency challenge, where surplus generation could be more effectively utilized if integrated with flexible demand applications such as electric cooking, water heating, pumping, or e-mobility.

For the hybrid PV-battery system, although the annual energy demand decreases from 21,576 kWh for no DSM to 19,874 kWh with DSM, DSM leads to a modest increase (about 2%) in the share of PV generation supplying the load, due to some shifting of refrigeration demand to coincide with PV production hours. Thus the improvement in PV energy consumption due to load shifting is not large.

More substantial benefits for the given objective and optimization approach could likely be achieved with a No DSM load profile characterized by a smaller morning peak, a larger number of shiftable loads, and smaller temporal resolution for load-shifting decisions.

- **Battery Performance**

In Figure 4-6 and Figure 4-7, positive battery energy values represent charging, while negative values indicate discharging. DSM reduces the maximum charging and discharging power requirements, while also lowering the depth of discharge (DOD).

The maximum hourly average charging power decreases from 7.17 kW in the No DSM case to 6.78 kW with DSM, while the maximum hourly average discharging power decreases from 4.70 kW to 3.61 kW, respectively. The reduction in battery depth of discharge (DOD = 1 − SOC) has positive implications for extending battery lifetime, which is influenced by DOD, number of cycles, battery temperature [69][65][70] and ambient temperature [247]. The implementation of the DSM would hence reduce lifetime battery replacement costs.

- **Self sufficiency**

Figure 4-6 and Figure 4-7 show, respectively, the No DSM and with DSM hourly average energy profile for the lowest-irradiance day in 2022 at the Lwak site based on irradiance data from the NASA website. With DSM, evening consumption is reduced, allowing the battery to supply the load until 23:00, with grid power required thereafter (Figure 4-7). This represents an improvement relative to the No DSM case, where grid imports begin as early as 20:00 due to a faster discharge toward the 50% SOC lower threshold (Figure 4-6).

Future research could expand DSM to additional flexible loads, implement finer control intervals, and examine longer-term seasonal variations. Improving appliance thermal mass or insulation, addressing compressor rebound effects, and integrating dynamic pricing signals could further enhance energy savings, load shifting, and battery performance.

4.4 Case study 4 - Temperature and battery SOC-based control for refrigeration appliances

4.4.1 General findings

Figure 4-8 shows measured power profiles for the refrigeration appliances over 6 hours,. It is noted that gaps occurred in the measurement data primarily due to intermittent communication connection failures between the smart plugs and the raspberry pi controller, site-specific power outages and/or data logging problems. Ambient temperature was not considered and was not measured.

Fridge 5 and Freezer 6 have an on-off cycling pattern, typical of fixed-speed compressor appliances. The rest of the appliances run with a 100% duty cycle similar to the Russel Hobbs refrigerator in [104] that uses thermoelectric cooling.

Also notable is that here the duty cycles for Fridge 5 and Freezer 6 appear larger than those presented in Figure 3-25. This is attributed to the lower granularity of this measurement setup data as here the data was recorded in minute intervals, compared to the setup described in Section 3.3.2 where data was recorded in intervals of several seconds. Thus Figure 4-8 is not able to capture in full detail the periodic cyclical pattern for Fridge 5 and Freezer 6 shown in Figure 3-25.

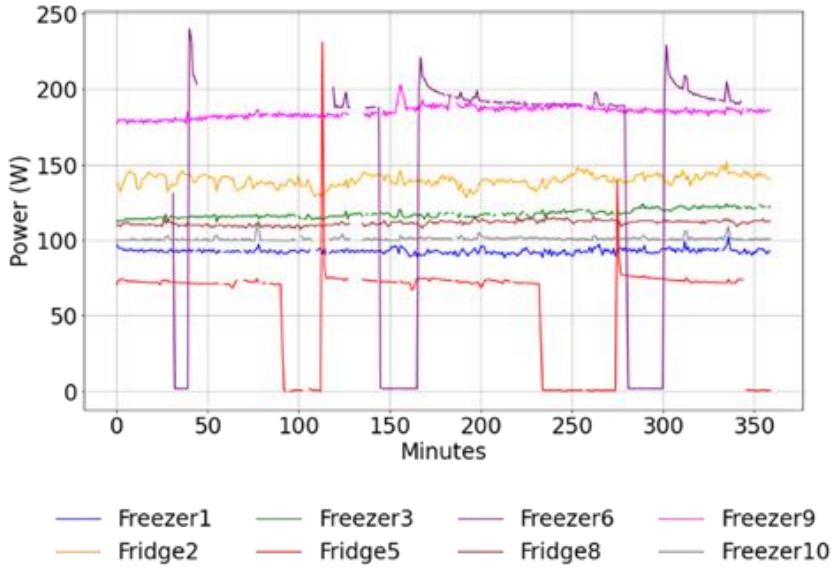

Figure 4-8: Typical power consumption patterns of the refrigeration appliances

Measurement results for the 2 Cases over 6 hours are described below.

Case 1:

For Case 1, as shown in Figure 4-9 and Figure 4-10, the power and temperature profiles reveal distinct appliance behaviour. During the first 100 minutes, Fridge 2 exhibits a gradual decline in power consumption as its internal temperature reduces following a door opening and closing event. At about 130 minutes, Fridge 5 shows a noticeable spike in both power demand and temperature, as does Fridge 8 at around 255 minutes; these fluctuations are attributed to door-opening events. The other appliances demonstrate relatively stable power consumption, albeit the temperature data contains more pronounced gaps. The limited variability in the temperature and power profiles of Freezers 1, 3, 6, 9, and 10 is consistent with expectations, given their larger size, bigger contents volume and hence greater thermal mass, plus possibly better insulation, which dampen fluctuations and contribute to steadier values.

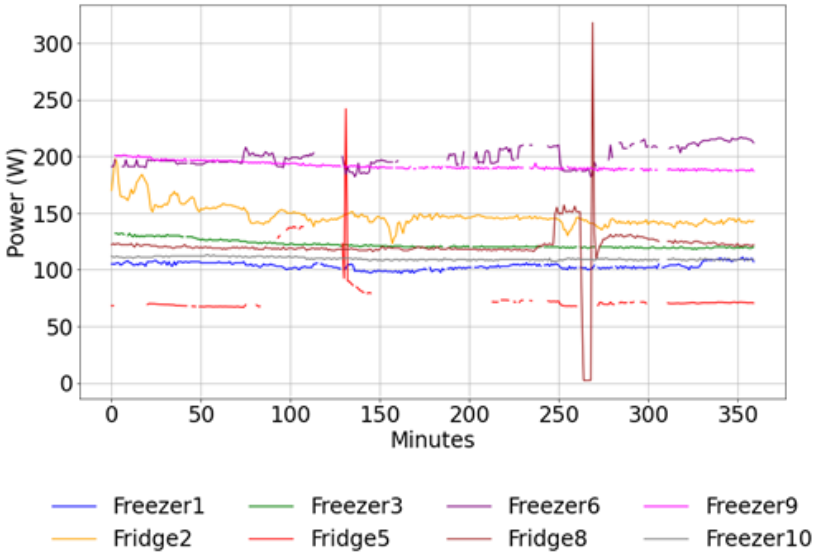

Figure 4-9: Case 1 – Power for the No Control case

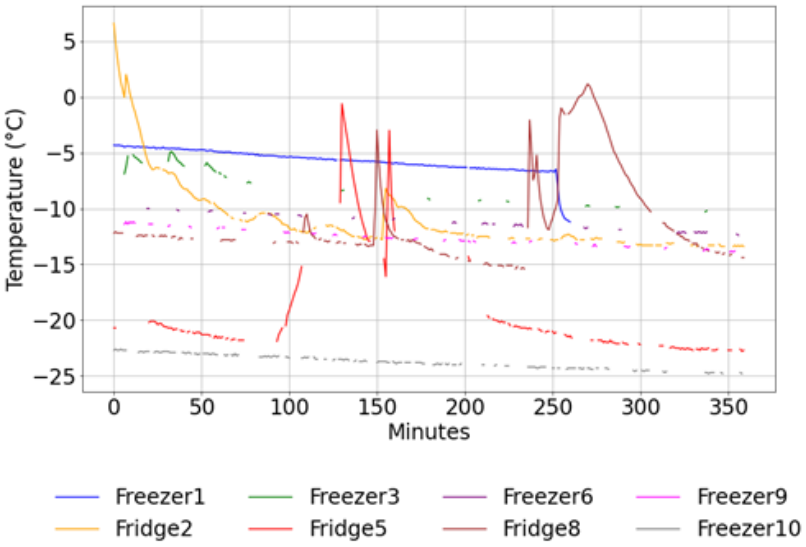

Figure 4-10: Case 1 – Temperatures for the No Control case

Case 2:

For Case 2, where SOC and temperature-based control is implemented, the power, temperature and SOC over a 6-hour period are shown in Figure 4-11, Figure 4-12 and Figure 4-13.

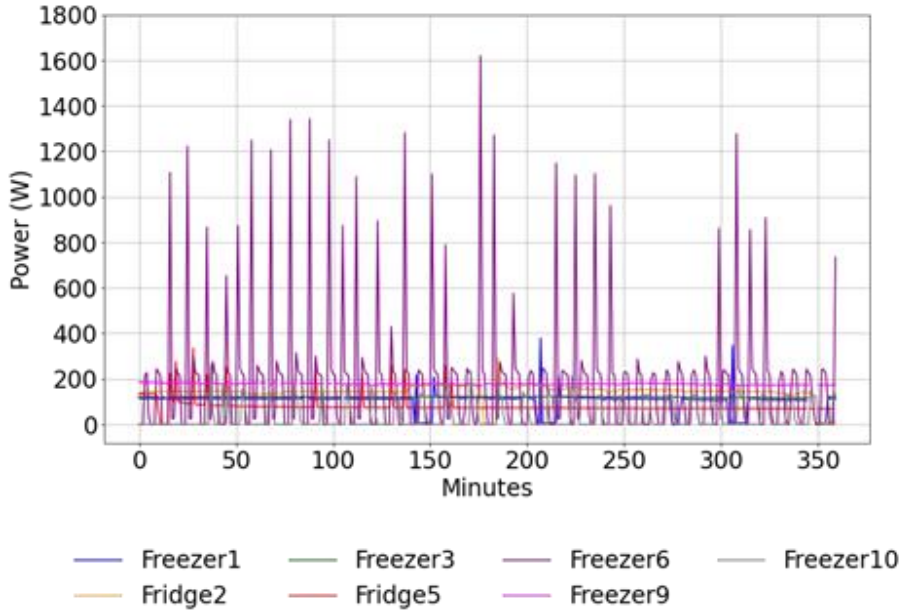

Figure 4-11: Case 2 – Power for SOC and temperature-based control (except for Fridge8)

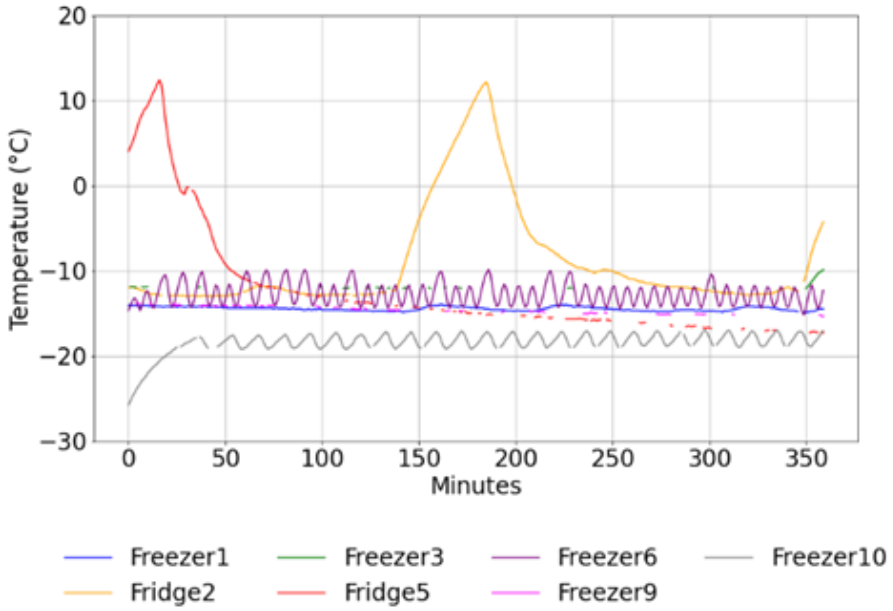

Figure 4-12: Case 2 – Temperature for SOC and temperature-based control (except Fridge8)

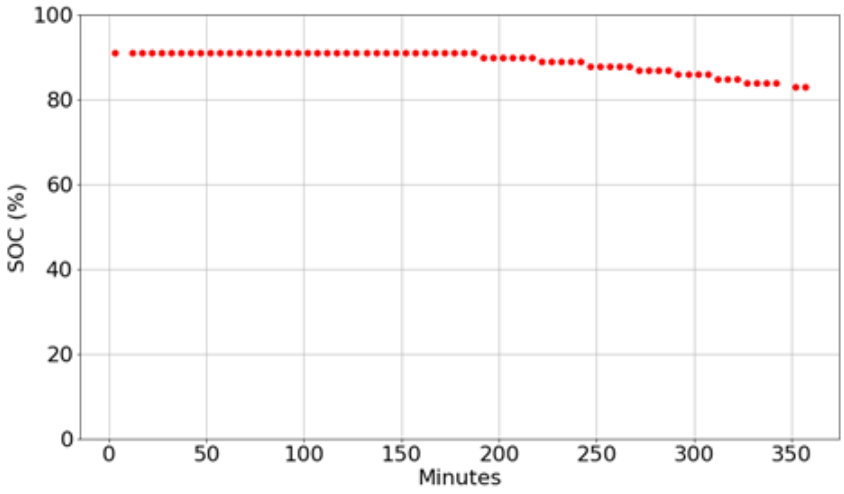

Figure 4-13: Case 2 – SOC values for SOC and temperature-based control

During this interval, the battery SOC declined from 91% to 83% (Figure 4-13), and as SOC > soc_{TH}, the appliance temperatures generally remained within the elevated deadband limits (-10 °C to -6 °C). Notable deviations are observed for Fridge 2 and Fridge 5, where temperature increases occur up to about 15 minutes, and from around 140 minutes to a peak at around 185 minutes, respectively. This is attributed to door openings as well as lower thermal mass given their smaller freezer compartments. Freezer 6 exhibits pronounced power spikes, occasionally reaching up to seven times its average power value. Under SOC and temperature-based control, several significant power peaks ranging from three to seven times those in the no-control case are observed. These are due to compressor startup inrush currents, which can sometimes reach up to 10 times the nominal operating current [19].

Lu et al. [33] propose a strategy to mitigate the rebound effect in systems with multiple thermostatically controlled loads by staggering appliance restarts after a blackout, beginning with the warmest units. While this approach is effective in large-scale direct load control (DLC) scenarios with many controllable devices, it was not implemented in this residential setup due to the relatively small number of appliances.

It is also noted from the measurement data that temperature-based switching influences power consumption differently across appliances, suggesting that this control strategy is more suitable for certain appliances than others.

4.4.2 DSM analysis

A 24-hour analysis was carried out for Freezer 1, Fridge 2, and Freezer 3 to evaluate the performance of DSM using temperature and SOC-based control. Case 1 represents the baseline scenario without DSM, while Case 2 is for the DSM strategy. The corresponding power, temperature, and SOC profiles with DSM are presented in Figure 4-14 and Figure 4-15, while Figure 4-16 shows the energy consumption for the 3 appliances with no DSM (Case 1).

With DSM (Case 2), Fridge 2 occasionally exceeded the upper deadband limit $T_{high2} = -6\ °C$ during the period when the battery SOC was below the soc_{TH} threshold (i.e. SOC ≤ 75%), exhibiting relatively large temperature swings due to its lower thermal mass. In contrast, Freezers 1 and 3 exhibited smaller temperature fluctuations, consistent with their larger thermal inertia arising from their bigger size and volume of contents. With Case 2, operation at the lower deadband (i.e. when SOC > soc_{TH}) between 9:00 and 21:00 for all 3 appliances reveals occurrence of fewer power spikes relative to periods when the appliances are at the higher deadband (i.e. when SOC ≤ 75%), as shown in Figure 4-14.

These observations indicate that SOC- and temperature-based DSM can effectively manage appliance operation in alignment with battery availability, thereby reducing grid dependence during low SOC periods. Appliances with higher thermal mass are better able to buffer temperature variations, minimizing energy waste and smoothing power demand. Conversely, appliances with smaller thermal mass, such as Fridge 2, are more sensitive to temperature deadband adjustments, which may lead to temporary overshoot events. Overall, the results demonstrate that incorporating battery-aware load control can improve PV-battery system efficiency, enhance load shifting, and contribute to longer battery lifespan by reducing avoidable discharge during periods of limited energy availability.

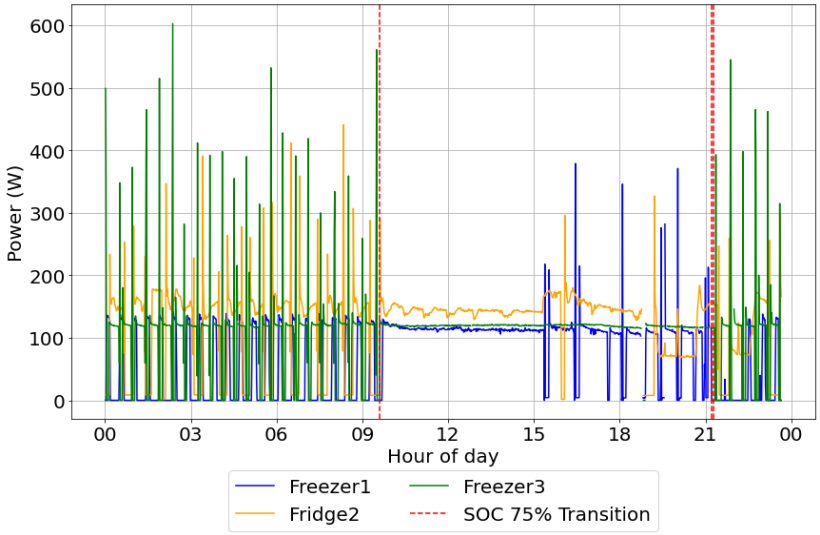

Figure 4-14: Case 2 – with DSM: Power over 24 hours for three appliances

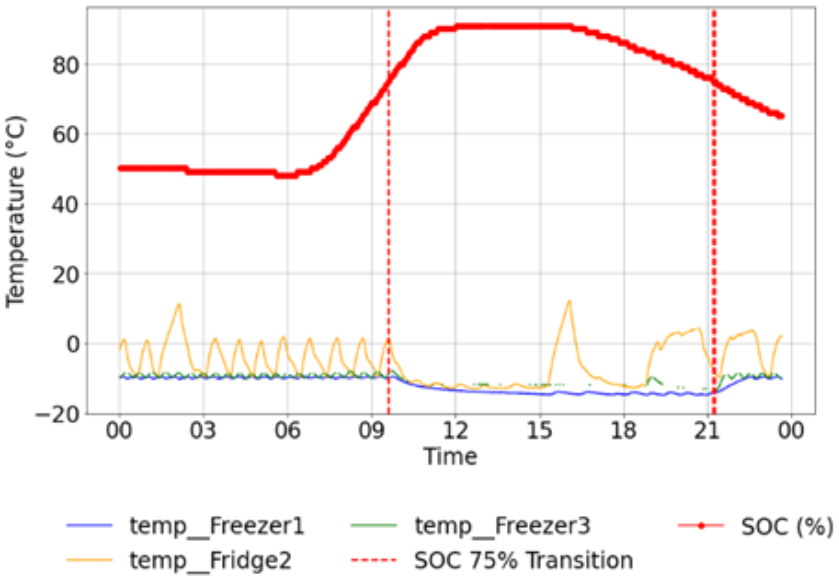

Figure 4-15: Case 2 – with DSM: Temperature (°C) over 24 hours for three appliances

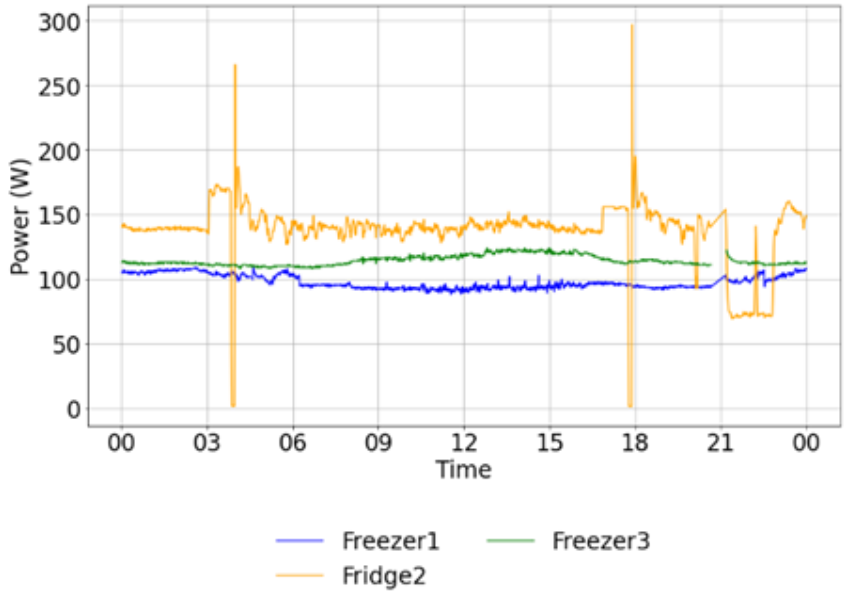

Figure 4-16: Case 1 – No DSM: Power over 24 hours for three appliances (No Control)

The toral power for all 3 refrigeration appliances over the 24 hour period for Case 1 (no DSM) and Case 2 (with DSM) is shown in Figure 4-17. The observed peak total refrigeration power values are 502.9 W (Case 1) and 885.0 W (Case 2), while the corresponding daily average values are 344.4 W (Case 1) and 294.5 W (Case 2). Although DSM leads to an increase in peak refrigeration power, the maximum value remains well below the inverter capacity limits of 5 kW (PV inverter) and 6 kW (battery inverter).

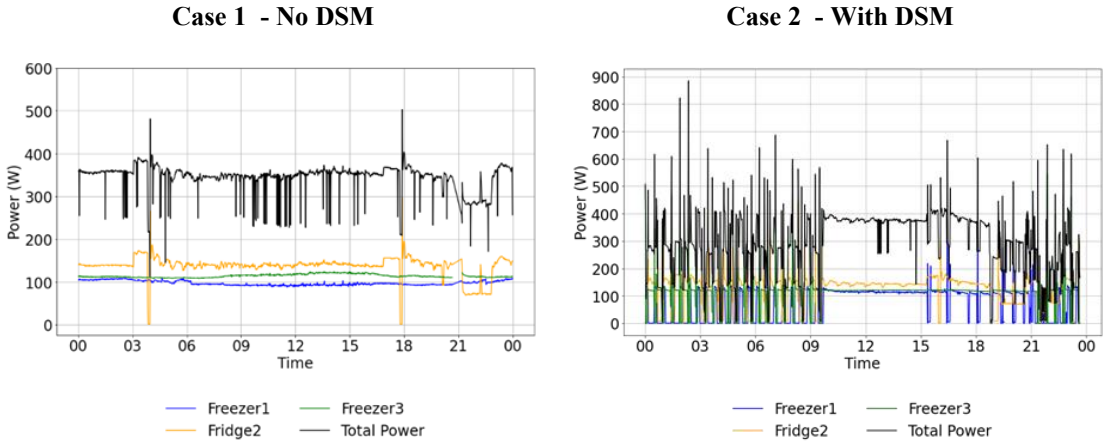

Figure 4-17: Total refrigeration appliance power for three appliances without DSM (Case 1) and with DSM (Case 2)

The elevated total refrigeration power observed between 9:00 and 15:00 in Case 2 relative to Case 1 may be attributed to factors such as increased power draw as a result of DSM control, or possibly higher ambient temperatures during this period.

Average power analysis

The average hourly consumption of the three selected appliances over a 24-hour period, for both Case 1 (no DSM) and Case 2 (DSM with SOC and temperature-based control), is presented in Figure 4-18. For Case 1 (No DSM), the appliances exhibit a relatively flat power profile throughout the day.

For Case 1, Freezer 1 shows a slight dip in power draw between 06:00 and 16:00, a trend that does not match either the expected solar irradiation profile or the higher daytime ambient temperatures, which would normally increase cooling demand. A possible explanation is user behavior such as more frequent door openings in the evening and night, or the addition of warm contents late in the day that could have created the higher refrigeration load in the evening and early morning period.

In contrast, under Case 2 with DSM, Freezer 1's consumption is higher during the daytime, when SOC levels are generally above the defined threshold (soc_{TH}).

Figure 4-18 illustrates the effect of the control algorithm in aligning cooling loads with periods of PV availability and higher battery energy levels, with all 3 appliances showing elevated consumption during 09:00 to 21:00, coinciding with solar production hours and / or relatively high SOC levels. This redistribution of load is consistent with DSM objectives, reducing stress on the battery during low SOC periods and improving utilization of local PV generation.

The impact of DSM varies across appliances. These percentage energy savings are summarized in Table 4-12. Freezer 1 benefits the most, with an average daily power reduction of about 30% (see Figure 4-18). Fridge 2 achieves a moderate reduction of 13%, reflecting its smaller compartment size and lower thermal mass, which make it less equipped for retention of lower temperatures. Freezer 3 shows negligible change. Overall, the results suggest that DSM effectiveness is appliance-dependent, with freezers offering greater controllability than refrigerator-freezers, due to their higher thermal storage capacity. The alignment of consumption with PV generation also points toward improved system-level efficiency by reducing the reliance on battery discharge during lower SOC periods.

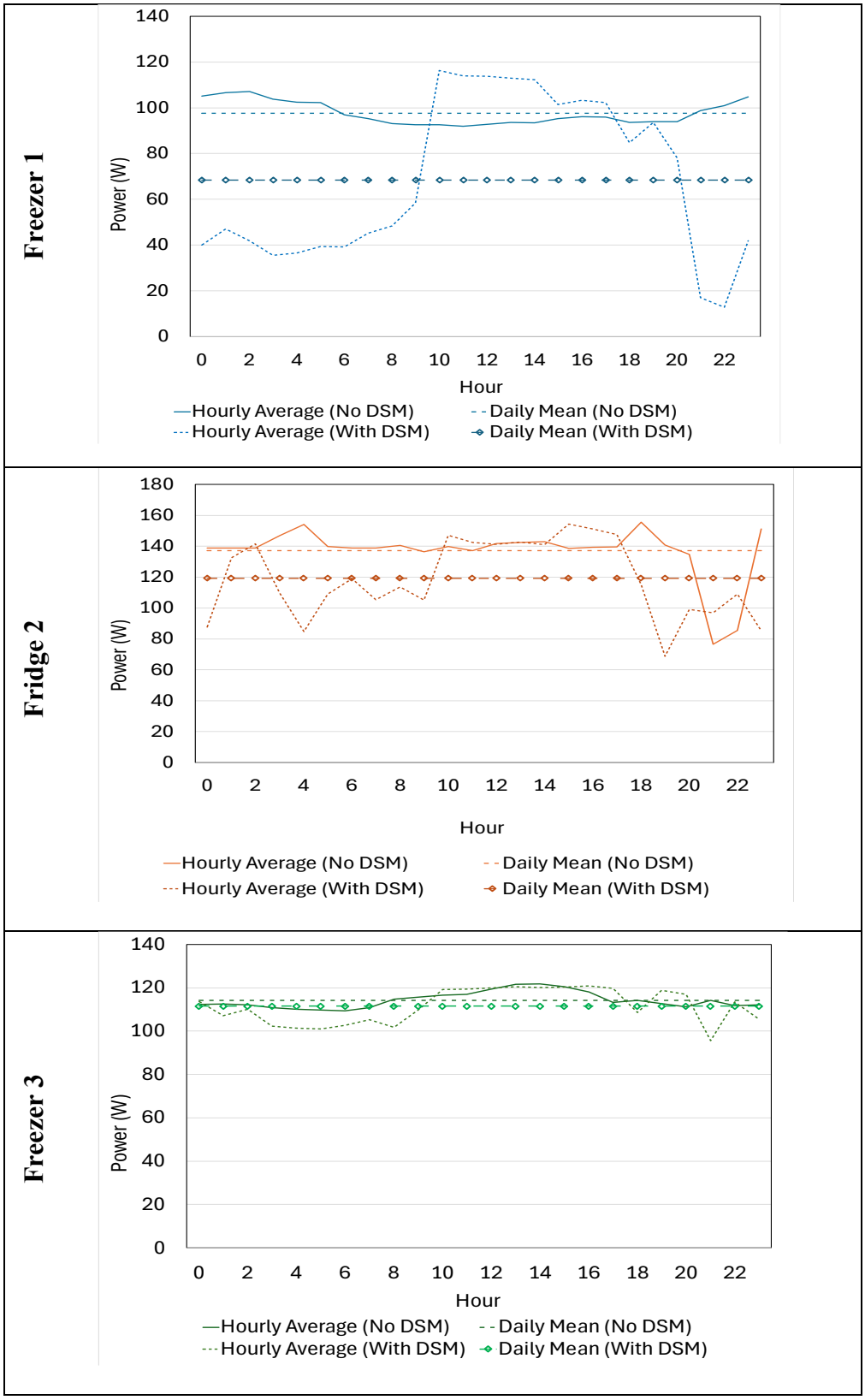

Figure 4-18: Average hourly and daily mean power for Freezer 1, Fridge 2 and Freezer 3, for Case 1 (No DSM) and Case 2 (With DSM)

Table 4-12: Mean power for Case 1 (No DSM) and Case 2 (with DSM)

Appliance	Case 1: No DSM (no control)	Case 3: With DSM (SOC & temperature-based control)	
	Average Power (W)	*Average Power (W)*	*Average Power change relative to Case 1 (%)*
Freezer1	97.6	68.4	-30%
Fridge2	137.1	119.3	-13%
Freezer3	114.2	111.5	-2%

The 24-hour energy consumption of the three appliances is presented in Figure 4-19, showing the different levels of daily energy savings achieved under DSM (Case 2) using the temperature thresholds defined in this study, compared to No DSM (Case 1). It is noted that the magnitude of these savings is dependent on the selected temperature limits; alternative thresholds would likely yield different outcomes.

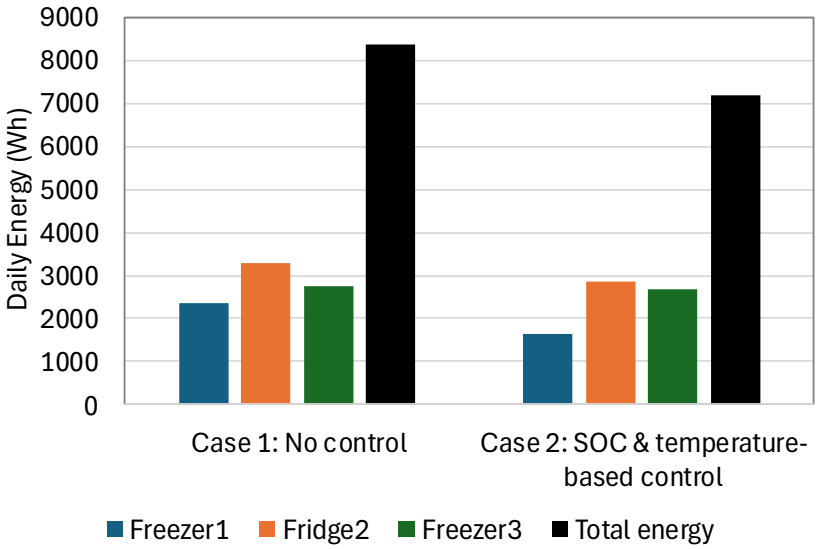

Figure 4-19: Average daily energy for 3 refrigeration appliances for no DSM and with DSM

Unlike the approach in [186] where compressor inrush current spikes were disregarded and only nominal power values were used in demand response energy calculations, this work explicitly included startup transients in the analysis. Incorporating these short-duration peaks provides a more accurate representation of average power and energy demand, which is more important in solar PV and battery storage systems where instantaneous loads can influence required inverter sizing and battery operation performance. The contribution of these spikes to total daily energy consumption, given their short duration, is found to be not significant, indicating that they primarily affect peak demand characterization rather than total energy needs.

Previous studies have explored precooling under time-of-use (TOU) pricing schemes [157] or achieving load shifting by enhancing the thermal storage capacity of appliances using PCM [272]. While such approaches can further shift or reduce refrigeration loads, they were not implemented here.

The focus of this work was instead on improving alignment of refrigeration demand with PV energy production and limiting battery energy requirements through using battery SOC information for control. Cooling refrigeration appliances to lower temperatures during periods of high battery state of charge, and then, when the battery state of charge is low, allowing appliances to operate at higher temperatures reduces cooling demand and eased stress on the system and battery storage. The strategy lowers overall energy consumption while improving the balance between supply and demand in solar-powered microgrids with storage.

Incorporating PCM to increase appliance thermal mass could potentially yield even greater energy reductions and more operational flexibility as noted in [179][273], but that was outside the scope of this study. Modification of the appliance insulation was also not within the scope of this work.

Implications of findings

If temperature-based control is to be applied, careful selection of target appliances is crucial, since energy efficiency and operational behavior can vary significantly across devices. For example, appliances such as Freezer 6 may not be ideal candidates for peak demand reduction despite their potential to lower overall energy consumption, as their startup transients introduce substantial power spikes. Such peaks, if unmanaged, could undermine the objective of demand reduction and energy system sizing reduction, and instead exacerbate system stress. While previous studies on demand-side management have often assumed homogeneity of thermostatically controlled loads (TCLs) [274] [275], this work highlights the importance of accounting for heterogeneous appliance

behavior. A clustering approach, where devices are grouped based on similar operating characteristics, would allow tailored control strategies to be applied, improving both effectiveness and efficiency.

In battery-based systems, frequent and large power spikes accelerate degradation, particularly for lead-acid batteries. Battery lifetime is adversely impacted by factors such as elevated temperatures, partial cycling, high charge and discharge rates and durations between charges to full capacity [69]. The demand spikes associated with the preset switching thresholds in this study could be buffered through integration of alternative storage technologies such as flywheels, which offer better tolerance for short-duration spikes due to their rapid charge/discharge capability. In grid-connected scenarios, these transients could alternatively be handled by the grid supply.

It should also be noted that the SOC and temperature-based DSM control introduces more frequent appliance switching than the uncontrolled case, which may accelerate wear of appliances and of the compressors. Practical mitigation measures could include implementing minimum switching delays or capping maximum switching frequency to extend appliance lifetimes.

As the Shelly devices only operated in the 2.4 GHz band, it was not possible to take advantage of the higher data rates and lower interference of the 5 GHz band which the routers and Raspberry pi 4's also supported. On the communication side, replacing IEEE 802.11 Wi-Fi with LoRaWAN offers advantages in scalability and robustness, particularly in rural and distributed systems such as in microgrids contexts. LoRaWAN enables long-range, low-power communication, supporting reliable data exchange across devices spread over several kilometers [207]. As systems scale to include larger numbers of devices and end-users, the complexity of the DSM algorithm, communication overhead, and computational requirements also will increase. Methods such as batched or staggered load management [276], clustered or aggregated appliance control, and adaptive, dynamic measurement and control intervals [277] could help address these challenges.

Finally, it is acknowledged that factors such as door opening, item loading and unloading, and fluctuations in ambient temperature influence both temperature dynamics and power consumption, thereby affecting the achievable energy savings from the presented DSM strategy. To address this, future implementations could integrate sensors for detecting door activity and/or employ predictive methods such as model predictive control (MPC) to improve the responsiveness and real-time adaptability of the DSM algorithm.

4.5 Case study 5 - E-mobility and portable storage integration analysis for a rural microgrid

4.5.1 Silale results

During the monitoring period for Silale microgrid from 15th - 29th December 2022 (see Section 3.2.3), several interruptions in electricity supply were recorded, comprising of both shorter duration nighttime outages and more extended periods of power loss. Importantly, these interruptions did not occur uniformly across the three supply phases. For instance, from 25 - 27 December 2022, Phase 2 experienced a continuous multi-day outage, whereas Phases 1 and 3 remained on. This selective power interruption is particularly significant, as Phase 2 had been allocated to commercial loads. The loss of power supply therefore affected the phase with the greatest revenue-generating potential.

The peak aggregate demand across all phases was about 2 kW during the measurement period (Table 4-13). Phase B (businesses) had the highest demand, while Phase C (households) had the lowest average consumption, with Phase A (organizations) falling in between.

Table 4-13: Silale microgrid measured power

	Phase A	**Phase B**	**Phase C**	**Total**
Average Power (kW)	0.344	0.374	0.121	0.839
Maximum Power (kW)	0.721	1.242	0.418	2.093

As shown in Figure 4-20, the total microgrid load was lowest between midnight and 08:00, then increased until 10:00 after which, as is characteristic of commercial demand, it remained fairly stable at around 1 kW until 16:00. An evening load ramp up, characteristic of residential demand, was observed from 16:00, peaking at about 1.8 kW at 20:00, followed by a drop in power demand.

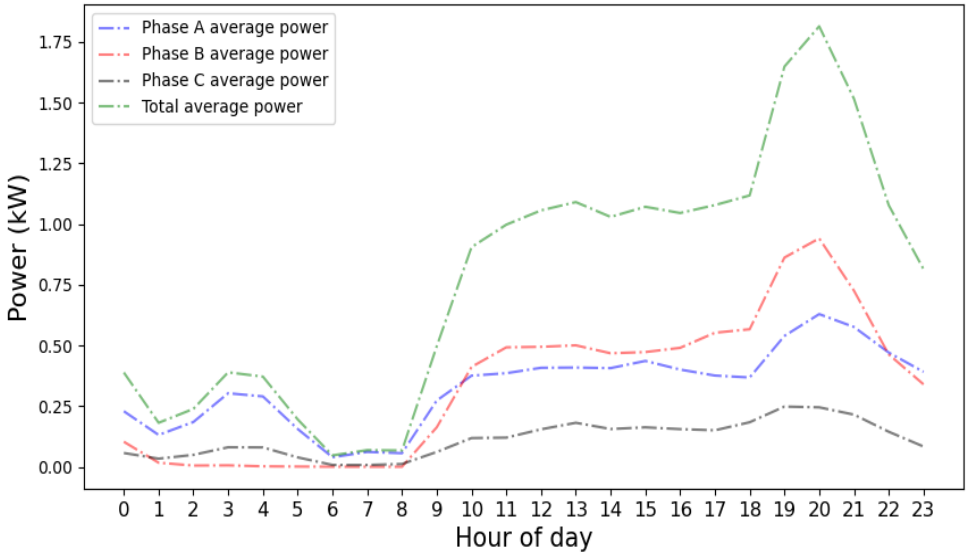

Figure 4-20: Average load profile for Silale microgrid for 15th - 29th December 2022

Total demand remained well below the system's rated capacity. While equipment damage contributed to reduced generation and storage capacity (Figure 3-7), the scale of underutilization points to untapped potential to grow demand. In particular, the relatively modest daytime load suggests opportunities to stimulate productive or commercial use, thereby improving the load factor, reducing the peak-to-average ratio, and enhancing both system efficiency and financial sustainability.

The prolonged downtime of Phase 2 demonstrates that supply reliability is unevenly distributed across the microgrid system. This tallies with findings mentioned in [278] which showed that a monthly subscription tariff model contributed to overloading of a microgrid in Tanzania, as it provided customers with little incentive to moderate their electricity consumption, hence impacting reliability.

From a planning and operational perspective, this highlights the need to assess phase load allocation and carry out periodic load balancing. Such measures would reduce phase-specific outages and improve overall system reliability.

Recommendations for enhancing microgrid sustainability

To improve sustainability of Silale microgrid and of microgrids in general, the following measures are recommended:

- Promote productive energy use: Encourage strategic load growth and load shifting to increase daytime consumption, thus supporting valley filling by adding or moving demand to low-consumption periods.
- Community sensitization: Train communities on proper handling of microgrid equipment and appropriate behaviour near installations to prevent damage (e.g. stones thrown on PV panels). Preventing such issues avoids premature equipment replacement costs and maintains generation capacity and reliability.
- Ensure line balancing: Regularly monitor and redistribute loads across distribution lines to ensure equitable loading. This reduces frequency load shedding and mitigates poor power quality caused by line overloading.
- Plan for decommissioning: Establish end-of-life and handover strategies, including provisions for safe equipment handling and disposal, e.g. battery recycling and disposal.
- Capacity building for local technicians: Train technicians in microgrid configuration, operation, and maintenance to ensure independent management. For example, inability to retrieve system data via the Sunny WebBox highlighted the need for locally accessible monitoring and data logging systems that do not rely on internet connectivity.

4.5.2 Senyondo microgrid results

As discussed in Section 3.5.5.2, PV and battery system characteristics were incorporated into modelling and lifecycle assessment of Senyondo microgrid. The schematic layout of the microgrid, including the proposed e-mobility and portable storage loads, is depicted in Figure 4-21.

Four scenarios were simulated:

- Scenario 1 (Base case): No DSM
- Scenario 2: DSM applied through the introduction of additional loads
- Scenario 3: PV, battery, and converter capacities are halved relative to Scenario 1
- Scenario 4: PV, battery, and converter capacities halved with additional loads introduced.

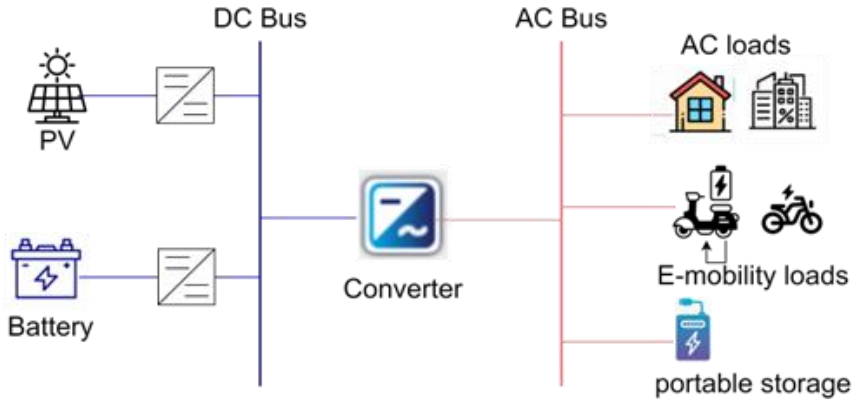

Figure 4-21: Proposed microgrid loads at Senyondo including e-mobility and portable storage

4.5.2.1 Technical Results

Scenario 1 - Business-as-usual with no DSM

The energy profiles without e-bike and portable storage loads are shown in Figure 4-22a. Battery discharge is indicated by negative values, while positive values represent charging. The average state of charge (SOC) is 85.4%, and the minimum SOC of 50% is rarely reached. With degradation considered, the computed battery lifetime is 14.11 years (Table 4-14). Overall, the PV and battery system adequately meet the load demand, achieving a low LPSP of 0.23%, which reflects the oversized PV capacity and resulting high reliability. However, this oversizing also causes significant annual PV curtailment of 60,139 kWh.

The simulated data for the first week is shown in Figure 4-22c. PV generation fluctuates with irradiance, with days 1, 3, and 7 experiencing low peaks probably due to cloudy conditions. Thus on day 2, load shedding occurs in the early hours (indicated by the unserved load curve dipping below 0) because the battery energy is insufficient to cover overnight and morning demand. From day 2 onwards, surplus PV energy is curtailed once the load is met and the battery is fully charged. During the rest of the week, the battery SOC remains relatively high (>70%). The day 2 load profile in Figure 4-22e illustrates the lost load when demand exceeds available supply, coinciding with the battery SOC reaching 50%. PV curtailment between 1500 h and 1700 h is also visible in the same figure.

Table 4-14: Technical results for Scenarios 1 to 4

Parameter	**Scenario 1 (Base Case)**	**Scenario 2 (Base Case Load with E-Bikes and Portable Storage)**	**Scenario 3 (Base Load Only)**	**Scenario 4 (Base Load, E-Bikes and Portable Storage)**
PV capacity (kWp)	75.84	75.84	37.92	37.92
Battery capacity (kWh)	296.64	296.64	148.32	148.32
Converter rating (kW)	80	80	40	40
LCC (USD)	499,918	499,918	367,053	367,053
LCOE (USD/kWh)	0.808	0.350	0.689	0.543
LCC change (%)		0%	−27%	−27%
LCOE change relative to Scenario 1 (%)		−57%	−15%	−33%
LCOE change Scenario 4 vs. Scenario 3 (%)				−21%
Battery lifetime (years)	14.11	14.11	7.62	7.62
Surplus PV energy (kWh/year)	60,138.84	879.05	10,669.76	155.17
Required Base load energy (kWh/year)	43,638.92	43,638.92	43,638.92	43,638.92
Base load energy (kWh/year)	43,539	43,539	37,482.85	37,482.85
E-bike and portable storage energy (kWh/year)	-	58,074.6	-	10,304.3
Unserved (lost) load (kWh/year)	101.96	101.96	6281.71	6281.71
LPSP (%)	0.23	0.23	14.11	14.11
Tariff (USD)	0.30	0.30	0.30	0.30
Increase in annual revenue due to e-bikes and portable storage (%)	-	134.6%	-	26.9%
Avoided CO_2 emissions (ton CO_2/year)	-	73.27	-	29.20
Average number of off-grid customers supplied annually	-	160	-	0
Number Bodawerk 50 km (/year)	-	6944	-	2006
Number Zembo 50 km (/year)	-	7466	-	2385
Number Africrooze 50 km (/year)	-	6644	-	3998
Number portable batteries charged fully (/year)	-	5858	-	3

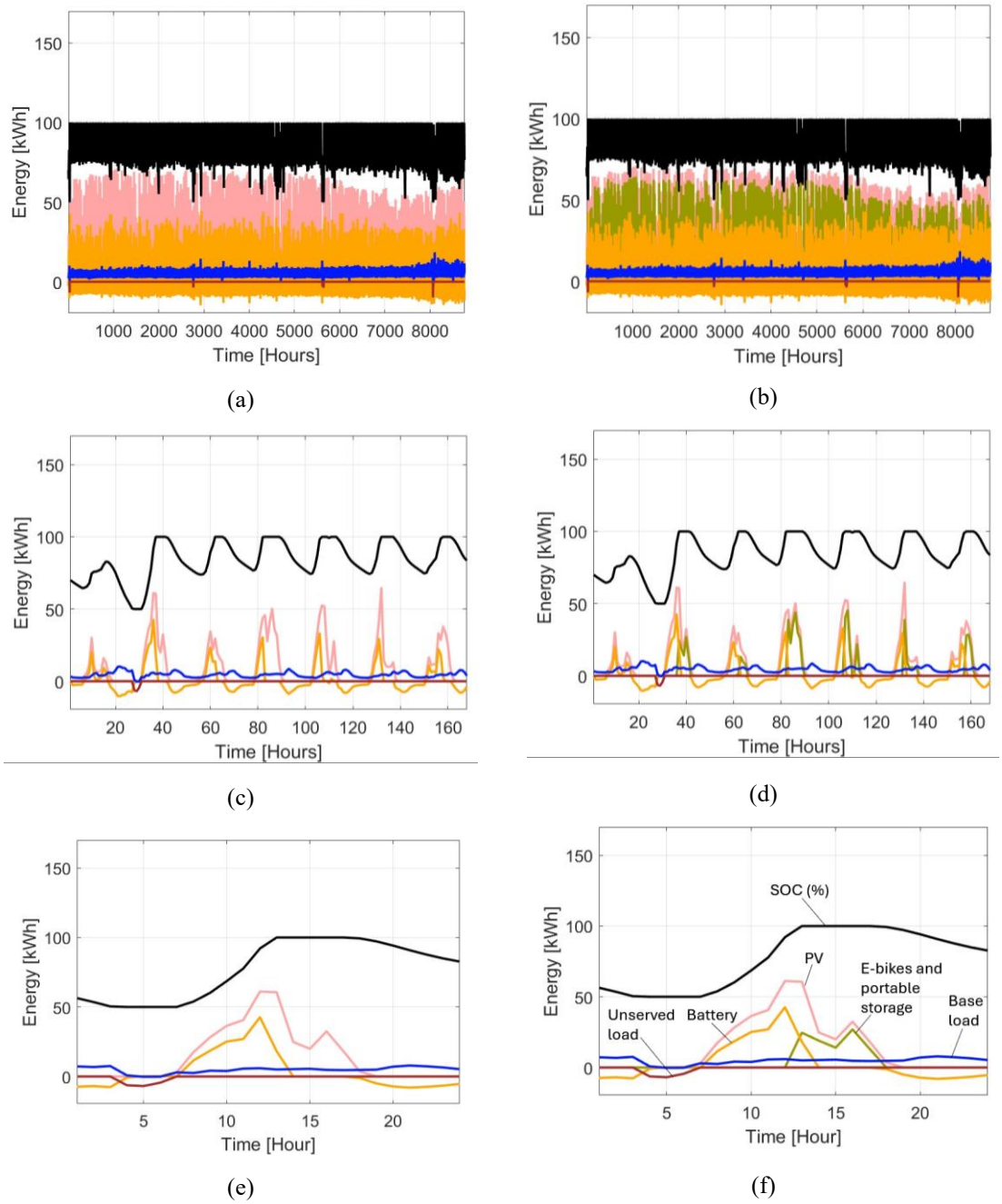

Figure 4-22: Average hourly energy and SOC profiles for the base case for a year: (a) Scenario 1; (b) Scenario 2 with e-bikes and portable storage. Average hourly energy and SOC profiles for the base case for the first week: (c) Scenario 1; (d) Scenario 2 with e-bikes and portable storage. Average hourly energy and SOC values for day 2: (e) Scenario 1; (f) Scenario 2 with e-bikes and portable storage.

Scenario 2 - Base Case with E-Bike and Portable Storage Loads

Introducing the e-bike and portable storage loads in Scenario 2 reduces annual PV curtailment by 98.5%, from 60,138.8 kWh to 879.05 kWh (Figure 4-22b, Table 4-14). Apart from the additional load energy values, all other energy values remained the same as in Scenario 1. From day 2 of week 1, the additional loads successfully absorb most of the surplus PV generation (Figure 4-22d). On day 1, insufficient irradiance limits both load supply and battery charging, while day 3, despite low PV generation, has some limited charging of e-bikes and portable storage once the BESS reaches full charge. Overall, from day 2 onwards, surplus PV energy is supplied to additional loads (Figure 4-22f).

Scenario 3 - Halved PV, Battery, and Converter Capacities without additional loads

In Scenario 3, the PV capacity, battery size, and converter rating are reduced to half the base case values (37.92 kW_p, 148.32 kWh and 40 kW respectively), while the base load is unchanged (see Figure 4-23a). This is feasible since the peak base load was below 20 kW. The reduced system capacity leads to a lower average SOC of 68.73%, with the 50% SOC lower limit reached more often. Consequently, the LPSP increases significantly to 14.11% (Table 4-14). Curtailment is significantly reduced to only 10,669.76 kWh, or about 18% of the curtailed energy in Scenario 1. The first week's energy profile (Figure 4-23c) highlights the greater battery depletion during low irradiance days (days 1 and 3), resulting in more frequent load shedding compared to the base case (Scenario 1). On day 2, the battery SOC falls to 50% before sunrise, leading to load loss until PV generation resumes around 7 a.m. (Figure 4-23e).

Scenario 4 - Halved PV, Battery, and Converter Capacities with Additional Loads

For Scenario 4, the PV capacity, battery size, and converter rating are reduced to half the base case values (37.92 kW_p, 148.32 kWh and 40 kW respectively), the base load is unchanged, and schedulable e-bike and portable storage loads are introduced (Figure 4-23b).

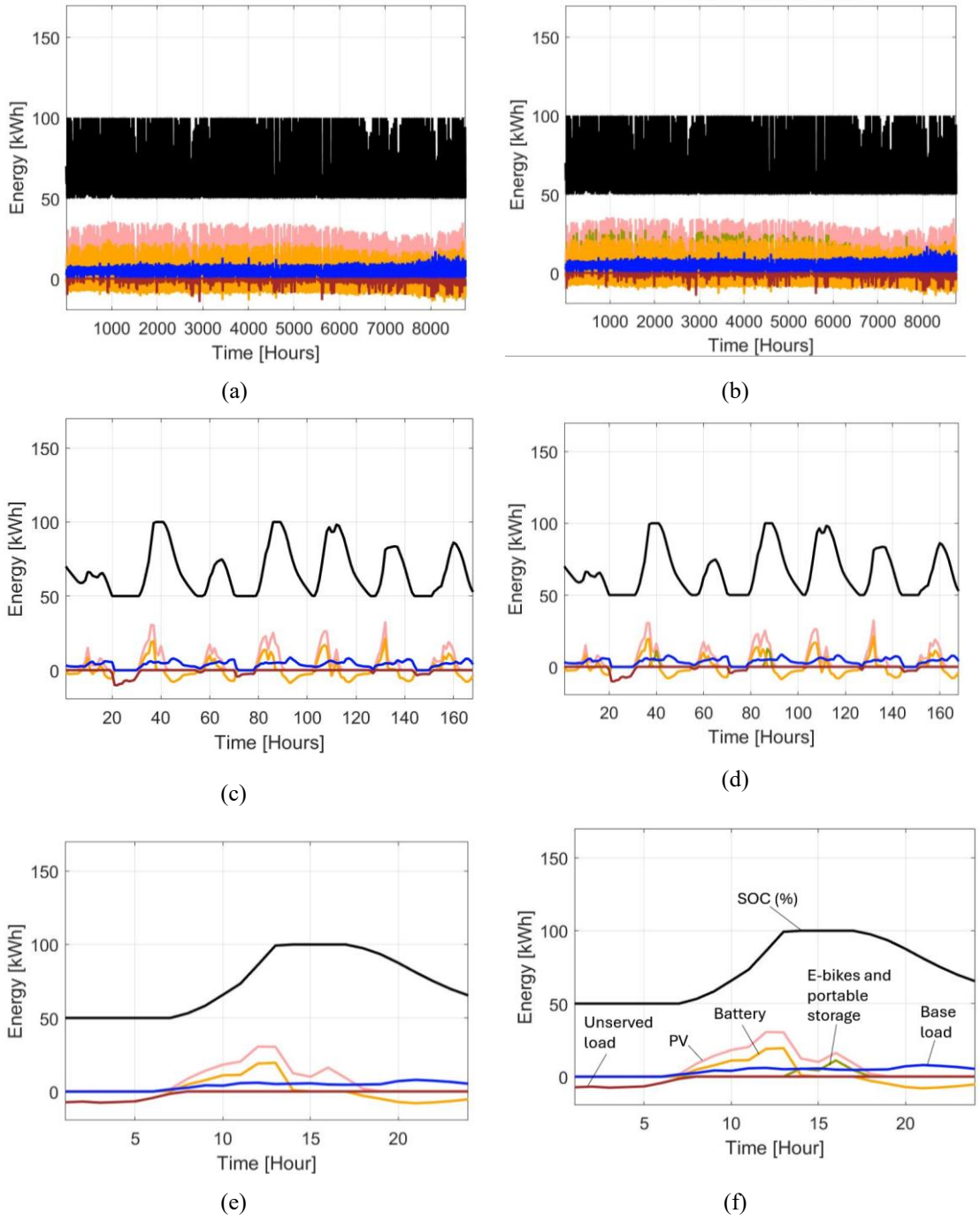

Figure 4-23: Average hourly energy and SOC profiles for a year: (a) Scenario 3; (b) Scenario 4 with e-bikes and portable storage. Average hourly energy and SOC profiles with half the base case PV, battery, and converter capacities for the first week: (c) Scenario 3; (d) Scenario 4 with e-bikes and portable storage. Average hourly energy and SOC values for day 2: (e) Scenario 3; (f) Scenario 4 with e-bikes and portable storage

After introducing the e-bike and portable storage loads, annual curtailed PV energy drops by 98.6% compared to Scenario 3, to only 155.2 kWh. The total energy supplied to the additional loads is 10,304.3 kWh, of which just 0.5% goes to the portable storage, which insufficient to meet the yearly energy demand of even a single off-microgrid customer (Table 4-14). This suggests that under constrained PV generation and the selected charging priority weights, surplus PV energy is best allocated exclusively to e-mobility loads, rather than portable storage. During week 2, some additional loads are supplied on days 2 and 4, after the base load and battery charging requirements are fully met (Figure 4-23d and Figure 4-23f).

4.5.2.2 E-Mobility and Portable Storage Results

The monthly number of e-bikes and portable batteries charged for Scenarios 2 and 4 is shown in Figure 4-24. In Scenario 4, where PV, battery, and converter capacities are halved, there was a significant reduction in e-bikes charged due to limited surplus PV. Notably, the integration of portable storage proves ineffective under the given charging priorities and system capacities, as evidenced by the annual total of portable batteries charged dropping to zero (Figure 4-24b). This highlights that choice of additional loads and their charging priorities should be tailored to the intended DSM objectives.

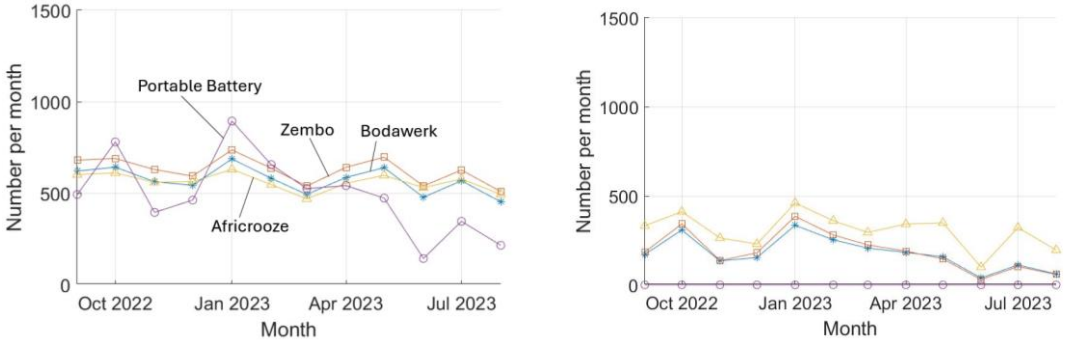

Figure 4-24: Number of portable batteries charged daily and e-bikes that can be charged daily with enough energy for 50 km daily distance (a) Scenario 2; and (b) Scenario 4.

Comparison with Figure 3-37 shows that the months with higher irradiance (September 2022, October 2022, January 2023 and February 2023) correspond to the greater numbers of additional loads charged (see Figure 4-24).

The integration of electric mobility in Scenario 2 results in 73.27 tons of CO_2 avoided annually, whereas Scenario 4 achieves only 29.20 tons of CO_2 avoided, representing a 60% reduction due to the 50% downscaling of PV capacity and the consequent decrease in surplus PV energy. 73.27 tons of CO_2 are the annual emissions from 57 petrol-fueled ICE two-wheelers running on petrol travelling 50 km daily

4.5.2.3 Economic Results

Most microgrids described in the literature use combinations of PV, battery, grid, fuel cells, hydro, biomass, and other energy resources. This study focuses on PV and battery systems. Reported LCOE values for different configurations [22][23][24][25][26][28] range widely from 0.034 USD/kWh to 1.9 USD/kWh, reflecting differences in technology types, capital costs, economic assumptions, grid connectivity, and site-specific weather conditions. For Senyondo microgrid, the calculated LCOE values for Scenario 1, Scenario 2, Scenario 3 and Scenario 4 fall within the lower half of this range (see Table 4-14).

The inclusion of e-bikes and portable storage significantly enhances the economic performance of the microgrid. In Scenario 2, LCOE reduces by 57% compared to Scenario 1, from 0.808 to 0.350 USD/kWh, approaching the typical Ugandan microgrid tariff of 0.30 USD/kWh [265]. Similarly, Scenario 4 achieves a 21% reduction relative to Scenario 3, dropping from 0.689 to 0.543 USD/kWh. These improvements result from strategic load growth DSM, which allocates surplus PV energy to additional loads, thereby minimizing PV curtailment and increasing the effective utilization of generated energy.

Despite halving the PV, battery, and converter capacities in Scenarios 3 and 4, the LCC decreases by only 27% compared to Scenarios 1 and 2, due to the shorter battery lifetime (7.62 years versus 14.11 years), which increases replacement costs. Nevertheless, the targeted use of e-mobility and portable storage allowed a greater proportion of PV generation to be consumed, enhancing cost-effectiveness.

Across all four scenarios, LCOE values are well below that of a stand-alone PV-battery system in Rwanda (1.82 USD/kWh) [22], demonstrating the economic advantage of integrating DSM-enabled loads in off-grid microgrids.

4.5.2.4 Sensitivity Analysis

The effect of varying battery and converter costs, interest rate, battery lifetime, and charging priority weights on system performance are evaluated relative to the base case

(Scenario 1). This analysis allows assessment of how changes in component costs, financial assumptions, and load management strategies impact LCC and LCOE.

Varying battery capital costs

The results in Table 4-15 highlight the critical influence of battery capital costs (C_{Bat}) on the LCC and LCOE. Even with a 20% increase in battery capital costs, integrating e-bikes and portable storage reduces LCOE by over 50% compared to the base case, emphasizing the strong economic advantage of DSM strategies that utilize surplus PV energy. Conversely, a 20% decrease in C_{Bat} results in an 11% reduction in LCC and a 61% decline in LCOE, showing that cost reductions in battery technology have a disproportionately positive effect on project viability.

This strong sensitivity to battery costs is expected, as energy storage systems (ESS) are typically the most replaced component of PV-battery microgrids, contributing heavily to both capital and replacement costs. The findings therefore reinforce the importance of ongoing cost declines in battery technologies, such as lithium-ion and emerging alternatives, in improving the competitiveness of PV-battery systems. From a policy and planning perspective, strategies that support battery cost reductions such as subsidies, local assembly, second-life applications, and recycling could significantly lower microgrid energy costs.

Table 4-15: Sensitivity analysis with varying battery capital costs (C_{Bat})

Parameter	**Scenario 1**	**Scenario 2**	**+10% C_{Bat}**	**+10% C_{Bat} (with Additional Loads)**	**+20% C_{Bat}**	**+20% C_{Bat} (with Additional Loads)**	**−10% C_{Bat}**	**−10% C_{Bat} (with Additional Loads)**	**−20% C_{Bat}**	**−20% C_{Bat} (with Additional Loads)**
C_{Bat} (USD/kWh)	300	300	330	330	360	360	270	270	240	240
LCC (USD)	499,918	499,918	527,418	527,418	554,917	554,917	472,419	472,419	444,919	444,919
LCOE (USD/kWh)	0.808	0.350	0.852	0.369	0.897	0.389	0.763	0.330	0.719	0.312
[1]ΔLCC (%)		0%	6%	6%	11%	11%	−6%	−6%	−11%	−11%
[2]ΔLCOE (%)		−57%	6%	−54%	11%	−52%	−6%	−59%	−11%	−61%

[1] Change in lifecycle cost (LCC) relative to Scenario 1 (%),

[2] Change in levelized cost of energy (LCOE) relative to Scenario 1 (%)

Varying converter capital costs

The sensitivity analysis of converter costs (C_{conv}) indicates that they have only a marginal impact on overall system economics. Even when varied by ±20% relative to the base case, the resulting changes in LCC are limited to ±3% (see Table 4-16), indicating that converter costs are not a dominant factor in total system expenditure. This contrasts sharply with the ESS, which demonstrates a far more significant influence on both LCC and LCOE.

When e-mobility and portable storage loads are introduced, the benefits of improved PV utilization greatly outweigh the small variations in converter costs, yielding reductions in LCOE of over 55% relative to the base case. This finding supports the notion that converter sizing need not be the primary focus of system design, especially when DSM strategies are integrated.

From a planning perspective, the results suggest that converter sizing strategies should prioritize flexibility and scalability rather than strict cost minimization. Aligning converter size with PV capacity rather than limiting it to the peak load [243] or 110% of peak demand [245] [97] provides an opportunity to support future load growth without incurring converter upgrade costs early. Such an approach ensures better long-term system resilience and adaptability, particularly in off-grid and rural microgrid contexts, where demand can evolve rapidly with electrification and promotion of productive uses of electricity.

Table 4-16: Sensitivity analysis with varying converter capital costs (C_{conv})

Parameter	**Scenario 1**	**Scenario 2**	**+10% C_{conv}**	**+10% C_{conv} (with Additional Loads)**	**+20% C_{conv}**	**+20% C_{conv} (with Additional Loads)**	**−10% C_{conv}**	**−10% C_{conv} (with Additional Loads)**	**−20% C_{conv}**	**−20% C_{conv} (with Additional Loads)**
C_{conv} (USD/kW)	300	300	330	330	360	360	270	270	240	240
LCC (USD)	499,918	499,918	507,331	507,331	514,743	514,743	92,506	492,506	485,093	485,093
LCOE (USD/kWh)	0.808	0.350	0.820	0.354	0.832	0.360	0.796	0.344	0.784	0.340
Δ LCC (%)		0%	1%	1%	3%	3%	−1%	−1%	−3%	−3%
Δ LCOE (%)		−57%	1%	−56%	3%	−55%	−1%	−57%	−3%	−58%

Varying battery lifetime

The results clearly demonstrate the dominant influence of the energy storage system (ESS) on overall system costs. Shorter battery lifetimes substantially increase the LCC, with rises of 23% and 64% for 7- and 5-year lifetimes, respectively, compared to the base case (Scenario 1), as shown in Table 4-17. This is primarily due to the need for more frequent battery replacements, which raises expenditure over the project lifetime.

When e-mobility and portable storage loads are integrated, the corresponding LCOE values for 7- and 5-year battery lifetimes increase to 0.571 and 0.432 USD/kWh, respectively, compared to 0.350 USD/kWh for Scenario 2 with additional loads. While the inclusion of additional loads raises the utilization of surplus PV energy, the benefits are partly offset by the higher replacement frequency of the batteries under shorter lifetimes. Thus, the cost-effectiveness of integrating e-mobility is strongly tied to the durability and performance of the ESS.

Table 4-17: Sensitivity analysis with varying battery lifetimes (L_{bat})

Parameter	**Scenario 1**	**Scenario 2**	**5 yrs L_{bat}**	**5 yrs L_{bat} (with Additional Loads)**	**7 yrs L_{bat}**	**7 yrs L_{bat} (with Additional Loads)**	**10 yrs L_{bat}**	**10 yrs L_{bat} (with Additional Loads)**
Battery lifetime (yrs)	14.11	14.11	5	5	7	7	10	10
LCC (USD)	499,918	499,918	817,827	817,827	616,382	616,382	616,382	616,382
LCOE (USD/kWh)	0.808	0.350	1.321	0.571	0.996	0.432	0.996	0.431
Δ LCC (%)		0%	64%	64%	23%	23%	23%	23%
Δ LCOE (%)		−57%	64%	−29%	23%	−47%	23%	−47%

These findings highlight the critical role of battery technology improvements, particularly regarding cycle life and degradation rates, in reducing long-term system costs. Investment in higher-quality batteries with longer lifetimes, even at higher initial capital cost, may prove more economical in the long run by avoiding multiple replacement cycles. Additionally, effective charging strategies and load management that minimize deep discharges could extend battery lifetime, further improving LCOE outcomes.

Varying interest rates

The interest rate sensitivity analysis reveals that financing assumptions play a noticeable role in shaping project economics. A 20% increase in the interest rate reduces the LCC by 16% (to USD 419,602), while a 20% decrease leads to a 24% increase in LCC (Table 4-18). This counterintuitive trend arises from the discounting effect, where higher interest rates reduce the present value of future replacement and operational costs, thereby lowering the overall LCC. Conversely, lower interest rates amplify the weight of long-term costs, increasing the LCC.

However, the effect of interest rate changes on LCOE is found to be negligible. This is because while the absolute project costs vary with the discount rate, the proportional relationship between costs and energy supplied remains largely unchanged. Therefore, the sustainability of the microgrid is more sensitive to technical and operational parameters (e.g. battery lifetime and cost) than to this financing assumption.

Table 4-18: Sensitivity analysis with varying interest rates (i_{nom})

Parameter	Scenario 1	Scenario 2	+10% i_{nom}	+10% i_{nom} (with Additional Loads)	+20% i_{nom}	+20% i_{nom} (with Additional Loads)	−10% i_{nom}	−10% i_{nom} (with Additional Loads)	−20% i_{nom}	−20% i_{nom} (with Additional Loads)
Interest rate (%)	13	13	14.3	14.3	15.6	15.6	11.7	11.7	10.4	10.4
LCC (USD)	499,918	499,918	455,919	455,919	419,602	419,602	553,497	553,497	619,090	619,090
LCOE (USD/kWh)	0.808	0.350	0.828	0.358	0.850	0.368	0.790	0.342	0.774	0.335
Δ LCC (%)		0%	−9%	−9%	−16%	−16%	11%	11%	24%	24%
Δ LCOE (%)		−57%	2%	−56%	5%	−54%	−2%	−58%	−4%	−59%

Varying charging priorities for the additional loads

The analysis of charging priority weights highlights the pivotal role of load prioritization in optimizing surplus PV energy utilization and aligning technical outcomes with social objectives. When all additional loads are given equal weighting i.e. $W_1 = W_2 = W_3 = W_4 = 1$, rather than the $W_1 = W_2 = W_3 = 1$ and $W_4 = 0.5$ of Scenario 1, portable storage absorbs most of the surplus PV energy (Figure 4-25), reducing the number of e-bikes charged compared to Scenario 2 (Figure 4-24). This trade-off shows how DSM strategies can be tailored for different aims; prioritizing portable storage enhances electricity access for off-microgrid customers, while prioritizing e-bikes supports e-mobility. The

maximum number of units of each additional load type that can be charged daily remains the same as before (Table 3-16), i.e. $n_{x_n daily_{max}}$ for each of the e-bike types is 20, and $n_{x_n daily_{max}}$ for the portable batteries is 60.

With equal priority weighting, curtailment of PV energy decreases by 72%, and the number of off-microgrid customers served annually increases by more than 90% to 304 (Table 4-19). These results underscore the effectiveness of charging priority adjustments as a flexible tool for balancing competing DSM objectives.

From a policy perspective, this finding is particularly relevant for rural electrification and sustainable transport planning. Regulators and microgrid operators could design incentive mechanisms or operational guidelines that encourage dynamic load prioritization based on local development goals. For example, in areas with low rural electrification rates, higher priority for portable storage could ensure that households without direct grid connections benefit from surplus energy. Conversely, in peri-urban or high-mobility regions, e-bike charging could be emphasized to replace fossil-fuel-based transport.

Ultimately, incorporating charging priority flexibility into microgrid planning frameworks can enhance system resilience, improve equity in energy access, and align renewable energy deployment with broader policy goals such as universal access (SDG 7) and decarbonized transport (SDG 11 and SDG 13).

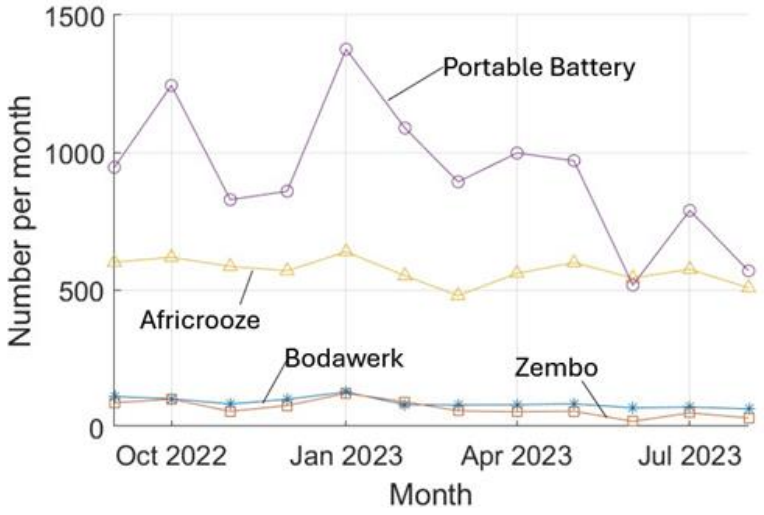

Figure 4-25: Monthly number of portable batteries and e-bikes charged for 50 km distance with equal charging priorities

Table 4-19: Results when weighted priorities for the additional loads are changed

Parameter	**Scenario 2—Base Case with E-Bikes and Portable Storage**	**Equal Weighting—(Base Load with E-Bikes and Portable Storage)**
LCC (USD)	499,918	499,918
LCOE (USD/kWh)	0.350	0.348
Surplus PV energy (kWh/yr)	879.05	248.64
E-bike and portable storage energy (kWh/yr)	58,074.6	58,692.4
Increase in annual revenue due to e-bikes and portable storage (%)	134.6%	132.1%
Avoided CO_2 emissions (ton CO_2/year)	73.27	30.34
Average number of off-grid customers supplied annually	160	304
Number Bodawerk 50 km (/yr)	6944	1068
Number Zembo 50 km (/yr)	7466	823
Number Africrooze 50 km (/yr)	6644	6825
Number portable batteries charged (/yr)	5858	11,078

5 Conclusion and Future Work

5.1 Conclusion

This thesis has examined the role of demand-side management (DSM) in enhancing the sustainability, affordability, and reliability of hybrid energy systems and rural microgrids in East Africa. Through a combination of techno-economic modeling, experimental analysis and policy-oriented assessment, the work has demonstrated that DSM offers a practical and impactful pathway for advancing rural electrification, improving appliance efficiency, and supporting decarbonization objectives.

For Lwak Convent in Western Kenya, hybrid PV-battery system modeling showed that DSM strategies such as peak clipping and load shifting can improve both technical and economic performance. The optimal configuration of the scenarios investigated reduced reliance on the grid, increased renewable utilization, lowered LCOE, and produced surplus energy that could be directed towards applications like thermal storage, electric cooking, water heating, water pumping or e-mobility.

Refrigeration, as one of the more energy intensive residential end-uses, was investigated. Appliance temperature monitoring and subsequent DSM modelling studies demonstrated annual energy and cost savings. The application of particle swarm optimization (PSO) further highlighted the value of coordinated load shifting and curtailment. Battery state of charge and temperature-based DSM was experimentally validated, showing that refrigeration loads can be aligned more closely with PV generation and battery availability. This not only reduced energy consumption but also mitigated stress on the battery system by moderating battery discharge, which has positive implications for lifetime costs and reliability.

The study also addressed a critical policy gap by considering the role of appliance ageing in shaping long-term efficiency performance. The Bonn method offers a practical, low-cost approach to evaluate insulation materials and monitor performance degradation in refrigeration appliances over time. An ageing model was proposed for integration into Minimum Energy Performance Standards (MEPS) for East Africa. Widespread adoption of ageing-aware MEPS and energy labeling standards has the potential to deliver significant energy savings at the regional level, as well as globally. By ensuring appliances sustain high efficiency throughout their operational life, electricity consumption for refrigeration could be substantially reduced. This reduction in energy demand would lower consumer electricity costs, reduce stress on microgrids and the grid, and decrease reliance

on backup generation. Moreover, enhanced appliance efficiency can contribute to lower greenhouse gas emissions, supporting broader climate mitigation objectives in the East African region. Over time, these standards could foster a positive cycle of energy efficiency, cost savings, and environmental benefits, while encouraging the market penetration of high-performance refrigeration appliances.

However, the success of such measures depends not only on technical evaluation but also on effective stakeholder engagement. Supplier and customer education and awareness programs are essential to foster understanding of lifetime energy requirements, encourage behavioral change, and promote the uptake of efficient appliances.

Beyond conservation, DSM analysis was extended to strategic load growth through modelling the integration of e-mobility and portable storage into a rural microgrid. Incorporating load profile data from eight microgrids in Uganda, the analysis showed that introducing electric two-wheelers and portable storage could lower PV curtailment (by 98.5%), reduce the levelized cost of electricity by more than half to 0.350 USD/kWh, and avoid emissions of over 73 tonnes of CO_2 annually. Importantly, portable storage enabled the extension of electricity access to an estimated 160 additional off-grid customers per year without additional distribution infrastructure, while also improving revenue generation for microgrid operators. These results illustrate the potential for DSM not only to reduce demand but also to stimulate productive use growth, thereby improving the long-term viability of rural microgrids.

Of particular importance is prioritization of local capacity building, investment towards locally stored and accessible microgrid data that can be used independently of internet connectivity, and the deployment of digital monitoring, control and load management tools. These measures collectively will enable operators and communities to effectively monitor, manage, and optimize energy system resources and components.

Overall, the findings of this thesis demonstrate that demand-side management (DSM) should be recognized as a central design element in sustainable microgrids and energy systems. By integrating conservation, flexible control strategies, and strategic demand growth, DSM improves both technical performance and socio-economic outcomes. This work spans the gap between appliance-level management, system optimization, and policy, presenting a holistic approach to planning and managing resilient microgrids and energy systems in rural areas and emerging economies.

5.2 Future work

Future research should extend the DSM analysis beyond refrigeration to a wider portfolio of deferrable and productive-use loads, supported by predictive and adaptive control techniques leveraging real-time sensing, machine learning, and weather forecasting.

Appliance ageing models should be studied and embedded into regional MEPS, supported by investments in laboratory capacity and standards certification centres as well as public awareness.

Further work is also needed to manage implementation challenges for appliance control and DSM implementation, such as local data storage, processing and access, and scalable low-cost communication for distributed microgrids and loads.

In addition, pilot-scale deployment of e-mobility and portable storage in rural microgrids is needed to assess adoption dynamics, economic viability, and long-term impacts on microgrid stability.

Extended modelling, experiments and studies on battery operation, degradation and DSM strategy impacts are essential to further understand trade-offs between energy savings and battery lifetimes and costs. Given that batteries often represent a major portion of microgrid expenses in systems with storage, such studies, as well as incorporating end-of-life management, would inform the design of reliable, cost-effective, and sustainable microgrids and storage systems in East Africa.

Finally, given the increasing variability of climate conditions, DSM strategies should be evaluated under extreme or adverse operating scenarios to ensure the reliability of rural energy supply and the resilience of cold-chain operations.

References

[1] M. Bhatia and N. Angelou, “Beyond Connections: Energy Access Redefined,” 2015. [Online]. Available: http://hdl.handle.net/10986/24368.

[2] A. Katre and A. Tozzi, “Assessing the sustainability of decentralized renewable energy systems: A comprehensive framework with analytical methods,” *Sustainability*, vol. 10, no. 4, 2018, doi: https://doi.org/10.3390/su10041058.

[3] United Nations, “SDGs Report 2023,” *The Sustainable development Goals Report 2023: Special Edition*. p. 80, 2023, [Online]. Available: https://unstats.un.org/sdgs/report/2023/The-Sustainable-Development-Goals-Report-2023.pdf.

[4] International Institute for Sustainable Development (IISD), “SDG7 Bulletin: Global Stocktaking on Sustainable Energy,” 2024. https://enb.iisd.org/sites/default/files/2024-04/global_stocktaking_sdg7_0.pdf (accessed May 25, 2024).

[5] IEA, “Africa Energy Outlook 2022,” Paris, France, 2022. doi: 10.1787/g2120ab250-en.

[6] K. Fritzsche, L. Shuttleworth, B. Brand, and P. Blechinger, “Exploring the nexus of mini-grids and digital technologies: Potentials, challenges and options for sustainable energy access in Sub-Saharan Africa.” doi: https://doi.org/10.2312/iass.2019.019.

[7] African Development Bank, “Annual Development Effectiveness Review 2023,” 2023. [Online]. Available: https://www.afdb.org/en/documents/annual-development-effectiveness-review-2023.

[8] BP, “Statistical Review of World Energy 2021,” *BP Energy Outlook 2021*. [Online]. Available: https://www.bp.com/content/dam/bp/business-sites/en/global/corporate/pdfs/energy-economics/statistical-review/bp-stats-review-2021-africa-insights.pdf.

[9] EIA, “Electricity net consumption in Africa from 2000 to 2019 (in terawatt hours),” *Statista*, 2021. https://www.statista.com/statistics/1276781/electricity-net-consumption-in-africa/ (accessed Jan. 09, 2025).

[10] R. Peters, J. Berlekamp, C. Kabiri, B. A. Kaplin, K. Tockner, and C. Zarfl, “Sustainable pathways towards universal renewable electricity access in Africa,” *Nat. Rev. Earth Environ.*, vol. 5, pp. 137–151, 2024, doi: 10.1038/s43017-023-00501-1.

[11] IEA, “Electricity consumption per capita - Africa,” *International Energy Agency (IEA)*. 2024.

[12] G. Baskaran and S. Coste, “Achieving Universal Energy Access in Africa amid Global Decarbonization.” Center for Strategic and International Studies (CSIS), 2024, [Online]. Available: https://csis-website-prod.s3.amazonaws.com/s3fs-public/2024-01/240131_Baskaran_Energy_Africa.pdf?VersionId=5H6XEl6W.3YisdwUoqotAo7aFeXIHLU3.

[13] S. Pelz, S. Pachauri, and N. Rao, “Application of an alternative framework for measuring progress towards SDG 7.1,” *Environ. Res. Lett.*, vol. 16, no. 8, 2021, doi: 10.1088/1748-9326/ac16a1.

[14] United Nations, “Leveraging energy action for advancing the Sustainable Development Goals,” 2021. [Online]. Available: https://sdgs.un.org/sites/default/files/2023-01/SDG 7 Policy Briefs 2021.pdf.

[15] S. R. Narlanka and P. Balachandra, “Measuring energy access for livelihoods, lifestyles, and welfare: Validating the Hierarchical Energy Access Framework in India,” *Energy Res. Soc. Sci.*, vol. 107, p. 103352, 2024, doi: 10.1016/j.erss.2023.103352.

[16] Shell Foundation, “Off-Grid Utilities Report: Bridging the Rural Energy Gap in Emerging Markets.” [Online]. Available: https://shellfoundation.org/app/uploads/2020/02/Shell-Foundation-Bridging-the-Gap-DCU-report.pdf.

[17] P. A. Trotter, N. J. Cooper, and P. R. Wilson, “A multi-criteria, long-term energy planning optimisation model with integrated on-grid and off-grid electrification – The case of Uganda,” *Appl. Energy*, vol. 243, no. March, pp. 288–312, 2019, doi: 10.1016/j.apenergy.2019.03.178.

[18] M. A. Cole, R. J. R. Elliott, G. Occhiali, and E. Strobl, “Power outages and firm performance in Sub-Saharan Africa,” *J. Dev. Econ.*, vol. 134, pp. 150–159, 2018, doi: 10.1016/j.jdeveco.2018.05.003.

[19] bidin A, “Lights, Power, Action: Electrifying Africa,” 2016. [Online]. Available: https://www.africa50.com/fileadmin/uploads/africa50/Documents/Knowledge_Center/APP_Lights_Power_Action_2016__PDF.pdf.

[20] Energy Sector Management Assistance Program, “Mini Grids for Half a Billion People: Market Outlook and Handbook for Decision Makers,” World Bank, Washington, DC, 2022. [Online]. Available: https://openknowledge.worldbank.org/server/api/core/bitstreams/32287154-1ccb-46ce-83af-08facf7a3b49/content.

[21] A. T. Dahiru, D. Daud, C. W. Tan, Z. T. Jagun, S. Samsudin, and A. M. Dobi, “A comprehensive review of demand side management in distributed grids based on real estate perspectives,” *Environ. Sci. Pollut. Res.*, vol. 30, pp. 81984–82013, 2023, doi: 10.1007/s11356-023-25146-x.

[22] C. Nsengimana, X. T. Han, and L. L. Li, “Comparative Analysis of Reliable, Feasible, and Low-Cost Photovoltaic Microgrid for a Residential Load in Rwanda,” *Int. J. Photoenergy*, vol. 2020, 2020, doi: 10.1155/2020/8855477.

[23] H. O. Omotoso, A. M. Al-Shaalan, H. M. H. Farh, and A. A. Al-Shamma’a, “Techno-Economic Evaluation of Hybrid Energy Systems Using Artificial Ecosystem-Based Optimization with Demand Side Management,” *Electron.*, vol. 11, no. 2, 2022, doi: 10.3390/electronics11020204.

[24] J. N. Kakande, G. H. Philipo, and S. Krauter, “Optimal Design of a Semi Grid-Connected PV System for a Site in Lwak, Kenya using HOMER,” in *8th World Conference on Photovoltaic Energy Conversion*, 2022, pp. 1463–1468, doi: 10.4229/WCPEC-82022-4CV.1.8.

[25] N. E. Seremba, F. Ssemakula, J. Namaganda-Kiyimba, and J. N. Kakande, “Integration of the Centralized Grid and Decentralized Renewable Energy Off-Grid Systems: A Techno-Economic Analysis,” in *2024 IEEE Conference on Technologies for Sustainability (SusTech)*, 2024, pp. 257–263, doi: 10.1109/sustech60925.2024.10553436.

[26] R. Mouachi, M. A. Jallal, F. Gharnati, and M. Raoufi, “Multiobjective Sizing of an Autonomous Hybrid Microgrid Using a Multimodal Delayed PSO Algorithm: A Case Study of a Fishing Village,” *Comput. Intell. Neurosci.*, 2020, doi: 10.1155/2020/8894094.

[27] G. H. Philipo, J. N. Kakande, and S. Krauter, “Demand-Side-Management for Optimal Dispatch of an Isolated Solar Microgrid,” in *IEEE AFRICON Conference*, 2023, pp. 1–6, doi: 10.1109/AFRICON55910.2023.10293343.

[28] C. A. Nallolla and P. Vijayapriya, “Optimal Design of a Hybrid Off-Grid Renewable Energy System Using Techno-Economic and Sensitivity Analysis for a Rural Remote Location,” *Sustain.*, vol. 14, no. 22, 2022, doi: 10.3390/su142215393.

[29] P. H. Kumar, R. R. Gopi, R. Rajarajan, N. B. Vaishali, K. Vasavi, and S. Kumar P, “Prefeasibility techno-economic analysis of hybrid renewable energy system,” *e-Prime - Adv. Electr. Eng. Electron. Energy*, vol. 7, p. 100443, 2024, doi: 10.1016/j.prime.2024.100443.

[30] N. K. Bahgaat, “Estimation of renewable energy systems for mobile network based on real measurements using HOMER software in Egypt,” *Sci. Rep.*, vol. 13, p. 16713, 2023, doi: 10.1038/s41598-023-43877-2.

[31] M. Meliani, A. El Barkany, I. El Abbassi, A. M. Darcherif, and M. Mahmoudi, “Energy management in the smart grid: State-of-the-art and future trends,” *Int. J. Eng. Bus. Manag.*, vol. 13, pp. 1–26, 2021, doi: 10.1177/18479790211032920.

[32] N. J. Williams, P. Jaramillo, B. Cornell, I. Lyons-Galante, and E. Wynn, “Load characteristics of East African microgrids,” *Proc. - 2017 IEEE PES-IAS PowerAfrica Conf. Harnessing Energy, Inf. Commun. Technol. Afford. Electrif. Africa, PowerAfrica 2017*, pp. 236–241, 2017, doi: 10.1109/PowerAfrica.2017.7991230.

[33] J. Lu, J. Hu, J. Yu, and J. Cao, “A dynamic demand response control strategy for isolated microgrid with primary frequency regulation,” *Electr. Power Syst. Res.*, vol. 224, p. 109691, 2023, doi: 10.1016/j.epsr.2023.109691.

[34] Z. A. Obaid, L. M. Cipcigan, L. Abrahim, and M. T. Muhssin, “Frequency control of future power systems: reviewing and evaluating challenges and new control methods,” *J. Mod. Power Syst. Clean Energy*, vol. 7, no. 1, pp. 9–25, 2019, doi: 10.1007/s40565-018-0441-1.

[35] C. J. Finck, “Activation of demand flexibility for heating systems in buildings: Real-life demonstration of optimal control for power-to-heat and thermal energy storage,” Eindhoven University of Technology, 2021.

[36] O. Elma, M. Kuzlu, and M. Pipattanasomporn, “A Smart Direct Load Control Approach Using Dynamic Voltage Control for Demand Response Programs,” *Electr. Power Components Syst.*, vol. 50, no. 13, pp. 738–750, 2022, doi:

10.1080/15325008.2022.2139869.

[37] J. Lukuyu, M. Shiran, R. Kennedy, J. Urpelainen, and J. Taneja, "Purchasing power: Examining customer profiles and patterns for decentralized electricity systems in East Africa," *Energy Policy*, vol. 172, p. 113331, 2023, doi: 10.1016/j.enpol.2022.113331.

[38] M. Sakah, S. de la Rue du Can, F. A. Diawuo, M. D. Sedzro, and C. Kuhn, "A study of appliance ownership and electricity consumption determinants in urban Ghanaian households," *Sustain. Cities Soc.*, vol. 44, pp. 559–581, 2019, doi: 10.1016/j.scs.2018.10.019.

[39] I. Gupta, G. N. Anandini, and M. Gupta, "An hour wise device scheduling approach for demand side management in smart grid using particle swarm optimization," in *2016 National Power Systems Conference, NPSC 2016*, 2017, doi: 10.1109/NPSC.2016.7858965.

[40] M. Jamil and S. Mittal, "Hourly load shifting approach for demand side management in smart grid using grasshopper optimisation algorithm," *IET Gener. Transm. Distrib.*, vol. 14, no. 5, pp. 808–815, 2020, doi: 10.1049/iet-gtd.2019.0566.

[41] B. Venkatesh, P. Sankaramurthy, B. Chokkalingam, and L. Mihet-popa, "Managing the Demand in a Micro Grid Based on Load Shifting with Controllable Devices Using Hybrid WFS2ACSO Technique," *Energies*, vol. 15, no. 3, 2022, doi: 10.3390/en15030790.

[42] G. K. Ayetor, I. Mbonigaba, and J. Mashele, "Feasibility of electric two and three-wheelers in Africa," *Green Energy Intell. Transp.*, vol. 2, no. 4, p. 100106, 2023, doi: 10.1016/j.geits.2023.100106.

[43] IEA, "Global EV Outlook 2022," Paris. [Online]. Available: https://iea.blob.core.windows.net/assets/ad8fb04c-4f75-42fc-973a-6e54c8a4449a/GlobalElectricVehicleOutlook2022.pdf.

[44] N. N. Opiyo, "Different Storage-Focused PV-Based Mini-Grid Architectures for Rural Developing Communities," *Smart Grid Renew. Energy*, vol. 09, pp. 75–99, 2018, doi: 10.4236/sgre.2018.95006.

[45] World Bank, "Global Horizontal Irradiation (GHI) solar resource map." https://commons.wikimedia.org/wiki/File:World_GHI_Solar-resource-map_GlobalSolarAtlas_World-Bank-Esmap-Solargis.png.

[46] Global Solar Atlas, "East Africa." https://globalsolaratlas.info/map?c=-5.441022,32.255859,5.

[47] Uganda Bureau of Statistics, "Statistical Indicators Bulletin." 2024, [Online]. Available: https://www.ubos.org/wp-content/uploads/2024/01/LIBERATION-DAY-BROCHURE-2024-FINAL.pdf.

[48] Electricity Regulatory Authority (ERA), "Electricity Supply Industry Performance Report for the Year 2022," 2023. [Online]. Available: https://www.era.go.ug/index.php/resource-centre/publications/reports/793-electricity-supply-industry-performance-report-for-the-year-2022.

[49] International Energy Agency (IEA), "Uganda 2023 Energy Policy Review," 2023. [Online]. Available: https://memd.go.ug/wp-

content/uploads/2020/07/Uganda2023-Energy-Policy-Review.pdf.

[50] Power for All, “Powering Jobs Census 2022 : Focus on Uganda Contents.” 2022, [Online]. Available: https://www.powerforall.org/application/files/9616/6619/4998/Powering-Jobs-Census-2022-Uganda-1.pdf.

[51] EleQtra, “Lake Albert Infrastructure Services.” https://eleqtra.com/projects/lake-albert-infrastructure/.

[52] “Uganda Vision 2040.” [Online]. Available: https://faolex.fao.org/docs/pdf/uga155949.pdf.

[53] MEMD, “Energy Policy for Uganda 2023.” 2023, [Online]. Available: https://nrep.ug/wp-content/uploads/2023/09/Energy-Policy-for-Uganda-2023_Final.pdf.

[54] Kenya National Bureau of Statistics, “2024 Economic Survey.” 2024, [Online]. Available: https://www.knbs.or.ke/wp-content/uploads/2024/05/Chapter-9-Energy-Tables.xlsx.

[55] S. K. Kimutai, I. K. Kimutai, and M. K. Kiplagat, “East Africa ’ s Renewable Energy Diversity Landscape : A case of Kenya ’ s Potential , Progress and Future Prospects,” *J. Energy Res. Rev.*, vol. 16, no. 9, pp. 13–27, 2024, doi: 10.9734/jenrr/2024/v16i9369.

[56] A. A. Abraham, “Choices, Challenges and Dilemmas in Tanzania’s Energy System,” 2024. [Online]. Available: https://ke.boell.org/en/2024/07/08/choices-challenges-and-dilemmas-tanzanias-energy-system-0.

[57] TanzaniaInvest, “Tanzania power.” https://www.tanzaniainvest.com/power.

[58] IEA, “Tanzania electricity information 2022.” https://www.iea.org/countries/tanzania/electricity.

[59] Danish Institute for Human Rights, *Scoping Paper : Human Rights and the Energy Transition in*. Copenhagen. Denmark, 2022.

[60] UNFPA, “World Population Dashboard, United Republic of Tanzania.” https://www.unfpa.org/data/world-population/TZ.

[61] TANESCO, “TANESCO Annual Report 2021/22.” [Online]. Available: https://www.tanesco.co.tz/attachments/media/publications/ugBmdTXeD8_Ag8sTDp2KXtrlYjHtA8RM_Annual Report 2021_22_2023_07_30_07_17_07.pdf.

[62] K. A. Philip, K. Jammeh, and J. Oduor, “An outlook of Tanzania’s Energy Demand, Supply and Cost by 2030,” Abidjan, Côte d’Ivoire, 2023. [Online]. Available: https://www.afdb.org/sites/default/files/documents/publications/wps_no_370_an_outlook_of_energy_demand_supply_and_cost_in_tanzania_.pdf.

[63] Daily News, “JNHPP third power turbine switched on,” 2024. https://dailynews.co.tz/jnhpp-third-power-turbine-switched-on/.

[64] T. Jiang, L. Yu, and Y. Cao, *Energy Management of Internet Data Centers in Smart Grid*, 1st ed. Springer, Berlin, Heidelberg, 2015.

[65] N. N. Opiyo, “Modelling Temporal Diffusion of PV Microgeneration Systems in

a Rural Developing Community," University of Leeds, 2016.

[66] X. Li, S. S. Booth, S. R. Esterly, E. I. Baring-Gould, J. Clowes, and ..., "Performance Monitoring of African Micro-Grids: Good Practices and Operational Data," 2020. [Online]. Available: https://www.osti.gov/biblio/1597244.

[67] E. I. C. Zebra, H. J. van der Windt, G. Nhumaio, and A. P. C. Faaij, "A review of hybrid renewable energy systems in mini-grids for off-grid electrification in developing countries," *Renew. Sustain. Energy Rev.*, vol. 144, 2021, doi: 10.1016/j.rser.2021.111036.

[68] F. Antonanzas-Torres, J. Antonanzas, and J. Blanco-Fernandez, "State-of-the-Art of Mini Grids for Rural Electrification in West Africa," *Energies*, vol. 14, no. 990, 2021, doi: doi.org/10.3390/en14040990.

[69] J. M. Delgado-Sanchez and I. Lillo-Bravo, "Influence of degradation processes in lead-acid batteries on the technoeconomic analysis of photovoltaic systems," *Energies*, vol. 13, no. 15, 2020, doi: 10.3390/en13164075.

[70] S. Ouédraogo, G. A. Faggianelli, G. Pigelet, G. Notton, and J. L. Duchaud, "Performances of energy management strategies for a Photovoltaic/Battery microgrid considering battery degradation," *Sol. Energy*, vol. 230, pp. 654–665, 2021, doi: 10.1016/j.solener.2021.10.067.

[71] G. Ireland, "Techno-Economic Modelling of Hybrid Renewable Mini-Grids for Rural Electrification Planning in Sub-Saharan Africa," University of Cape Town, 2018.

[72] N. Narayan *et al.*, "Stochastic load profile construction for the multi-tier framework for household electricity access using off-grid DC appliances," *Energy Effic.*, vol. 13, pp. 197–215, 2020, doi: https://doi.org/10.1007/s12053-018-9725-6.

[73] CrossBoundary LLC and Energy 4 Impact, "Innovation Insight: Machine Learning to Predict Mini-Grid Consumption," Nairobi, Kenya, 2019. Accessed: Mar. 15, 2021. [Online]. Available: https://crossboundary.com/wp-content/uploads/2024/02/CrossBoundary-Innovation-Lab-Innovation-Insight-Predicting-Consumption-12-December-2019.pdf.

[74] P. Henriot, "Unleashing the benefits of data for energy systems," 2023. https://www.iea.org/commentaries/unleashing-the-benefits-of-data-for-energy-systems (accessed May 16, 2023).

[75] M. T. İşyapar, "Classification of electricity customers based on real consumption values using data mining and machine learning techniques and its corresponding applications," Middle East Technical University, 2013.

[76] M. Fowlie and R. Meeks, "The economics of energy efficiency in developing countries," *Rev. Environ. Econ. Policy*, vol. 15, no. 2, 2021, doi: 10.1086/715606.

[77] N. J. Williams, P. Jaramillo, K. Campbell, B. Musanga, and I. Lyons-Galante, "Electricity Consumption and Load Profile Segmentation Analysis for Rural Micro Grid Customers in Tanzania," *2018 IEEE PES/IAS PowerAfrica, PowerAfrica 2018*, pp. 360–365, 2018, doi: 10.1109/PowerAfrica.2018.8521099.

[78] I. Mwammenywa and U. Hilleringmann, "Analysis of Electricity Power

Generation and Load Profiles in Solar PV Microgrids in Rural Villages of East Africa: Case of Mpale Village in Tanzania," *IEEE AFRICON Conference*. IEEE, Nairobi, Kenya, 2023, doi: 10.1109/AFRICON55910.2023.10293635.

[79] E. Yoder and N. J. Williams, "Load Profile Prediction Using Customer Characteristics," *2020 IEEE PES/IAS PowerAfrica, PowerAfrica 2020*, 2020, doi: 10.1109/PowerAfrica49420.2020.9219811.

[80] G. Falchetta, M. Hafner, and S. Tagliapietra, "Pathways to 100% Electrification in East Africa by 2030," *Energy J.*, vol. 41, no. 3, 2020, doi: 10.5547/01956574.41.3.gfal.

[81] J. Liu and P. Di, "New energy power system inertia weak position evaluation and frequency monitoring positioning," *Front. Energy Res.*, vol. 12, p. 1418302, 2024, doi: 10.3389/fenrg.2024.1418302.

[82] M. H. Moradi, M. Eskandari, and S. M. Hosseinian, "Cooperative control strategy of energy storage systems and micro sources for stabilizing microgrids in different operation modes," *Int. J. Electr. Power Energy Syst.*, vol. 78, no. September 2019, pp. 390–400, 2016, doi: 10.1016/j.ijepes.2015.12.002.

[83] K. Sirviö, K. Kauhaniemi, A. A. Memon, H. Laaksonen, and L. Kumpulainen, "Functional analysis of the microgrid concept applied to case studies of the Sundom smart grid," *Energies*, vol. 13, no. 6, 2020, doi: 10.3390/en13164223.

[84] B. Chen, J. Wang, X. Lu, C. Chen, and S. Zhao, "Networked Microgrids for Grid Resilience, Robustness, and Efficiency: A Review," *IEEE Trans. Smart Grid*, vol. 12, no. 1, pp. 18–32, 2021, doi: 10.1109/TSG.2020.3010570.

[85] N. Salehi, H. Martinez-Garcia, G. Velasco-Quesada, and J. M. Guerrero, "A Comprehensive Review of Control Strategies and Optimization Methods for Individual and Community Microgrids," *IEEE Access*, vol. 10, pp. 15935–15955, 2022, doi: 10.1109/ACCESS.2022.3142810.

[86] Y. Zong, L. Mihet-Popa, D. Kullmann, A. Thavlov, O. Gehrke, and H. W. Bindner, "Model predictive controller for active demand side management with PV self-consumption in an intelligent building," in *2012 3rd IEEE PES Innovative Smart Grid Technologies Europe (ISGT Europe)*, 2012, pp. 1–8, doi: 10.1109/ISGTEurope.2012.6465618.

[87] H. Bevrani, B. Francois, and T. Ise, *Microgrid Dynamics and Control*, First Edit. Hoboken, NJ: John Wiley & Sons, Inc, 2017.

[88] N. A. Luu, "Control and management strategies for a microgrid," Université de Grenoble, 2015.

[89] D. Atabay, "Comparison of optimization methods for model predictive control: An application to a compressed air energy storage system," Technischen Universität München, 2018.

[90] F. Durán, W. Pavón, and L. I. Minchala, "Forecast-Based Energy Management for Optimal Energy Dispatch in a Microgrid," *Energies*, vol. 17, no. 2, pp. 1–21, 2024, doi: 10.3390/en17020486.

[91] A. Micangeli, D. Fioriti, P. Cherubini, and P. Duenas-Martinez, "Optimal design of isolated mini-grids with deterministic methods: Matching predictive operating strategies with low computational requirements," *Energies*, vol. 13, no. 6, 2020,

doi: 10.3390/en13164214.

[92] H. K. Ringkjøb, P. M. Haugan, and I. M. Solbrekke, “A review of modelling tools for energy and electricity systems with large shares of variable renewables,” *Renew. Sustain. Energy Rev.*, vol. 96, no. August, pp. 440–459, 2018, doi: 10.1016/j.rser.2018.08.002.

[93] Y. Xiao, W. Sun, and L. Sun, “Dynamic programming based economic day-ahead scheduling of integrated tri-generation energy system with hybrid energy storage,” *J. Energy Storage*, vol. 44, p. 103395, 2021, doi: 10.1016/j.est.2021.103395.

[94] M. Dashtdar *et al.*, “Optimal Operation of Microgrids with Demand-Side Management Based on a Combination of Genetic Algorithm and Artificial Bee Colony,” *Sustainability*, vol. 14, 2022, doi: 10.3390/su14116759.

[95] M. Awais *et al.*, “An efficient genetic algorithm based demand side management scheme for smart grid,” in *2015 18th International Conference on Network-Based Information Systems*, 2015, pp. 351–356, doi: 10.1109/NBiS.2015.54.

[96] C. Menos-aikateriniadis, I. Lamprinos, and P. S. Georgilakis, “Particle Swarm Optimization in Residential Demand-Side Management: A Review on Scheduling and Control Algorithms for Demand Response Provision,” *Energies*, vol. 15, 2022, doi: 10.3390/en15062211.

[97] P. P Kumar and R. P. Saini, “Optimization of an off-grid integrated hybrid renewable energy system with various energy storage technologies using different dispatch strategies,” *Energy Sources, Part A Recover. Util. Environ. Eff.*, vol. 00, no. 00, pp. 1–30, 2020, doi: 10.1080/15567036.2020.1824035.

[98] R. Rigo-mariani *et al.*, “Comparison of optimization frameworks for the design of a multi-energy microgrid,” *Appl. Energy*, vol. 257, p. 113982, 2020, [Online]. Available: https://hal.archives-ouvertes.fr/hal-03016450 Submitted on 28 May 2021%0AHAL.

[99] E. Cuisinier, C. Bourasseau, A. Ruby, P. Lemaire, and B. Penz, “Techno-economic planning of local energy systems through optimization models: a survey of current methods,” *Int. J. Energy Res.*, vol. 45, pp. 4888–4931, 2021, doi: 10.1002/er.6208.

[100] S. Panda *et al.*, “Residential Demand Side Management model, optimization and future perspective: A review,” *Energy Reports*, vol. 8, pp. 3727–3766, 2022, doi: 10.1016/j.egyr.2022.02.300.

[101] B. Mota, P. Faria, and Z. Vale, “Residential load shifting in demand response events for bill reduction using a genetic algorithm,” *Energy*, vol. 260, p. 124978, 2022, doi: 10.1016/j.energy.2022.124978.

[102] K. Y. Lee and J. Park, “Application of Particle Swarm Optimization to Economic Dispatch Problem : Advantages and Disadvantages,” in *2006 IEEE PES Power Systems Conference and Exposition*, 2006, pp. 188–192, doi: 10.1109/PSCE.2006.296295.

[103] M. Jaradat, M. Jarrah, Y. Jararweh, M. Al-Ayyoub, and A. Bousselham, “Integration of renewable energy in demand-side management for home appliances,” in *Proceedings of 2014 International Renewable and Sustainable Energy Conference, IRSEC 2014*, 2014, pp. 571–576, doi: 10.1109/IRSEC.2014.7059843.

[104] M. R. Z. Sabegh and C. Bingham, “Model Predictive Control with Binary Quadratic Programming for the Scheduled Operation of Domestic Refrigerators,” *Energies*, vol. 12, no. 24, 2019, doi: https://doi.org/10.3390/en12244649.

[105] C. K. Das, O. Bass, G. Kothapalli, T. S. Mahmoud, and D. Habibi, “Overview of energy storage systems in distribution networks: Placement, sizing, operation, and power quality,” *Renew. Sustain. Energy Rev.*, vol. 91, no. November 2016, pp. 1205–1230, 2018, doi: 10.1016/j.rser.2018.03.068.

[106] Z. Banday and P. Yadav, “Demand Side Management in Power Grid Using Particle Swarm Optimization,” *Int. J. Sci. Res. Dev.*, vol. 8, no. 3, pp. 817–821, 2020, [Online]. Available: https://www.ijsrd.com/articles/IJSRDV8I30789.pdf.

[107] T. Logenthiran, D. Srinivasan, and T. Z. Shun, “Demand side management in smart grid using heuristic optimization,” *IEEE Trans. Smart Grid*, vol. 3, no. 3, pp. 1244–1252, 2012, doi: 10.1109/TSG.2012.2195686.

[108] K. K. P. Kumar *et al.*, “Day-Ahead DSM-Integrated Hybrid-Power-Management-Incorporated CEED of Solar Thermal/Wind/Wave/BESS System Using HFPSO,” *Sustain.*, vol. 14, no. 1169, 2022, doi: 10.3390/su14031169.

[109] N. Azlina, A. Aziz, and K. A. Aziz, “Particle Swarm Optimization for Constrained and Multiobjective Problems : A Brief Review,” in *International Conference on Management and Artificial Intelligence IPEDR*, 2011, vol. 6, pp. 146–150.

[110] H. L. Chen *et al.*, “Towards an optimal support vector machine classifier using a parallel particle swarm optimization strategy,” *Appl. Math. Comput.*, vol. 239, pp. 180–197, 2014, doi: 10.1016/j.amc.2014.04.039.

[111] “About EnergyPLAN.” https://energyplan.eu/about-energyplan/.

[112] “HOMER Pro.” https://homerenergy.com/products/pro/index.html.

[113] “LEAP.” https://www.sei.org/tools/leap-long-range-energy-alternatives-planning-system/.

[114] D. Bogdanov, A. Gulagi, M. Fasihi, and C. Breyer, “Full energy sector transition towards 100% renewable energy supply: Integrating power, heat, transport and industry sectors including desalination,” *Appl. Energy*, vol. 283, p. 116273, 2021, doi: 10.1016/j.apenergy.2020.116273.

[115] A. S. Oyewo, S. Sterl, S. Khalili, and C. Breyer, “Highly renewable energy systems in Africa: Rationale, research, and recommendations,” *Joule*, vol. 7, pp. 1437–1470, 2023, doi: 10.1016/j.joule.2023.06.004.

[116] IEA-ETSAP, “MARKAL.” https://iea-etsap.org/index.php/etsap-tools/model-generators/markal.

[117] “About oemof.” .

[118] “OSeMOSYS.” http://www.osemosys.org/.

[119] “PyPSA: Python for power system analysis.” https://pypsa.readthedocs.io/en/latest/.

[120] “RETScreen Clean Energy Management Software.” https://openei.org/wiki/RETScreen_Clean_Energy_Project_Analysis_Softwarehttps://openei.org/wiki/RETScreen_Clean_Energy_Project_Analysis_Software.

[121] “TIMES.” https://iea-etsap.org/index.php/etsap-tools/model-generators/times.

[122] Stockholm Environment Institute, “LEAP 2020: SEI’s flagship tool for low emissions analysis gets major upgrade.” .

[123] “Annex A. LUT Energy System Transition Model.” 2022, [Online]. Available: https://www.greens-efa.eu/files/assets/docs/09._annex_-_accelerating_the_european_renewable_energy_transition_-_2022.pdf.

[124] T. Kallai and M. Çengel, “Open Source Tools for Energy System Modelling in Europe and Africa.” 2022, doi: 10.13140/RG.2.2.28979.50727.

[125] Electric Power Research Institute (EPRI), “Principles and Practice of Demand Side Management,” 1993.

[126] C. W. Gellings, “The Concept of Demand-Side Management for Electric Utilities,” *Proc. IEEE*, vol. 73, no. 10, pp. 1468–1470, 1985, doi: 10.1109/PROC.1985.13318.

[127] K. Tamilarasu, C. R. Sathiasamuel, J. D. N. Joseph, R. M. Elavarasan, and L. Mihet-Popa, “Reinforced demand side management for educational institution with incorporation of user’s comfort,” *Energies*, vol. 14, p. 2855, 2021, doi: https://doi.org/10.3390/en14102855.

[128] A. S. Duran and F. G. Sahinyazan, “An analysis of renewable mini-grid projects for rural electrification,” *Socioecon. Plann. Sci.*, vol. 77, p. 100999, 2021, doi: 10.1016/j.seps.2020.100999.

[129] CrossBoundary, “Innovation Insight: Appliance Financing 3.0.,” 2022. [Online]. Available: https://www.crossboundary.com/wp-content/uploads/2023/01/CrossBoundary-Innovation-Lab-Appliance-Financing-3.0-Innovation-Insight-10-January-2023.pdf.

[130] H. Pourbabak, T. Chen, B. Zhang, and W. Su, “Control and energy management system in microgrids,” in *Clean Energy Microgrids*, S. Obara and J. Morel, Eds. London, United Kingdom: Institution of Engineering and Technology, 2017.

[131] J. Prasad, T. Jain, N. Sinha, and S. Rai, “Load Shifting Based DSM Strategy for Peak Demand Reduction in a Microgrid,” in *2020 International Conference on Emerging Frontiers in Electrical and Electronic Technologies, ICEFEET 2020*, 2020, pp. 1–6, doi: 10.1109/ICEFEET49149.2020.9186983.

[132] G. H. Philipo, J. N. Kakande, and S. Krauter, “Neural Network-Based Demand-Side Management in a Stand-Alone Solar PV-Battery Microgrid Using Load-Shifting and Peak-Clipping,” *Energies*, vol. 15, no. 5215, 2022, doi: https://doi.org/10.3390/en15145215.

[133] David Kathan, “Demand Response as Power System Resources.” Federal Energy Regulatory Commission, 2010, [Online]. Available: https://www.energy.gov/oe/articles/ferc-presendation-demand-response-power-system-resources-october-29-2010.

[134] IEA, “Energy Efficiency.” https://www.iea.org/energy-system/energy-efficiency-and-demand/energy-efficiency.

[135] M. A. Islam *et al.*, “Energy Conservation and Load Shifting based DSM approach in the residential sector: applicability and impacts analysis in the case of

developing countries," in *2022 International Conference on Innovations in Science, Engineering and Technology, ICISET 2022*, 2022, no. February 2022, pp. 498–503, doi: 10.1109/ICISET54810.2022.9775910.

[136] Federal Energy Regulatory Commission, "Assessment of Demand Response and Advanced Metering - Staff Report," 2008. [Online]. Available: https://www.ferc.gov/sites/default/files/2020-04/demand-response_4.pdf.

[137] M. S. Bakare, A. Abdulkarim, M. Zeeshan, and A. N. Shuaibu, "A comprehensive overview on demand side energy management towards smart grids: challenges, solutions, and future direction," *Energy Informatics*, vol. 6, 2023, doi: 10.1186/s42162-023-00262-7.

[138] P. Faria and Z. Vale, "Demand response in electrical energy supply: An optimal real time pricing approach," *Energy*, vol. 36, no. 8, pp. 5374–5384, 2011, doi: 10.1016/j.energy.2011.06.049.

[139] IEA Photovoltaic Power Systems Programme (IEA PVPS), "PV as an ancillary service provider project," 2021. [Online]. Available: https://iea-pvps.org/wp-content/uploads/2021/10/IEA-PVPS_T14_14_2021_PV_ancillary_service_provider_IEA_PVPS_report.pdf.

[140] B. Peng *et al.*, "A two-stage pattern recognition method for electric customer classification in smart grid," in *2016 IEEE International Conference on Smart Grid Communications, SmartGridComm 2016*, 2016, pp. 758–763, doi: 10.1109/SmartGridComm.2016.7778853.

[141] A. M. Jasim, B. H. Jasim, B. C. Neagu, and B. N. Alhasnawi, "Efficient Optimization Algorithm-Based Demand-Side Management Program for Smart Grid Residential Load," *Axioms*, vol. 12, no. 1, 2023, doi: 10.3390/axioms12010033.

[142] K. P. Schneider *et al.*, "Enabling resiliency operations across multiple microgrids with grid friendly appliance controllers," *IEEE Trans. Smart Grid*, vol. 9, no. 5, pp. 4755–4764, 2018, doi: 10.1109/TSG.2017.2669642.

[143] A. Arteconi and F. Polonra, "Demand side management in refrigeration applications," *Int. J. Heat Technol.*, vol. 35, no. Special Issue 1, pp. S58–S63, 2017, doi: 10.18280/ijht.35Sp0108.

[144] M. Buevich, D. Schnitzer, T. Escalada, A. Jacquiau-Chamski, and A. Rowe, "Fine-grained remote monitoring, control and pre-paid electrical service in rural microgrids," in *IPSN 2014 - Proceedings of the 13th International Symposium on Information Processing in Sensor Networks*, 2014, no. 1, pp. 1–11, doi: 10.1109/IPSN.2014.6846736.

[145] EACREEE, "Energy Efficient Lighting and Appliances (EELA) Project in Southern and Eastern Africa." https://www.eacreee.org/project/energy-efficient-lighting-and-appliances-eela-project-southern-and-eastern-africa.

[146] D. A. Mir, C. N. H. Doll, R. Lindner, and M. T. Parray, "Explaining the diffusion of energy-efficient lighting in India: A technology innovation systems approach," *Energies*, vol. 13, no. 5821, 2020, doi: 10.3390/en13215821.

[147] K. Reiss-haimbala, T. Grader, M. Gullberg, and R. Makaliki, "Lighting and Appliances for Lives and Livelihoods ; a Foundation for Strategic Energy

Efficiency Policies in East and Southern Africa," 2024. [Online]. Available: https://www.eela-project.org/sites/default/files/2024-07/ECEEE paper.pdf.

[148] C. C. Okafor, C. N. Madu, C. C. Ajaero, K. Agomuo, and E. Abu, "Toward Sustainable Power Supply and Consumption of an Emerging Economy (Nigeria)," *J. Econ. Dev. Environ. People*, vol. 9, no. 4, 2020, doi: 10.26458/jedep.v9i4.674.

[149] M. J. Booysen, J. A. Samuels, and S. S. Grobbelaar, "LED there be light: The impact of replacing lights at schools in South Africa," *Energy Build.*, vol. 235, p. 110736, 2021, doi: 10.1016/j.enbuild.2021.110736.

[150] S. de la R. du Can, D. Pudleiner, D. Jones, and A. Khan, "Energy efficiency roadmap for Uganda: Making energy efficiency count," 2017. [Online]. Available: https://international.lbl.gov/publications/energy-efficiency-roadmap-uganda.

[151] IIF-IIR, "The Role of Refrigeration in the Global Economy (2019). 38th Note on Refrigeration Technologies," 2019. doi: http://dx.doi.org/10.18462/iif.NItec38.06.2019.

[152] NASA, "Temperatures Rising: NASA Confirms 2024 Warmest Year on Record," 2025. https://www.nasa.gov/news-release/temperatures-rising-nasa-confirms-2024-warmest-year-on-record/ (accessed Jul. 25, 2025).

[153] Mohammad Reza Zavvar Sabegh, "Deep Reinforcement Learning And Model Predictive Control Approaches For The Scheduled Operation Of Domestic Refrigerators," University of Lincoln, 2022.

[154] A. Postnikov, I. Albayati, S. Pearson, C. Bingham, R. Bickerton, and A. Zolotas, "Facilitating static firm frequency response with aggregated networks of commercial food refrigeration systems.pdf," *Appl. Energy*, vol. 251, 2019, doi: 10.1016/j.apenergy.2019.113357.

[155] J. Tran, J. Gilles, R. Mann, and V. Murthy, "Automated Demand Response Refrigerator Project," *Tran2015AutomatedDR*, vol. 186, no. October, pp. 1–7, 2015, [Online]. Available: https://ecal.berkeley.edu/files/ce186/projects/mannryancasey_4883549_63830968_CE 186 Final Paper.pdf.

[156] A. Ovca, T. Skufca, and M. Jev, "Temperatures and storage conditions in domestic refrigerators - Slovenian scenario," *Food Control*, no. January, 2021, doi: 10.1016/j.foodcont.2020.107715.

[157] A. U. Zaman and J. Doyle, "Smart Grid Control: Demand Side Management in Household Refrigerators as a tool for Load Shifting," *Macalester J. Phys. Astron.*, vol. 10, no. 1, 2022, [Online]. Available: https://digitalcommons.macalester.edu/cgi/viewcontent.cgi?article=1170&context=mjpa.

[158] National Environment Agency, "Guidelines on Proper Storage of Food in Refrigerators and Use of Refrigerators," 2016. [Online]. Available: https://www.nea.gov.sg/docs/default-source/resource/guidelines-on-proper-storage-of-food-in-refrigerators.pdf.

[159] Food and Drug Administration (FDA), "Are you storing food safely?," 2023. https://www.fda.gov/consumers/consumer-updates/are-you-storing-food-safely.

[160] V. V. Arun Kappen, Titto John George, "Performance Improvement of a Domestic

Refrigerator By Using Phase Change Material," *Int. J. Sci. Eng. Res.*, vol. 7, no. 3, pp. 58–68, 2016, [Online]. Available: https://www.ijser.org/researchpaper/Performance-Improvement-of-a-Household-Refrigerator-by-Use-of-a-Phase-Change-Material.pdf.

[161] J. M. Belman-Flores, D. Pardo-Cely, M. A. Gómez-Martínez, I. Hernández-Pérez, D. A. Rodríguez-Valderrama, and Y. Heredia-Aricapa, "Thermal and energy evaluation of a domestic refrigerator under the influence of the thermal load," *Energies*, vol. 12, no. 3, 2019, doi: 10.3390/en12030400.

[162] L. W. Harrington, "Prediction of the energy consumption of refrigerators during use," University of Melbourne, 2018.

[163] European Commission Directorate-General for Energy, "Ecodesign & Labelling Review Household Refrigeration: Preparatory/review study - Commission Regulation (EC) No. 643/2009 and Commission (Delegated) Regulation (EU) 1060/2010," 2015. [Online]. Available: https://ecodesign-fridges.eu/sites/ecodesign-fridges.eu/files/Household Refrigeration Review TASK 1_6 DRAFT REPORT 20151114.pdf.

[164] K. A. Agyarko, R. Opoku, and R. Van Buskirk, "Removing barriers and promoting demand-side energy efficiency in households in Sub-Saharan Africa: A case study in Ghana," *Energy Policy*, vol. 137, p. 111149, 2020, doi: 10.1016/j.enpol.2019.111149.

[165] L. W. Davis, A. Fuchs, and P. Gertler, "Cash for coolers: Evaluating a large-scale appliance replacement program in Mexico," *Am. Econ. J. Econ. Policy*, vol. 6, no. 4, pp. 207–238, 2014, doi: 10.1257/pol.6.4.207.

[166] F. X. Trias, C. Oliet, J. Rigola, and C. D. Pérez-Segarra, "A simple optimization approach for the insulation thickness distribution in household refrigerators," *Int. J. Refrig.*, vol. 93, pp. 169–175, 2018, doi: 10.1016/j.ijrefrig.2018.06.014.

[167] C. Hueppe *et al.*, "Age-related efficiency loss of household refrigeration appliances: Development of an approach to measure the degradation of insulation properties," *Appl. Therm. Eng.*, vol. 173, p. 115113, 2020, doi: 10.1016/j.applthermaleng.2020.115113.

[168] EACREEE, "Key milestone achieved in the development of Minimum Energy Performance Standards," 2024. https://www.eacreee.org/article/key-milestone-achieved-development-minimum-energy-performance-standards.

[169] S. Agarwal, S. Dela Rue Du Can, V. Letschert, W. Y. Park, and U. Kaggwa, "A review of the legislative landscape and refrigeration market for introducing an energy efficiency standards and labeling program for refrigeration appliances in Uganda," 2022.

[170] UNEP U4E, "Regional harmonization of energy-efficient and climate-friendly cooling in East and Southern Africa." 2022, [Online]. Available: https://united4efficiency.org/wp-content/uploads/2021/09/U4E_FACT-SHEETS_EAC-SADC_2021-09-24.pdf.

[171] W. Y. Park, N. Shah, P. Blake, and M. Edl, "Technical Note on Quality and Performance Metrics of Cooling Products for East African Community (EAC) and Southern African Development Community (SADC)," 2021. [Online]. Available:

https://united4efficiency.org/wp-content/uploads/2021/04/Technical-Note-on-Ref-in-EACSADC_Final_April-2021.pdf.

[172] G. Coccia, A. Arteconi, P. D'Agaro, F. Polonara, and G. Cortella, "Demand side management of a commercial refrigeration system with cold thermal energy storage," *Refrig. Sci. Technol.*, vol. 2019-Augus, no. September, pp. 2504–2511, 2019, doi: 10.18462/iir.icr.2019.1088.

[173] I. M. Saleh *et al.*, "Impact of demand side response on a commercial retail refrigeration system," *Energies*, vol. 11, no. 2, 2018, doi: 10.3390/en11020371.

[174] T. G. Hovgaard, L. F. S. Larsen, K. Edlund, and J. B. Jørgensen, "Model predictive control technologies for efficient and flexible power consumption in refrigeration systems," *Energy*, vol. 44, no. 1, pp. 105–116, 2012, doi: 10.1016/j.energy.2011.12.007.

[175] EERE, "Energy Efficiency: Buildings and Industry | Department of Energy." https://www.energy.gov/eere/energy-efficiency-buildings-and-industry.

[176] G. Sonnenrein *et al.*, "Copolymer-bound phase change materials for household refrigerating appliances: experimental investigation of power consumption, temperature distribution and demand side management potential," *Int. J. Refrig.*, vol. 60, pp. 166–173, 2015, doi: 10.1016/j.ijrefrig.2015.06.030.

[177] E. Oró, L. Miró, M. M. Farid, and L. F. Cabeza, "Improving thermal performance of freezers using phase change materials," *Int. J. Refrig.*, vol. 35, no. 4, pp. 984–991, 2012, doi: 10.1016/j.ijrefrig.2012.01.004.

[178] I. Javeri-Shahreza, M. Fakhroleslam, and S. M. Sadrameli, "Application of phase change materials for performance enhancement of open-display supermarket refrigerators: Numerical simulation and parametric study," *J. Energy Storage*, vol. 66, no. 107506, 2023, doi: 10.1016/j.est.2023.107506.

[179] I. Javeri-Shahreza, L. Abdolmaleki, S. M. Sadrameli, and M. Fakhroleslam, "Dynamic modeling and experimental validation of household refrigerators/freezers equipped with phase change materials towards improved energy efficiency," *Therm. Sci. Eng. Prog.*, vol. 46, p. 102227, 2023, doi: 10.1016/j.tsep.2023.102227.

[180] R. Barzin, J. J. J. Chen, B. R. Young, and M. M. Farid, "Peak load shifting with energy storage and price-based control system," *Energy*, vol. 92, pp. 505–514, 2015, doi: 10.1016/j.energy.2015.05.144.

[181] L. S. Rodrigues, D. L. Marques, J. A. Ferreira, V. A. F. Costa, N. D. Martins, and F. J. Neto Da Silva, "The Load Shifting Potential of Domestic Refrigerators in Smart Grids: A Comprehensive Review," *Energies*, vol. 15, no. 20, 2022, doi: 10.3390/en15207666.

[182] J. Sánchez Ramos, M. Pavón Moreno, M. Guerrero Delgado, S. Álvarez Domínguez, and L. F. Cabeza, "Potential of energy flexible buildings: Evaluation of DSM strategies using building thermal mass," *Energy Build.*, vol. 203, p. 109442, 2019, doi: 10.1016/j.enbuild.2019.109442.

[183] S. Naderi, G. Pignatta, S. Heslop, I. MacGill, and D. Chen, "Demand response via pre-cooling and solar pre-cooling: A review," *Energy Build.*, vol. 272, p. 112340, 2022, doi: 10.1016/j.enbuild.2022.112340.

[184] A. Maiorino, M. G. Del Duca, A. Mota-Babiloni, and C. Aprea, “Achieving a running cost saving with a cabinet refrigerator incorporating a phase change material by the scheduling optimisation of its cyclic operations,” *Int. J. Refrig.*, vol. 117, pp. 237–246, 2020, doi: 10.1016/j.ijrefrig.2020.05.017.

[185] M. M. Almenta, J. Morrow, R. Best, B. Fox, and A. Foley, “An aggregated fridge-freezer peak shaving and valley filling control strategy for enhanced grid operations,” in *2015 IEEE Power and Energy Society General Meeting*, 2015, pp. 1–5, doi: 10.1109/PESGM.2015.7285851.

[186] V. Lakshmanan, K. Gudmand-Hoyer, M. Marinelli, A. M. Kosek, and P. Norgard, “Energy shift estimation of demand response activation on refrigerators - A field test study,” 2014, doi: 10.1109/UPEC.2014.6934681.

[187] N. Baghina, I. Lampropoulos, B. Asare-Bediako, W. L. Kling, and P. F. Ribeiro, “Predictive control of a domestic freezer for real-time demand response applications,” in *IEEE PES Innovative Smart Grid Technologies Conference Europe*, 2012, pp. 1–8, doi: 10.1109/ISGTEurope.2012.6465809.

[188] Siemens Stiftung, “E-Mobility Solutions for Rural Sub-Saharan Africa: Leveraging Economic, Social and Environmental Change,” 2020. https://www.siemens-stiftung.org/wp-content/uploads/medien/publikationen/publication-emobility-emobilitysolutionsforruralsubsaharanafrica-siemensstiftung.pdf (accessed Apr. 04, 2023).

[189] T. Bishop *et al.*, “Enhancing understanding on safe motorcycle and three-wheeler use for rural transport,” 2019.

[190] KCCA, “Analysis of Boda-Boda Operations Paratransit Modernization and Street Usage Study Final Report,” 2020. https://transportforcairo.com/wp-content/uploads/2022/11/GKMA_Bodaboda_Final_Report.pdf (accessed Jul. 06, 2024).

[191] J. Park, J. Calzavara, and T. Courtright, “Environmental and Social Impact Assessment of Electric Motorcycle Taxis in Kampala , Uganda,” 2021. [Online]. Available: https://dx.doi.org/10.7302/1037.

[192] A. Bugaje, M. Ehrenwirth, C. Trinkl, and W. Zoerner, “Investigating the Performance of Rural Off-Grid Photovoltaic System with Electric-Mobility Solutions: A Case Study Based on Kenya,” *J. Sustain. Dev. Energy, Water Environ. Syst.*, vol. 10, no. 1, 2022, doi: 10.13044/j.sdewes.d9.0391.

[193] RENAC, “Fact Sheet E-mobility.” Accessed: Aug. 02, 2024. [Online]. Available: https://www.renac.de/fileadmin/renac/media/Projects/Soaring/Soaring_Fact_sheet_E-Mobility.pdf.

[194] Uganda Investment Authority and UNDP, “Lamwo District Investment Profile.” [Online]. Available: https://www.undp.org/sites/g/files/zskgke326/files/migration/ug/UNDPUg17--DistrictProfile_Lamwo.pdf.

[195] L. D. Namujju, I. Mwammenywa, G. M. Kagarura, U. Hilleringmann, and B. Hehenkamp, “Smart Metering and Choice Architecture in Demand-Side Management: A Power Resource-Constrained Perspective,” in *2024 IEEE 8th*

Energy Conference, ENERGYCON 2024 - Proceedings, 2024, pp. 1–6, doi: 10.1109/ENERGYCON58629.2024.10488738.

[196] T. Raji, L. Maqelepo, N. J. Williams, and A. Bett, "Money and Power: The Impact of Tariff Structures on Electricity Consumption in Solar Microgrids in Africa," in *2022 IEEE PES/IAS PowerAfrica, PowerAfrica 2022*, 2022, pp. 1–5, doi: 10.1109/PowerAfrica53997.2022.9905330.

[197] T. Reber, S. Booth, D. Cutler, X. Li, and J. Salasovich, "Tariff Considerations for Micro-Grids in Sub-Saharan Africa," 2018. [Online]. Available: www.nrel.gov/publications.%0Awww.nrel.gov/publications.%0Ahttps://www.nrel.gov/docs/fy18osti/69044.pdf.

[198] I. S. Alsaidan, "Optimal Planning of Microgrid-Integrated Battery Energy Storage," University of Denver, 2018.

[199] L. Bhamidi and S. Sivasubramani, "Optimal Sizing of Smart Home Renewable Energy Resources and Battery under Prosumer-Based Energy Management," *IEEE Syst. J.*, vol. 15, no. 1, pp. 105–113, 2021, doi: 10.1109/JSYST.2020.2967351.

[200] J. Xu, C. Yan, Y. Xu, J. Shi, K. Sheng, and X. Xu, "A Hierarchical Game Theory Based Demand Optimization Method for Grid-Interaction of Energy Flexible Buildings," *Front. Energy Res.*, vol. 9, no. 736439, 2021, doi: 10.3389/fenrg.2021.736439.

[201] "Tesseract OCR." https://github.com/tesseract-ocr/tesseract.

[202] D. Restrepo, B. Restrepo-Cuestas, and A. Trejos, "Microgrid analysis using HOMER: A case study," *DYNA*, vol. 85, no. 207, pp. 129–134, 2018, doi: 10.15446/dyna.v85n207.69375.

[203] "Docker overview." https://docs.docker.com/get-started/overview/.

[204] "MQTT: The Standard for IoT Messaging." https://mqtt.org.

[205] "Eclipse Mosquitto." https://mosquitto.org/.

[206] HiveMQ, "HiveMQ." https://www.hivemq.com/ (accessed Apr. 17, 2024).

[207] N. Hosseinzadeh, A. Al Maashri, N. Tarhuni, A. Elhaffar, and A. Al-Hinai, "A Real-Time Monitoring Platform for Distributed Energy Resources in a Microgrid—Pilot Study in Oman," *Electronics*, vol. 10, no. 15, p. 1803, 2021, doi: 10.3390/electronics10151803.

[208] OpenJS Foundation, "Node-RED." https://nodered.org/about/ (accessed Apr. 18, 2023).

[209] OpenJS Foundation, "Node-red-contrib-sma-webconnect." https://flows.nodered.org/node/node-red-contrib-sma-webconnect (accessed Jul. 18, 2023).

[210] "InfluxDB." https://www.influxdata.com/products/influxdb-overview/.

[211] "Grafana." https://grafana.com/.

[212] "Twingate vs. VPNs." https://www.twingate.com/docs/twingate-vs-vpn.

[213] "What is Tailscale?," *Tailscale Inc*, 2022. https://tailscale.com/kb/1151/what-is-tailscale/.

[214] J. Taneja, “Measuring Electricity Reliability in Kenya,” 2016.

[215] K. Olaniyan, B. C. McLellan, S. Ogata, and T. Tezuka, “Estimating residential electricity consumption in Nigeria to support energy transitions,” *Sustainability*, vol. 10, no. 5, p. 1440, 2018, doi: 10.3390/su10051440.

[216] R. Dharani, M. Balasubramonian, T. S. Babu, and B. Nastasi, “Load shifting and peak clipping for reducing energy consumption in an indian university campus,” *Energies*, vol. 14, p. 558, 2021, doi: 10.3390/en14030558.

[217] EnergySage, “SunPower E-Series SPR-E20-327.” https://www.energysage.com/solar-panels/sunpower/778/spr-e20-327/ (accessed Jan. 21, 2022).

[218] R. Samu, G. Poyrazoglu, and M. Fahrioglu, “The Potential and Economic Analysis of Grid-connected Solar PV Power in Kenya,” in *2019 1st Global Power, Energy and Communication Conference (GPECOM)*, 2019, pp. 298–301, doi: 10.1109/GPECOM.2019.8778467.

[219] L. Uwineza, H. G. Kim, and C. K. Kim, “Feasibilty study of integrating the renewable energy system in Popova Island using the Monte Carlo model and HOMER,” *Energy Strateg. Rev.*, vol. 33, p. 100607, 2021, doi: 10.1016/j.esr.2020.100607.

[220] C. Hueppe *et al.*, “Investigating the real life energy consumption of refrigeration appliances in Germany: Are present policies sufficient?,” *Energy Policy*, vol. 155, p. 112275, 2021, doi: 10.1016/j.enpol.2021.112275.

[221] A. Paul *et al.*, “Impact of aging on the energy efficiency of household refrigerating appliances,” *Appl. Therm. Eng.*, vol. 205, p. 117992, 2022, doi: 10.1016/j.applthermaleng.2021.117992.

[222] EAC, “Draft East African Standard: Refrigerating appliances for household and similar use - minimum energy performance - Requirements,” *Draft East African Standards*. 2024, [Online]. Available: https://members.wto.org/crnattachments/2024/TBT/UGA/24_03695_00_e.pdf.

[223] S. L. Arun and M. P. Selvan, “Intelligent Residential Energy Management System for Dynamic Demand Response in Smart Buildings,” *IEEE Syst. J.*, vol. 12, no. 2, pp. 1329–1340, 2018, doi: 10.1109/JSYST.2017.2647759.

[224] EPRA, “Retail electricity tariff review for the 2022/23-2025/26 4th Tariff Control Period (TCP) effective 1st April 2023.” 2023, [Online]. Available: https://www.epra.go.ke/retail-electricity-tariff-review-for-the-2022-23-2025-26-4th-tariff-control-period-tcp-effective-1st-april-2023/.

[225] J. N. Kakande, G. H. Philipo, and S. Krauter, “Demand side management potential of refrigeration appliances,” 2023, doi: 10.1109/PowerAfrica57932.2023.10363161.

[226] NASA, “NASA data access viewer.” https://power.larc.nasa.gov/data-access-viewer/ (accessed May 31, 2024).

[227] F. Brihmat and S. Mekhtoub, “PV Cell Temperature/ PV Power Output Relationships Homer Methodology Calculation,” 2013, [Online]. Available: https://www.semanticscholar.org/paper/PV-Cell-Temperature-PV-Power-Output-Relationships-Brihmat-

Mekhtoub/81ca5f5da5e2e77ef9b420439c6d057fcae70849.

[228] Hoppecke, “Hoppecke Sun Power VR M brochure.” [Online]. Available: https://www.hoppecke.com/fileadmin/Redakteur/Hoppecke-Main/Products-Import/sun_power_vrm_brochure_en.pdf.

[229] SMA, “SUNNY ISLAND 4.4M / 6.0H / 8.0H Datasheet.” [Online]. Available: https://files.sma.de/downloads/SI44M-80H-13-DS-en-31.pdf.

[230] K. Ma, P. Liu, J. Yang, and X. Guan, *Control and Communication for Demand Response with Thermostatically Controlled Loads*. Springer Nature Singapore, 2023.

[231] J. Wang, C. Yik Tang, and L. Song, “Analysis of precooling optimization for residential buildings,” *Appl. Energy*, vol. 323, no. July, 2022, doi: 10.1016/j.apenergy.2022.119574.

[232] “Winch Energy.” https://www.winchenergypower.com/about-us/.

[233] M. K. M. Shapi, N. A. Ramli, and L. J. Awalin, “Energy consumption prediction by using machine learning for smart building: Case study in Malaysia,” *Dev. Built Environ.*, vol. 5, no. July 2020, p. 100037, 2021, doi: 10.1016/j.dibe.2020.100037.

[234] S. Hussain, M. W. Mustafa, K. H. Ateyeh Al-Shqeerat, B. A. Saleh Al-rimy, and F. Saeed, “Electric theft detection in advanced metering infrastructure using Jaya optimized combined Kernel-Tree boosting classifier—A novel sequentially executed supervised machine learning approach,” *IET Gener. Transm. Distrib.*, vol. 16, no. 6, pp. 1257–1275, 2022, doi: 10.1049/gtd2.12386.

[235] H. Dhungana, F. Bellotti, R. Berta, and A. De Gloria, “Performance Comparison of Imputation Methods in Building Energy Data Sets,” in *Applications in Electronics Pervading Industry, Environment and Society*, S. Saponara and A. De Gloria, Eds. Springer Nature Switzerland, 2021, p. 150.

[236] B. O. Petrazzini, H. Naya, F. Lopez-Bello, G. Vazquez, and L. Spangenberg, “Evaluation of different approaches for missing data imputation on features associated to genomic data,” *BioData Min.*, vol. 14, no. 44, 2021, doi: 10.1186/s13040-021-00274-7.

[237] H. Rosado-Galindo and S. Dávila-Padilla, “Tree-Based Missing Value Imputation Using Feature Selection,” *J. Data Sci.*, vol. 18, no. 4, pp. 606–631, 2020, doi: 10.6339/JDS.202010_18(4).0002.

[238] P. Dixneuf, F. Errico, and M. Glaus, “A computational study on imputation methods for missing environmental data,” *ArXiv*, pp. 1–19, 2021, [Online]. Available: https://arxiv.org/pdf/2108.09500.

[239] A. A. Kebede *et al.*, “A techno-economic optimization and performance assessment of a 10 kWP photovoltaic grid-connected system,” *Sustain.*, vol. 12, no. 18, 2020, doi: 10.3390/su12187648.

[240] Y. Wu, Z. Liu, B. Li, J. Liu, and L. Zhang, “Energy management strategy and optimal battery capacity for flexible PV-battery system under time-of-use tariff,” *Renew. Energy*, vol. 200, pp. 558–570, 2022, doi: 10.1016/j.renene.2022.09.118.

[241] M. Schreiber, M. E. Wainstein, P. Hochloff, and R. Dargaville, “Flexible electricity tariffs: Power and energy price signals designed for a smarter grid,”

Energy, vol. 93, no. 2, pp. 2568–2581, 2015, doi: 10.1016/j.energy.2015.10.067.

[242] K. Mongird, V. Viswanathan, J. Alam, C. Vartanian, V. Sprenkle, and R. Baxter, "2020 Grid Energy Storage Technology Cost and Performance Assessment," 2020. [Online]. Available: https://www.pnnl.gov/sites/default/files/media/file/Final - ESGC Cost Performance Report 12-11-2020.pdf.

[243] A. A. Kebede *et al.*, "Techno-economic analysis of lithium-ion and lead-acid batteries in stationary energy storage application," *J. Energy Storage*, vol. 40, p. 102748, 2021, doi: 10.1016/j.est.2021.102748.

[244] SMA, "Sunny Tripower 15000TL/ 20000TL/ 25000TL." Accessed: Jul. 07, 2024. [Online]. Available: https://files.sma.de/downloads/STP15-25TL-30-DS-en-41.pdf.

[245] P. P. Kumar, V. Suresh, M. Jasinski, and Z. Leonowicz, "Off-grid rural electrification in india using renewable energy resources and different battery technologies with a dynamic differential annealed optimization," *Energies*, vol. 14, no. 18, 2021, doi: 10.3390/en14185866.

[246] V. A. Silva, A. R. Aoki, and G. Lambert-Torres, "Optimal day-ahead scheduling of microgrids with battery energy storage system," *Energies*, vol. 13, p. 5188, 2020, doi: 10.3390/en13195188.

[247] N. Ya'acob, A. S. G. A. Apandi, A. L. Yuso, M. Kassim, and N. F. Naim, "Prediction of Battery Lifetime using Hybrid Solar Power System," *Math. Stat. Eng. Appl.*, vol. 71, no. 2, pp. 208–224, 2022, doi: 10.17762/msea.v71i2.80.

[248] Hoppecke, "Manual for Hoppecke VRLA batteries." Accessed: Sep. 10, 2024. [Online]. Available: https://www.hoppecke.com/fileadmin/Redakteur/Hoppecke-Main/Products-Import/vrl_manual_de.pdf.

[249] R. Khezri, S. Member, A. Mahmoudi, S. Member, M. H. Haque, and S. Member, "A Demand Side Management Approach For Optimal Sizing of Standalone Renewable-Battery Systems," *IEEE Trans. Sustain. Energy*, vol. 12, no. 4, pp. 2184–2194, 2021, doi: 10.1109/TSTE.2021.3084245.

[250] T. Dragičević, H. Pandžić, D. Škrlec, I. Kuzle, J. M. Guerrero, and D. S. Kirschen, "Capacity Optimization of Renewable Energy Sources and Battery Storage in an Autonomous Telecommunication Facility," *IEEE Trans. Sustain. Energy*, vol. 5, no. 4, pp. 1367–1378, 2014, doi: 10.1109/TSTE.2014.2316480.

[251] C. A. Correa, A. Gerossier, A. Michiorri, and G. Kariniotakis, "Optimal scheduling of storage devices in smart buildings including battery cycling," *2017 IEEE Manchester PowerTech, Powertech 2017*, pp. 1–6, 2017, doi: 10.1109/PTC.2017.7981199.

[252] X. Luo, J. V. Barreras, C. L. Chambon, B. Wu, and E. Batzelis, "Hybridizing lead–acid batteries with supercapacitors: A methodology," *Energies*, vol. 14, no. 507, 2021, doi: 10.3390/en14020507.

[253] S. Mandelli, C. Brivio, E. Colombo, and M. Merlo, "A sizing methodology based on Levelized Cost of Supplied and Lost Energy for off-grid rural electrification systems," *Renew. Energy*, vol. 89, pp. 475–488, 2016, doi: 10.1016/j.renene.2015.12.032.

[254] S. D. Downing and D. F. Socie, "Simple rainflow counting algorithms," *Int. J.*

Fatigue, vol. 4, no. 1, pp. 31–40, 1982, doi: 10.1016/0142-1123(82)90018-4.

[255] M. Weiss, K. C. Cloos, and E. Helmers, "Energy efficiency trade-offs in small to large electric vehicles," *Environ. Sci. Eur.*, vol. 32, no. 46, 2020, doi: 10.1186/s12302-020-00307-8.

[256] ARE, "Bodawerk – Shareable & circular Li-Ion batteries for Africa (Uganda)." https://www.ruralelec.org/case-study/bodawerk-shareable-circular-li-ion-batteries-africa-uganda/ (accessed Jul. 27, 2024).

[257] A. Bugaje, M. Ehrenwirth, C. Trinkl, and W. Zörner, "Electric two-wheeler vehicle integration into rural off-grid photovoltaic system in kenya," *Energies*, vol. 14, no. 23, 2021, doi: 10.3390/en14237956.

[258] ARE, "Hybrid Solar PV System Installed for Zembo Motorcycles in Uganda," 2022. https://aptechafrica.com/hybrid-solar-pv-system-installed-for-zembo-motorcycles-in-uganda/ (accessed Jul. 27, 2024).

[259] T. R. Courtright, "Introducing the quarterly Kampala boda report," 2022. https://medium.com/lubyanza/introducing-the-quarterly-kampala-boda-report-718426589984 (accessed Jul. 06, 2024).

[260] "Bodawerk homepage." https://bodawerk.com/energy (accessed Aug. 20, 2024).

[261] N. R. Kuranel and D. Mohapatra, "E-mobility & DRE Innovations in Emerging Economies," 2022. Accessed: Jul. 27, 2024. [Online]. Available: https://itpo-germany.org/PDF/E-Mobility & DRE Innovations.pdf.

[262] "Zembo homepage." https://www.zem.bo (accessed Aug. 20, 2024).

[263] "AfricroozE homepage." https://africrooze.com/en/ (accessed Aug. 20, 2024).

[264] M. H. Elkholy *et al.*, "Techno-economic configuration of a hybrid backup system within a microgrid considering vehicle-to-grid technology: A case study of a remote area," *Energy Convers. Manag.*, vol. 301, p. 118032, 2024, doi: 10.1016/j.enconman.2023.118032.

[265] S. Mahomed, R. Shirley, D. Tice, and J. Phillips, "Business model innovations for utility and mini-grid integration : Insights from the Utilities 2 . 0 initiative in Uganda," no. October. 2020, Accessed: Mar. 27, 2021. [Online]. Available: https://www.energyeconomicgrowth.org/publication/business-model-innovations-utility-and-mini-grid-integration-insights-utilities-20.

[266] MoFPED, "Performance of the Economy - Monthly Report August 2021." [Online]. Available: https://mepd.finance.go.ug/documents/POE/2021/POE-2021-08-AUG.pdf.

[267] MathWorks, "Mixed-Integer Linear Programming (MILP) Algorithms." https://de.mathworks.com/help/optim/ug/mixed-integer-linear-programming-algorithms.html.

[268] A. Bugaje, M. Ehrenwirth, C. Trinkl, K. Bär, and W. Zörner, "Development of a load management algorithm using nonlinear programming (NLP) for optimum integration of electric-mobility solutions into rural off-grid PV systems," in *NEIS 2020 - Conference on Sustainable Energy Supply and Energy Storage Systems*, 2020, no. September, [Online]. Available: https://dspace.uib.es/xmlui/bitstream/handle/11201/160802/149IntegrationOfElec

tro-Mobility.pdf?sequence=1.

[269] A. I. Bugaje, “Standalone Solar-Based Power Supply for Electric Mobility in Rural Areas of Developing Countries,” Technische Universität Berlin, 2023.

[270] W. Afzal, L.-Y. Zhao, G.-Z. Chen, and Y. Xue, “Hybrid Wind/PV E-Bike Charging Station: Comparison of Onshore and Offshore Systems,” *Sustainability*, vol. 15, no. 20, p. 14963, 2023, doi: 10.3390/su152014963.

[271] Liebherr, “BluRoX: Innovative vacuum perlite insulation.” https://www.liebherr.com/en-gb/fridges-freezers/blurox-vacuum-perlite-insulation-3011725.

[272] S. Bourne and A. Novoselac, “Compact PCM-based thermal stores for shifting peak cooling loads,” *Build. Simul.*, vol. 8, pp. 673–688, 2015, doi: 10.1007/s12273-015-0243-6.

[273] R. R. Yenare *et al.*, “A comprehensive review of portable cold storage: Technologies, applications, and future trends,” *Alexandria Eng. J.*, vol. 94, pp. 23–33, 2024, doi: 10.1016/j.aej.2024.03.014.

[274] S. Acha, Y. Du, and N. Shah, “Enhancing energy efficiency in supermarket refrigeration systems through a robust energy performance indicator,” *Int. J. Refrig.*, vol. 64, pp. 40–50, 2016, doi: 10.1016/j.ijrefrig.2015.12.003.

[275] S. Lin *et al.*, “Grouping control strategy for aggregated thermostatically controlled loads,” *Electr. Power Syst. Res.*, vol. 171, pp. 97–104, 2019, doi: 10.1016/j.epsr.2019.02.005.

[276] K. Zhang, J. Yu, and Y. Ren, “Demand side management of energy consumption in a photovoltaic integrated greenhouse,” *Int. J. Electr. Power Energy Syst.*, vol. 134, p. 107433, 2022, doi: 10.1016/j.ijepes.2021.107433.

[277] S. Tindemans and G. Strbac, “Low-complexity control algorithm for decentralised demand response using thermostatic loads,” 2019, doi: 10.1109/EEEIC.2019.8783359.

[278] J. M. Ngowi, L. Bångens, and E. O. Ahlgren, “Benefits and challenges to productive use of off-grid rural electrification: The case of mini-hydropower in Bulongwa-Tanzania,” *Energy Sustain. Dev.*, vol. 53, pp. 97–103, 2019, doi: 10.1016/j.esd.2019.10.001.

Appendices

Appendix A: Python Code for Tesseract OCR to log the Edimax SP-2101W V3 smart plug data

```
import csv
import os
import cv2
import numpy as np
import pytesseract
from PIL import Image
import re

pytesseract.pytesseract.tesseract_cmd = r'D:\Program Files\Tesseract-OCR\tesseract.exe'
# Remember to add this line to where the tesseract.exe is

def image_to_text(image_path):
    image = cv2.imread(image_path)  # read image as a numpy array
    hsv = cv2.cvtColor(image, cv2.COLOR_BGR2HSV)  # convert to HSV color space

    # define range of orange and gray colors in HSV color space
    orange_lower = np.array([5, 40, 50])  #tweak these to ornage
    orange_upper = np.array([15, 90, 100])
    gray_lower = np.array([0, 0, 0])
    gray_upper = np.array([180, 255, 40])

    # threshold the HSV image to get only orange and gray colors
    mask = cv2.inRange(hsv, orange_lower, orange_upper) + cv2.inRange(hsv, gray_lower,
                                gray_upper)
    image = cv2.bitwise_and(image, image, mask=mask)

    # convert image to grayscale
    image = cv2.cvtColor(image, cv2.COLOR_BGR2GRAY)

    # run OCR on the grayscale image
    text = pytesseract.image_to_string(image)
```

```
    return text

def extract_text_and_write_to_csv(images_dir, csv_file):
    with open(csv_file, 'w', newline='') as file:
        writer = csv.writer(file)
        writer.writerow(["Image", "Text"])

        for image_name in os.listdir(images_dir):
            if not image_name.endswith(".png") and not image_name.endswith(".jpg") and not
                                image_name.endswith(".jpeg"):
                continue
            image_path = os.path.join(images_dir, image_name)
            text = image_to_text(image_path)
            writer.writerow([image_name, f'"{text}"'])

def extract_info(text):
    pattern = r"\s*(\d+(?:\.\d+)?)\s*\|\s*(\d+w@)"
    #re-edit this after colour changes
    match = re.search(pattern, text, re.IGNORECASE)
    if match:
        return match.group(1), match.group(2)
    return None, None

if __name__ == '__main__':
    images_dir = "./input" #./inout is the directory of images
    csv_file = "./input/output.csv"
    extract_text_and_write_to_csv(images_dir, csv_file)

    with open("./input/output.csv", "r") as input_file, open("./input/new_output.csv", "w",
                                newline="") as output_file:
        reader = csv.reader(input_file)
        writer = csv.writer(output_file)
        writer.writerow(["Image", "Text", "A", "B"])
        next(reader)  # skip header row
        for row in reader:
            image_name, text = row[0], row[1]
            a, b = extract_info(text)
            writer.writerow([image_name, text, a, b])
```

Appendix B: Masters Theses Supervised

Omid Malki, Analyse und Auslegung eines Stromversorgungssystems für das Mädcheninternat am Standort Lwak in Kenia zur Minimierung des CO2-Fußabdrucks und der Kosten. (28.08.2023, Paderborn University)

Waddah Alturk, Development of an energy management system to control a Load system through IoT platform. (09.04.2024, Paderborn University)

Bibhavari Bandyopadhyay, Demand Side and Food Safety Management using Fuzzy Logic Control. (15.10.2024, Paderborn University)